Human Powered Vehicle Frame Design

By

Matthew Allen

msallen@calpoly.edu

Peter Aumann

paumann@calpoly.edu

Trent Hellmann

thellman@calpoly.edu

Project Advisor: John Fabijanic

Instructor's Comments:

Instructor's Grade: _____

Date: _____

Final Design Report

Human Powered Vehicle Frame Design

Sponsored by the Cal Poly Human Powered Vehicle Team

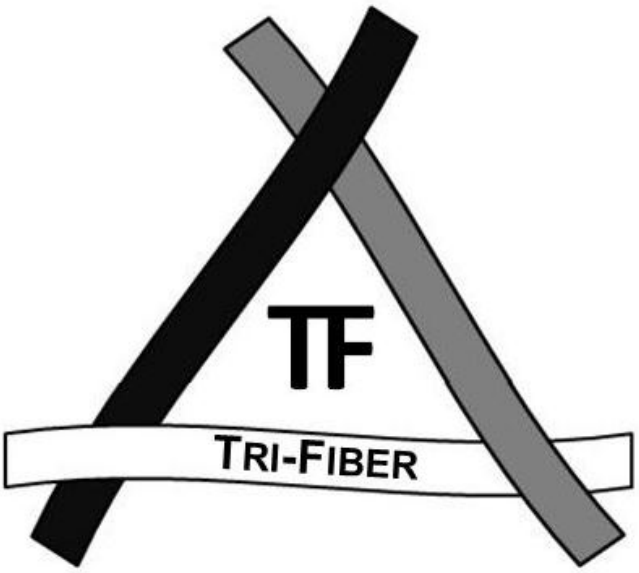

Matthew Allen

Peter Aumann

Trent Hellmann

Mechanical Engineering Department

California Polytechnic State University

San Luis Obispo

2015

Statement of Disclaimer

Since this project is a result of a class assignment, it has been graded and accepted as fulfillment of the course requirements. Acceptance does not imply technical accuracy or reliability. Any use of information in this report is done at the risk of the user. These risks may include catastrophic failure of the device or infringement of patent or copyright laws. California Polytechnic State University at San Luis Obispo and its staff cannot be held liable for any use or misuse of the project.

Table of Contents

List of Figures

List of Tables

Executive Summary

This report discusses the Human Powered Vehicle Frame Design senior project's contributions to the design, manufacture, testing, and competition of the Cal Poly Human Powered Vehicle Club's 2015 vehicle, Sweet Phoenix. The project's guiding rules and timeline were dictated by the ASME Human Powered Vehicle Challenge (HPVC), held in April 2015. The Club sought to improve upon its previous vehicle, Aria, which suffered from a range of faults including a catastrophic structural failure at the 2014 HPVC. Largely in response to this failure, the Frame Design project's major focus was Sweet Phoenix's frame, from concept to manufacturing.

During the design process in the Spring and Fall of 2014, several other issues were tackled in order to define the frame's design parameters. These secondary efforts included the fairing shape, vehicle stability requirements, handling characteristics, and rider ergonomics. A handling prototype was constructed in late Fall 2014, which successfully validated the solutions to these secondary requirements before the final design was constructed. Ultimately, Sweet Phoenix's frame is a hybrid design – a composite monocoque fairing to which several weldments are mechanically fastened. The team used extensive finite element analysis to evaluate structural properties for both of these frame subsystems during the final development stages.

Sweet Phoenix was produced during the Winter quarter of 2015, with much physical help from the HPV Club members and financial support from several sponsors. The production effort was quite successful, in part thanks to two significant manufacturing improvements – sponsored out-of-house machining of the fairing tools, and a frame-to-fairing alignment jig. The vehicle's construction quality was recognized at HPVC with a "Best Craftsmanship" award.

Testing of the final vehicle revealed very low stiffness of the weldments' fairing mounts, which was resolved by adding additional bracing locations to the fairing. In addition, the team discovered several drivetrain-related issues that were attacked with numerous attempted solutions, but were not solved prior to HPVC. The drivetrain also contributed to localized delamination of the fairing near a chain idler pulley mount. Unfortunately, these drivetrain issues resulted in several broken chains and poor performance in the acceleration-heavy Endurance Event at HPVC. On the other hand, Sweet Phoenix placed 1st in Design and Men's Sprint, both satisfying results for the Club, and the Frame Design project was an overall success.

Chapter 1: Introduction

Each year, the American Society for Mechanical Engineers (ASME) hosts a competition titled the Human Powered Vehicle Challenge (HPVC) in two separate locations across the United States and in two locations internationally. The purpose of the competition is to encourage the advancement of Human Powered Vehicles (HPVs) by providing design guidelines, challenges, and events to exhibit the innovation and design abilities of collegiate teams. Cal Poly has been competing in this competition since 1978, fielding innovative and new designs each year that push the envelope of what can be designed, manufactured, and ridden.

Human Powered Vehicles traditionally consist of a two part structure – an aerodynamic shell called a fairing, and the structural frame that supports the rider and other vehicle systems. These two components can be combined or be separate, however, both must be present in some form for a vehicle to be considered an HPV. The scope of this Senior Project involved designing, manufacturing, testing, and ultimately competing in the Human Powered Vehicle at the 2015 ASME HPVC – West competition in conjunction with the Cal Poly Human Powered Vehicle Club. Specifically, this project focused on the vehicle's structural frame and its overall integration with the fairing that was designed and built by the club.

The goals of this project were two-fold: to meet the requirements put forth by the sponsor – the Human Powered Vehicle Club – and to adequately design, manufacture, and test the vehicle to ensure its competitiveness at the ASME HPVC competition. Through collaboration with the club's team, a vehicle was created to reach the team's goal of winning the overall competition. A competitive vehicle needs to be well designed, professionally built, and adequately tested while keeping competition requirements in mind. Therefore, Tri-Fiber focused on these points throughout the duration of the project. Cal Poly's Human Powered Vehicle Team has a long history of success when competing at HPVC, which this project sought to continue.

Objectives

The overall goals of this Senior Project were to research, design, construct, and test a human powered vehicle with the end goal of competing in the 2015 ASME Human Powered Vehicle Challenge - West. This event, also known as HPVC-West, took place from April 24-26, 2015.

This project required a broad list of requirements in order to define its success. In order to determine which requirements were the most important to the customer, the Cal Poly Human Powered Vehicle Team (HPVT), Quality Function Deployment (QFD) was utilized. This method centers on a tool called a House of Quality (HOQ), which enabled the team to systematically evaluate requirements and benchmarks, evaluate the correlation between customer requirements and product specifications, and set product goals. The HOQ used to determine our list of design requirements is located in Appendix A.

In order to evaluate designs effectively, we came up with a set of core project objectives from the requirements table in conjunction with trade studies, and are as follows:

- Place in the top 15% of competitors in the Sprint Event, top 20% in the Endurance Event, top 10% in Design, and top 25% in Innovation.
- Construct a vehicle that can fit all riders between the heights of 5’5” and 6’2”.
- Conduct testing of all major final vehicle systems and all major events prior to competition.
- Complete the final vehicle frame by February 23, 2015.
- Achieve a stand-alone frame weight under 6 lbs (not including drivetrain components, wheels, and other add-ons.
- Achieve a vehicle cargo capacity of 10 lbs, and capable of holding an un-deformed full standard grocery bag (1000 in^3)
- Allow for an unassisted vehicle ingress/egress in conjunction with the fairing built by the club team to achieve endurance event pit stop speeds of less than 45 seconds.
- Construct two prototypes before final competition vehicle – a rolling proof of concept, and a full mockup of all major vehicle systems.
- Improve upon Aria’s stiffness under pedaling, steering, braking, and turning loads.
- Create a vehicle that is inherently stable at low speeds and while stopped.
- Integrate the vehicle’s frame with aerodynamic efficiency devices during the preliminary design stages.

The requirements that the team came up with are outlined in Table 1. Since the purpose of this vehicle was to compete in a well-defined competition, many of the requirements were derived from the 2014 ASME HPVC rules. For instance, the competition’s endurance event required

vehicles to negotiate a slalom, multiple tight corners, and a stop sign. There were also several safety requirements, including a rollover protection system test, a braking distance test, and a maximum turning radius. Therefore, the vehicle had to pass these tests as defined in Table 1 with a reasonable margin of safety.

Further requirements were determined from the HPVT's past experience. These included a realistic operating temperature range, adequate rider visibility, rider comfort over rough surfaces, a large span of rider sizes, and a reasonable amount of labor required for production and assembly. In addition, the sprint event had been held on a banked velodrome in 2013 and 2014, so the vehicle had to remain laterally stable on banked straight surfaces.

Finally, some requirements were derived from the desire to maintain Cal Poly's role as a competitive team in every HPVC. For example, the vehicle was desired to be lightweight, have an efficient drivetrain, an aerodynamically efficient shape, remain stable and predictable at both low and high speeds, and be adequately stiff.

As shown in the requirements list (Table 1), some of the parameters had a high risk, or a high expected difficulty for success. Therefore it was necessary to address these requirements with additional care and effort, and so they are discussed here in greater detail than the other requirements.

Table 1. Engineering requirements.

#	Parameter Description	Requirement	Tolerance	Risk	Compliance
1	Weight	55 lb	Max	H	I
2	Track Width	28 in	+/- 0.1 in	L	I
3	Wheelbase	43 in	+/- 0.1 in	L	I
4	Ground Clearance	4 in	+/- 0.1 in	L	I
5	Fwd Dist to Ground Visibility	20 ft	Max	M	I
6	Side Slope to Tip-over	25 deg	Min	L	A,T
7	Front Slope to Tip-over	15 deg	Min	L	A,T
8	Vertical Vehicle Stiffness	2500 lb/in	+/- 200 lb/in	H	A,T
9	Bottom Bracket Lateral Deflection with Maximal Starting Load	0.25 in	Max	H	A,T
10	Drive Wheel Lateral Stiffness, Including Frame Deflection	200 lb/in	+/- 20 lb/in	H	A,T
11	Rollbar Vert. Test SF	1.15	Min	M	A,T
12	Rollbar Horiz. Test SF	1.15	Min	M	A,T
13	Max Rider Height	74 in	Min	M	T
14	Min Rider Height	65 in	Max	M	T
15	Cargo Volume & Shape	8 in x 8 in x 15 in box	Min	M	I
16	Max Cargo Weight	10 lb	Min	M	T
17	Highest Gear	140 gear inches	Min	L	I
18	Lowest Gear	45 gear inches	+/- 5 gear inches	M	I
19	Stopping Distance from 15 mph	15 ft	Max	M	T
20	Speed at 200 W	25 mph	Min	H	A,T
21	Torque at Cranks to Backpedal	3 in-lb	Max	M	T
22	Reflective Surface Area on Vertical Fairing Surfaces	100 in^2	+/- 25 in^2	L	I
23	Forward Lighting System Brightness	1200 lumens	+/- 200 lumens	L	I
24	Front Wheel Change Time	60 s	Max	M	T
25	Rear Wheel Change Time	120 s	Max	H	T
26	Vehicle Production Costs	$6,000	Max	M	I
27	Tire Life	10 hrs	Min	M	I
28	Serviceable Riding Hours	100	Min	M	I
29	Production Man-Hours	2500 hrs	+/- 500 hrs	H	I
30	Assembly Man-Hours	100 hrs	Max	M	I

First, the vehicle's weight would be difficult to minimize while passing all safety requirements and remaining sufficiently stiff. This difficulty stemmed from several sources, including unknown component weights, last minute solutions to small system requirements, and manufacturing difficulties to make some parts lightweight. One major source of un-anticipated weight gain in past years came from the last-minute addition of small systems such as lighting, and so extra efforts were made to account for as many systems as possible when predicting vehicle weight. Another source of excessive weight for Aria was the need to construct certain components, specifically the steering knuckles and the central frame lug, using relatively heavy materials due to manufacturing limitations. To prevent this issue, the team worked early on to complete as much of the design as possible from a comprehensive perspective that included manufacturing and component integration.

While not a necessarily difficult requirement to meet, the forward distance to ground visibility had caused significant conflict and confusion in years past, and its evaluation will be described in detail here. Previously, only direct forward ground visibility had been evaluated, leading to the incorporation of an unnecessary forward camera system in Aria. In reality, the ground could be seen out of Aria's windshield quite close to the vehicle if the rider looked only a few degrees either left or right, and the visibility was not an issue. To take this idea of complete external view area into account, Aria's visibility was "mapped" by sitting a rider in the vehicle while it was stationary in a large flat area, and marking the limit of ground visibility for the full 180° visibility sweep. This technique provided some insight into the real needs for windshield visibility. In Aria's year, a fairing mockup was created from several cross sections cut out of foam in order to evaluate the planned forward visibility (Figure 1). A similar technique was an option this year depending on the fairing decision. In the end, the team sought to at least reproduce, if not improve upon, Aria's external visibility.

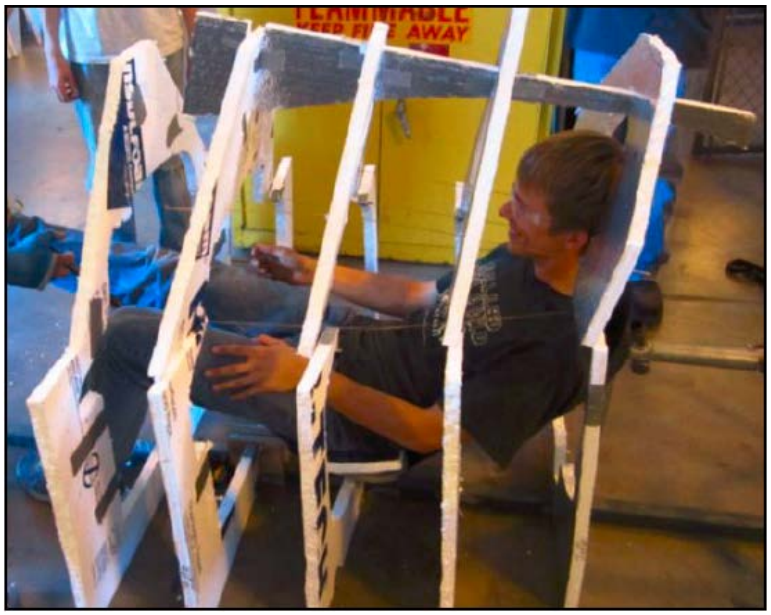

Figure 1. Aria fairing mockup to test rider fit and visibility.

Another difficult specification to meet was the accommodation of a large range of rider sizes. The HPVT has many enthusiastic, strong riders, but to take full advantage of this resource, the vehicle needed to fit individuals from 5’5” to 6’2”. The major obstacles Tri-Fiber expected to encounter when finding a solution to this requirement included fairing clearances, stability changes with a shift in CG location, and the viable execution of adjustable seat-to-pedal distance.

We also expected the inclusion of the required cargo volume to present difficulty. The HPVC rules require adequate cargo volume to hold a full, standard paper grocery bag, though for the past two years, this much volume has not been needed in the competition. In addition, the cargo compartment must support significant weight while the vehicle negotiates sharp speed bumps, all without inhibiting the handling characteristics of the vehicle. Since Cal Poly has historically included less-than-adequate cargo compartments as an afterthought, Tri-Fiber endeavored to provide a more robust cargo solution to meet the HPVC requirement in full.

The final difficult task for this vehicle design was enabling a fast rear wheel change. Typically, faired vehicles must be significantly disassembled in order to access the rear wheel, which could result in large amounts of time lost in the endurance race due to a flat tire. To avoid these issues, the vehicle was designed with the goals of fast and easy disassembly for rear wheel removal, or perhaps no need of disassembly altogether.

Though the list of requirements is long and presented a sizeable challenge, Tri-Fiber felt this project could be successful with a thorough and well planned method of approach.

Chapter 2: Background

Human Powered Vehicles vary widely in design, shape, size, and scope, but the fundamental idea behind each vehicle remains the same: to efficiently apply human power to create a viable form of sustainable transportation. Up until recent centuries, human power has been the main form of local and long distance transportation, and civilizations have adapted to channel human power in the most efficient way. From the first canoe to modern day bicycles and skateboards, human power has been a cheap but relatively inefficient mode of transportation for travel and cargo transportation over long distances. Modern transportation is no longer dominated by human power. According to the U.S. Census Bureau's American Community Survey, only 0.61% of all commutes are done on bicycle [1], the most widely used form of human powered commute transportation. Automobile transportation is by far the dominant choice, making up 87% of all commutes [1]. While bicycles and human powered vehicles have many similarities, HPVs seek to mitigate the disadvantages of bicycle transportation while offering a viable alternative to automobiles for recreation and commuting. Aerodynamic drag most significantly limits the top speed and overall efficiency of conventional bicycles, requiring large human power outputs by riders at moderate road speeds. These shortcomings limit bicycles' practicality as a long distance transportation option. While bicycles are currently the most efficient and most accessible form of human powered transportation, Human Powered Vehicles seek to improve upon their design.

Throughout HPVs' long history, there have been two distinct categories of vehicles being produced and ridden: speedbikes and utility-commuter vehicles. Speedbikes are built solely for the purpose of maximizing the efficiency of human power for speed while limiting comfort or utility considerations. These bikes usually consist of compact, highly aerodynamic shells that house only the rider and frame, often with electronic vision systems rather than windshields to allow for greater aerodynamics. Other common features, including a limited turning radius and streamliner (two wheeled recumbent) configuration, make these vehicles impractical for everyday use. Most recently, the fastest human powered speedbike topped 83.2 mph at the International Human Powered Speed Challenge held in Battle Mountain, Nevada [2]. While speeds of that magnitude are often unobtainable or even impractical in everyday situations, speedbikes serve as the extreme example for what human powered vehicles can achieve.

On the other end of the spectrum, utility commuter human powered vehicles are often less focused on speed and more focused on rider comfort and utility. These HPVs often have a tricycle configuration, allowing for static stability, and feature more robust, spacious fairings designed to allow for comfort, safety, and storage in addition to aerodynamic advantage. These vehicles tend to be relatively large, heavy, and expensive; however they create an alternative to automobile transportation. The ASME Human Powered Vehicle Challenge draws ideas from both categories of HPVs to challenge of engineers to create the most efficient utilitarian vehicle.

Figure 2. Comparison of a Fiester WAW utility HPV[3] (left) and the Delft University speedbike[4] (right).

HPVC Rules and Considerations

Our client, the Cal Poly Human Powered Vehicle Team, requested that the frame of the vehicle be in compliance with the rules of the ASME Human Powered Vehicle Challenge. Therefore, to be competitive, each event at the competition was thoroughly considered and designed for in the final vehicle. The event includes four main events with a sample score breakdown as seen in Appendix A. A summary of the scoring can be seen in Table 2[3] with the objective of each event as stated by ASME below.

Table 2. Breakdown of scoring at HPVC West.

Event	Percentage of Total Score
Design Event	30
Speed Event	25
Innovation Event	20
Endurance Event	25

1. Design Event[3]: "To demonstrate the effective application of established principles and practices of design engineering to the development of the team's vehicle."
2. Speed Event[5]: "To provide teams the opportunity to demonstrate the top speed of their vehicles."
3. Innovation Event[5]:
   "1) To encourage innovation that advances the state of the art in human-powered vehicles.
   2) To provide teams an opportunity to demonstrate significant innovations."
4. Endurance Event[5]: "To provide teams the ability to demonstrate the functionality, agility, and durability of their vehicles."

The two performance driven aspects, the endurance and speed events, are what the team asked Tri-Fiber to cater the characteristics of the vehicle to, and thus they are discussed in further detail below.

The speed event can be one of two formats to be determined by the event coordinators prior to the competition: a head-to-head drag race or flying 200 meter format. Despite being classified under the same category, these formats have quite different design requirements. A flying 200 meter event allows the rider to gradually accelerate to top speed before going through a time "trap," where the average speed over 200 meters is calculated. Therefore, the flying 200 event requires a stable vehicle with a high top speed, where acceleration is not critical. On the other hand, the drag race format favors quick acceleration to nearly top speed. The drag race format favors a stiff and light bike with a lower overall top speed. Additional considerations for the speed event include rider familiarity with the design and a possible velodrome (oval banked track) location. For the 2015 HPVC West, the speed event was to be a flying 200m held in the Hellyer Velodrome, similar to the previous two years. Therefore, the team placed focus on the required vehicle characteristics that are specific to this location – stability on inclined surfaces, a well bolstered seat for rider stability, and adequate time for the riders to familiarize themselves with the vehicle's behavior at high speed.

The endurance event typically takes place on a closed track where obstacles are intermittently placed to challenge the durability and versatility of a vehicle's design. These obstacles include stop signs, cargo pick-ups and drop-offs, quick lane change simulations, hairpin turns, and

slaloms. New additions to the 2015 ASME rules indicated that vehicles would be required to back out of designated spots for grocery pick-up and drop-off. Traditionally, vehicles that are well tested prior to competition, stable at a stop, have quick ingress and egress, and are free of mechanical problems do well in these events. In the past two years, Cal Poly has been plagued with mechanical issues that have caused low placements in endurance events. The club team asked that Tri-Fiber attempt to eliminate mechanical problems prior to the event and focus on designing for fast rider changes, quick acceleration, and static stability.

To satisfy the sponsor's requirements, these two events, speed and endurance, were considered heavily when designing and were used as a mode of analysis to benchmark the performance of the vehicle. A further discussion of the competition format, requirements, and how it would affect the frame design can be found in the subsequent objective section design requirements.

Previous Cal Poly Vehicle Designs and Performance

The Cal Poly Human Powered Vehicle Team has been building competitive vehicles since 1978, and therefore it was our goal to improve upon the previous vehicles. However, because of the shift to an integrated utility and speed class at the HPVC competition in 2012, only the vehicles from the previous three years were thoroughly analyzed.

Gemini (2012)

The year that Gemini was built was the first year the competition integrated its utility and speed classes. This brought new competition requirements of speed bumps, unassisted starts and stops, and an overall emphasis on stability at low speeds.

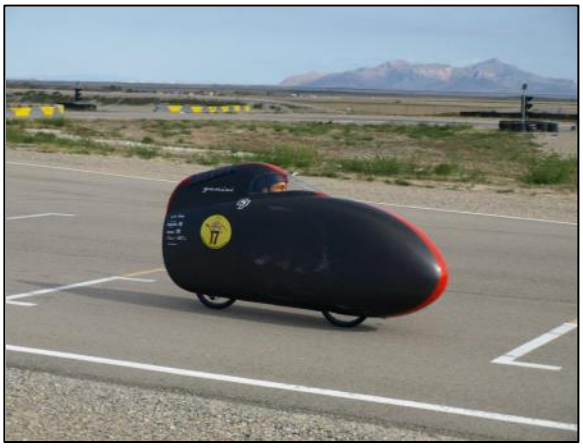

Figure 3. Cal Poly's Gemini in the 2012 Speed Event.

Gemini sought to iterate on the design of Atlas (2008) and improve upon the fully carbon fiber monocoque streamliner frame design. The high vertical stiffness, compact design, and relatively low weight (60 lbf) allowed Gemini to fare well in the speed and endurance events.

While Gemini placed second overall, the flaws of a fully enclosed streamliner in the new competition format were apparent. Inherent static stability was absent, so Gemini relied on a "landing gear" system to provide the stability required to start and stop unassisted. Other

complaints of riders were the high vertical stiffness causing an uncomfortable riding quality and poor cornering stability, and the limited range of rider sizes able to fit in the bike comfortably. None the less, Gemini placed in the top two in each event because of an overall well-designed vehicle. Due to a shift in the competition focus toward more utility oriented vehicles that have stability at low speed, Gemini was the last generation of streamliner that Cal Poly has made.

Figure 4. Gemini's high vertical stiffness caused it to launch off speedbumps and caused an uncomfortable ride quality.

Figure 5. Cal Poly's Black Stallion in the Speed Event (2013).

Black Stallion (2013)

Black Stallion sought to bridge the gap between streamliner and tricycle characteristics by incorporating a leaning mechanism. The leaning mechanism could be unlocked for a tighter turning radius and similar handling to a streamliner, and locked to theoretically maintain the static stability of a rigid trike. Black Stallion also addressed the vertical stiffness and rider sizing complaints from Gemini.

Figure 6. Black Stallion's lean mechanism in action. The nose of the fairing had to be cut off due to a low speed crash from instability at low speeds.

Despite the trike design, however, low speed and static stability were still a problem as the leaning mechanism caused instability if not locked correctly. Black Stallion also suffered aerodynamically after the door had to be removed following a crash-caused hinge failure. Additionally, riders complained of poor drivetrain efficiency due to the chain twist design coupled with a Rohloff internally geared hub. The vehicle's high weight (70 lbf) due to the steel frame and leaning mechanism didn't allow it to reach its full potential in the competition. Even with these flaws, Black Stallion finished in 4th place overall.

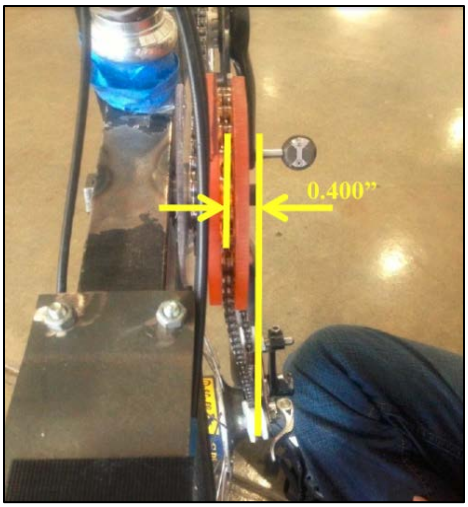

Figure 7.The chain-twist design implemented on Black Stallion. The chain twist caused seizure in the drivetrain, drastically lowering efficiency.

Aria (2014)

Aria sought to improve upon the poor low speed stability that plagued Black Stallion by implementing a rigid tadpole trike configuration and striving to keep the weight as low as possible. To reduce weight, the frame was built in a fully carbon fiber tube-lug configuration that allowed for ease of manufacture and assembly. However, due to a rider striking a pothole with one wheel on the endurance course at high speed, the central lug cracked and a strut arm debonded, debilitating the vehicle for the remainder of the endurance event. While the club achieved both of its goals by building a trike with a weight below 50 pounds, the design was inadequately strong and unstable at high speed. Additionally, riders complained about restricted fit, low torsional stiffness, and a non-bolstered seat that did not allow for a secure riding position. Fairing integration, while adequate, could have been improved by increasing stiffness in both the frame and fairing.

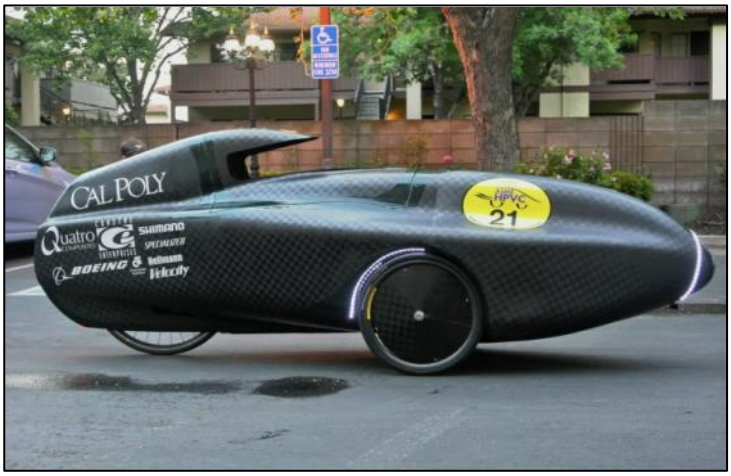

Figure 8. Cal Poly's Aria (2014).

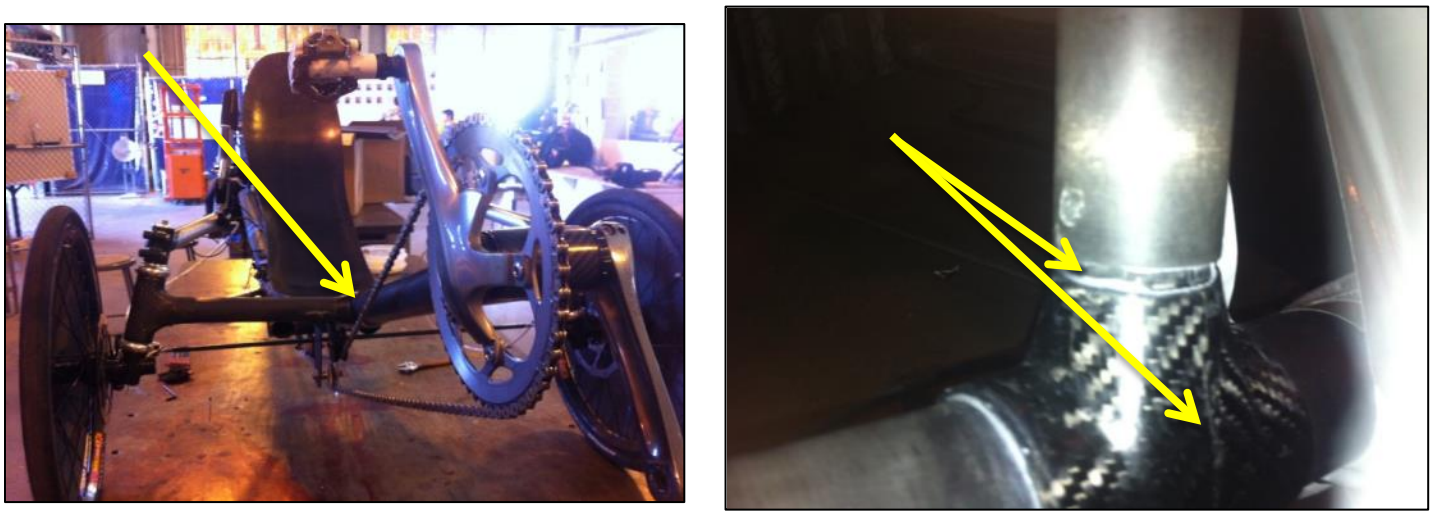

Figure 9. Strut debond and lug cracking that debilitated Aria.

Slight adjustments to geometry and layup schedules used could have yielded a very competitive vehicle. Aria proved the need for extensive testing before competition to allow for iteration and adjustment, especially when using composite materials. Despite these deficiencies, Aria achieved the low speed stability necessitated by the competition and proved that the club could build trikes to a low weight. Aria achieved a top 25% finish by placing 6th overall.

A summary of the issues with the three previous year's bikes can be seen in Table 3. From this table, Tri-Fiber identified a few common trends. First, stiffness is a major concern across the designs. Second, stability, whether at low or high speed, majorly affects the bike's competitive potential. Finally, each design could have benefited from more testing and subsequent iteration. Tri-Fiber sought to learn from these failures, address the corresponding design aspects, and implement testing to produce a competitive vehicle.

Table 3. Previous years' bikes issues.

	Problem	Cause	Effect
Gemini (2012) 2nd	Vertical stiffness	Excessive ply thickness	Uncomfortable ride, large impacts
	Low speed stability	Landing gear mechanism failed	Fell over at stop signs
	Cornering stability	High control sensitivity @ cornering speeds	Sudden roll velocity when entering turn
Black Stallion (2013) 4th	Excessive drivetrain drag	Chain twist coupled with jackshaft bearings	Decreased power output
	Heavy	Steel frame/components and large fairing	Slow acceleration
	Broke door hinge	Fell repeatedly on fairing, cracking the mount	Ran majority of endurance w/o door
Aria (2014) 6th	Low headtube torsional stiffness	Too few ±45° plies in struts	Brake dive, possibly contributed to steering problems
	"Twitchy" steering	Low stiffness?	Difficult to handle at high speeds
	Broke strut lug	Insufficient plies in layup/thin wall	17th place in endurance event
	Fairing vibration at high speeds	Poor fairing integration	Sheared nose mounts necessitating repairs
	Did not fit all riders	Seat bonded in wrong location/fixed	Limited number of available riders, riders not fitted properly
	Excessive Bottom Bracket Deflection	Low Boom Torsional/Bending Stiffness	Reduced acceleration and drive train efficiency
	Difficult ingress/egress w/o assistance	No sufficient support on fairing/frame to lift oneself	Required assistance when exiting the vehicle

Past Competitions Results

Appendix A includes a breakdown of the previous 3+ years of HPV competitions including Cal Poly, overall winners, and individual event winners. The purpose of this resource is to collect relevant data into one spreadsheet to identify trends in recent winners. Tri-Fiber then determined event placement goals in order to achieve first place overall, as summarized in Table 4.

Table 4. Past competition results summary event targets.

Design Event	Innovation Event	W. Speed	M. Speed	Endurance Event
90% Top Score	85% Top Score	Top 15% (26 mph)	Top 15% (29 mph)	Top 20% (14 mph)

Trends identified when analyzing the data included the tendency for the top team to place in the top three in the speed events consistently. This is due a tested and efficient design and strong riders to achieve high speeds. There has been a shift for the overall winning team to not win or place in the top 15% of each category, since more and more teams are very competitive in specific events and not others. With the shift in the competition, designs are often endurance or sprint oriented, whereby winning one inhibits the other. Based on previous competition results, the endurance event is least critical for placement, since design, innovation, and speed events often dictate the overall winners. While all events should be weighted evenly, Tri-Fiber used these results to evaluate prospective designs.

Chapter 3: Design Development

The team was largely satisfied with the decision made in 2014 to switch to a rigid tadpole tricycle layout for the associated benefits in stationary stability, ease of ingress and egress, reliability, and simplicity. This choice was re-evaluated objectively to ensure it was the best choice, as shown in the decision matrix below (Table 5).

Table 5. Vehicle layout decision matrix

Criteria	Factor	**Rigid Trike, Tadpole (Baseline)**	2-wheeled Recumbent	Rigid Trike, Delta	Leaning Delta Trike	Leaning Tadpole Trike	2-Wheel Upright
Low-speed stability	2.86	**D**	-1	0	-1	-1	-1
Cornering Stability	1.90	**D**	-1	-1	0	0	0
High Speed Stability	2.38	**D**	1	1	1	0	0
Weight	0.95	**D**	1	0	-1	-1	1
Complexity	0.00	**D**	1	0	-1	-1	1
Drivetrain Options	1.43	**D**	0	-1	-1	0	1
Aerodynamics	0.48	**D**	1	0	0	0	-1
TOTALS		**D**	-0.95	-0.95	-2.86	-3.81	-0.95

The results suggest that a rigid tadpole trike offers the most desirable characteristics to satisfy the customer requirements. The general consensus of the team following the 2014 competition seemed to be that a few changes to the design of Aria could produce a winning vehicle as the majority of riders were satisfied with the overall “feel” and performance of the vehicle. In past years, the learning curve for riders has been steep due to the fact that most individuals are unfamiliar with the handling characteristics of two wheeled recumbent vehicles. However, the rigid tadpole frame of Aria provided a stable platform that riders were able to jump on and ride the first time. The decision to iterate on the rigid tadpole layout also enables the team to expand upon the successes of Aria and make favorable improvements.

The second criteria held constant during the design process was the use of a fully enclosed fairing. This is partly due to team tradition, but a full fairing also comes with safety and aerodynamic advantages over partial or no fairings.

Time-to-Speed Model

In order to gain a better grasp for which vehicle characteristics were most important to improve over the course of the entire vehicle design, a time-to-speed model was constructed for two race scenarios, the ½ mile sprint race starting from rest, and acceleration from a slow corner in the endurance race. The power profile model for the sprint race was a gradual increase from 150 to 275 W over 1 minute, and the corner acceleration assumed a constant 225W input. These power values were selected to replicate the performance of Aria at the 2014 HPVC. They represent the net applied power, after taking into account drivetrain losses and other inefficiencies.

Both of these models were run for Aria as a baseline (50 lb, CdA = 1.69), and then with hypothetical 20% changes of lower aerodynamic drag, higher power, and lower vehicle weight. As the resulting graphs show (Figure 10 and Figure 11), rider power is the most important area to improve upon, followed by aerodynamics and finally weight. With this in mind, the overall vehicle design focused on improving the ability of riders to produce maximum power through increased vehicle stiffness, improved ergonomics, and higher confidence. The team estimated that design alterations to achieve these goals would increase vehicle weight, increase power, and increase aerodynamic drag. The projected performance of the 2015 vehicle is shown for reference. Results of this study are summarized in Table 6.

Table 6. Time-to-speed model results summary.

Vehicle	Sprint Model Performance		Endurance Model Performance	
	Performance (mph)	Change	Performance (mph)	Change
Aria	28.3 mph		16.5 mph	
20% Less Weight	28.6 mph	+ 1.1%	16.6 mph	+ 0.6%
20% Less Aero Drag	29.6 mph	+ 4.6%	16.6 mph	+ 0.6%
20% More Power	30.2 mph	+ 6.7%	17.1 mph	+ 3.6%
2015 (Projected) 60 lb, CdA = 1.82 ft^2, 20% more power	30.0 mph	+ 6.0%	16.9 mph	+ 2.4%

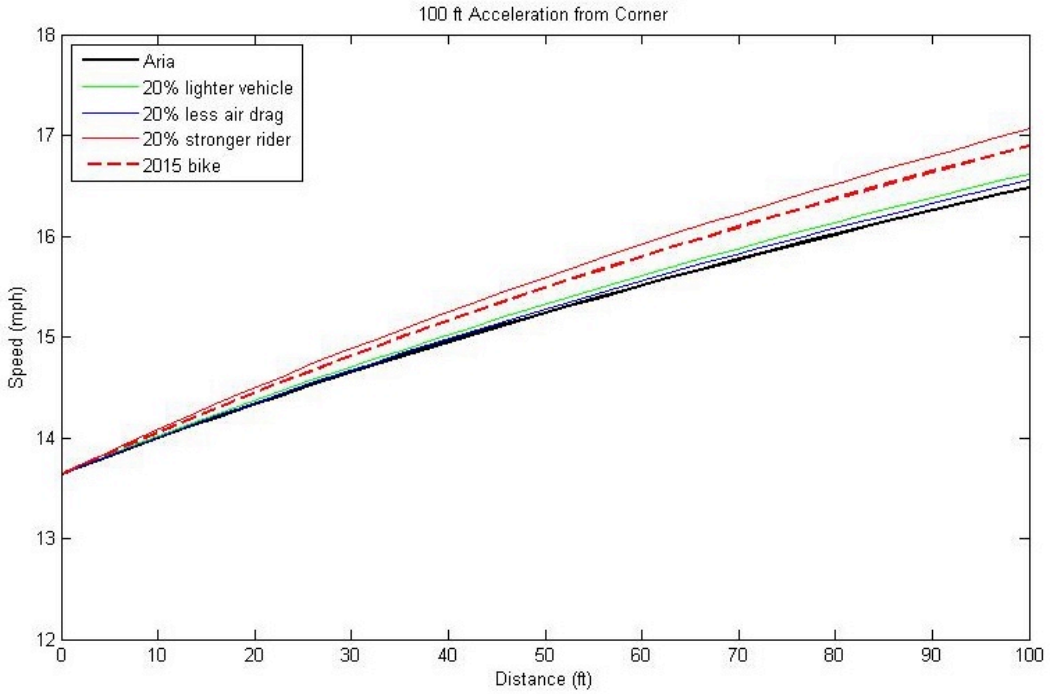

Figure 10. Time-to-speed model for endurance race, accelerating out of a tight corner for 100 ft. Increased rider power is by far the most significant improvement.

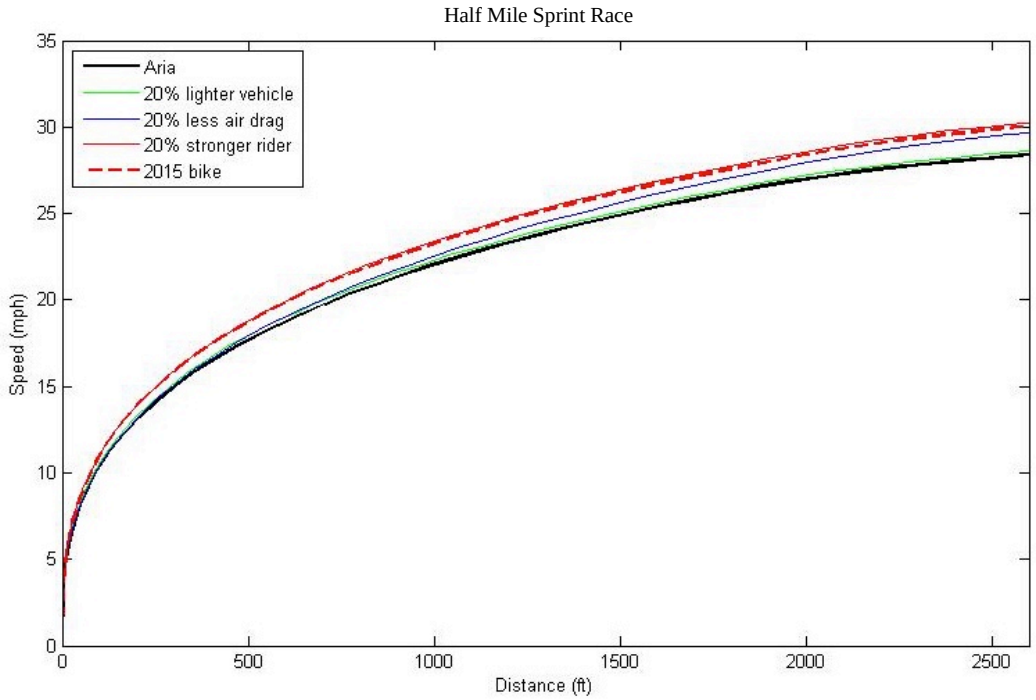

Figure 11. Time-to-speed model for standing start 1/2 mile sprint race. Rider power is again the most significant improvement, followed closely by aerodynamics, especially as speed increases.

Rider Position

As mentioned previously, rider fit has been a significant problem in past years. From the club's experience, fit and ergonomics have large impacts on confidence and power, especially with novice racers. Based on the results of the time-to-speed model discussed previously, it is clear that power is of utmost importance in both the sprint and endurance races. Rider fit was therefore a major point of emphasis for this design project.

Contrary to velomobiles on the market today, which are often designed for one-time adjustment to accommodate a range of *average* rider sizes, the HPV vehicle is built specifically for the ASME competition, which is a race environment. Therefore, it is critical that each of the team's riders can pedal efficiently and achieve their maximum capabilities without any hindrance. The club provided a range of rider sizes from 5' 5" to 6' 2", and accommodating this size range was a primary design requirement. Each rider varied significantly in anthropometric measurements, so it was decided that individual rider measurements were necessary to develop a 2-D model, which would be utilized in the fairing design. Body measurements shown in Figure 12 were measured and tabulated for each rider. Shoulder width and hip width were also included. The complete measurement data are shown in Appendix E. The table shows critical maximum values from the entire data set (highlighted red). These values provided no-go zones for fairing sizing.

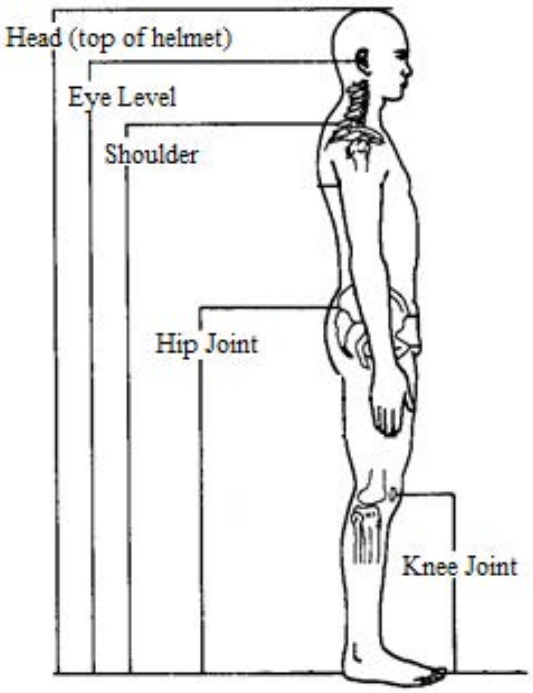

Figure 12. Body measurement parameters. Shoulder and hip width not shown.

One major concern with several previous bikes was compromised rider visibility. This was due to the sight line pointing over the fairing's nose, which enclosed the volume of pedaling feet. In the worst case scenarios, riders couldn't see the ground ahead of the vehicle for upwards of 50 ft. This limited visibility impacted rider safety and confidence when racing in close proximity to hazards, especially other moving vehicles. To improve visibility, the bottom bracket was placed as low as possible (18" off the ground) while still maintaining 4" of clearance under the pedal volume, to maximize the visibility over the pedal volume.

Another rider position parameter that has a large effect on visibility, stability, and power output is the rider's hip angle (Figure 13). Several studies have been completed with the goal of determining the ideal hip angle for a rider in the recumbent position, most notably a Cal Poly senior project from 2008[9] and a Northern Arizona University capstone design project report from 2014[3]. Both of these studies found that an angle of 120° - 125° allowed the largest number of tested individuals to achieve close to their maximum power and efficiency. Therefore this range of hip angles was selected as the target for all riders' positions.

Finally, the rider was placed as low as possible in the fairing, in order to minimize CG height and maximize stability for a given wheel layout.

With these considerations in mind, the 2-D sketches were created from the dimensions of each rider, and each rider's position was adjusted to obtain a forward sight distance of less than 30 ft.

Figure 13. Hip angle is defined as the angle between shoulder, hips, and vehicle bottom bracket.

From these measurements, a 2-D model was created for each rider, as shown in Figure 14, with the wheels appropriately placed. This sketch was coupled with a previously-created pedal volume model, helping to package the front end of the vehicle and ensuring adequate fairing clearance.

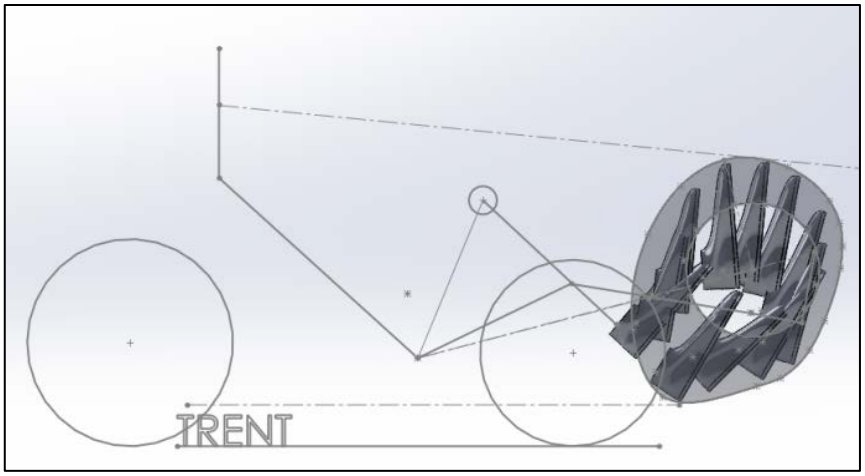

Figure 14. Rider position model created with 2-D SolidWorks sketch.

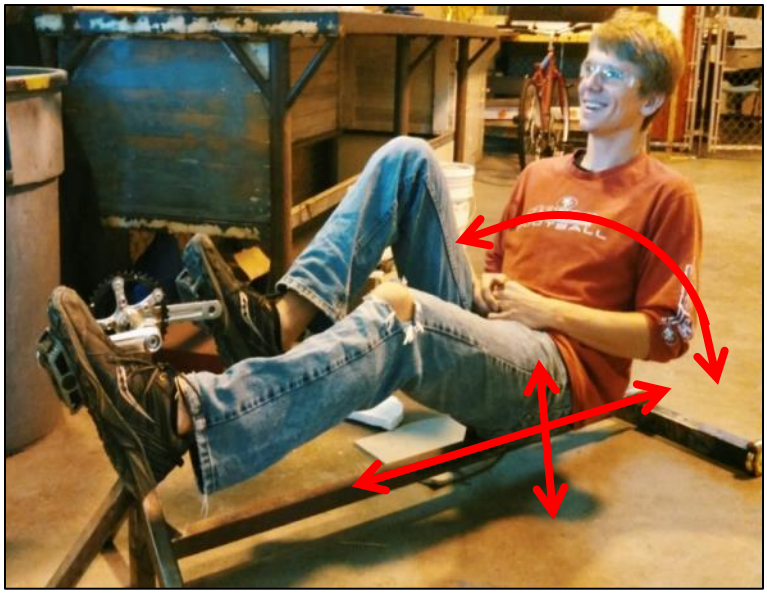

Figure 15. The rider position jig used to verify seat locations for each rider. The bottom bracket location is fixed, and arrows show the available seat adjustments.

Once the model was completed, rider positions and measurements were confirmed by having riders throughout the height range sit in a sizing jig (Figure 15). The seat fore-aft position and back angle were adjustable via pin locations in the seat mount, and rider height was adjusted by placing pads on the seat. For nearly every rider, the seat needed to be placed further forward than in the model, and the height of the riders' heads was consistently lower as compared to the model.

These observations were used to update the 2D rider position models. Additional parameters were then derived from the models, such as CG location, bottom bracket height, and forward sight distance. The CG location was approximated as the rider's navel. This value was used in further stability calculations. The forward sight distance was based on the assumption that the rider cannot see through the pedal volume. In actuality, a significant increase in forward visibility was achieved by lowering the windshield, as discussed further in this report, which enabled looking forward through the pedal volume and over the bottom bracket.

Stability

With the rider position confirmed, the CG location of the vehicle-rider system was determined in order to carry out stability calculations. The CG of each rider was assumed to be at his or her navel. As an initial assumption, the vehicle's CG was chosen to be 1.5" lower than that of Aria (Table 7), and located 33% of the way from front to rear wheels. These assumptions were checked throughout the design process as the locations of significant vehicle parts were finalized.

Table 7. Vehicle CG location summary.

Vehicle	CG Height	% Front	% Rear
Aria	13.6"	72	28
2015 Vehicle	12.0"	67	33

Aria's CG location was calculated using data from a set of lifting tests. Black Stallion's CG location was then estimated based on major differences from the previous year, such as lower rider position and frame placement. Again, these estimations were checked throughout the design process. The locations of the rider and vehicle CG were combined for each rider, and this system of CG location was used for subsequent stability calculations. Each rider-vehicle combination was evaluated to better understand and work around the impacts of different rider sizes. This set of CG locations was used for selecting a wheelbase, track width, and bottom bracket fore/aft position. These dimensions were selected to be as small as possible in order to minimize vehicle footprint, while still meeting certain safety and performance goals for all riders.

The first goal used to determine wheel layout was the safe completion of the ASME-specified stopping distance test, with a safety factor of 1.1 on forward tip of the vehicle (Table 8). The low safety factor is due the rules' allowance of multiple attempts at completing this test, without penalty, and the fact that the braking deceleration in this test is significantly higher than would be usually encountered in everyday vehicle use. The lowest safety factor out of all riders was 1.08, but this was not cause for concern because any rider can complete the braking test, and the largest safety factor was 1.20.

Table 8. Stability goals and performance.

Requirement	Braking Distance	Cornering, 8 m radius
Goal	6.00 m	15.0 mph
Worst Case	5.55 m	15.2 mph
SF	1.08	1.01

Second, the vehicle was required to perform an 8m radius turn at 15 mph, for about 0.57g of turning acceleration, with a safety factor of 1.0 (Table 8). The safety factor on this requirement is 1.0 because of an innovative safety system in the vehicle, designed outside the scope of this senior project, which alerts the rider to dangerously high lateral accelerations.

Table 9. Wheel layout summary.

Track Width	Wheelbase	BB Dist. Ahead of Front Wheels
28"	43"	17.5"

The table of calculations carried out for these analyses can be found in Appendix E.

Steering System

In selecting the steering actuation method for this year's vehicle, the team hoped to remedy the ergonomic and handling shortcomings of Aria through conceptual re-evaluation and steering geometry improvements. Aria's tie rod linkage, however, worked well, and was chosen again over a heavier steering rack to turn the wheels. Geometrical analysis for the steering system may be found in Chapter 4.

Figure 17. Left: Over-seat push/pull (Gemini, 2012). Right: Under-seat rotation (Greenspeed GTS).

Figure 16. Left: Direct knuckle (Catrike Expedition). Right: Over-seat tiller (AVD Windcheetah).

Several common steering systems found in HPVs and other small vehicles (Figure 16 & Figure 17) were evaluated for several characteristics relating to performance, ergonomics, and manufacturability (Table 10).

Table 10. Steering actuation method decision matrix.

Criteria	Factor	Direct Knuckle	**Overseat Wheel/bar**	**Overseat Tiller**	Overseat Push/Pull	**Underseat Rotation**
Highly intuitive steering motion	0.67	D	**1**	**1**	-1	**0**
Easy ingress/egress	0.67	D	**-1**	**-1**	-1	**0**
Simple to manufacture	0.17	D	**-1**	**-1**	-1	**-1**
Lightweight	0.33	D	**-1**	**-1**	-1	**-1**
Fairing space requirements	0.17	D	**1**	**1**	1	**1**
Adequate rider lateral support	1.00	D	**1**	**1**	1	**1**
Adjustable to wide range of rider sizes	1.00	D	**1**	**1**	0	**1**
Easy braking/shifting component integration	0.67	D	**0**	**0**	0	**0**
TOTALS:		D	**1.67**	**1.67**	-0.67	**1.67**

The decision matrix resulted in a three-way tie between a steering wheel, tiller, and under-seat rotation. To try to break the tie, scores were cleared and the weighting factors re-evaluated independently. The weighting factors for this decision matrix adjusted to more accurately reflect the team's thoughts. Unfortunately, a three-way tie between the same systems was still the result, so rider opinions were sought in an attempt to find a better solution. Riders were asked to rank their choices in order, with 2 points awarded for first choice and 1 point awarded for second choice (Table 11). As the table shows, the steering wheel and under-seat rotation concepts remained tied. Ultimately, the steering wheel concept was selected as the least polarizing choice amongst the riders.

Table 11. Rider feedback on steering actuation methods.

Rider	**Steering Wheel**	Over-seat Tiller	**Under-seat Rotation**
Rider 1	**1**	2	**0**
Rider 2	**2**	0	**1**
Rider 3	**1**	0	**2**
Rider 4	**1**	2	**0**
Rider 5	**1**	0	**2**
Rider 6	**1**	0	**2**
TOTALS:	**7**	4	**7**

Steering Analysis

As discussed briefly in Chapter 3, the steering characteristics of Aria were a major area of issues and complaints, and are remedied in part by switching from knuckle-mounted handlebars to the knuckles to a steering wheel. Specifically, Aria had overly twitchy steering, pronounced brake steer characteristics, and insufficient tire life. These issues are summarized in Table 12 below.

Table 12. Steering issues and solutions.

Problem	Cause	Parameter at Fault	Dimension on Aria	Solution	Dimension on 2015 Vehicle
Brake Steer	Kingpin axis intersects ground inside of wheel	Kingpin angle	15°	Increase kingpin angle	17°
Twitchy	Steering ratio too low	Steering ratio	$\frac{1° \; input}{1° \; output}$	Increase steering ratio	$\frac{2.5° - 3.5° \; input}{1° \; output}$
	Insufficient trail	Caster angle	12°	Increase caster angle	14°
High Tire Wear	Improper Ackerman Geometry	Knuckle Tie Rod Mount Angle	10° off from drawing	Improve manufacturing tolerances	± 1° tolerance

Ackerman steering geometry is a method of wheel angle control that ensures all wheels are traveling along curved paths centered at the same point. This method provides maximum traction and eliminates unnecessary tire wear. One key assumption with Ackerman geometries is that all wheels travel in the direction they are pointed. In other words, that there should not be deformation of the tires that would affect wheel trajectory otherwise. However in car racing, for example, the slip angle caused by deformation of the tires under load can greatly influence the effective wheel trajectory. Ackerman steering geometries do not necessarily provide ideal tire friction grip in this case.

From simple calculations with curves found in Zapletal's "Heavenly Angles"[1], this HPV's maximum tire slip angle was estimated at less than 1°, far lower than the 6°-10° slip angle racing cars encounter[1]. This small slip angle implies negligible effects of tire deformation, mostly due to the low normal forces on the tires of lightweight vehicles such as. From this estimation, it was determined that the HPV should utilize a true Ackerman steering geometry.

The final major consideration when designing the steering geometry was the steering ratio, defined as the ratio of steering input angle to wheel turning angle. Since Cal Poly has recently constructed HPVs with handlebar steering, where the steering ratio is fixed at 1:1, the team did not have a good understanding of what steering ratio produces a good compromise between responsiveness, steering weight, and stability. Therefore, the steering geometry to be used on the handling prototype had an adjustable ratio from 2.5:1 to 3.5:1. This range was selected based on the corner radii expected during the endurance event and advice from Cal Poly SAE clubs. Once a final steering ratio was selected, the final vehicle was produced with a single steering ratio.

In order to test the range of steering ratios, a tie rod geometry had to be derived that would work with the selected steering system. Peter Eland's tricycle steering geometry spreadsheets[2] were used to determine a geometry that deviated less than 5% from Ackerman through the minimum turning radius of 6 m, allowed for an adjustable steering ratio without affecting Ackerman geometry, worked with a symmetric tie rod linkage, and did not interfere with the crotch clearance required by the riders with the shortest legs. The final steering geometry is summarized in the tables and figure below, and in-depth calculations may be found in Appendix E.

Table 13. Steering performance summary.

Minimum Turning Radius	6 m
Steering Ratio Options	2.5:1, 3.0:1, 3.5:1
Max. Ackerman Deviation	4.1%
Min. Ackerman Deviation	-2.6%

Table 14. Steering geometry summary.

Kingpin – Kingpin (a)	22.5 in
Steering Arm Lengths (b)	4.0, 4.5, 5.0 in
Steering Arm Angle (c)	70°
Handlebar Pivot Offest (d)	2.5 in
Handlebar Arm Length (f)	1.5 in

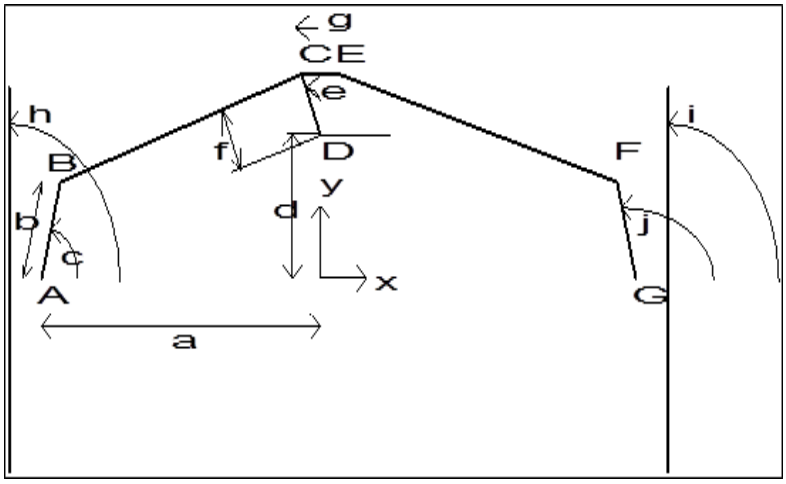

Figure 18. Steering linkage geometry parameters as defined in Eland's spreadsheets [2].

Component Selection

Wheel sizes were selected for a balance of lateral stiffness, weight, tire availability, fairing integration, and drivetrain ratio. Decision matrices were used for both front and rear wheels to evaluate these criteria, resulting in 18" front wheels and a 20" rear wheel. The front wheel matrix

resulted in a tie, after which 18” wheels were chosen because the team already had several 18” front wheels. The 20” rear wheel will allow a significantly stiffer rear end when compared to Aria’s 700c rear wheel, but comes at a cost of a smaller drivetrain ratio. This issue was solved with a mid-drivetrain step up, discussed later in the Development section of this report.

Table 15. Front wheel size decision matrix.

Criteria	Weight	**18"**	20"	16"
Stiffness	2	**D**	-1	1
Weight	2	**D**	-1	1
Packaging	0	**D**	-1	1
Tire Availability	2	**D**	1	-2
TOTALS		**0**	-2	0

Table 16. Rear wheel size decision matrix.

Criteria	Weight	700c	26"	**20"**
Stiffness	3	D	0	**1**
Weight	3	D	0	**1**
Packaging	2	D	0	**0**
Tire Availability	2	D	-1	**-1**
Drivetrain Ratio	0	D	0	**-1**
TOTALS		0	-2	**4**

Frame Layout

Once the frame configuration was selected, the team researched various methods of construction for the vehicle. From research, it was found that the traditional methods of construction included a standalone frame integrated with a shell fairing (such as Aria, Gemini, and Black Stallion), a completely monocoque “tub”-style vehicle (Figure 19), or a vehicle that integrated the two – a monocoque tub with a sub-frame for component mounting (Figure 19).

Figure 19. Left: The University of Toronto Full monocoque tub bike[07] with their bonded in frame members. Right: The Cygnus WHPSC Bike[07] with its sub-frame monocoque assembly.

Full monocoque vehicles are traditionally a tub style configuration where the aerodynamic fairing is the structural component. The rider sits directly on the tub floor and all drivetrain, steering, and other sub-system components are bonded or bolted to the structural tub. This allows very high spatial efficiency to be achieved, with all the space in the fairing available for mounting or use. Additionally, the large vehicle geometry can be used to tune stiffness in both

the torsional and vertical directions. The drawbacks to this method include the unfamiliarity of the team in construction methods and analysis, and the more permanent nature of the components in the bike, stinting the ease of maintenance.

Stand-alone frames are advantageous in that they can be constructed, maintained, and analyzed separate from the fairing. Downsides include that the configuration requires flawless integration between the fairing and the frame which the team has been unable to achieve in the previous three years. Additionally, it limits the amount of usable space inside the fairing for sub-frame components, and it lacks the large cross-section for use in stiffness considerations. The sub-frame configuration brings together the ease of maintenance of a stand-alone frame with its removable components, while still retaining all of the advantages of the full-monocoque configuration.

The Cal Poly Human Powered Vehicle Team has traditionally constructed stand-alone frames with a shell fairing. The only recent deviation from this trend was the 2009 vehicle, Atlas, which won the ASME Speed-Class competition that year. Similar success has been seen by two teams who have consistently put out winning vehicles in the monocoque-tub configuration: University of Toronto and Rose-Hulman University. Similarly, stand-alone frames with shell fairings have been successful, with the second and third place teams in 2014 fielding a stand-alone frame. At the World Human Powered Speed Challenge (WHPSC) 2014, an event where enthusiasts try to break the Human Powered Speed Record in HPVs, the preferred method for construction were full-monocoque or sub-frame style configurations; however, the trike that broke the trike speed record, Trisled's "All Over-Zealous," was constructed in a stand-alone frame configuration (Figure 20).

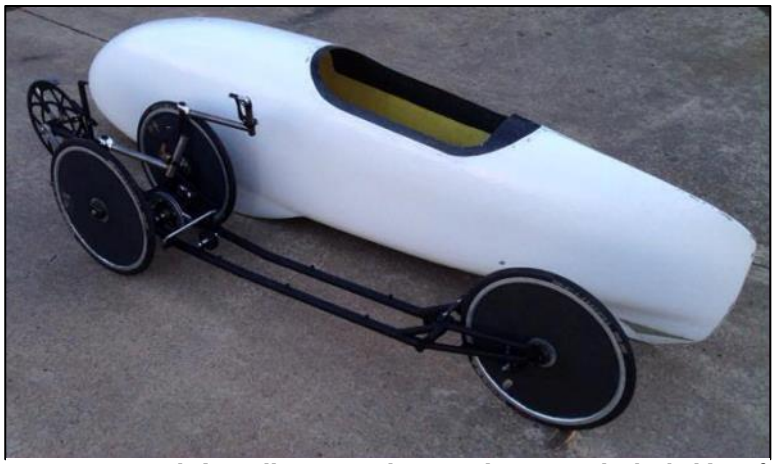

Figure 20. Trisled's "All-Over Zealous" Trike, currently the holder of the trike speed record of 74 mph [08]. It was built in a separable frame-fairing configuration.

Because the trade studies on configurations of previous winners of the ASME Event and the WHPSC vehicles was inconclusive, Tri-Fiber derived criteria to evaluate the three construction methods. The resulting decision matrix can be seen in Table 17.

The criteria chosen was assigned a factor based on importance to the design. Aria, a stand-alone frame, was used as a datum to which the full monocoque and sub-frame configurations could be evaluated. The overall winner was the sub-frame monocoque configuration.

Table 17. Frame layout decision matrix. A sub-frame was selected as the best option.

Criteria	Factor	Stand-Alone Frame	Full Monocoque	**Sub-Frame**
Ease of Manufacturability	1.78	D	-1	**-1**
Ease of Achieving Torsional Stiffness	1.33	D	1	**1**
Ease of Maintenance	1.56	D	-1	**0**
Ease of Analysis	0.22	D	-1	**-1**
High Spatial Efficiency	0.67	D	1	**1**
Layout Simplicity	0.67	D	1	**1**
Ease of Rollbar Integration	0.67	D	1	**1**
High Rider Position Adjustability	2.00	D	0	**0**
Ease of Achieving Vertical Stiffness	1.11	D	0	**0**
TOTALS		0	-0.22	**1.33**

Vision System

Achieving adequate visibility for each rider operating the vehicle was of utmost importance to the HPV team. While the ASME Competition Rules only state that riders must have 180 degree lateral visibility, the team set additional requirements based on rider input and empirical calculations.

Design History

Shown in Table 17 is a comparison of the visibility of the previous two years' bikes, Black Stallion and Aria. Black Stallion had the common complaint from riders that forward visibility was severely limited. This was due to the incorrect mounting of the fairing to the frame causing the nose of the bike to be 2 degrees higher than the design intent. Aria improved upon the

visibility of Black Stallion for most riders, however the shorter riders had slightly more limited forward vision. To give the rider a full view in front of him or her during slow-speed or precise maneuvers, a forward-facing wide angle camera was added under the nose of the bike. As seen in Figure 21, this gave the rider a full view of his or her forward surroundings; however, riders commented that they rarely if ever used the forward view camera when operating the vehicle due to unnecessary extra vision and inconvenience of taking their eyes off the road.

Table 18. Forward sight distance comparison of Cal Poly HPVs. Black Stallion's fairing was mounted incorrectly and severely limited the rider's forward vision.

Vehicle	Minimum Forward Sight Distance (ft)
Aria (sight only)	29.2
Aria (with camera)	1.0
Black Stallion	50.3
Gemini	33.3

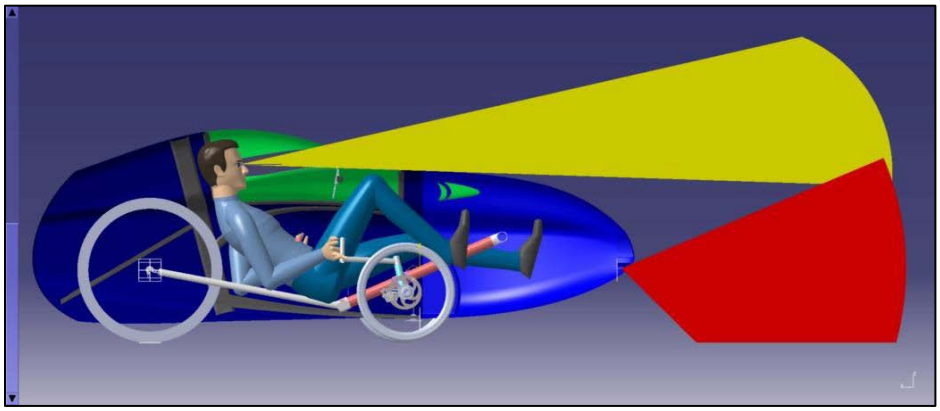

Figure 21. Forward visibility area plot for Aria with the windshield in yellow and camera in red.

Vision Requirements

Ideally, the rider would have unobstructed 360 degree lateral vision and forward vision beginning at the vehicle's nose. However due to the use of a fairing and the rider's position in the vehicle, this is impossible to implement. Therefore, to compromise, a baseline vision level must be set that allows riders to be confident and aware of the surroundings while riding. In his book *Cyclecraft,* John Franklin outlines a minimum reaction distance of 6 meters at 15 mph and 10 meters at 25 mph[4]. Riders in Sweet Phoenix can always see above the horizon, so the rider's sight distance is always greater than the required reaction distance. In 2014, riders found Aria's 31-foot vision to be adequate for safely operating the vehicle among the endurance race's well-marked obstacles. Because of these two considerations, a minimum forward sight distance of 30 ft. was chosen.

System Choice

Three options arose as choices of vision system. The first option was a clear plastic windshield. Historically, the team has chosen this method and placed a small windshield the front of a head bubble. This design requires a relatively upright rider position to see over the fairing's nose, which increases vehicle height. The next option was a windshield and camera hybrid system as implemented in Aria. While camera augmentation allows for a less upright rider position, the camera's utility is questionable. Riders noted the difficulties of switching focus between a windshield and a camera while moving. Thus the reality of this system is a windshield with inadequate visibility and an unused camera. The final option eliminates the windshield entirely and creates a "camera bike" where the rider sees only through video cameras. Record breaking speed bikes at the WHPSC often use camera systems, since riders can be laid flatter once the rider position and forward sight distance are de-coupled. To reduce the possibility of system failure, two independently wired camera circuits (Figure 22) are commonly used. According to Gareth Hanks, who set the trike land speed record in a camera-only vehicle, finding the right camera and display to mimic direct vision was challenging, and riding through a camera never felt "right." A camera system may hinder the overall performance of the bike through reduced rider comfort and increased weight.

Figure 22. Trisled's All-Overzealous camera configuration. The sting at the top holds two cameras wired independently to the redundant monitors below.

Through criteria generation and evaluation of each option, a windshield-only configuration was chosen for Black Stallion. Table 19 shows the decision matrix that led to this choice.

Table 19. Decision matrix for deciding on the vision system for the vehicle.

Criteria	Factor	**Windshield Only**	Camera Only	Camera + Windshield
Aerodynamics	1.00	**D**	1	1
Simplicity	1.00	**D**	-1	-1
Cost	1.00	**D**	-1	-1
View range	2.00	**D**	-1	1
Reliability	3.00	**D**	-1	0
Rider comfort	2.00	**D**	-1	-1
TOTALS		**0**	-8	-1

Fairing Concepts

Fairing concepts were developed based on rider position. Two dimensional models of each rider provided a sizing tool from which fairing shapes were designed. Due to the team's lack of experience in fairing design as well as aerodynamic analysis of streamlined bodies, it was decided to develop initial concepts that were comparable in size and shape to Aria with smooth contours and a tapered closeout to try and minimize boundary layer separation. These concept designs are shown in Figure 23.

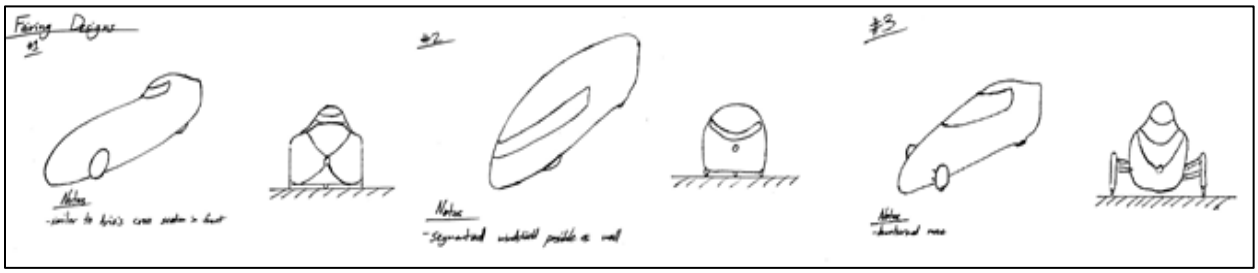

Figure 23. Initial fairing concepts.

Concept #1 was similar in size and shape to Aria with the characteristic head bubble that has become common on Cal Poly's bikes in recent years. One downside to including a head bubble is the issue of rider fit and visibility. As was the case with Aria, the shoulder curve that follows the rider profile was too low at the top of the shoulder, resulting in the larger riders contacting the door seam when riding. The head bubble also limited rider visibility as the forward vision was limited by the fairing height above the knees. Concept #2 was a simpler design than the previous with a gradual taper to the rear of the vehicle and a wrap-around front windshield, which could also be partitioned. The front wheels are enclosed but the design could be modified to have wheel cutouts. Concept #3 was essentially a hybrid of the first two designs with a tapered front windshield from the top of the pedal volume back to the top of the rider's head. This design had the front wheels completely removed from the fairing, which could be altered as well.

Windshield Considerations

The windshield design was an important consideration in the fairing shape. Basic vision requirements consisted of a 180° lateral field of vision (per ASME rules) and adequate forward visibility as defined in the Vision System section.

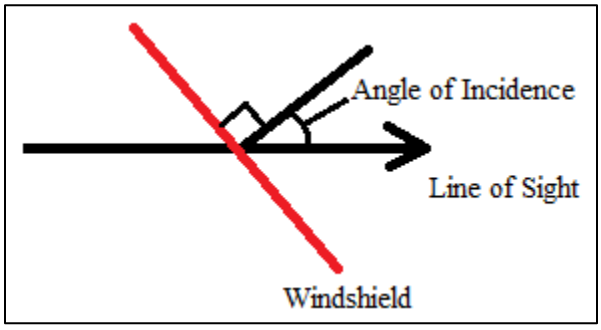

Figure 24. Definition of angle of incidence

Two parameters that weigh heavily in the windshield design are the angle of incidence and radius of curvature. The angle of incidence is defined in Figure 24. A study on the effects of windshield geometry on aircraft pilot visual performance[5] was used to establish bounds for these two parameters. The study defined certain optical characteristics present in windshields and their effects on vision. One such effect is distortion, which results from minor variations in windshield thickness. Figure 25 shows the impact angle of incidence has on the deviation and distortion. Both curves begin to increase drastically around 60°, suggesting the upper limit for the angle of incidence should be close to this value.

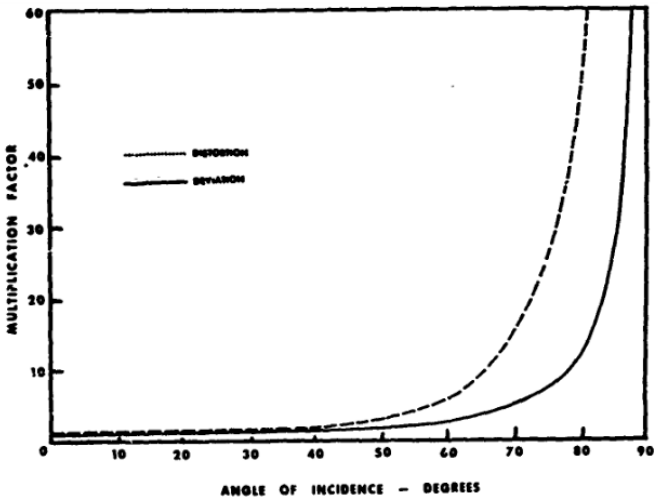

Figure 25. Effect of angle of incidence on distortion (dashed) and deviation (solid).

In addition, the study cited certain military requirements at the time for the design of aircraft windshields. Multiple sources stated that the angle of incidence should not exceed 60° in an attempt to avoid impaired vision. No such requirements were established for radius of curvature. However, the study recommended that large angles of incidence coupled with a small radius of curvature (<10") be avoided as this can greatly amplify angular deviations. Compound curvatures should also be avoided. With these factors in mind, the fairing shapes were further refined to avoid undesirable optical effects in the windshield shape.

Concept Selection

Based on previous years' issues with head bubbles, concept #1 was discarded in favor of larger wrap-around windshields. The larger fairing volume around the rider ensured there would be adequate clearance around the rider's head and shoulders to allow for small movements while seated. This is advantageous as riders must be able to turn their heads to meet the lateral visibility requirement. Solid models were then created for both concepts (2 and 3) to further develop the shapes and identify any issues with the designs.

As both designs provided ample room for rider adjustment, the windshield was the deciding factor in the design decision. Figure 26 shows the angles of incidence for each model relative to the rider's presumed line of sight when riding. Concept #2 is slightly above the maximum 60° angle of incidence recommendation as put forth in the windshield study whereas concept #3 is significantly larger (~73°) which could produce negative optical effects that would compromise the rider's ability to react quickly in a race environment.

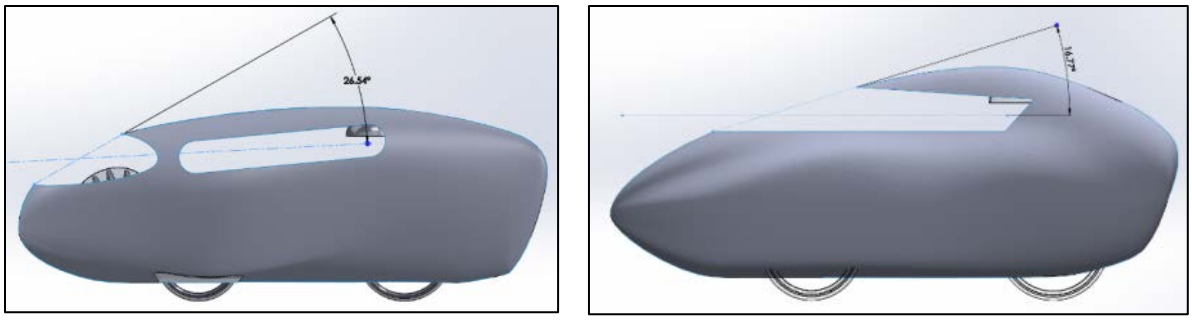

Figure 26. Left: Concept #2 iteration with 63 degree angle of incidence and 16 ft. forward visibility. Right: Concept #3 iteration with 73 degree angle of incidence and 40 ft. forward visibility.

As it was decided to avoid the use of an auxiliary camera, the forward distance to ground visibility was driven purely by rider line of sight. This distance for concept #2 was considerably smaller in comparison since the front windshield enabled the rider to see through their feet just above the bottom bracket. In addition, the windshield of concept #3 contained compound curvature and pulling the bottom line of the windshield any lower would only increase the area of complex curves. Consequently, concept #2 was chosen in favor of the increased rider visibility.

Design Development

Two iterations, shown in Figure 27, were then developed from the selected concept – one fairing enclosed the front wheels, and the other left them exposed. The aerodynamic performance of these concepts relative to one another is not immediately clear. The enclosed wheel version is approximately 5" wider at the front wheels to accommodate wheel rotation. However, the exposed wheels of the other version could significantly increase air turbulence on the sides of the fairing. To identify a final model design, analysis of the aerodynamic drag of the two vehicles was performed. An empirical approach to the analysis was taken as the team lacked knowledge and experience in the analysis of complex streamlined bodies using analytical tools such as computational fluid dynamics (CFD).

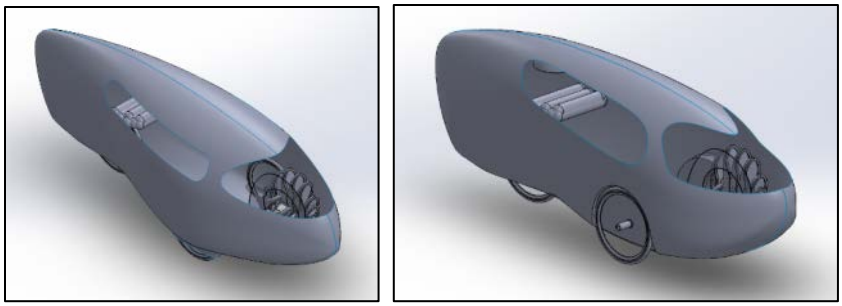

Figure 27. Iterations with front wheels enclosed (left) and with wheel cutouts (right).

Wind Tunnel Testing

Testing of fairing models in the Cal Poly Mechanical Engineering wind tunnel was chosen as the most feasible option for determining the differences in drag force between the two models. The first step in this process required the calculation of the appropriate model scale in order to prevent excessive blockage in the test section and ensure the wind tunnel could reach a high enough velocity. Cal Poly professor Dr. Russ Westphal, who provided assistance with the initial testing plan, recommended that the frontal area of the models not exceed 10% of the overall test section area (2 ft. x 2 ft.) to avoid excessive blockage. This can negatively influence the test results as the boundary layer at the test section walls can interfere with the flow around the body if the model is too large. A 1/6th scale model was chosen for the tests as it resulted in 5% blockage for the enclosed wheel model and 4% for the wheel cutout model, considerably less than the recommended 10%. This scale also enabled the team to use existing 20 lbf/ft^3 HDU foam that was available to the club for the machining of the two models. The goal with model testing is to match the Reynolds number (a dimensionless quantity) from the full-scale to the model scale. The Reynolds number is defined as:

$$Re = \frac{\rho_{air} U L}{\mu_{air}}$$

where L is a characteristic length and U is the air velocity. The desired 1/6th scale model would require an air velocity six times that experienced by the full-size vehicle. The Cal Poly ME wind tunnel has a published maximum air speed of 110 mph at 60 Hz (fan speed), which translates to a full-scale velocity of 18.3 mph. Although this velocity was significantly less than our maximum expected vehicle speed, it was deemed sufficient for a comparative study of the two models.

Manufacturing

The fairing shapes were partitioned down the centerline and scaled to the appropriate sizes, with each half as a separate part to simplify the machining operation. CAMWorks was utilized for developing tooling paths, and the models were cut from HDU foam using the Haas VF3 CNC vertical mill in the Cal Poly Mustang ’60 machine shop. The foam halves still had visible tooling paths following the machining process (Figure 28), which were removed out with 220 grit sandpaper. To complete the models, the halves were bonded together with epoxy and discontinuities filled with Bondo or sanded down. A thin coat of Duratec mold sealer was then applied to the models to seal any porous regions (Figure 29). The final additions to the models included acrylic wheels and threaded aluminum inserts, which were bonded into cavities on the bottom of each model in order to mount the sting assembly. These inserts sat flush with the fairing surface, in order to maintain the fairing contour for display purposes.

Figure 29. Newly machined model halves.

Figure 28. Models following Bondo and sanding.

The Cal Poly ME wind tunnel included an optional sting mount for mounting the model. However, it was too long and would have placed the models well above the wind tunnel’s centerline unless a large slot was machined in the base of each model for embedding the sting. This approach was avoided, as the complex model shapes would make machining difficult and any machining on the models could damage the foam. Instead, a shorter aluminum sting was machined to center the model within the tunnel and match the bolt pattern of the wind tunnel’s dynamometer. Slotted blocks with mating threaded inserts were machined to bolt the model to the top of the sting.

Testing Setup/Procedure

To complete the setup, a false floor was included as a means of modeling the ground effects that are present when riding the full-size vehicle. George Leone loaned the team his existing false floor, which had been constructed for similar testing of his bike in the same wind tunnel. The floor was mounted on wooden dowels and rested just below the models’ wheels to prevent

contact with the model. A clearance hole already existed in the false floor to accommodate the sting and the floor's leading edge was cut with a beveled edge (facing down) to split air flow around the floor.

The dynamometer is a measurement tool to which the sting mounts in order to measure aerodynamic drag and lift on the test object. The loads experienced by the model during testing are transferred through the sting to two flexion beams. The corresponding displacement is proportional to the applied force on the sting. This deflection is measured with a Linear Voltage Displacement Transducer (LVDT) and an output voltage is transmitted to the readout assembly. As this value is a voltage, calibration was required in order to calculate the drag or lift force in the desired units. This procedure was laid out in detail in the wind tunnel manual and was performed prior to testing. A provided mounting fixture was implemented to fix the dynamometer with the sting oriented horizontally (drag component) as shown in Figure 30. A series of known weights were loaded on the end of the sting and the corresponding voltage recorded. The LVDT and dynamometer span were adjusted to a fixed datum value. From this data, a calibration equation that related force to voltage output was obtained.

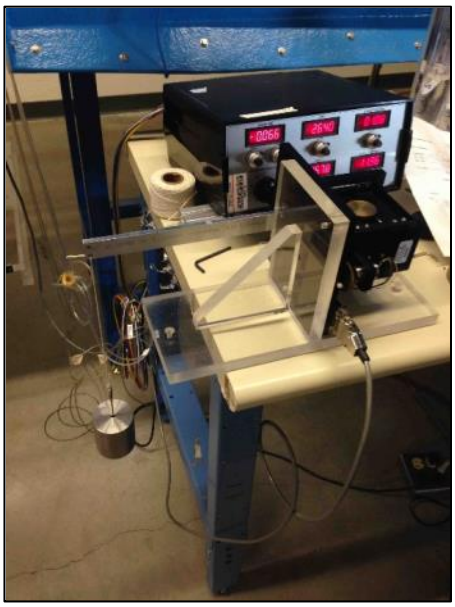

Figure 30. Calibration setup for drag component.

Due to the fact that a custom sting was used, the existing shroud was unusable. The purpose of this device is to surround the sting and place it in quiescent air so that the added drag from the sting does not adversely impact the data. However, rather than manufacture a new shroud, the decision was made to perform a sample run at maximum velocity (60 Hz) with only the sting mounted (no model) to establish a baseline drag force, which was then tared from the model data. The final test setup is shown in Figure 31 with the model mounted and the false floor in place.

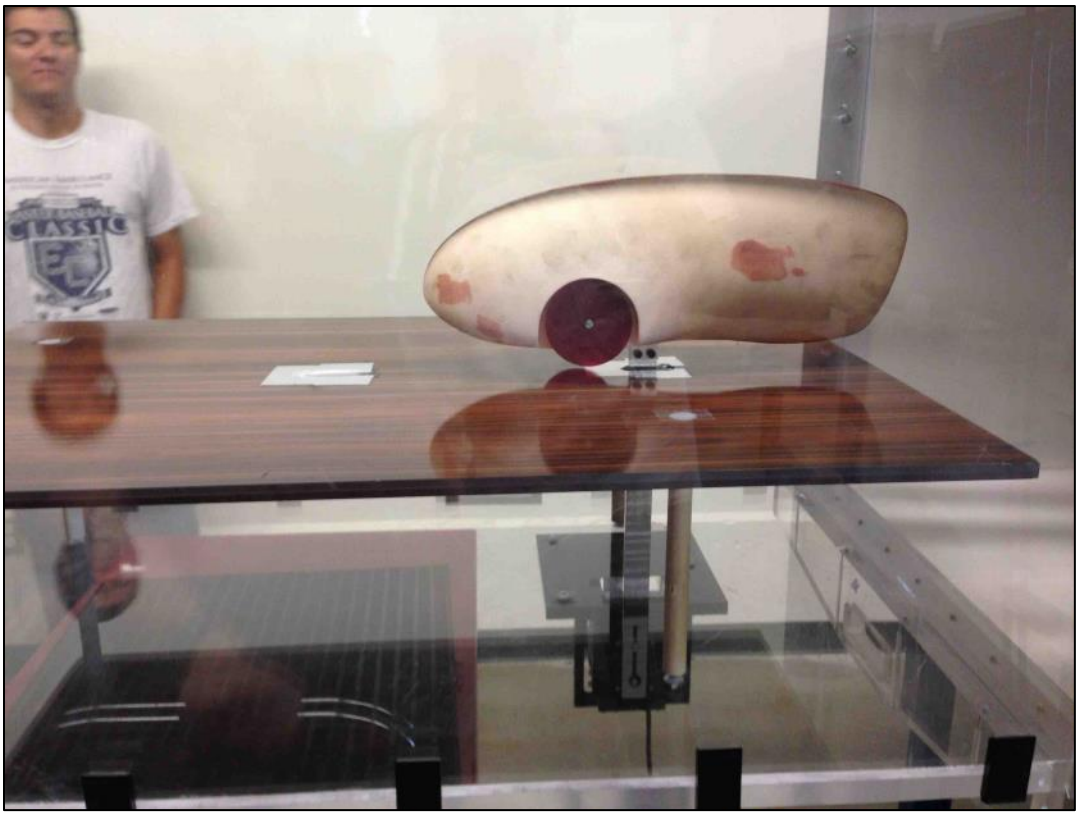

Figure 31. Final wind tunnel test setup.

Because the maximum possible velocity was desired due to the 1/6th scaling factor, all trials were run at 60 Hz fan speed. A Pitot-static tube was placed at the inlet of the test section to measure pressure differential, which was used to calculate the true velocity, as it never actually reached the published value of 110 mph. Drag and pressure values were measured and recorded for ten trials for each model. The raw data is included in Appendix E along with the calculations for the drag and velocity at full-scale. A tabulated summary of the calculated full-scale results is shown below in Table 20.

Table 20. Wind tunnel testing results summary. Values represent full-scale vehicle.

Model	Drag (lbf)	Velocity (mph)	Cd	Required Power (W)
Wheels Enclosed	1.22	17.26	0.23	42.11
Wheel Cutouts	1.26	17.24	0.28	43.47

When analyzing the data, it was necessary to keep in mind the fact that the test was purely comparative and was by no means a method for calculating the *absolute* drag force value present on the full-scale vehicle. Numerous parameters in the test were ignored (i.e. surface finish, blockage correction) since the only critical aspect was ensuring consistent test conditions between the two models.

The data indicated that there was a slight advantage in terms of drag force (~3% decrease) for the wheels enclosed model. This demonstrated that although the frontal area of the wheel cutout model was approximately 15% smaller than the wheels enclosed model, the discontinuity that exists at the wheel wells results in excessive turbulence, contributing a significant amount to the overall drag on the vehicle. Although a 3% decrease in drag is relatively insignificant, it was enough to justify a decision between the two designs as any decrease is to the advantage of the riders. Thus, the wheels enclosed model was chosen for the final design of the vehicle.

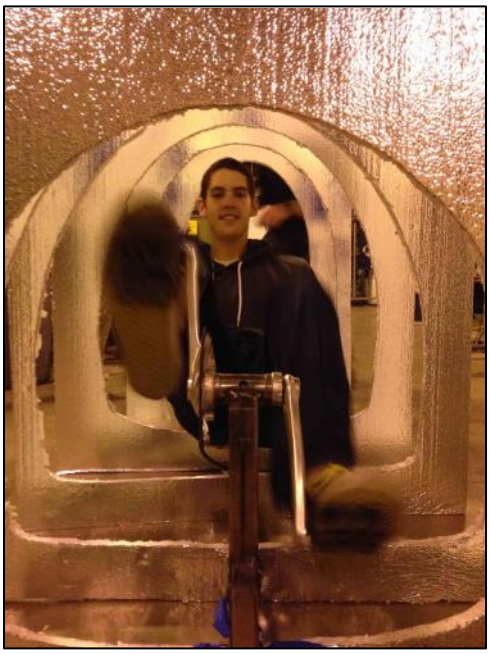

Figure 32. Rider fit test with the largest rider.

Rider Size Verification

As further validation that all riders would fit comfortably in the fairing shape, full-scale cross-section profiles at uniform increments along the length of the fairing were printed and cut out of board insulation. These cutouts were used in conjunction with the rider position trainer to obtain a full-scale model of the outer fairing skin that riders could pedal in and verify fit. A test with the team's tallest rider is shown in Figure 32. Following testing, it was decided to reduce the fairing height by an inch to approximately 38.5" (relative to ground) and raise the bottom bracket to 18" above the ground. These changes maintained adequate clearance for both rider's helmet and heel at the bottom of the pedal stroke.

Stiffness Testing

One requirement set that required further clarification through testing was the target frame stiffness. As discussed in the Background section, Gemini was too stiff vertically, and Aria suffered from excessive deflection in nearly every loading case. In order to design the vehicle to be adequately stiff for handling purposes and yet not too stiff to be uncomfortable, static deflection tests were performed on the frames of Gemini, Black Stallion, and Aria. These tests helped the team determine ideal stiffness values by correlating quantitative stiffness values with qualitative rider feedback about their perceived comfort on each frame. Both vertical and torsional stiffness tests were performed to obtain a more complete overall vehicle target stiffness.

Dr. Joe Mello granted the team access to the composites lab where the T-slot strong floor was used to provide stiff mounting locations for each of the frames. The first test involved vertical deflection measurements on each of the three frames. This required the frames be rigidly fixed at one end with a roller support mounted at the opposite end to realistically model the deflection of the frame in a riding situation. In order to properly mount the frames, custom dropout inserts were machined as seen in Figure 33. Radial ball bearings were press-fit onto the axles to allow for horizontal translation of the frames under a vertical load. In addition to these inserts, mock hubs and mounting brackets were fabricated for each frame as shown in Figure 33 below.

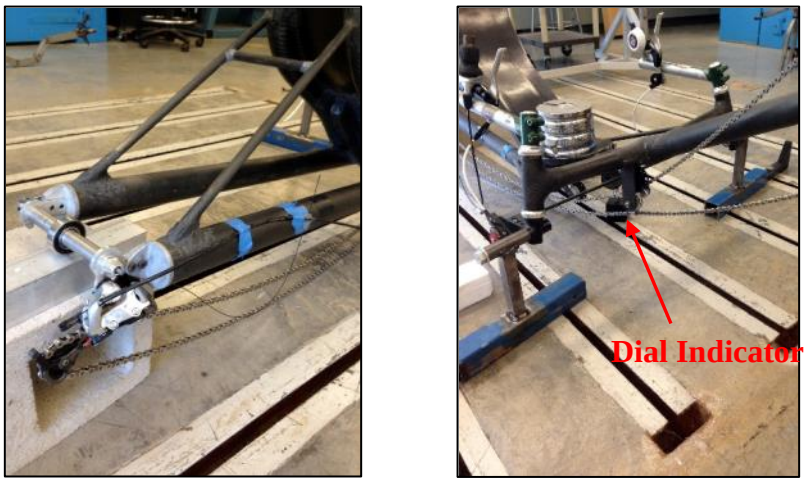

Figure 33. Machined dropout inserts with press-fit radial ball bearings (left) and welded box steel "fake hubs" for mounting Aria to the strong floor (right). The right image also displays the test setup with weights and dial indicator.

Once each frame was securely mounted, weights ranging from 10-50 lbf were applied at the seat and the vertical deflection at the seat was measured with a dial indicator as shown in Figure 33. Following the placement of weights, Peter (143 lbf) and Trent (165 lbf) stood on the seat to obtain additional data points to check the linear elastic response of each frame. Load and deflection data was tabulated and an effective vertical frame stiffness number was obtained for each frame as seen in Table 21 below. The test data can be seen in Appendix E.

The second test performed was a torsional loading of Aria's frame. Neither Gemini nor Black Stallion were subjected to torsional testing as their designs were too dissimilar to this year's, whereas Aria had essentially the same layout. Aria was of particular interest since the rear end exhibited excessive deflection when cornering, which resulted in the need to enlarge the wheel cutout at the 2014 competition to eliminate tire abrasion on the fairing. The torsional test was

performed with the same mounting hardware as used in the vertical stiffness tests (Figure 34). A C-clamp was fixed to the rear axle mount with a dial indicator oriented to measure transverse displacement of the resulting moment arm. The club's digital force gauge (spring scale) was used to apply incremental loads along the same line of action as the dial indicator and the corresponding deflections were measured. The moment arm was measured in order to calculate the resultant angular displacement. The test was not ideal as the C-clamp contributed to the overall lateral deflection. Therefore, the C-clamp's stiffness was evaluated separately and later tared from the calculated frame torsional stiffness. Table 21 shows the torsional stiffness data and Appendix E contains the test data.

Figure 34. Torsional testing setup with applied force location.

Table 21. Vertical and torsional stiffness test data from the three vehicles along with corresponding rider perception.

Vehicle	Vertical Stiffness (lbf/in)	Rider Perception	Torsional Stiffness (in-lbf/deg)
Aria	2520	Good	91.5
Black Stallion	2250	Ok / Low	--
Gemini (low weight)	2960	High	--
Gemini (high weight)	4520	High	--
2015 TARGETS	2500	--	150

Table 21 provides a summary of the results along with the qualitative observations from past riders. The data provided target stiffness values that were later used for refinement of the layup schedule and core thickness of the monocoque tub. The testing of Gemini's frame returned some interesting results as shown in the table. When the 10 to 50 pound weights were applied, the calculated stiffness was roughly 17% greater than that of Aria. However, when Peter and Trent stood on the frame, the effective stiffness was approximately 50% greater than with the smaller loads. This may have been a result of any slop in the system causing the initial stiffness at low force to be significantly less than the actual frame stiffness. As additional weight was added, any slop in the system would have been removed and the measured frame stiffness closer to the actual value.

Wheel Stiffness

Further investigation into the source of the large rear-end deflections of Aria prompted a test of lateral stiffness for different wheel sizes. The 20 inch rear wheel from Gemini was fixed in an available front fork from a BMX bike and a lateral force applied to the rim with a force gauge. The subsequent lateral displacements were measured with the dial indicator and used to calculate the effective torsional stiffness. The same process was repeated for the 700c wheel of Aria with the wheel fixed in the HPV Club's rider training jig. Test data is included in Appendix E.

Table 22. Wheel stiffness testing results for 20 inch and 700c wheel.

Wheel Size	Torsional Stiffness (in-lb/deg)
Gemini, 20 in.	1082
Aria, 700c	292

Table 22 shows the large deviation in stiffness between the two wheels as the effective stiffness of the 20 inch wheel is 73% stiffer than the 700c wheel. This factor would greatly stiffen the rear of the vehicle, allowing for tighter packaging around the rear wheel.

Monocoque-Tub Construction Method

Once the vehicle layout and material had been selected, the method of carbon fiber tool construction was considered. Traditionally the team has used High Density Urethane (HDU) Foam that is donated each year by Coastal Enterprises to construct large female molds similar to the molds seen in Figure 35 for the fairing skin and rollbar layups. Constructing and finishing these HDU foam molds consistently requires the largest time commitment and often the resulting molds are fragile and unwieldy to work with. Complaints from team members include the large amount of finishing work, particularly sanding of the mold surface; the susceptibility of the molds to damage by simple actions such as dropping a tool or resting one's elbows on the surface; and the high part cycle time when multiple layups must be

Figure 35. HDU foam molds that the team has traditionally made. The foam is CNC machined and finished with Duratec, a sandable mold sealer.

performed in the same mold. Therefore, Tri-Fiber explored alternative manufacturing methods to mitigate or reduce complaints from team members.

The first option explored was using a lost-foam “male” (positive) tool. An example of this process which was utilized by the University of Toronto, is seen in Figure 36. The Toronto team used a hand shaped male foam plug with mild finishing as a “core” for their layups. Then the foam was removed through the windshield cutouts after all of the layups were completed. This method is simple, requires limited surface finishing due to the inside mold surface, and thus would significantly reduce manufacturing time. For instance, Toronto completed this whole production process in a little over one month. The drawbacks to this method, however, are that the tool may only be used once, the final part’s outside surface finish is at best the same as the coarse breather material used; and the male plug cannot be machined on the school’s CNC router (Shop-bot). These three factors had the potential to add countless hours to the post-layup finishing work, likely negating any time saved during the mold development process.

Figure 36. University of Toronto creating their male foam plug. Internal ribbing and overall vehicle shape can be fine-tuned before layups start.

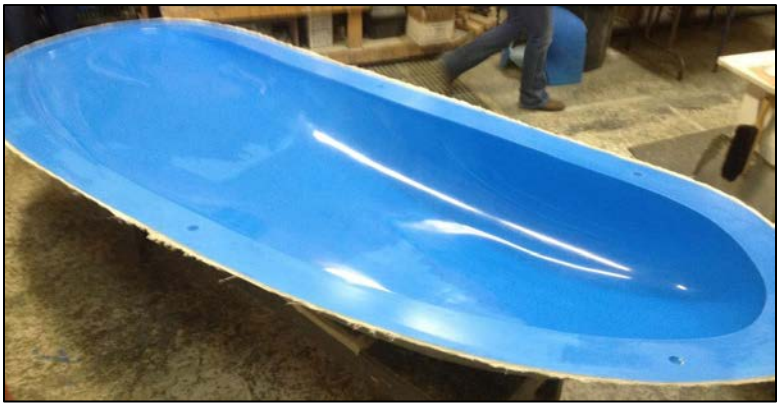

Figure 37. Fiberglass female mold half constructed by Northern Arizona University's HPV team. The tool is more durable than an HDU mold.[3]

The next option explored was to create a male plug, finish it to the team’s high surface standards, and then lay-up fiberglass on the plug to create female molds. A carbon fiber wet-layup process can then be used to create the desired parts. An example of a female mold created with this process can be seen in Figure 37. Fiberglass molds are much more durable than those made from HDU foam, and allow for more robust finishing work to be done. The downsides of this method include the extra work involved with doing fiberglass layups and the cost of extra material.

The final method explored involved using tooling carbon to make a female mold off of a male plug, and subsequently using pre-impregnated ("prepreg") carbon fiber to construct the part. Prepreg is advantageous to dry carbon fiber traditionally used by the team in that it has B-staged resin impregnated in the cloth, allowing for a quick elevated temperature cure with optimal resin content. Additional advantages of using Prepreg are the long working time of the material, eliminating time constraints when performing a large lay-up; the ability to use unidirectional fibers instead of cloth weaves to more precisely customize strength and stiffness; and the high availability of prepreg material for donation from industry sponsors due to the limited shelf life. While this is the optimal construction method from the perspective of material efficiency on the final product, special tooling carbon is required to withstand the heat of the curing oven and limit any thermal expansion of the tool. This material and its specialty resin are not as readily available as standard prepreg, are very expensive, and subsequently were out of the team's budget for the 2015 competition vehicle.

Through the use of the decision matrix seen in Table 23, Tri-fiber decided to pursue the traditional method of vehicle construction involving HDU female tools. The team's familiarity with the process and the low material cost were both leading deciding factors for the decision.

Table 23. Decision matrix for the construction of the molds to manufacture the vehicle. Wet layup with a female HDU foam tool was chosen as the best option.

Criteria	Factor	**Wet Layup with Female HDU Foam Molds**	Prepreg with Female Fiberglass Molds	Male Plug Only Wet Layup	Wet Layup with Fiberglass Molds
High Carbon Availability / Low Price	1.07	**D**	1	0	0
High Team Familiarity	1.43	**D**	-1	-1	-1
High Mold Material Availability	2.14	**D**	-1	0	-1
High Mold Durability	1.43	**D**	1	-1	1
Low Part Cycle Time	0.00	**D**	1	-1	0
Low Mold Manufacturing Lead Time	0.71	**D**	0	1	0
Facilities Availability/Constraints	2.50	**D**	-1	0	0
Complexity of Mold Required	0.71	**D**	0	1	1
TOTALS		**0**	-3.57	-1.43	-1.43

Proof of Concept Handling Prototype

In order to ensure the success of team's rider comfort and confidence goals, a proof of concept prototype was constructed. Comfort and confidence were especially critical because flaws in the rider-vehicle interaction significantly affect the rider's ability to produce power. As explained earlier, power output has a greater effect on the vehicle's racing performance than both weight and aerodynamics. Notably, Aria had very sensitive steering and poor ergonomics that hindered rider confidence. Thus riders did not race as hard as possible at the 2014 HPVC.

The prototype helped accomplished three other tasks as well: testing and selecting of a finalized steering geometry, verifying the viability of a steering wheel, and providing the HPV team with a means of practice and experimentation while the final vehicle was being constructed.

Design Considerations

The team was unfamiliar with the geometry parameters that would produce desirable handling qualities, but Aria's overly sensitive steering was thought to be an issue with poor steering geometry design. Therefore a testing-heavy approach was taken instead of an analysis focus that likely would not have yielded meaningful results. The prototype incorporated adjustable steering ratios to allow riders to provide feedback throughout testing. Due to the use of a new steering input system compared to previous years, the brake lever mounting points, hand grip width, and arm reach were also adjustable.

Figure 38. Handling prototype.

Due to the amount of testing and riding on the prototype, durability was a leading design consideration. The prototype was not intended to mimic the stiffness, strength, or manufacturability of the final frame. While the drive train was operational, it was also not intended to be representative of the final chain routing, gearing ratio, or overall efficiency of the final design.

Design

The prototype frame was constructed from low-carbon box section steel as seen in Figure 38. The prototype was designed to allow for easy testing of three different steering ratios and quickly remaking any component needed to confirm design changes. Figure 39 shows the implementation of adjustable steering ratios. A course was set up to have riders evaluate the handling at low and high speeds by simulating a straight line sprint, slalom and hairpin turns. Rider feedback for each steering ratio, summarized in Table 24, shows that a steering ratio of 3.5 felt most natural and had a balanced handling characteristic. This ratio was implemented in the final vehicle.

Figure 39. Prototype knuckle with adjustable steering ratios.

Table 24. Rider observations for each steering ratio

Steering Ratio	Preference Ranking	Low Speed Handling Observations	High Speed Handling Observations
3.0	2	Required excessive upper body movement	Not responsive enough
3.5	1	Turning felt in line with vehicle	Limited twitchiness and responsive
3.9	3	Twitchier than 3.5 ratio	Easy to oversteer

Door Location and Actuation (Rider Ingress and Egress)

Rider ingress and egress has traditionally been a place for improvement in Cal Poly's HPV designs. A recent rule change required that entering and exiting the vehicle must be done unassisted, emphasizing the advantages of full door designs that some teams have implemented in the past. At least eight times during the ASME endurance event, a rider must exit and re-enter the vehicle - five rider changes and a total of three grocery pick-ups and drop-offs. Therefore it was in the team's best interest to reduce the ingress and egress times of the vehicle significantly. Estimated times from previous year's bikes can be seen in Table 25.

Table 25. Estimated ingress and egress times for the previous three years' vehicles. Note that Gemini was an assisted ingress and egress.

Vehicle	Ingress Time (s)	Egress Time (s)
Gemini	100	120
Black Stallion	90	90
Aria	35	45

Due to its similar trike platform and recent ASME competition rule changes, Aria was used as a primary comparison for evaluating rider change times. On Aria, a door cutout was positioned at the shoulders of the rider, allowing the rider to stand on the frame and then step up and over the edge of the cutout. Alternatively, the rider could be assisted with a “pull-up” bar held by other team members when in the pits, significantly decreasing the pit-stop time. While Aria’s rider changes proved faster than previous years, problems with a single hinge design on the door and the inability of the rider to step on the fairing floor caused troubles when performing the maneuver alone. To improve upon Aria’s door design, the team identified two major features that would significantly help the ingress and egress process: a larger surface area capable of bearing body weight, and a better method of securing the door.

The first concern was addressed by the monocoque tub frame, allowing the rider to step on the large surface area floor. Components were also to be designed to reduce clutter in the expected standing area on the fairing floor. Greater door security was researched by Tri-fiber, and three potential designs were selected: a hinged door, a sliding door, or a separate door.

A hinged door as seen in Figure 40 on Trisled’s Aquila Race Trike can be placed at any suitable location and doesn’t require the rider to worry about alignment. However, the design requires two collinear hinge axes to counteract moment loads and still operate smoothly. Due to complex curvature on trikes, collinear hinge mounting points are limited and would have to be precisely made to avoid misalignment. Additionally, a door which hinged to the left or right would block one side of entry to the vehicle, potentially becoming hazardous if the vehicle capsized.

Figure 40. Trisled Aquila with an example of a hinged door. The hinges require special mounts to keep concentricity of the pins on the curved mounting surfaces.

A sliding door also allows the rider to ignore alignment of the door when closing it. Additionally, a sliding door with motion forward or aft would place the door in a position where both sides of the vehicle can be accessed. The downsides to a sliding door, however, are that an overturned bike would prove difficult to exit due to interference with the ground, and the door requires a specific path to clear the remainder of the vehicle forward or aft. Also, the sliding components add weight and complexity to the vehicle design.

A separate door, as seen in Figure 41, allows the rider to completely remove the door and store it either inside the bike or outside of the vehicle. This design is the least complex, allows multiple points of access, operation of the vehicle without the door to aid in ventilation, and easy removal when the bike is capsized. Downsides include that the rider has to align the door without any mechanical assistance when inside the vehicle.

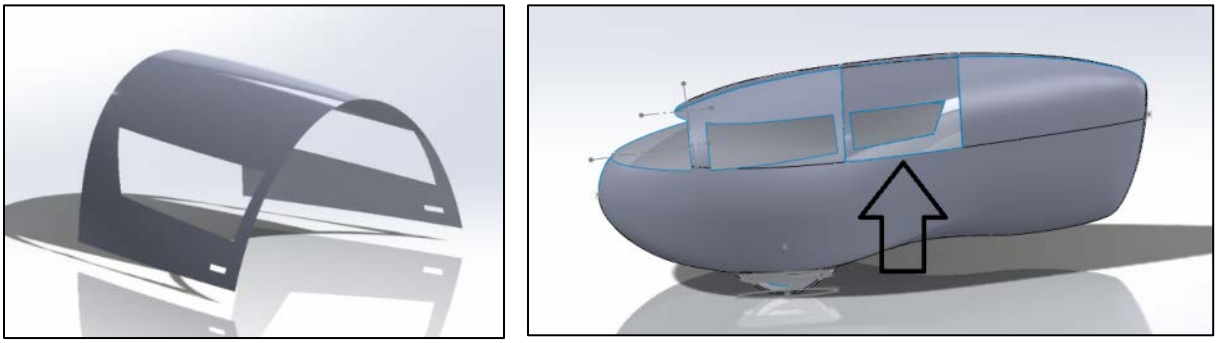

Figure 41. Door Shape and Location

Shown in Table 26 is the decision matrix for the door design. The overall winning design is the separable door.

Table 26. Decision matrix for door actuation. A separable door with a hook attachment was chosen.

Criteria	Weight	**Hinged**	Sliding	Separate
Low Complexity	0.91	**D**	-1	1
Low Mounting Requirements	1.82	**D**	-1	1
Removability	0.91	**D**	0	1
Removal in Crash	3.64	**D**	0	1
Low Hardware Required	0.91	**D**	-1	1
Rider Alignment Ease	1.82	**D**	1	-1
TOTALS		**0**	-1.82	6.36

Loading Cases

Preliminary Testing

Following the strut arm failure on Aria at the 2014 competition, the loading cases used in the analysis and sizing of the frame were brought into question. Valid and accurate loading cases were needed in order to predict the maximum loads experienced by the vehicle during the competition. Since two of the team members were enrolled in ME 410 (experimental methods in mechanical design) the previous quarter, the required term project was used to investigate certain loading cases experienced in a competition setting. The steel geometry prototype of Aria was used for testing in order to validate some of the critical loading cases to be used in the analysis of the current vehicle design.

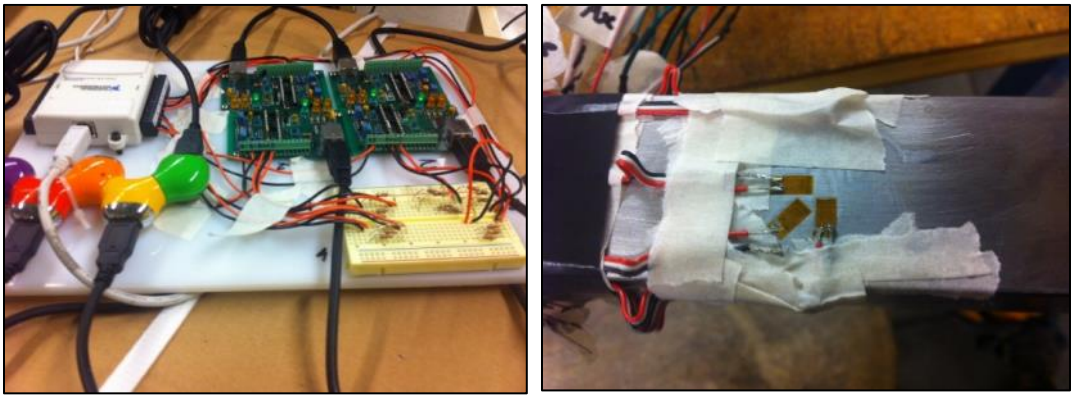

Figure 42. Portable data acquisition board (left) and strain gauges bonded to strut arm in rosette orientation.

The testing involved the placement of strain rosettes on each face of the strut arm at a highly stressed location as shown in Figure 42. The data acquisition system (DAQ) contained Wheatstone bridge circuits, which were wired to four “hacked” minestrone boards (Figure 42). Due to the limited number of minestrones, it was necessary to run three tests to obtain a complete set of data (12 strain gauges). These boards served as bridge amplifiers that transmitted output voltage to a National Instruments USB-6008 DAQ board for a single strain gauge. The analog input was converted to a digital signal and output to a laptop running LabVIEW. All equipment was mounted to the frame of the vehicle in order to allow for dynamic testing. The two loading cases under investigation were a pothole impact at 10 mph and braking from 15 mph in 10 feet.

Impact Test Procedure

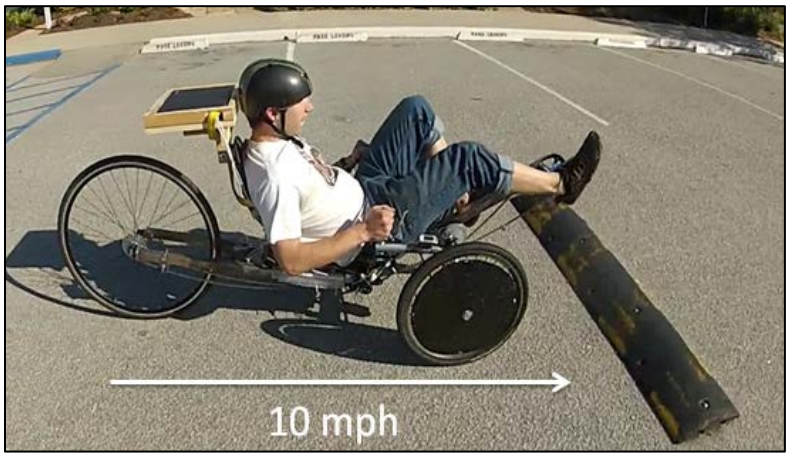

Figure 43. Impact test setup.

To model a sudden impact during competition, the speed-bump impact test was developed. While this test doesn't model the largest possible impact seen during competition, a lower speed was used to save the testing equipment and rider sanity. If validated, the results could be scaled to higher speed impacts for more accurate estimates of loads. The following procedure was developed to achieve the most repeatable results:

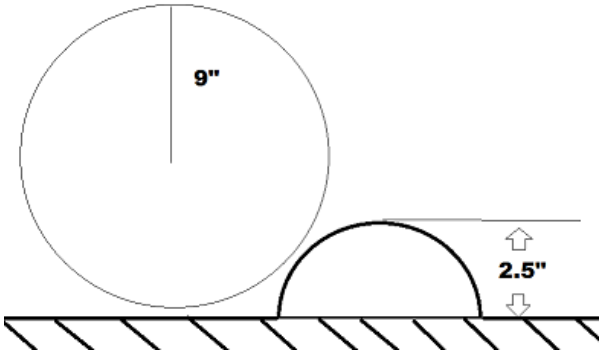

Figure 44. Speed bump and wheel geometry schematic.

1. *Set the desired tire pressures (30 psi front, 80 psi rear)*
2. *Obtain desired speed bump to verify model (2.5 inch radius – see schematic, Figure 44)*
3. *Position rider to have adequate run up time to achieve desired speed (20 yards – on hill – no pedaling was required for run up, increasing stability and rider concentration)*
4. *Perform an unloaded offset calibration run to record an offset from zero voltage*
5. *Perform the test, ensuring adequate speed is reached and data is recorded without errors*
6. *Repeat desired number of tests (10 x 3 = 30 repetitions for 10 complete samples)*

Braking Test Procedure

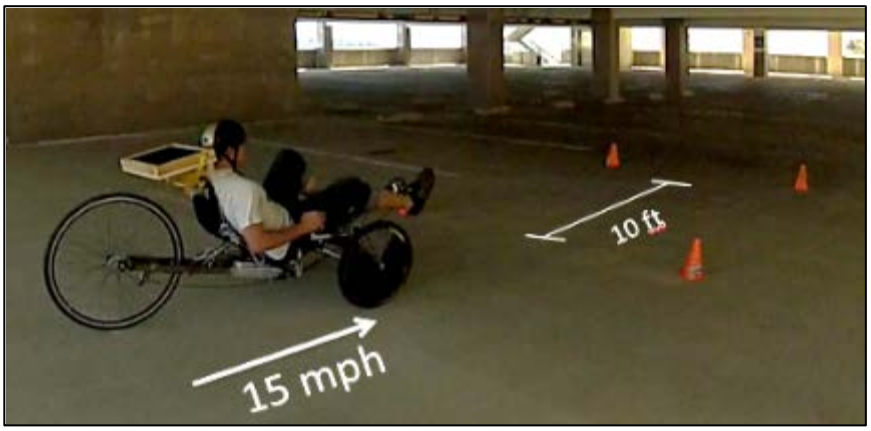

Figure 45. Braking test setup.

To model a hard braking scenario, the following procedure was developed with speeds and distances based on the ASME HPVC safety rule of being able to complete a stop in 6 meters from 25 kph. The team misread the rule set prior to testing and designed the test with a stopping distance of 3 meters rather than 6, which proved difficult to achieve consistently.

1. *Set the desired tire pressures (30 psi front, 80 psi rear)*
2. *Mark out a visible 10 ft. braking area at which the rider will come to a complete stop from the desired speed (15 mph)*
3. *Position rider to have adequate run up time to achieve desired speed (30 yards)*
4. *Perform an unloaded offset calibration run to record an offset from zero voltage*
5. *Perform the test, ensuring adequate speed is reached and data is recorded without errors*
6. *Repeat desired number of times with consistent rider and braking strategy (10 x 3 = 30 repetitions for 10 complete samples)*

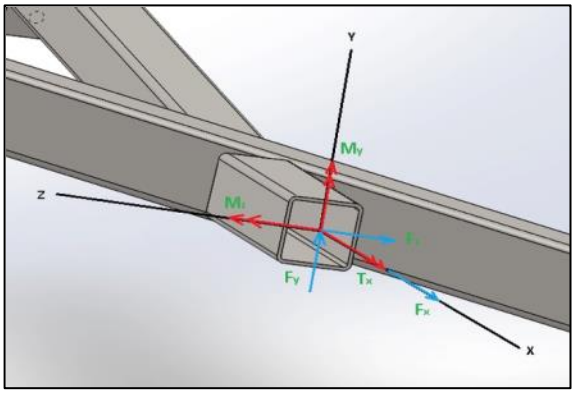

Figure 46. Loading cases coordinate system on Aria prototype strut arm.

Analysis of Results

The signal data was then processed in Microsoft Excel to obtain peak strain values. Statistical analysis of the trial data was utilized to calculate a 95% statistical maximum from these peak strain values. The resulting reaction forces on the front wheel hub were calculated and are summarized in Table 27 in addition to the theoretical determined values. Hand calculations for the loading cases are attached in Appendix E.

Table 27. Comparison of theoretical and experimental loading cases.

			Front Axle Loads (one wheel), lbf					
			Theoretical Results			*Experimental Results*		
Loading Case	Notes	Speed (mph)	X	Y	Z	X	Y	Z
Pothole impact	Using speed bump in tests	10	0	305	254	-21	396	162
Braking	Stopping in 10 ft.	15	0	167	158	0	333	116

The discrepancy between the results for the impact test is likely attributed to the differing geometry of the speed bump, since the theoretical model assumed a sharp bump rather than a rounded one as used in the testing. However, it was decided that the results were similar enough to use the impulse-momentum model for predicting maximum loads experienced during competition and may be scaled to differing parameters (i.e. speed of impact). The one variable that highly influences the model calculations is the impact time duration, Δt. The value used in the calculations at the 10 mph impact speed was derived from a frame-by-frame analysis of the wheel impacting the actual speed bump. Due to the fact this value is on the order of 50 milliseconds (@ 10 mph), and the equations for the impulse forces are inversely related to impact duration, the loads are highly sensitive to small changes in this time. Therefore, further testing may be required in the future to determine a ballpark impact duration value at different speeds, or a conservative estimate of this time could be assumed from the known value at 10 mph. Thus, based on the previous discussion, the deviation between the theoretical and experimental results was deemed acceptable as the selection of a higher speed impact for the critical loading case was a conservative decision.

The braking loading case results do not compare as well as the impact loading, which may be attributed to a number of factors. The most likely cause was the large variation in test data due to the short stopping distance. On certain runs the vehicle would skid and on others it would have a tendency to roll forward about the front wheels which likely caused deviations in the maximum loading on the strut arm. Thus, when using the calculated braking loads, a conservative safety factor was utilized.

Other Loading Cases

The aforementioned impact and braking loading cases were used in the detailed design of the tub and sub-frame. Other loading conditions were also considered to account for the variety of loads the vehicle may experience when in operation. By designing to these loads, the tub and other structural components can be strengthened and stiffened in the appropriate regions while minimizing excess material in an effort to reduce the overall vehicle weight.

The additional loading cases considered are presented in Table 28. The hand calculations for each case are presented in Appendix E.

Table 28. Additional loading cases considered.

Loading Case	Notes
Rider ingress/egress	Loading applied to bottom of tub, seat structure, and door seam
Start-up pedal force	Max. expected loading on bottom bracket
Steady-state pedaling	Fatigue analysis of bottom bracket mount
Cornering	0.6 g turn
Rollbar (RPS)	Per ASME rules

Potted Insert Selection and Testing

The selected semi-monocoque design required a means of joining the sub-frame and the carbon fiber tub structure. Research into industry practice revealed the advantages of potted inserts, including their ease of implementation. Blind threaded inserts were selected as they only require a hole to be drilled on the inside of the vehicle and do not extend past the bottom facing skin. This characteristic was advantageous due to the low ground clearance of the vehicle and the need to avoid protrusions on the underside of the tub that could catch on external objects. Because manufacturers often do not publish load capacities for their potted inserts, the team decided to perform tensile testing to determine the failure load of the inserts. By quantifying the average failure point of a number of inserts, a minimum failure value could be obtained in order to calculate the number of inserts required at each mount. Both steel and Torlon (thermoplastic composite) #10-32 potted inserts were tested to determine if one had a significant advantage in pullout strength (vendor information in Appendix D).

Carbon fiber sandwich plates (roughly 3”x15”) were laid up with three plies of carbon ([0/45/0]) on either side of the core material. The potted inserts were then installed using the procedure outlined in Figure 47 with four inserts per plate, spaced at least 3” apart.

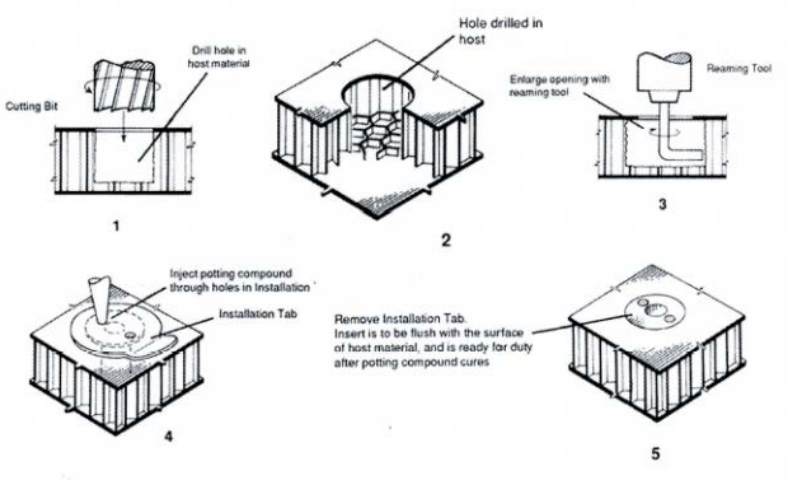

Figure 47. Potted insert installation procedure.[10]

In order to rigidly hold the test panels during testing, a fixture was constructed as shown in Figure 48. The top plate of the fixture was made from a ½" plate of 6061 aluminum with a 1.5" diameter hole drilled in the center. A 3/16" steel plate was used for mounting to the lower jaws of the Instron and was offset from the aluminum with spacers. A welded tab on the bottom side of the steel was used to clamp the fixture in place. A steel tab was welded to a #10-32 bolt that was threaded into the insert during the test in order to adequately transmit the load. The basic principle in the design of potted inserts is that the applied force is transmitted from the surrounding epoxy to the top face sheet of carbon. Thus, each test sample was placed on the bottom side of the aluminum plate and loaded through the hole in an attempt to isolate the insert while minimizing the stressed skin area surrounding it.

Figure 48. Potted insert testing setup.

The inserts were tested in two core materials, aluminum honeycomb and end-grain balsa, to gain an understanding of any advantages. Table 29 shows the results of the potted insert testing analysis including the first fiber failure load (FFFL). The discrepancy between the FFFL of the potted inserts in the aluminum honeycomb core and in the balsa core come as a

Figure 49. Face sheet failure of potted inserts subjected to tensile loading.

direct result of the installation method. When potted inserts are installed, the surrounding core must be removed to allow excess epoxy to fill the void and establish contact with the face sheet (step 3 of Figure 47). The end-grain balsa core samples were not prepared correctly in this manner, and subsequently achieved lower strength values. Nonetheless, this minimum load was used in the design as a conservative worst case scenario. The Torlon inserts were selected as they were roughly 1/3 the weight of the steel inserts. In addition, the testing results did not show a significant increase in strength for either material. End-grain balsa was chosen for the sub-frame mounting locations due to its availability and would likely exceed the testing results with proper installation.

Table 29. Potted insert testing results, normalized to statistical minimums using student-t analysis.

Core Material	FFFL, Mean (lbf)	Std. Deviation (lbf)	FFFL, 99% minimum (lbf)
Aluminum Honeycomb Core (1/2”)	723	63.1	604.4
End-Grain Balsa (1/2”)	351	76.7	263.7

Seat Adjustment Mechanism Design Development

As the team includes a large variety of body sizes and physiques, it was important for the club to be able to accommodate anyone who wished to ride the vehicle. Additionally, as seen in the time to speed model, a small increase in power outweighs any aerodynamic or weight reductions in the vehicle speed range. This therefore points to rider comfort and fit as driving factors. Speed of position change was also considered, as pit-stop time was of major importance to the team.

To account for the large variety in rider sizes, the first step was to quantify rider measurements and develop a model based on largest and smallest rider sizes. Both riders were seated in the trainer and measurements were taken from the bottom bracket centerline to the glutes, shoulders, and top of the head. From this data, maximum and minimum positions were developed. These positions required 10 inches of adjustability.

Figure 50. Car seat adjustment mechanism. This would allow for the most effortless seat adjustment, but would require overly complex and heavy mechanisms.

To maintain the same rider position while shifting the seat position linearly, the seat back position must be changed concurrently. It was decided this achievement would require an overly complex and bulky mechanism. Additionally, between the largest and smallest rider positions, the hip angle changed less than 10 degrees, which is within the range of desirable hip angles (see rider position section). Therefore, a nominal hip angle of 130 degrees was chosen, allowing a range of hip angles of approximately 125° to 135° at smallest and largest riders, respectively.

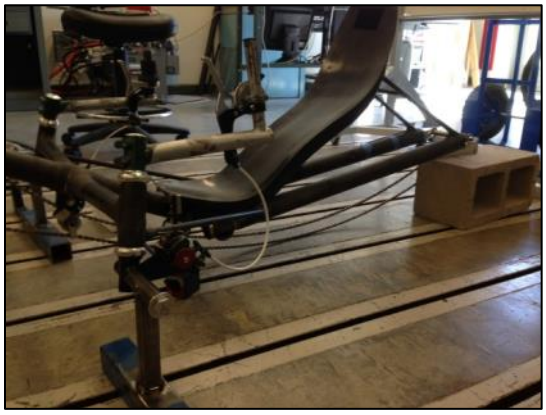

Figure 51. Aria's fixed seat design. This design used spacer pads behind the rider's back to adjust sizes.

Three designs were considered for adjustment. The first involved a mechanism similar to a car seat that allowed quick adjustment by lever actuation and roller bearings (Figure 50). The second design involved fixed seat and custom spacing pads for smaller riders, similar to the method used on Aria (Figure 51). Finally, the last design considered used indexed holes with pin locators (Figure 52) as seen on pedal kayak designs.

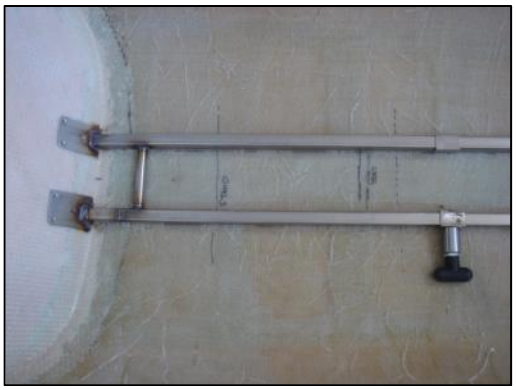

Figure 52. Seat adjustment design for a pedal kayak.

The selected design was based on the kayak seat adjustment design, but also incorporated elements of the car adjustment mechanism. The final design's key features were the use of Delrin-lined sliding brackets to allow the rider to quickly adjust their position, and spring-loaded locator pins to index the seat positions. Additionally, tie rods were used to connect all sliding members to allow for ease of alignment. This design allowed for the most adjustability while maintaining sinplicity. The final design can be seen in Figure 53.

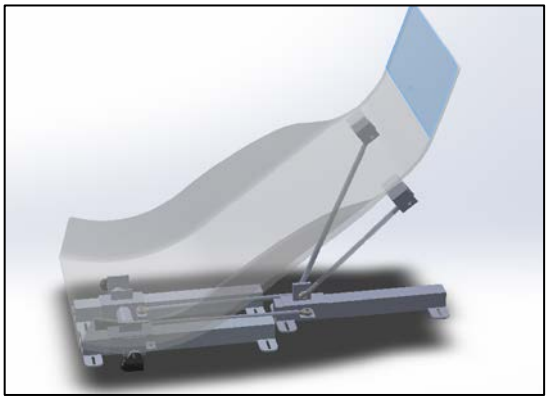

Figure 53. Final Seat Adjustment Mechanism.

Seat Design Development.

An ergonomic and comfortable seat design was important to increase the power output of the rider. Traditionally, the team has used standard recumbent seats based on molds developed by George Leone to manufacture an ergonomically correct seat. However, due to the decision to pursue a trike design, lessons learned from Aria required a bolstered seat design. Bolstering (Figure 54) supports the rider while cornering, minimizing the amount of unwanted steering inputs or sliding off of the seat.

To achieve this requirement of a bolstered seat, the team either had to design a seat from scratch or modify a current design. It was chosen to design a seat from scratch as it allowed for the most freedom in the design; however it also presented challenges from an ergonomic standpoint. Achieving proper lumbar support was of utmost concern, as a seat with incorrect fit could reduce the power output capability of the rider.

Figure 54. Trisled Carbon Fiber Racing Seat with mild bolstering.

A design primer by JetTrike[13] on recumbent seat design was used for basic measurements, and lumbar support was to be added post-manufacturing via Velcro and a foam pad. This allowed a bucket seat design to be made with ergonomic fine-tuning to occur based on rider feedback. The final seat bucket design can be seen in Figure 55. The key features include the added bolstering around the lower back, added glute and hamstring support, and carbon-epoxy sandwich design for ease of manufacturing.

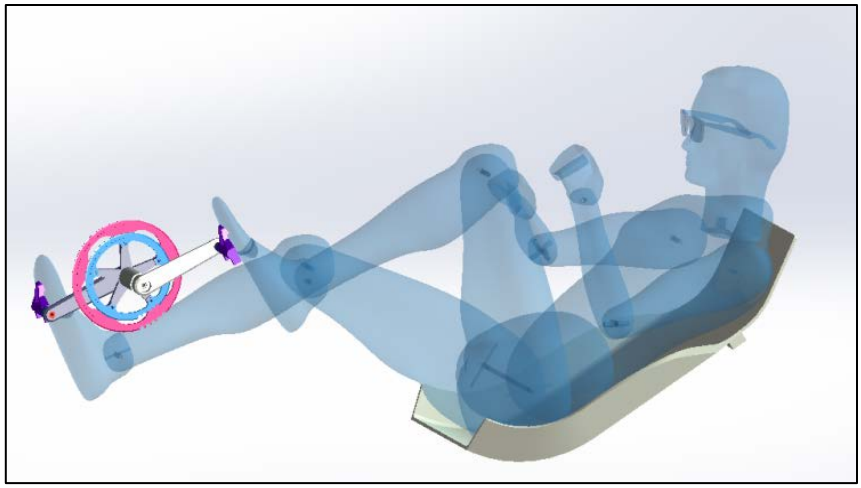

Figure 55. Final seat design with mock-up of the largest rider in position

Drivetrain Design Development

Because of the need to ensure efficient transfer of power between the rider and the vehicle to maximize rider output, the most efficient drivetrain with adequate gearing ratios for both the sprint and endurance events was sought. Other points of emphasis were to limit chain derailment and to simplify the parts of the drivetrain that are often inaccessible due to the full fairing design. A decision matrix comparing researched configurations can be seen in Table 30. A primary concern was achieving a high enough gearing ratio due to the smaller 20" rear wheel.

Table 30. Decision matrix for the drivetrain configuration.

Criteria	Factor	Direct to Rear Wheel Shifting	Behind the seat mid-drive	**In front of seat Mid-drive**
Simplicity of parts	1	D	-1	**-1**
Shifting Simplicity	3	D	0	**1**
Gearing Range	3	D	1	**1**
Gearing Adjustability	2	D	1	**1**
Custom Parts Required	1	D	-1	**-1**
TOTALS		D	3	**6**

The chosen design was to implement a mid-drive in front of the seat with a left drive hub at the rear wheel. This held a few advantages over directly shifting a cassette on the rear wheel. Firstly, the shifting is localized to a shorter chain line of the same length as an upright bicycle. This minimizes the amount of chain that physically has to move, reducing binds and resistance in the drive train. Secondly, the mid-drive configuration allows standard size front chain rings to be implemented without outsourcing a large chain ring to achieve adequate gearing ratios. Additionally, the mid-drive allowed the step-up ratio to be easily changed by changing the step-

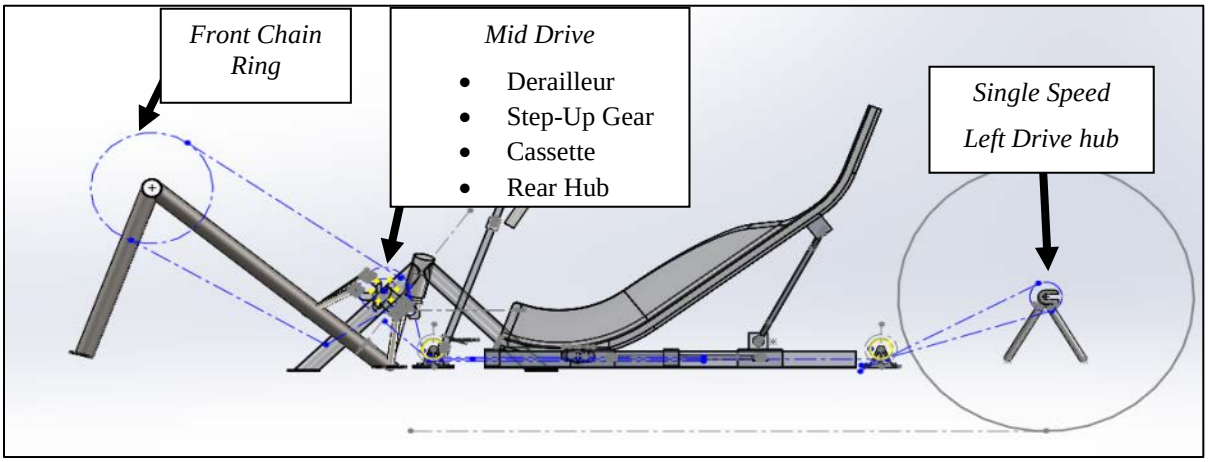

Figure 56. Visual representation of the final drivetrain with chain path in blue.

up and drive sprockets without changing out the cassette or front chain ring. Finally, the single speed chain to the rear wheel allowed tight clearances to be implemented and limited the chance for a chain derail, a potentially dangerous situation for a recumbent on the road.

The proposed layout of the design is shown in Figure 56 with subsystems highlighted. A summary table of the gearing ratios available for the endurance and sprint races is shown in Table 31 along with component selection when compared to the datum of a race road bicycle.

Table 31. Drivetrain setups for Sweet Phoenix in the endurance (E) and sprint races (S).

Vehicle	Front Chain Ring	Mid Drive Cassette	Mid Drive Step-up	Drive Sprocket	Rear Wheel Diameter	Gear Inch Max	Gear Inch Min	Max Speed at 100 rpm
Sweet Phoenix (S)	53 Teeth	12 - 21 Teeth (9spd)	17 teeth	13 teeth	20 in (451)	115.5	60.3	34.4
Sweet Phoenix (E)	53 teeth	12 - 21 Teeth (9spd)	17 teeth	15 teeth	20 in (451)	100.1	53.2	29.8
Upright Bicycle	53 teeth	12 - 21 Teeth (9spd)	n/a	n/a	27.5 in (700c)	121.5	63.4	36.1

The mid-drive was the main point of emphasis of the drivetrain design. To implement the system, a rear hub was proposed, with a machined sprocket mounted to the 6-bolt pattern disc brake mount used as a step-up gear (Figure 57). The mid-drive required careful placement to ensure a 400 mm minimum front chain length, while also allowing adequate derailleur extension, leg, and heel clearances. To ensure that the proposed placement was adequate, a mockup jig was made to simulate the position of the mid-drive derived from chain length and derailleur clearances while the rider was pedaling. Figure 58 shows the test setup with the shortest rider. Adjustments were made after initial testing until a proper placement was found.

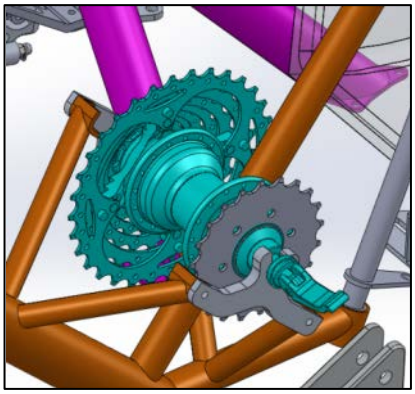

Figure 57. Mid-Drive Setup with disc brake bolt pattern mounted step-up gear.

Figure 58. Preliminary placement of the mid-drive.

Routing of the chain was also debated. While the front chain line was relatively simple, the mid-drive to rear wheel provided many complications. Space constraints required the chain to go through the left seat rail and pass through two idlers with rather steep chain angles. The first iteration of the design routed both chains through the left seat rail and passed through two side by side idlers (Figure 59) with plastic tubing separating the two chains. While not ideal, this design was thought to be the simplest way to route the chain.

Figure 59. Side-by-side chain routing initial design

Chapter 4: Description of the Final Design

Overall Description

Sweet Phoenix is a recumbent tricycle built for the 2015 ASME Human Powered Vehicle Challenge. The three wheels are arranged in a tadpole formation, with two steering and braking wheels in front and a single drive wheel in the rear. Its structural system is comprised of a semi-monocoque carbon-epoxy fairing to which several sub-frame weldments are bolted using potted inserts. Also integrated into the fairing is a rollover protection system (RPS) designed to withstand vertical and side impacts. The rider is connected to the RPS with a four-point harness. A wide range of rider sizes is accommodated with a sliding seat mounted to three rails on the vehicle's floor. A steering wheel is connected to the front wheels via universal joints, a bell crank, and two tie rods. The drivetrain consists of two stages. A primary chain connects a single chainring at the cranks to a 10-speed road bike cassette mounted beneath the rider's legs. A bicycle derailleur shifts this "mid-drive" transmission. A secondary chain continues from the mid-drive to the rear wheel. A shelf located behind the rider and above the rear wheel carries cargo. Five windows provide 180° of visibility. The rider may enter and exit through a removable door on the vehicle's left side.

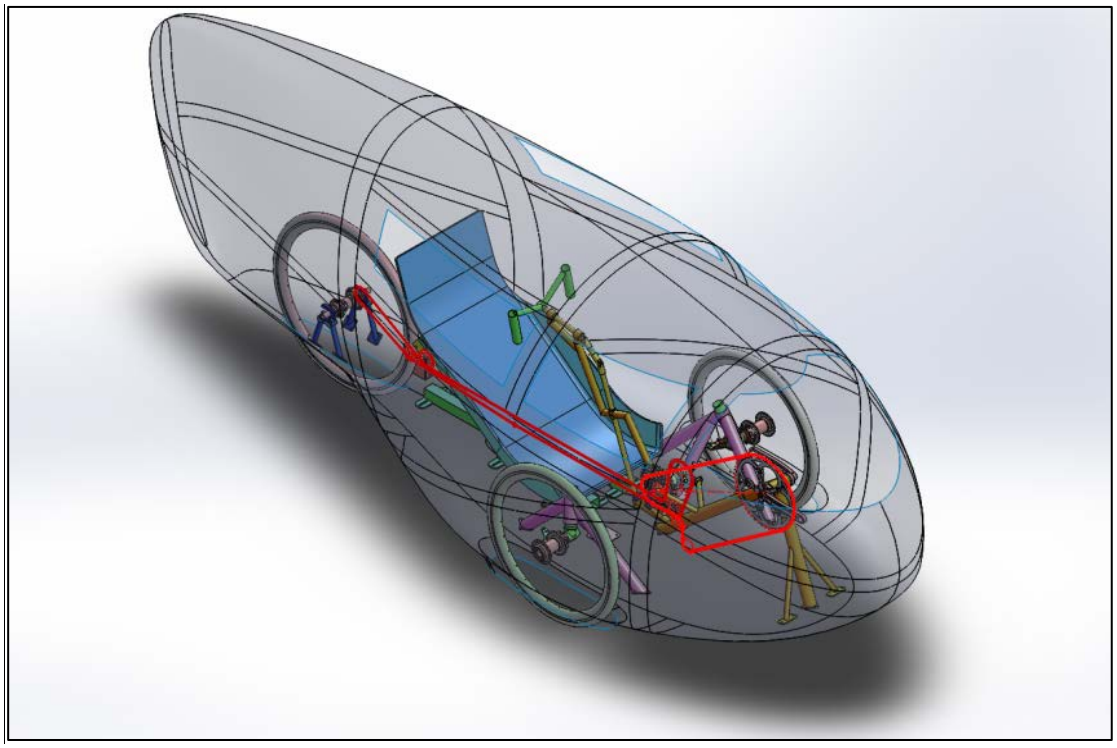

Figure 60. Vehicle subsystem and component layout. Primary and secondary drive chains are shown in red.

Materials Selection

The frame layout for Sweet Phoenix required selecting materials for each sub-system – the monocoque fairing and sub-frame components. As a starting point, it was assumed that the fairing would be made from a fiber-reinforced composite (FRP) in order to make use of the club's manufacturing skillset. The materials selection process was accomplished using two decision matrices (Table 32 and Table 33), which evaluated the properties of several materials for use in each structural sub-system. Datum materials were selected based on recent material usage by the team. The cost projections included in these matrices take into account that the team already had a large amount of carbon fabric available. The final design used CFRP and steel for the fairing and sub-frame, respectively, mostly out of cost and manufacturability concerns.

Table 32. Monocoque fairing laminate material decision matrix

Criteria	Factor	**Carbon FRP**	Glass FRP	Kevlar FRP
Strength	1.00	**D**	0	0
Stiffness	0.67	**D**	-1	-1
Weight	0.33	**D**	-1	-1
Cost	0.00	**D**	-1	-1
TOTALS		**0.0**	-1.0	-1.0

Table 33. Sub-frame material decision matrix

Criteria	Factor	**Steel**	Aluminum	Carbon FRP
Strength	1.00	**D**	0	0
Stiffness	0.50	**D**	0	-1
Weight	0.25	**D**	1	1
Manufacturability	0.75	**D**	-1	-1
Cost	0.00	**D**	0	-1
TOTALS		**0.0**	-0.5	-1.0

Fairing Layout

The final core and ribbing layout for the monocoque tub is shown in Figure 61. All ribbing in the vehicle is constructed with a sandwich core structure, consisting of either Divinycell or Nomex honeycomb core surrounded by carbon fiber-epoxy laminate (details are discussed in Fairing Analysis section).

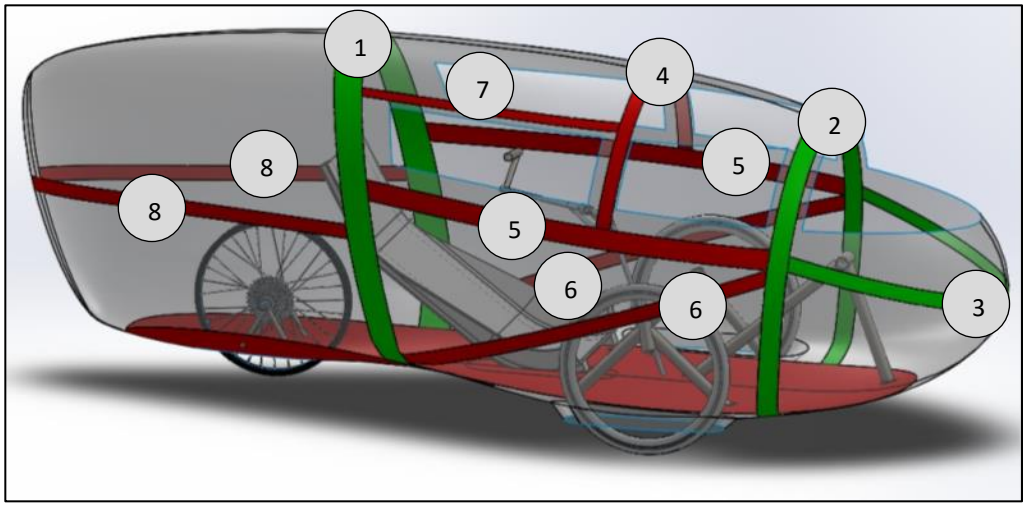

Figure 61. Sweet Phoenix RPS rib key. Green members have Divinycell core and red members have Nomex honeycomb core.

As mandated by the ASME competition rules, a rollover protection system (RPS) is included in the vehicle's design. The primary member of this system is represented by Rib #1 in Figure 61. This roll bar is situated directly behind the rider and serves to protect them in the event of a lateral or vertical impact. Analysis and testing of the roll bar was completed to validate the structural loading cases set forth by the ASME competition rules, and can be seen in the RPS Analysis and RPS Testing sections, respectively. Although not required for the rules-specified RPS, additional ribbing throughout the fairing serves several purposes. The vertical ribs increase the overall stiffness of the vehicle, provide local reinforcement to mitigate deflection of the carbon skin under wind loading, and increase protection during unforeseen impact scenarios. The horizontal rib that runs parallel to the tub bottom acts as the bottom door seam, providing a support for easy ingress/egress. In addition, the cargo volume shown in Figure 62 is the appropriate size as specified in the rules (8"x 13"x 15"). The gradually tapered tail of the fairing provides room for storage of this cargo, which is carried on a carbon-epoxy honeycomb sandwich plate shelf. Riders can access the cargo by reaching above or around the seat.

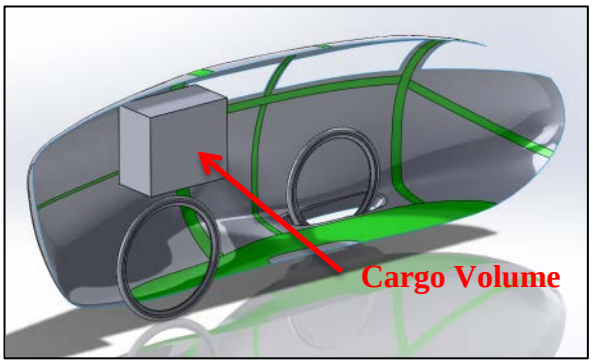

Figure 62. Cargo volume location behind rider.

Structural Analyses

The overall fairing stiffness and strength were analyzed to ensure desirable vehicle handling and structural integrity. In addition, an RPS analysis was conducted. Requirements for each analysis were established with tests discussed further in the Design Development chapter.

Fairing Stiffness

The stiffness testing section outlines the derivation of target stiffness values for Sweet Phoenix. The vertical stiffness provided a baseline from which the layup schedules and core sizes throughout the fairing could be developed while keeping the overall weight as low as possible. While the vertical stiffness value remained a target goal, the torsional stiffness value from testing was an absolute minimum. The team believed that excessive rear tire deflection on the previous year's vehicle resulted in poor handling characteristics and had to be mitigated.

In order to adequately analyze the complex geometry of the fairing, a finite element model of the fairing and rib structure was developed in Abaqus/CAE using 3-D shell elements and corresponding core sizes and layup schedules. Material properties for Aramid Fiber Honeycomb and Divinycell H45 are contained in Appendix D. Standard material properties for 3K 2x2 twill weave carbon fiber (Appendix D) were obtained from Dr. Mello and utilized in the analysis. On the final vehicle, it was decided to add a single ply of TeXtreme® carbon fiber on the outer layer of the fairing for aesthetic appeal. However, this ply was not included in the analysis due to a lack of both material properties and time to perform material testing, implying that all results obtained in the analyses would be conservative.

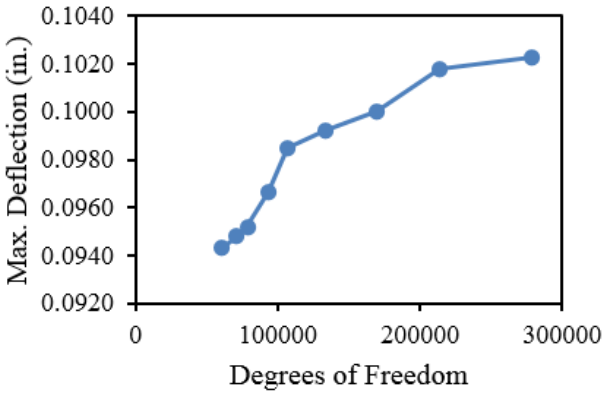

Figure 63. Mesh convergence plot for fairing model.

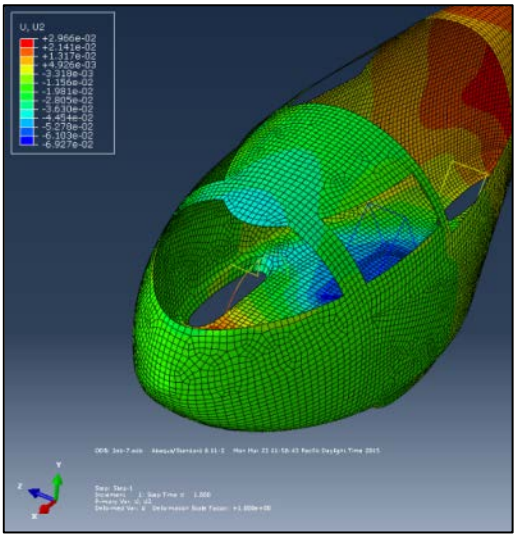

Figure 64. Displacement plot with rider weight.

A mesh convergence study was then performed to ensure an adequate mesh size was used. As seen in Figure 63, the model approached convergence with approximately 275,000 degrees of freedom.

Although the plot does not demonstrate total asymptotic behavior, it was decided that the convergence was sufficient to achieve accurate results without requiring more computing power than was available.

Beam elements with infinite stiffness were used to model the internal sub-frame components as a means of transferring the load from the front axles down into the tub floor. These beam elements were tied with wire features directly to the tub, modeling the potted-insert locations. A rider weight of 170 lbf was then applied to the seat location with the axles simply supported to model a rider sitting in the vehicle. A displacement plot with the rider load is shown in Figure 64. The torsional stiffness was calculated by applying a moment to the rear axle and determining the maximum angular deflection of the fairing. The results of three layup iterations are shown in Table 34.

Table 34. Comparison of vertical stiffness and weight for three fairing layup and core iterations. All plies are cloth with a 0 implying a 0°-90° ply and 45 implying ±45°.

		Layup Schedule	Core Material	Core Thickness (in.)	Vertical Stiffness (lbf/in)	Total Weight (lbf)
#1	Skin	[0/45/0]	---	---	2081	21.1
	Ribs	$[0/45/0/core]_{sym}$	Divinycell	0.375		
	Rollbar	$[0/45/0/45/core]_{sym}$	Divinycell	0.500		
	Tub	$[0/45/0/core]_{sym}$	Divinycell	0.500		
#2	Skin	[0/45/0]	---	---	**2454**	**21.3**
	Ribs	$[0/45/0/core]_{sym}$	Div. & Honey	0.375 & 0.394		
	Rollbar	$[0/45/0/45/0/core]_{sym}$	Divinycell	0.750		
	Tub	$[0/45/0/core]_{sym}$	Honeycomb	0.472		
#3	Skin	[0/45/0/45]	---	---	2835	26.0
	Ribs	$[0/45/0/45/core]_{sym}$	Div. & Honey	0.375 & 0.394		
	Rollbar	$[0/45/0/45/core]_{sym}$	Divinycell	0.500		
	Tub	$[0/45/0/45/core]_{sym}$	Honeycomb	0.472		

As seen in the results, iteration #2 was chosen as it differed by only 1.9% from the goal of 2500 lbf/in. The overall weight of the corresponding layup and core configuration was the lightest iteration that still met the stiffness requirements. During analysis, it was determined that the torsional stiffness minimum of 150 lbf-in/deg was easily attainable with a semi-monocoque structure as the entire roll-hoop resisted rotation due to cornering loads in the rear of the vehicle. The resulting torsional stiffness was approximately 1200 lbf-in/deg, which far exceeded the required minimum.

Fairing Strength

Following determination of the required layup schedule to meet stiffness requirements, the strength of the fairing under critical loading was evaluated. The impact testing (see Developmental Testing section) resulted in a 15 mph pothole impact loading case with tire force components of 610 lbf upwards and 510 lbf rearwards.

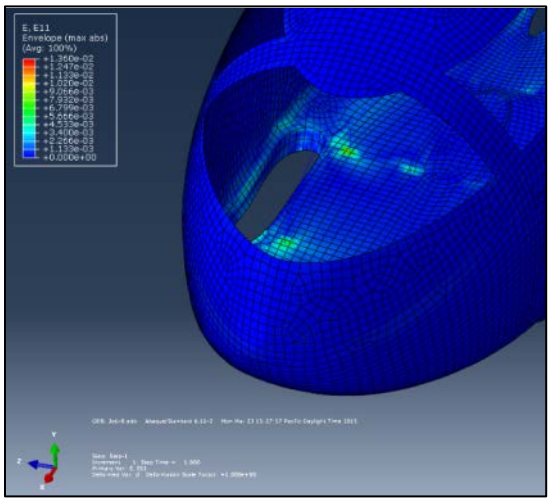

Figure 65. Plot of maximum longitudinal strains through the laminate.

As a conservative model and to ensure convergence, the left axle was fixed in the x (along length of vehicle) and y directions (vertical) while the rear axle was fully fixed. The critical forces determined previously were applied to the right axle and the subsequent ply strains were checked for failure. An envelope plot of the maximum longitudinal strains in the x-direction is shown in Figure 65. The results of the analysis are shown in Table 35 below.

Table 35. Major results from fairing strength FE analysis.

Loading Case	Max. Vertical Deflection (in)	Ply Max Failure Index (Longitudinal)	Ply Max Failure Index (Shear)
15 mph Impact Load	2.944	0.907	0.964

Post-processing of the data revealed discontinuities at the sub-frame to fairing connections, and the results in these areas were ignored as invalid. The surrounding unaffected region was therefore used in scanning the plies for maximum strains. From the results, it was evident that excessive deflection occurred and that certain plies were close to fiber failure. However, this was considered acceptable as all aspects of the analysis were conservative in nature.

Sub-Frame Mounts

Detailed analysis was also performed on the sub-frame components to verify adequate strength and stiffness. The knuckle mounts and the bottom bracket mount were determined to be the critical sub-frame components as they experience the greatest loads on the vehicle and must transmit the input forces to the fairing without excessive deflection or yielding. As mentioned previously, the mounts were both constructed of 1018 low carbon steel with mitered and welded joints. The main strut arms were 0.049” wall thickness with 1.25” outer diameter. Steel plate (3/32” thick) was used for the base-plates for bolting the mounts to the potted inserts.

Due to their geometry, both components were modeled with 3-D shell elements in Abaqus/CAE. The bolt hole locations on the base-plates of each mount were fully fixed to conservatively model the mounting on the vehicle. In actuality, the fairing tub would deflect with the input load, acting as a form of suspension and damping, thus decreasing the localized stress on the sub-frame components. A 300 lbf horizontal load on one pedal at the top of the pedal stroke was assumed to be a conservative maximum force a rider could output. For the loading on the knuckle mount, the same 15 mph impact forces were translated from the axle to the center of the head tube along with the resulting moments. Plots of von Mises equivalent stress are shown below in Figure 66 for both mounts.

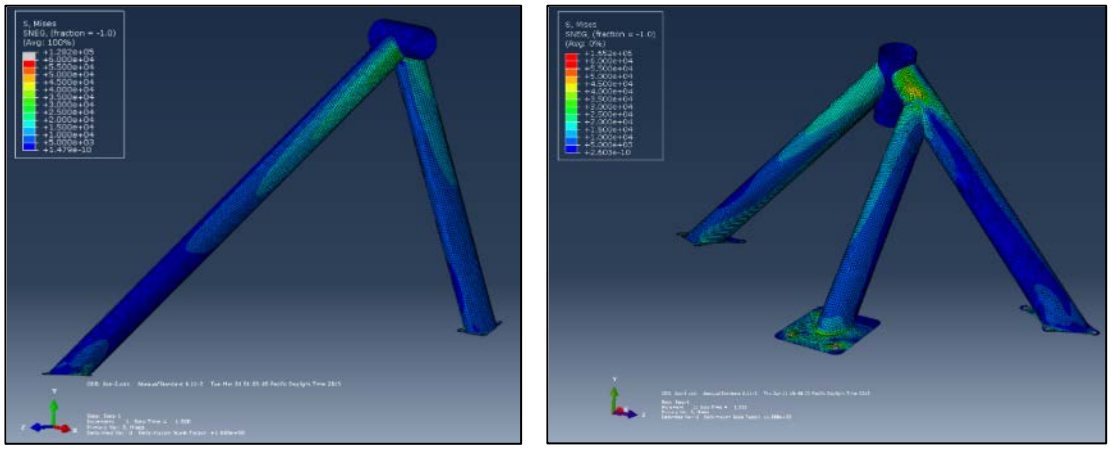

Figure 66. Von Mises equivalent stress plots of the bottom bracket and knuckle mounts under critical loading conditions.

Similar to the fairing impact analysis, discontinuities existed in both models at the mounting boundary locations, and so these areas were ignored as invalid. The results of the analysis are summarized in Table 36. Of most concern was the lateral deflection of the bottom bracket, as large values can have undesirable effects on drivetrain efficiency. However, this value was decided to be well within an acceptable range based on prior years' experiences.

Table 36. Summary of major results from critical loading for sub-frame mounts.

Component	Loading Case	Minimum F.O.S. (Yield)	Max Deflection (in)
Knuckle Mount	15 mph Impact Load	1.15	0.056
BB Mount	300 lbf pedal load	1.84	0.015 (lateral at BB)

RPS Analysis

The rollover protection system utilized in Sweet Phoenix was designed to meet the required ASME HPVC specifications of 1.5" horizontal deflection when subjected to a 300 lbf horizontal

load and 2.0” resultant deflection when subjected to a 600 lbf load applied 12° from vertical, sloping towards the rear of the vehicle. In this analysis, the boundary conditions were a major concern, and utilizing a fully fixed bottom quarter of the rollbar as in previous years’ analyses was deemed to be unrepresentative of reality. Instead, the boundary conditions in this analysis focus upon reactions caused by the seat harness mounts.

In past years, the team has performed destructive rollbar testing before determining final composite layup schedules, but two changes implemented in this year’s design made this strategy impractical. First, Sweet Phoenix relies on a larger degree of structural complexity within the RPS than previous vehicles. Stand-alone tests of the primary rollbar were determined to poorly represent the nature of this system, and creating a second entire roll structure before constructing the fairing was not feasible within the club’s timeline or budget. Second, and discussed further below, the reactions to be used in analysis and testing have been clarified since the preliminary design of this RPS, and the team would like to verify the constructed design with a more thorough analysis.

The dimensions, materials, and layup schedules of the ribs of the RPS had already been determined during the design phase and Table 37 summarizes the proposed core sizing and layup schedules of each structural component outlined by Figure 61. A cross sectional diagram of the primary roll structure can be seen in Figure 67, where previous year’s teams had determined that this is offers the best weight-to-stiffness ratio.

Table 37. Manufactured fairing structural member summary.

Rib	RPS Section	Layup Schedule	Core Material	Core Base Width (in)	Core Height (in)
1	Primary	$[0_{CL}/+45_{CL}/0_{CL}/+45_{CL}/0_{CL}/\text{Core}]_S$	Divinycell	3.00	0.750
2	Secondary	$[0_{CL}/+45_{CL}/0_{CL}/\text{Core}]_S$	Divinycell	2.00	0.500
3	Secondary	$[0_{CL}/+45_{CL}/0_{CL}/\text{Core}]_S$	Divinycell	1.50	0.500
4	Secondary	$[0_{CL}/+45_{CL}/0_{CL}/\text{Core}]_S$	Nomex Honeycomb	1.25	0.375
5	Secondary	$[0_{CL}/+45_{CL}/0_{CL}/\text{Core}]_S$	Nomex Honeycomb	2.00	0.375
6	Secondary	$[0_{CL}/+45_{CL}/0_{CL}/\text{Core}]_S$	Nomex Honeycomb	1.50	0.375
7	Secondary	$[0_{CL}/+45_{CL}/0_{CL}/\text{Core}]_S$	Nomex Honeycomb	0.75	0.375
Floor	N/A	$[0_{CL}/+45_{CL}/0_{CL}/\text{Core}]_S$	Nomex Honeycomb	Varies	0.500

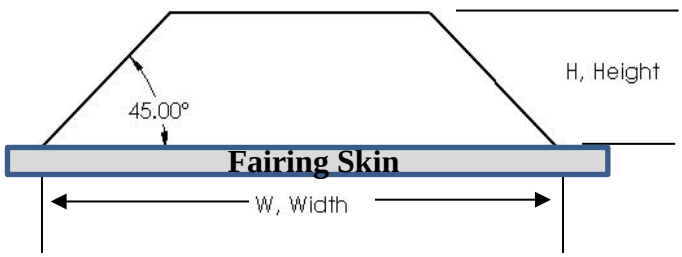

Figure 67. Rib core profile.

A model of the RPS was developed and imported into Abaqus CAE. It was decided that the reactions would be at the roll harness mounting locations. The primary load reactor would be from the potted inserts located at each harness mounting point as shown in Figure 68. These reaction points were fully encastred to simulate a roll harness attached to a rider on a seat while allowing for the roll structure to deform around the rider in the event of a crash. This boundary case was manufactured as two rows of three potted inserts on each side, to which a steel plate is bolted and epoxied onto the rib face of the primary roll structure. The specified vertical impact load was applied at the top of the roll bar with a distributed load. Tangential surface traction and normal pressure loads over an area 2 inches wide by 3 inches deep were chosen to adequately simulate a crash scenario in which the vehicle impacted a large blunt object. The horizontal load was applied at the location of the rider's shoulders. Using quadratic quadrilateral conventional shell elements, a convergence study was conducted for the isolated rollbar and entire roll structure, as shown in Figure 69.

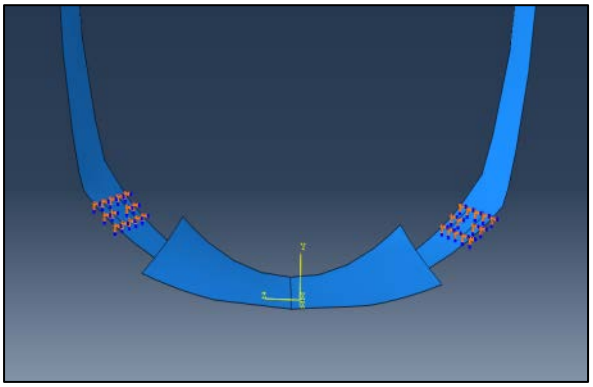

Figure 68. Boundary conditions applied to rollbar.

Table 38 shows a summary of the results for the analyses, including the maximum deflections in the direction that the load was applied, the maximum reaction forces at the boundary conditions, and the maximum compression and tension failure indices on the laminate. Figure 70 shows the isolated rollbars deflection for each loading case and Figure 71 shows the deflection with each loading case on the entire RPS.

Table 38. Table of major results from the analyses.

	Load Case	Deflection (in)	RF max (lbf)	Ply Max Failure Index (Tens.)	Ply Max Failure Index (Comp.)	Pass / Fail
Rollbar Only	Horizontal	-0.971	150.4	0.474	0.529	Pass
	Vertical	-2.778	487.5	0.846	0.559	Fail
Full Roll Structure	Horizontal	-0.942	205.0	0.438	0.478	Pass
	Vertical	1.506	302.0	0.571	0.826	Pass

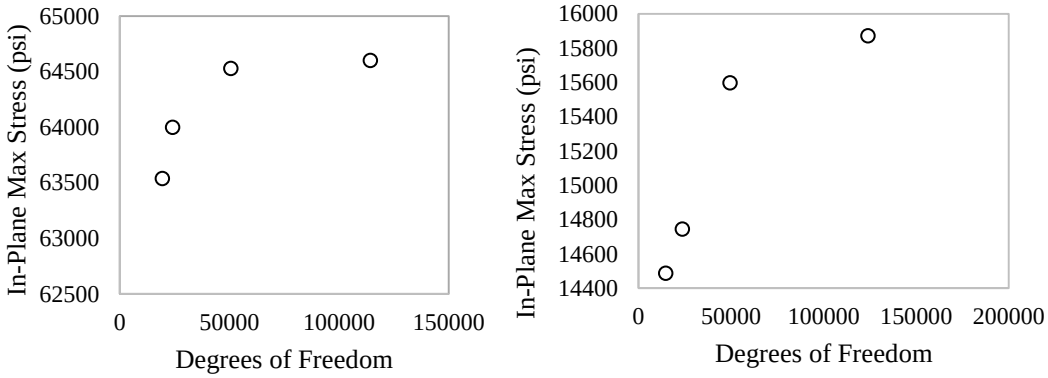

Figure 69. Convergence plots for the roll bar only (left) and roll structure (right)

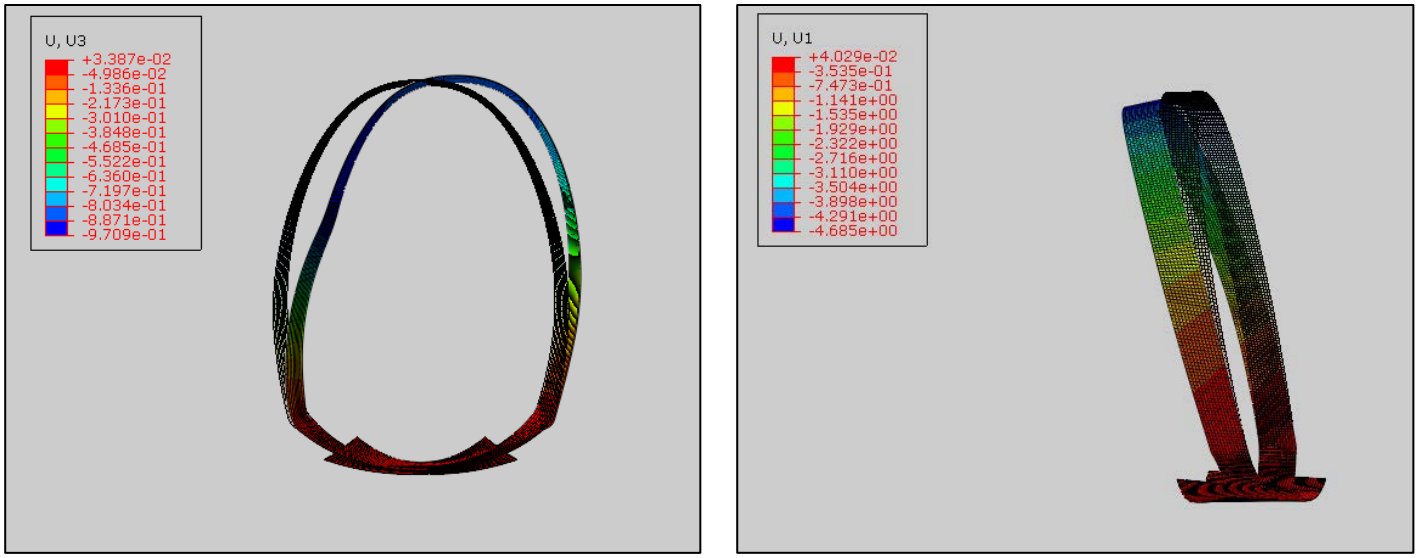

Figure 70. Deflection plots with deformed shapes for the roll bar only. Horizontal (left) and Vertical (right).

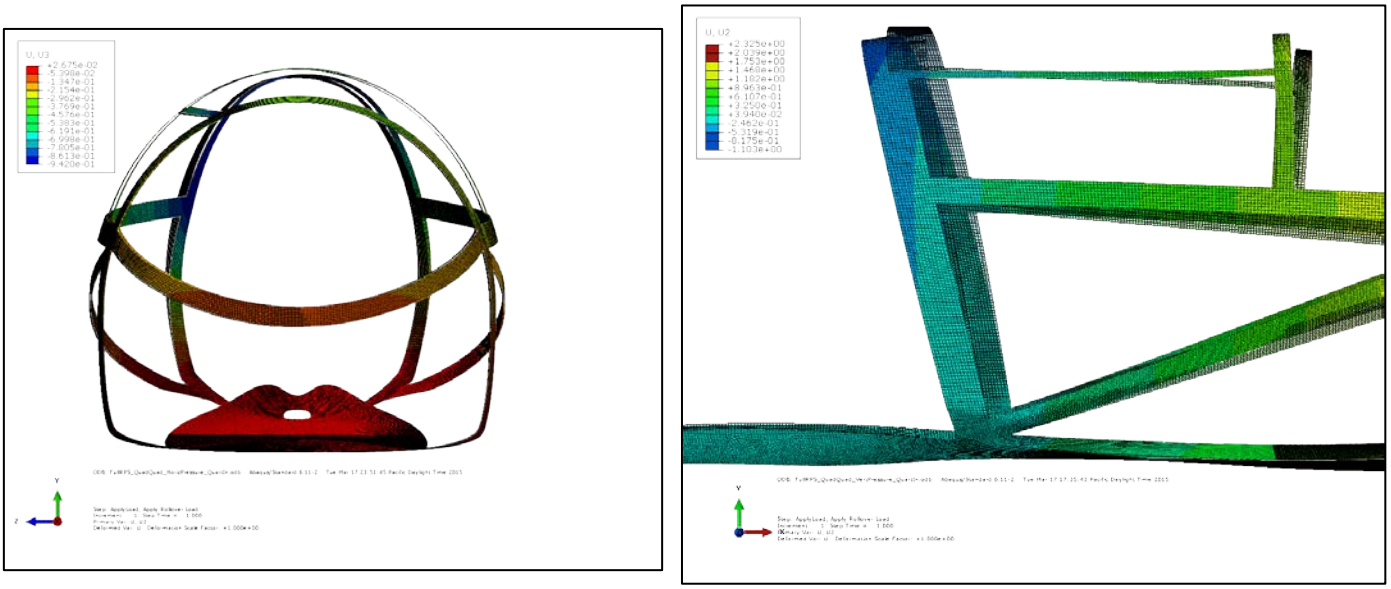

Figure 71. Full roll structure deformed shapes for the vertical load (right) and side load (left).

When isolated for this analysis, the primary rollbar is significantly less stiff than the past years' rollbars and does not meet the required loading specifications. This is likely due to reduced layup schedule used this year, as well as the more realistic boundary conditions used in comparison with the past strategy of fully constraining the lower 20-30% of the rollbar with an encastre boundary condition. However, the required specifications are met when the full ribbed RPS structure is analyzed. Therefore, to verify the FEA model, a mockup of the isolated roll bar will be created and that FEA model will be verified. Because the same boundary conditions and loading cases will be used, this will then verify the roll-over system.

Sub-Frame/Fairing Integration

One of the critical aspects of the semi-monocoque design was the proper integration of the steel components and the carbon fiber tub. The developmental testing of the potted inserts provided a conservative baseline for the load carrying capacity of each insert. However, because of the difficulty in modeling the carbon to steel interface, the team decided upon a factor of safety of at least two for a pullout failure on the inserts. This decision was made with the goal of maintaining the structural integrity of the critical members of the vehicle under any unexpected loading conditions. Figure 72 below shows the selected potted insert layout, which ensured this criteria was met or exceeded.

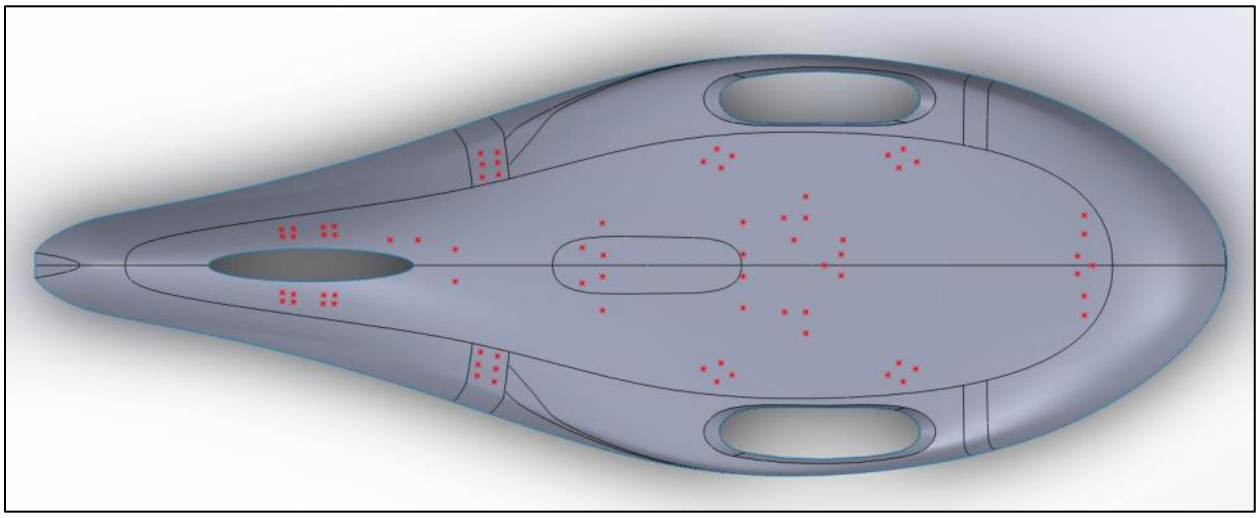

Figure 72. Potted insert locations.

Geometry Selection

Sweet Phoenix's layout, steering, and rider position geometries were determined using analyses outlined in Chapter 3. The fairing geometry was driven by these dimensions, in addition to

surface modeling concerns and aerodynamics testing. The resulting vehicle geometries are stated at the end of in their respective sections, and again in Table 39 below.

Table 39. Summary of important geometry descriptors.

Parameter	Value	Units	Parameter	Value	Units
Wheelbase	43.0	in	Fairing Width	28.0	in
Track Width	28.0	in	Fairing Height	38.7	in
Turning Radius	20.0	ft	Fairing Length	103.5	in
Front Tire Dia.	20.0	in	Rear Tire Dia.	27.5	in
Rider Hip Angle (approx.)	122	deg	Steering Ratio	3.0:1	-

Components

Wheels

The front wheels are built around 20mm thru-axle mountain bike hubs. This large axle diameter accommodates the increased stress of mounting only one side of the wheel to the steering knuckles. In contrast to Aria, which relied on custom-machined, hollow aluminum shoulder bolts for axles, Sweet Phoenix uses Catrike 20mm thru-axles. The decision to purchase instead of fabricate the axles saved time and allowed for faster wheel changes.

The rear wheel selection was driven by the drivetrain requirement of a left-hand drive hub. By coincidence, the team found a suitable wheel buried in their parts cache. This wheel was used to reduce production time and costs.

Rear Dropouts

The dropouts used in Sweet Phoenix (Figure 74) were chosen for several reasons. A horizontal orientation was required in order to adjust chain tension of the single-speed secondary drive chain. The modular bolted design included very simple aluminum dropouts bolted to a more complex steel base. New dropouts had to be machined in order to accommodate the BMX hub's large axle diameter, but the 2D shape and simple attachment made this task quite simple.

Figure 73. Rear dropouts, as purchased. The lighter colored aluminum pieces were replaced with custom parts parts with altered slot dimensions and orientations.

The steel base allowed welding the dropout sub-frame members directly to the dropouts, which was chosen as the easiest fabrication method.

Drivetrain

Each drivetrain component was chosen for various reasons, depending on its location and function. The selected components and associated reasoning are summarized in Table 40.

Table 40. Drivetrain selection summary.

Component	Selected Product	Deciding Factor	Advantage of selection
Crankset	FSA Carbon Track 165mm	Cost, weight, clearance	Already owned by team, low weight, short crank arms helped foot clearance
Chainring	Unknown 52t, 42t	Cost	Already owned by team
Cassette	SRAM 11-21, verify	Gear ratio step, size	Close ratios provided many cadence options for different rider preferences, small diameter fit below riders' legs
Derailleur	SRAM X9, short cage	Fairing clearance	Short cage derailleur fit between fairing floor and riders' legs
Mid-drive hub	WTB	Cost	Already owned by team
Output gear	Unknown, 21t	Size, machinability	Solid gear allowed machining 6-bolt hole pattern to mount to mid-drive hub
Rear hub	Unknown	Left-hand drive	LH drive enabled mid-drive design to function, already owned by team
Shifter	SRAM X9 Gripshift	Ergonomics, Cost	Grip shifter compatible with steering wheel design, already owned by team

Brakes

Cable-actuated Avid BB7 brake calipers were selected to allow pairing two calipers to one lever. Hydraulic-actuated calipers, while more powerful, cannot be paired as easily since the master cylinder built into the brake lever cannot handle twice the amount of hydraulic fluid required by two calipers. This would have required the fabrication of a custom brake lever and master cylinder, which was deemed beyond the team's abilities. To execute the paired caliper design, a Problem Solvers Cable Doubler 1:2 was used, which allowed one input cable to pull on two output cables. A Pyramid Tech locking brake lever was chosen to allow use of the brakes as a parking brake.

Seat and Seat Adjustment

The seat and seat mounting system was derived as seen in the design development section. The seat mounting system allowed adjustable travel to accommodate riders in the range of 5'5" to 6'2" by using sliding rails with indexing pins. A total of six usable rider positions were

established along the aluminum rails and quick adjustment between them was allowed through the use of Delrin® bushings to act as sliders.

The seat was designed as a bucket seat with no ergonomic lumbar support to allow for customization by each rider. As per ASME HPVC rules, a four point harness was used to secure the rider in the event of a crash. A detailed analysis of the roll-over protection system can be seen in the RPS analysis section.

Sub-frame

The sub-frame was designed to meet the target stiffness while minimizing the weight of each mount. Initially, the sub-frame was designed with two supporting struts per mount, which allowed for adequate strength and minimum weight. After construction, testing revealed that to achieve the desired stiffness and prevent core failure at the mounting points, a third strut had to be added to the mounts. The final mounts are shown in Figure 74.

Figure 74. Triangulated headtube mounts.

Potted Inserts

Two different versions of potted inserts were used for the sub-frame mounting locations. Marketing Master's AEP1036-3 (#10-32 bolts) Torlon® composite potted-in inserts were used for the majority of the inserts throughout the tub due to their weight advantages over steel. Genuine Aircraft Hardware Co.'s NAS1832-3 (#10-32) carbon steel inserts were used as well.

Cost Analysis

The Cal Poly Mechanical Engineering Department supplied the HPVT with a budget of $6000 for the 2015 vehicle. As the spending of this senior project team coincided with practically all of the club's expenses, it was decided to set the $6000 club budget as the senior project's maximum spending limit. The cost breakdown shown in Table 41 summarizes the construction costs for the final vehicle. However, this does not include sponsorships and donations from external sources. For example, the HDU foam for the fairing molds was donated from Coastal Enterprises, which would cost roughly $3000 if purchased. Without the additional resources and supplies, the team would have far exceeded the allocated funds for the club.

Table 41. Cost breakdown for construction of a single prototype.

	Item	Description	Quantity	Cost
Composite Tooling Supplies	Duratec Primer/Sealer	1 gallon can	4	$400.00
	Gorilla Glue	36 ounce bottle	5	$150.00
	Sandpaper	120, 220, 300, 400, 600 grit packs	10	$50.00
	Bondo Body Filler	1 gallon can w/ hardener	1	$22.00
	Frekote Mold Release/Sealer		1	$150.00
	Wood Dolly	Lumber, casters, wood screws	--	$150.00
Layup Materials	Carbon Fiber, Fiberglass, Kevlar	(150 yd^2)	1	$1,700.00
	West Systems Resin/Hardener	2.5 gallon resin/1 gallon hardener	1	$500.00
	Vacuum Bagging Material	Perf, Peel Ply, Breather, Vac Bag	1	$500.00
	Sealant Tape	25 ft. rolls	10	$80.00
	Core Material	Honeycomb & Divinycell	--	$200.00
Layup Supplies	Scissors		5	$50.00
	MDF Sheets	For layups	2	$50.00
	Gloves	100 per box	6	$60.00
	Respirators	Including replacement filters	10	$200.00
	Sharpies	2 per pack	3	$11.00
Frame & Prototype Materials	Raw Materials	Bar, round, and tube stock	--	$300.00
	Bicycle Components	Wheels, tubes, tires, chains, etc.	--	$500.00
	Epoxies/Adhesives	Loctite 5-minute, etc.	--	$150.00
	Paint	Aerosol cans	5	$50.00
	Windshield Materials	Polycarbonate & PETG	--	$100.00
	Hardware	Nuts, bolts, wiring, etc.	--	$300.00
			Total	$5,673.00

Hazard Analysis

Vehicle Occupants

Rider safety is of utmost concern, and in the case of a crash (i.e. rollover), a four point harness installed in Sweet Phoenix keeps the rider strapped into the seat to prevent them from being ejected out or injuring themselves on the steering wheel. There is also a plastic guard installed above the mid-drive sprockets that prevents the rider from injuring themselves with the chain or sprocket itself. Furthermore, to prevent even the rollover from happening, a sensor was built and installed to detect and alert the rider if the HPV is being pushed close to tipping.

Bystanders

Compared to a traditional upright bicycle, the trike design is exceedingly safer for bystanders. The stability in having three points of contact at all times means that the likeliness of the rider losing control and injuring bystanders is greatly reduced. In low speed conditions, the rider can quickly and safely come to a complete stop if someone were to step out in front of the trike without needing to consider deploying a landing gear or other form of assisting device. In high speed conditions, the most common crashes for a bicycle are low siding in a corner or harmonic instability (i.e. speed wobbles), both of which are mitigated by having three wheels in contact with the ground at all times. In addition, the head/tail lights, reflectors, bell and fading in/out under glow lighting makes Sweet Phoenix more apparent to pedestrians and motorists when ridden at night.

Vehicle Builders

Alongside designing to ensure safety for the rider and bystanders, much care was put into the fabrication of the final vehicle as well as its prototype and other related parts to ensure the safety of the builders. Numerous hazardous chemicals, vapors, and dust particles were used and present during the construction process and so anyone who assisted in manufacturing was required to wear safety glasses as well as any other appropriate forms of safety (welding helmets/gloves/aprons, respirators, safety masks, safety gloves, etc.) that abided by OSHA (Occupational Safety and Health Administration) and Cal Poly Machine Shop standards. With various machinery being used, a Red-Cross First Aid/CPR/AED certified shop technician club member was always present to provide any form of support whether it be technical or medical. Finally, Material Safety Data Sheets (MSDS) were always made available and kept up to date for all materials and chemicals used.

Chapter 5: Product Realization and Manufacturing

Mold Tool Design

As previously discussed, the method for constructing the molds for Sweet Phoenix was determined to be most effectively done by using female high density urethane (HDU) foam tools with a wet layup process. The Human Powered Vehicle club has a well-established method that was further used and refined for Sweet Phoenix's construction. This method, along with the mold design will be described fully in this section.

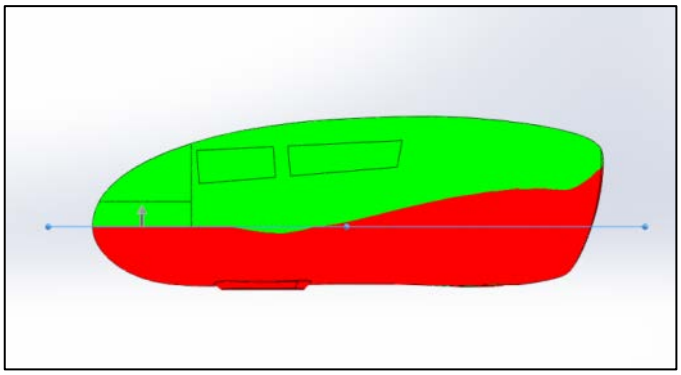

Figure 75. Draft analysis on the fairing. To pull from a female mold at the proposed parting plane, one side must be green and the other red. The shape of the tail requires a left-right mold for the top.

In the past, the HPV team has designed their molds to be two or more parts (Figure 76), with generally left and right halves that are seamed together down the whole length of the bike. For a monocoque construction such as the one chosen for Sweet Phoenix, the traditional tool layout posed structural concerns stemming from a stressed seam along the bottom of the vehicle. The bottom "tub" of the vehicle would experience the largest loads during riding, with multiple sub-frame members along the centerline of the vehicle. These locations would be subjected to high stress; something that the team was not sure would be favorable at a seam. Ideally, the vehicle would be constructed seamlessly over a male plug or with a "block" mold design, however, this provided additional unknowns for the team. Therefore, it was decided that a top-bottom mold design would be pursued to create a seamless tub for structural integrity and sub-frame locational accuracy.

Figure 76. Traditional Cal Poly HPV left / right half molds.

A top-bottom mold design presented numerous challenges that the team had never had to deal with. Firstly, the seam between the top and bottom molds had to be placed at a position where it divided the shell into two sections at the apex of a curve (Figure 75). This allows the tools to be cut by a 3 axis CNC machine rather than requiring 5 axis features (capabilities the Cal Poly machine shop does not have). Because of the shape of the shell, the tub allowed this without problems, but the top half required splitting into left and right halves dues to the angle of the tail (Figure 77). This was deemed to be an inconsequential decision, as the top half of the vehicle carried significantly less stress as determined by the FEA models. Additionally, it reduced the depth of each mold, allowing easier access to features at the very top of the vehicle. Splitting the top into left and right halves, however, provided a new sense of complexity to the manufacturing, as two seams, instead of the traditional one seam, had to line up.

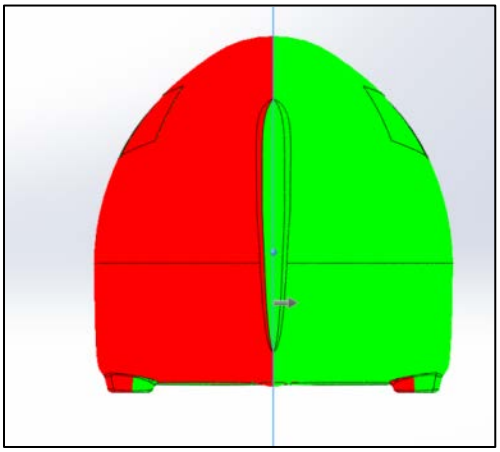

Figure 77. Draft analysis of the fairing for the top parting line. The tail required a parting line for the top mold at the centerline of the vehicle, adding another seam.

Figure 78. The ShopBot CNC router at the Cal Poly Hanger. Molds are traditionally machined with the shopbot and are subject to its limitations.

Sources of misalignment between the machined molds typically come from inaccuracies when cutting the tools on the school ShopBot CNC Router (Figure 78) and when finishing the molds by hand. Firstly, the ShopBot's lack of rigidity proves to be a problem consistently and secondly, the lower densities of the HDU foam traditionally used (4, 6, & 8 lb density) allow for easy "oversanding" of the molds. As both of these problems originated from the ShopBot's limitations, the team sought alternative options to machine the molds. C&D Zodiac Aerospace in Santa Maria, CA generously offered to professionally machine the tools for the team, thus offering a means to mitigate both problems.

The final consideration for the mold design was to ensure proper draft angle to prevent the parts from locking in the tool after curing. Draft angle, as its name implies, is the overall taper angle

that is normal to the parting line. The HPV team has traditionally built in a draft angle of 1-3° depending on the depth. For this mold, a 3° draft angle was built in for anything greater than 3 inches below the parting line. An exploded view of the final tool design can be seen in Figure 80, with the subsequent draft angle analysis seen in Figure 79.

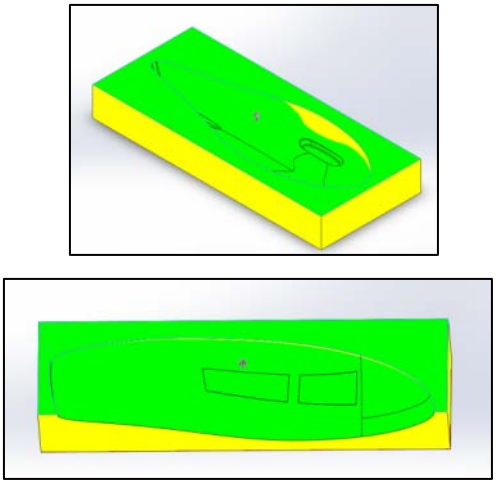

Figure 79. Mold draft angles. Yellow indicates a draft less than 3 degrees but greater than 0 degrees.

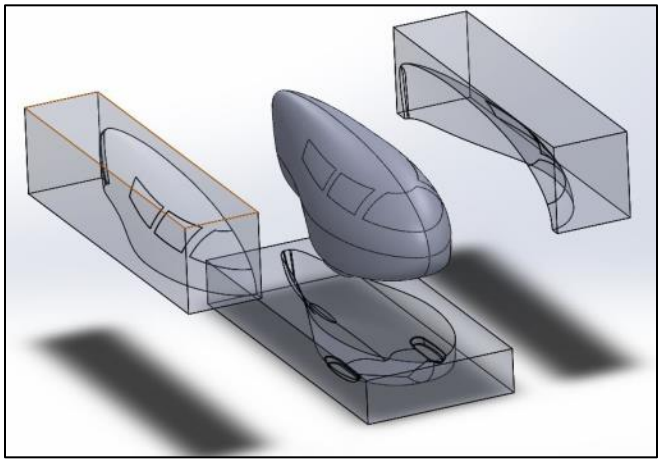

Figure 80. Final Tool design.

Other mold improvements built into the design were dowel alignment holes and windshield location bosses. The dowel alignment holes allowed a frame alignment jig to be made with specified distances from these holes to hold higher precision on the sub-frame (see Alignment Jig section). The windshield bosses were offset 0.100” from the surface of the mold and created an inset in the final part where the windshields could be cut out from, instead of measuring from the nose. Both of these tool improvements allowed for higher precision of features on the final part.

Construction & Finishing

The final tool density was chosen to be 10 lb HDU foam. This was thought to provide the best machinability and durability, while still keeping the overall mold weight in mind. To prepare the tool stock, the team used Gorilla Glue to form three large blocks to the size of the proposed tools out of 1”-3” thick 4’ x 8’ 10 lb density sheets provided as a donation by Coastal Enterprises. Gorilla Glue was used as it provided a similar cured density to the foam, allowing for easy sanding later on. The tools were put together three sheets at a time, and steel angle iron was used to provide compression (Figure 81).

Figure 81. Gluing of foam to create stock for tools. The foam was laid up in blocks of three (left) and guerilla glue was used to adhere the layers. Weight was used to minimize separation between layers of foam while curing.

The tools were cut by Zodiac Aerospace during Fall quarter of 2014 and were delivered to the team at the beginning of winter break. The tools were cut on a 5-axis gantry router (Figure 82), which provided much higher precision and surface finish than possible on the school ShopBot. Once the team had possession of the tools, finishing and preparation still had to be done to prepare for layups.

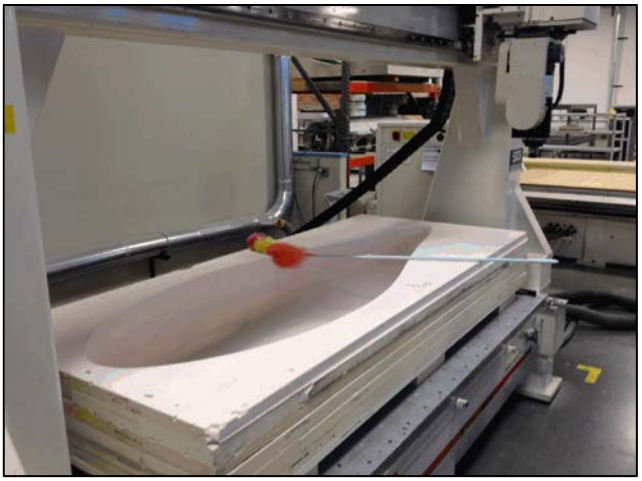

Figure 82. Machining setup at C&D Zodiac Aerospace in Santa Maria, CA.

The first step in finishing the molds was to light sand the bare foam and fill any large flaws on the mold surface (Figure 83). Bondo® Lightweight Filler was used to fill any low spots, as it has sanding characteristics close to the Duratec surface to be applied after. The team made the mistake of sanding the Bondo® to be flush with the surface before applying a Duratec layer, easily burning through the surrounding foam in the process and creating new low spots. Once noticed, sanding was halted until a layer of Duratec was applied. The seams between layers of foam proved the toughest to make flush with the surface, requiring many subsequent Bondo layers.

Figure 84. Initial foam sanding and Bondo® application before spraying Duratec primer.

After the pre-sanding, Duratec mold sealer was applied to each of the molds with a spray gun (Figure 84) to seal the pores of the foam and allow the Duratec primer to lay on top of the surface instead of soaking into the mold. Two layers of mold sealer were applied and allowed to cure overnight before Duratec primer was applied. After the sealer had cured, Duratec EZ Sand Primer was combined with Duratec Thinner and sprayed onto the mold via a paint spray gun at 45 psi (Figure 84). The primer was applied to the surface of the mold in layers dyed with alternating colors of paint dye and allowed to cure for two hours before applying a second layer. Initially, one layer was applied per spraying round, however, the team decided after further investigation of the instructions that up to three layers could be applied before allowing the primer to cure overnight.

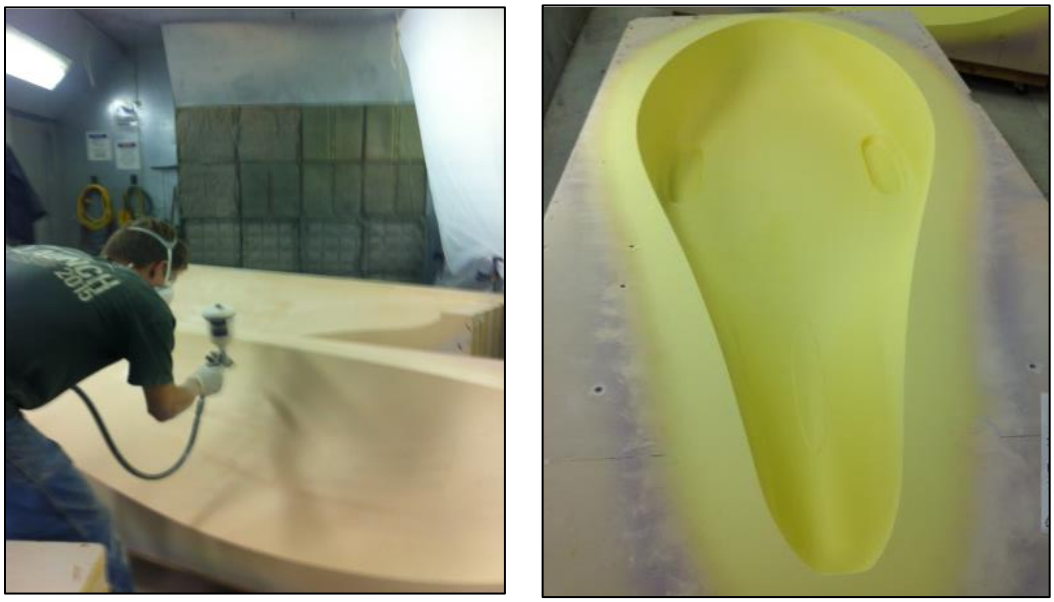

Figure 83. Molds were sprayed with Duratec Sealer and EZ Sand Primer using a paint spray gun.

Once the primer had cured, sanding of the surface with 220 grit sandpaper commenced to knock down any blemishes, and Bondo® was used to fill low spots. Overall, 3 gallons of Duratec EZ Sand Primer were used to cover the molds before high grit sanding took place. Once the team was satisfied with the quality of the surface with respect to blemishes, higher grit sanding was done to polish the surface. The order of sanding was as follows: 120, 220, 300, 400, and 600 grit with each layer above 220 being wet-sanded. “Scratch coats” of Bondo were applied to fill any

pin-holes found during these steps to ensure a smooth surface finish and adequate release of the parts. Finally, the molds were cleaned with Acetone and sent to be prepared for layups. The final surface finish can be seen in Figure 85, where the minimal surface defects and polished surface provide a high quality surface finish on the final part.

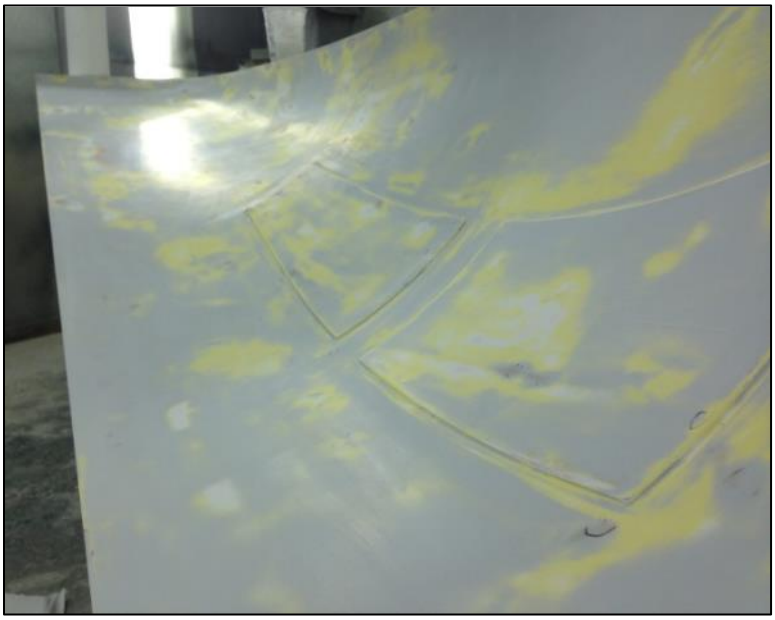

Figure 85. Final surface finish of the molds.

The final step in mold construction was to apply the mold sealer and mold release to the surface. Arguably, this is the most important step in the process, as locking a part in the mold will destroy the tool and negate any work done to make the mold surface. Chemlease mold sealer was first applied to the Duratec surface using cloth rags, ensuring any surface that carbon would touch was coated. A total of five layers of mold sealer were applied to each surface, with an hour waiting period between applications. Next, 10 layers of Frekote 700-NC were applied to the same surfaces as the mold sealer. This provided a base layer of mold release that could be supplemented before each layup. Finally, one layer of Axle F57-NC was applied to the mold surface. After the molds had been released, they were covered and only water could touch them to be cleaned as any contact with a solvent would negate the mold release and require the process to be repeated. Before each layup, three layers of Frekote and one layer of Axle were applied to ensure release of the parts.

Once the molds were finalized, they required minimal care throughout the course of layups. Maintenance included fixing dents or scratches, scraping cured resin off the surface, and reapplying release where needed. Overall, molds took about 500 man hours, or $1/5^{th}$ of the total manufacturing hours of the project, but ensured high quality finished parts that the team was proud of.

Fairing Construction

Following the completion of the molds, the layups and post-bonds began. The team made extensive use of their composite layup knowledge, specifically that pertaining to wet-layups, which was the method of choice due their experiences in past years. Prior to applying the mold release, 20 mil. PVC tape was placed around the perimeter of the molds just below the flange as well as along the door outlines as shown in Figure 86. This provided a recessed border along all seams, accounting for the carbon fiber strips used in bonding the three parts together. The resulting post-bonded seam was thus flush with the outer skin. In the case of the door, the tape border was used to incorporate an inset flange that the door would rest on, creating a smooth surface along the length of the vehicle.

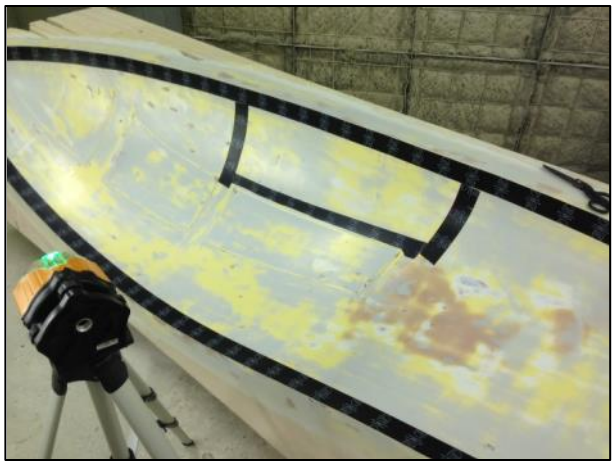

Figure 87. Layup preparation with 20 Mil. Tape.

Figure 86. Cutting carbon fiber to size.

For the most part, the general layup procedure was the same throughout the construction of the fairing and will therefore only be outlined once.

<u>Layup Procedure</u>

1. Carbon fiber pieces cut from roll to required sizes (Figure 87)
2. Bagging materials (Peel Ply, perforated release film, breather fabric, vacuum bag) cut to corresponding sizes to fit within vacuum bag sealant tape
3. Vacuum bag sealant tape placed around part, with adequate room for flange and vacuum parts
4. All carbon weighed and resin/hardener ratio calculated based on total weight of fabric (using West

Figure 88. Wetting out carbon fiber.

Systems 105 epoxy resin)

   a. West Systems 206 Slow Hardener, resin to hardener weight ratio - 5:1
   b. West Systems 209 Extra Slow Hardener, resin to hardener weight ratio - 3.5:1

5. Resin & hardener mixed according to proper ratio
6. Carbon plies placed between 10 mil. plastic sheeting
7. Top sheet of plastic pulled back and resin mixture spread evenly over carbon
8. Top sheet laid over wet carbon and plastic squeegees used to evenly distribute resin, known as “wetting out” (Figure 88)
9. After spreading of resin within plastic, excess resin pulled out of plies
10. Carbon pieces cut out of plastic and remaining plastic removed from front and back
11. Wet carbon placed in molds according to layup schedules (Figure 89)
    a. Working times for epoxy resins contained in technical data sheets (Appendix D)
12. Single layer of each dry fabric (Figure 90) placed over wet carbon
    a. Peel Ply
    b. Perforated release film (avoid overlapping)
    c. Breather fabric
    d. Vacuum Bag (with excess beyond sealant tape)
13. Vacuum bag securely adhered to sealant tape with vacuum line passing from tool side (on flange) to vacuum pump (ensured no air gaps existed)
14. Vacuum pump turned on
15. Squeegee or quarter used to press in tight concave corners to avoid bridging

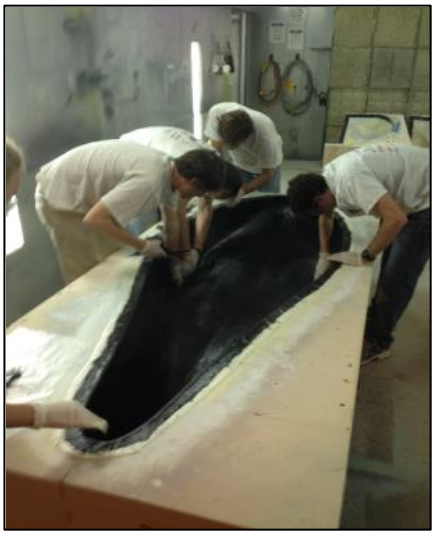

Figure 89. Placing carbon in tub mold.

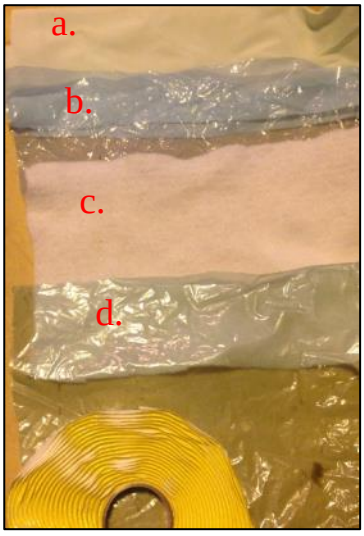

Figure 90. Layup bagging materials & sealant tape.

This proven methodology was utilized throughout the fairing construction to ensure consistency from part to part. Following the completion of the three fairing skins, the next step involved adding core material to create a stiffened sandwich plate structure. The process for the post-bonds was essentially the same as the aforementioned layup procedure, with the addition of core material (divinycell or honeycomb) between the existing skin and the new plies of carbon fiber. In order to ensure accurate geometry and increase the chances of alignment between fairing parts, the post-bonds were performed with the existing skin placed in the respective mold. Prior to laying up the fabric, the core material was laid out on the part and adhered to the skin with spray adhesive to avoid movement during the layup process. The placement of the ribbing was important as alignment across the seams was critical. In addition, the carbon sizes were double-checked in the part to ensure that the fabric extended beyond the core material so that no core edges were exposed, as this can drastically decrease the structural properties of the panels. As seen in Figure 91, the edges of all core material were beveled to approximately 45° to mitigate bridging of the carbon fiber.

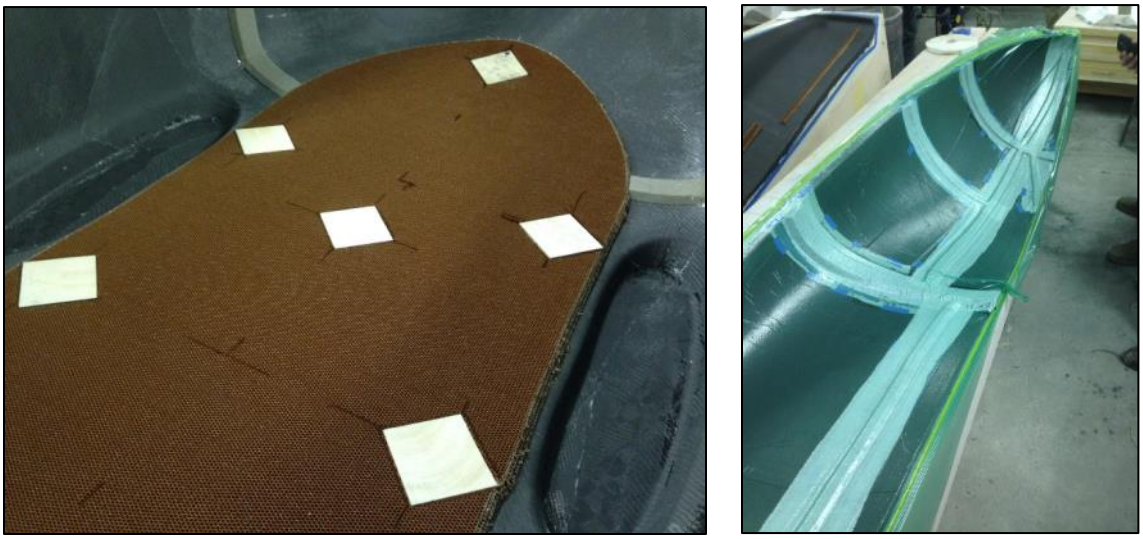

Figure 91. Tub core material layout with honeycomb & end-grain balsa (at potted insert locations) on the left. Completed post-bond layup for one upper half of fairing on right.

With the post-bonds completed, the final step involved seaming the three fairing parts together. The flanges were removed from all parts with a Dremel® rotary tool and the mating core sections sanded flush. The top two halves were joined first since the tub was needed for potted insert installation and sub-frame and construction. The seaming process began by aligning the halves over the tub mold and using 2”x2” squares of 3K carbon fiber covered in 5-minute epoxy as alignment tabs on the inside of the fairing to temporarily tack the parts together. Once full cure of the epoxy was reached, the parts were then seamed down the center with two stacked

four inch wide strips of carbon that spanned the entire length of the fairing. Rather than employing the standard vacuum bagging procedure, the wet carbon was covered directly with Saran wrap and taped tight across the seam as shown in Figure 92. This technique was introduced by Cal Poly Shop Technician, George Leone, and saved much time and effort as attempts in previous years to pull vacuums on open seams were relatively unsuccessful due to the permeability of the carbon fiber skin. The method provided adequate pressure across the seam and resulted in a workable surface for finishing and painting. The windshield cutouts and wheel fairings were cut out at this point for easier access when working.

After the outer seam had fully cured, it was necessary to layup three additional strips of carbon fiber ([0/45/0]) along the inside of the seam and add carbon caps over the adjoining ribs. These additional plies would increase the strength and stiffness across the major stress concentrations that exist at both seams. The layup schedule for the rib caps was matched to the post-bond layup for the corresponding rib (i.e. [0/45/0/45/0] for rollbar with 5” x 5” carbon squares). In an attempt to achieve better resin content for the inner seam, it was decided to utilize a vacuum for the layup. To try and minimize air leaks through the outside of the seam, the vacuum bag was placed on both the inside and outside as shown in Figure 92. This resulted in a decent vacuum pull and provided adequate pressure to extract some of the resin.

Figure 92. Saran wrap technique for seaming (left) and secondary post-bond inside the fairing with vacuum pump (right).

Lastly, the outer seams were patched with epoxy resin and Bondo and sanded to form a smooth transition across all seams in preparation for painting. The completed inner and outer seams with core reinforcements and windshield cutouts are shown in Figure 93.

Figure 93. Completed inner seams (left). Outer seam patching and sanding (center). Completed seam with paint (right).

Alignment Jig Construction

In order to produce the sub-frame components within desired tolerances, an alignment jig was constructed. Of utmost concern were the location and alignment of the four main geometry hard points – the rear hub, left and right headtubes, and bottom bracket. As part of the initial fairing mold machining process, four holes were machined in the top flange and durable plaster inserts placed at each corner of the bottom fairing mold. Dowel pins were press-fit into each of these holes, both to anchor the alignment jig and provide datum locations amongst the otherwise organic fairing curves.

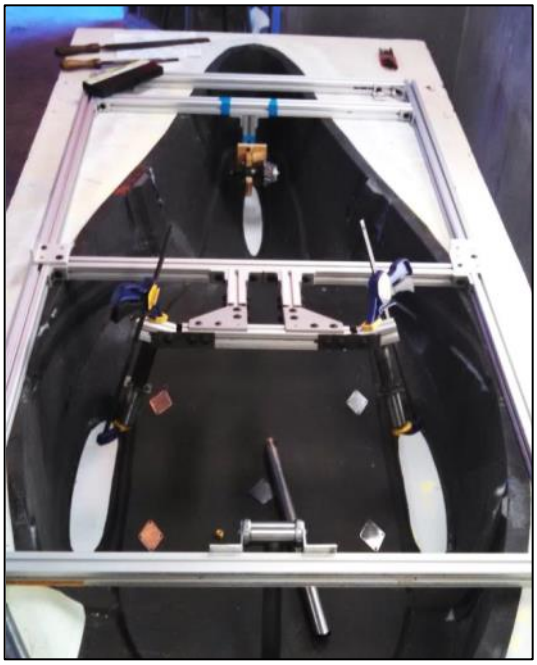

Figure 94. Alignment jig secured to bottom fairing mold, with all four hard points in place.

The jig was primarily a frame of extruded aluminum T-slot bars, known as 80/20, fastened together with bolts and a combination of stock and custom brackets. The 80/20 bars were cut to length from leftover stock made available after an old Cal Poly ME department project. They were then joined with stock 80/20 brackets into a rectangular datum frame with three additional cross braces for the rear dropout, headtubes, and bottom bracket. The stock brackets were loaned by Allen Capatina, an AERO graduate student who had used them for another

previous project. The rough frame was then placed on the dowel pins and aligned with the mold to form four datum edges.

Custom brackets were needed to locate and orient each hard point. First, a short 80/20 bar was extended down from the rear-most cross brace. A wooden bracket with a pair of semi-circular clamping halves was constructed to hold the hub's shell securely. Since the bracket was made from asymmetric scrap materials, it was measured to allow the hub to be centered within the fairing. The hub was then clamped into the wooden bracket, which was bolted onto the vertically oriented 80/20 bar. This rear assembly was then located and aligned with respect to the datum frame with a combination of plumb bob, measuring tape, and electronic angle finder.

The headtubes were then located and aligned. Each headtube required two inclinations – caster and kingpin. The inclined caster plane was defined from the middle cross brace by using short sections of 80/20 bar and custom rotation brackets cut from sheet metal (Figure 95). From this plane, each kingpin plane was defined in a similar manner off of the right and left sides of the caster plane. At this point, one length of 80/20 bar was aligned normal to each headtube axis. Next, these aligned bars were located with respect to the datum frame, in order to locate the headtubes.

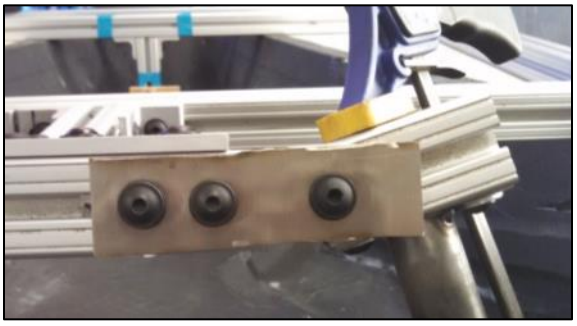

Figure 96. Custom sheet metal rotation bracket on the left headtube.

The bottom surface of the aligned bars were not low enough to directly clamp the headtubes, so normal extensions were fabricated by welding end plates onto the ends of scrap tubing. The upper endplate was centered on the aligned bar, and the lower endplate had a circular recess to ensure the headtube was reliably located concentric to its axis. Finally, the headtube locations were checked numerous times with iterative measurements of caster angle, kingpin angle, and headtube location. The headtubes were then clamped into their locator recesses, as shown in Figure 96.

Figure 95. Left axial headtube extension, with headtube clamped in place.

The bottom bracket shell was located by first installing a plastic

dummy crank spindle. Two right-angle brackets were then machined to locate the bottom bracket vertically. These brackets were bolted to the front crossbar on the datum frame, and the dummy spindle was bolted onto the brackets. Finally, the bracket assembly was located within the datum plane.

This alignment jig was quite successful, especially when compared to previous years' production tolerances. The four hard points were located and aligned to within 0.07 in. and 0.5°, respectively. This is at least twice as accurate as the 2014 frame's tolerances of 0.15 in. and 2°.

The only major flaw in the jig's use was the difficulty in defining the dual-axis inclination of the headtubes. The kingpin angle was set with a rotation bracket off of the caster plane, not the horizontal datum plane. This coupling effect meant the angle swept by the kingpin rotation bracket was not equal to the actual headtube axis' kingpin angle. To work around this issue, the headtube itself had to be measured with an electronic angle finder. The accuracy of the final sub-frame members was not compromised by this issue, but the iterative measurement required made for quite a tedious process.

Sub-Frame Construction

With the alignment jig constructed and the critical member locations (bottom bracket, head tubes, rear dropouts) verified on the tub mold, the next step was to manufacture the bolt-in steel sub-frame components. All sub-frame members were designed as mitered and welded low carbon steel tubing in order to simplify the fabrication of the components. The primary method for mitering the tubes was an angle grinder and file. An online tube coping calculator[11] was used for creating 2-D profiles based on the angle between mating tubes and the tube diameters. The other option, which was used for a few of the more difficult miters (knuckle mounts) was a tube miter fixture, provided by Cal Poly's Frame Builders Club as seen in Figure 97. The required hole patterns for each baseplate were drilled in 3/32" plate steel and then the plates were cut to size. The tubes were then fit to match the baseplate locations and the adjoining member (i.e. head tube, bottom bracket) as seen in Figure 98. The process was tedious, but the attention to detail ensured the mating joints were

Figure 97. Cutting knuckle mount on tube miter fixture.

tight with minimal gaps. Next, the joints that were elevated off the tub floor were tack welded in place. However, due to the contact between the baseplates and the carbon tub, it was decided to tack the tube to the baseplate with a drop of 5-minute epoxy, which would then be taken off prior to full welding.

Figure 98. Knuckle mount alignment (left). Full welded knuckle mount and bottom bracket mount (right).

The potted inserts were installed following completion of the sub-frame members. Each baseplate was used as a template to transfer the hole pattern to the tub floor. The procedure outlined in Figure 99 was followed for each install, making certain to bore out excess core beneath the top facing skin. Figure 99 below outlines the procedure.

Figure 99. Potted insert installation procedure.

Seat and Seat Adjustment Mechanism Manufacturing

To manufacture the seat, a male tool was machined from high density urethane foam and finished in a similar manner to the fairing tools. Due to the lower quality of foam used and low availability of Duratec Primer, Bondo® was used as the primary mold surface. In efforts to speed up the process, the team also employed a method known as "double bagging" as seen in Figure 100. Double bagging the mold involved pulling an initial vacuum over the mold surface, thereby using the initial vacuum bag as a mold surface. The material was laid directly over the vacuum bag and then a subsequent vacuum bag was pulled over the entire assembly.

This method allows for rapid mold processing, requiring a much lower quality of mold surface to release the part and create a vacuum seal. The surface finish provided by the vacuum bag is of medium quality, showing any creases or folds in the surface bag, and showing any imperfections in the mold surface. Additionally, the process requires a male mold with gentle curves to ensure the vacuum bag pulls over the surface without pleats.

In an effort to minimize material costs, carbon fiber was only used for the outer layer of the seat, with aluminumized fiberglass used for the inner layers of the layup. A total of six cloth layers and a 0.25" honeycomb core $[0/45/0/Core]_s$ were used in the seat construction. Problems were encountered when laying up the aluminumized fiberglass, as it was difficult to conform to complex contours of the mold and did not adhere well to the carbon fiber. Additionally, the core was cut into three sections (2 sides, 1 middle) to reduce anticlastic curvature when bending the core; however the core was found to be cut too small. This resulted in gaps between the core sections that were later filled to smooth the surface. Post-bonds of end close-outs for the exposed edges (Figure 101) and for seat bracket mounting bosses were done with hand-shaped Divinycell core.

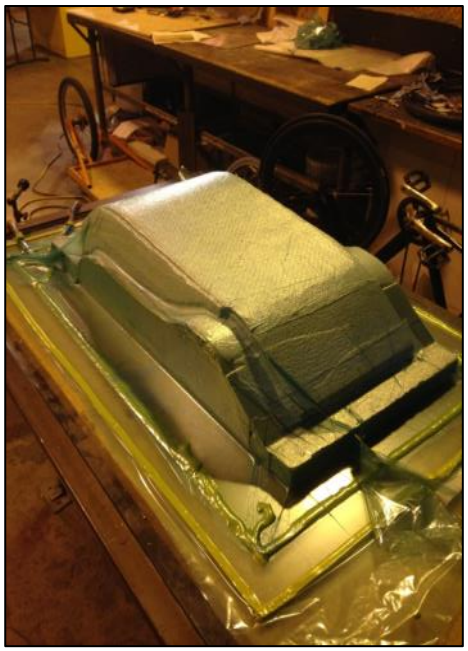

Figure 100. Double bagging technique used for the seat lay-up. All other procedures (wetting out, etc.) were similar to the traditional layup method.

The seat bracket mechanism was largely constructed of TIG-welded steel components with aluminum seat rails. Delrin was used as a bushing to allow ease of sliding between the steel brackets and aluminum rails (Figure 102). Each bracket was fabricated separately and then connected with the spanner tube. Alignment was critical on these components, as the pins had to line up almost perfectly with the seat rail holes, and the brackets had to be exactly parallel in order to slide smoothly. Both of these factors caused a longer manufacturing time for these components. Much time was spent hand sanding the holes to enlarge them to accommodate the barrel pin, while the brackets had to be consistently tacked and checked to ensure smooth sliding.

Figure 101. Seat released from the mold with exposed core requiring edge closeouts.

The sheet metal bracket to attach the sliding rails to the composite seat was deemed inadequate when only epoxied due to rider movement on the seat. Therefore, six bolts were added to ensure a mechanical connection between the seat and the rail assembly. A pad was put over the bolt heads to ensure there was no rider discomfort.

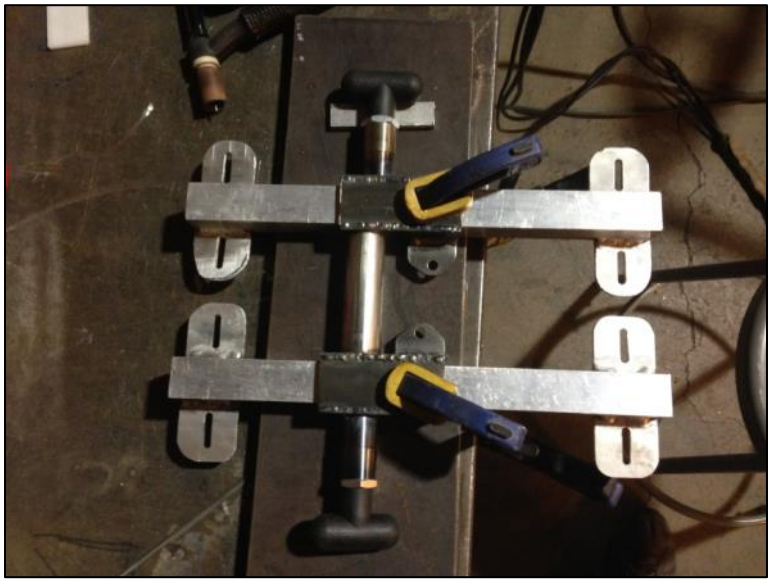

Figure 102. Steel rails and aluminum rails fixtured for welding.

Tie rod connections with adjustable ball ends allowed the seat angle to be changed and any manufacturing inconsistencies to be accounted for easily. Potted inserts were installed in the tub at approximate locations and the seat rails had slots machined for easy alignment. Even with the slots, the parts had to be bored out further to align the rails to parallel. This was expected,

however, and washers were used under the bolt heads to ensure adequate holding force for the rails. Final seat and adjustment mechanism in the completed vehicle can be seen in Figure 103.

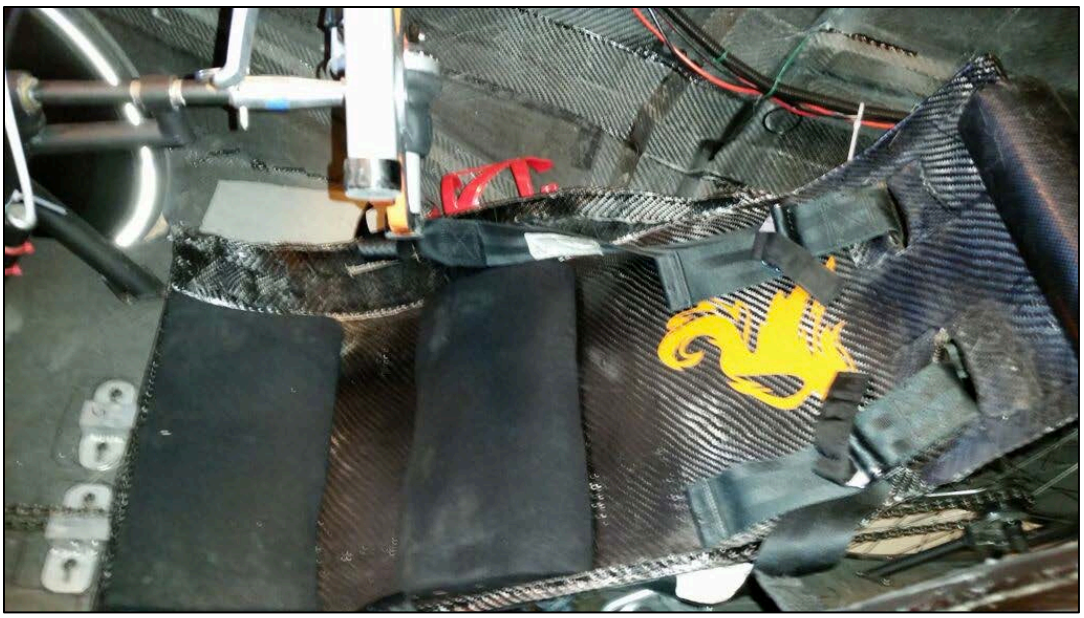

Figure 103. Mounted seat in final vehicle.

Drivetrain Manufacturing

While the drivetrain was a complex system, relatively few parts were manufactured by the team for use in the vehicle. Traditional OEM bicycle chain, chainrings, sprockets, cassettes, and idlers were used to limit the number of team manufactured components. Despite this, the drivetrain provided many obstacles to overcome during manufacturing.

Figure 104. TerraTrike Idler.

The idler mounts and step up-gear bolt pattern were CNC machined on the Cal Poly Machine Shop's Haas Mini Mill. The Terra Trike idlers (Figure 104) were mounted using screws and nuts, allowing the bearing to spin freely. The first iteration of the drivetrain (side-by-side rear chain routing) proved to have many problems stemming from width of the chain required. The chain used had to be a larger than expected 1/8" single speed chain (versus a 3/32" 10-speed chain) due to the left drive hub available. This caused two major problems that ultimately invalidated the initial design: the wider chain would not fit into the purchased idlers and the larger chain was more reluctant to twist than the narrower, 10-speed chain. Two fixes were attempted before redesigning the system. First, the chain pins were ground to attempt to fit inside

the idlers. While this worked initially, it weakened the chain significantly to the point where normal load would break the pins. The second solution was to modify the idlers to remove the flange and use the idler mount as a guide. While this worked to stop some problems, it still required a large redesign.

The re-designed rear chain routing and idler design to accommodate for the larger chain can be seen in Figure 105. This drivetrain incorporated a top-bottom chain routing by routing the drive chain under the seat and over the rail, while routing the return side through the left seat rail. The modified idlers without the flanges were incorporated by using the idler mount as a guide for the chain. The updated idlers mounts can be seen in Figure 106.

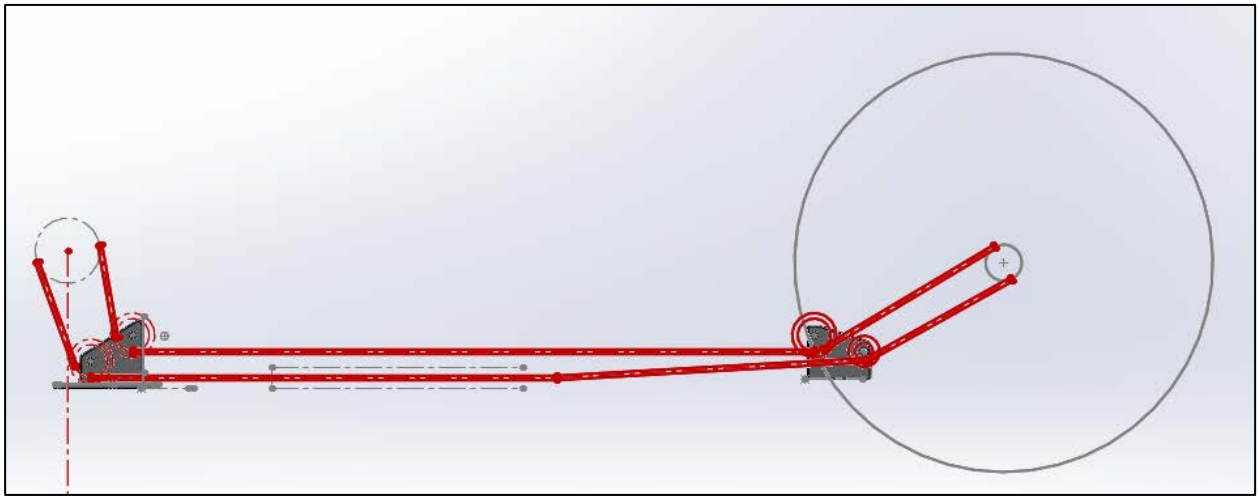

Figure 105. Redesigned drivetrain layout, with rear chain routing shown in red.

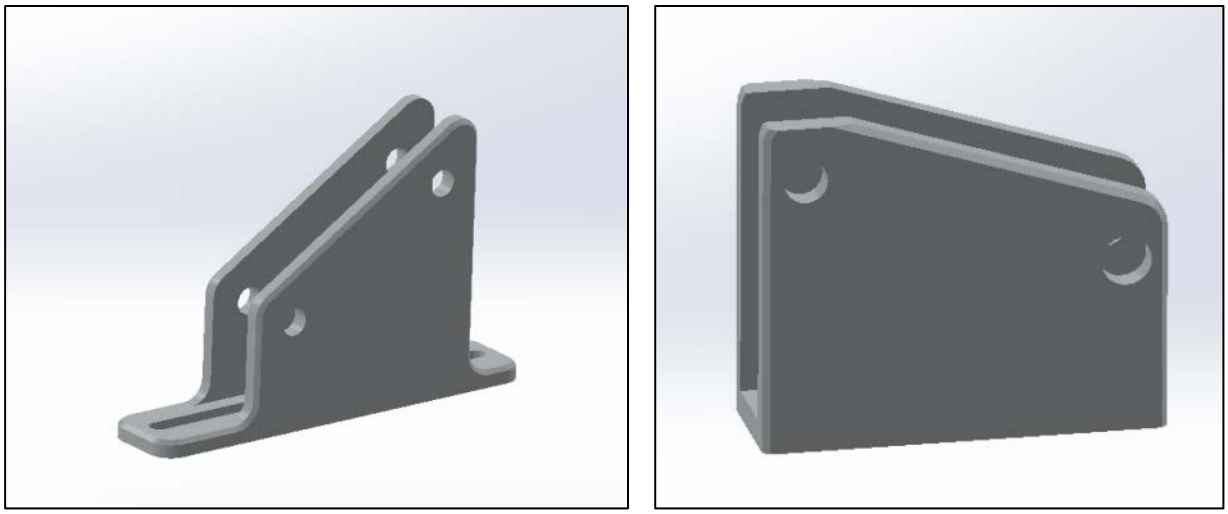

Figure 106. Revised idler mount design.

This design ultimately worked well enough to ride, despite having more friction and catches than desired. Larger chain loads than expected required longer bolts to be incorporated on the potted inserts and ultimately, an extra through bolt was used to support the potted inserts. After testing, alignment and realignment, fixes and theories, a continual "popping" of the chain still persisted during low cadence/high torque scenarios. This popping was the cause of four broken chains at competition; however, the cause for it was never discovered. The fully realized drivetrain can be seen in Figure 107 without the seat routing.

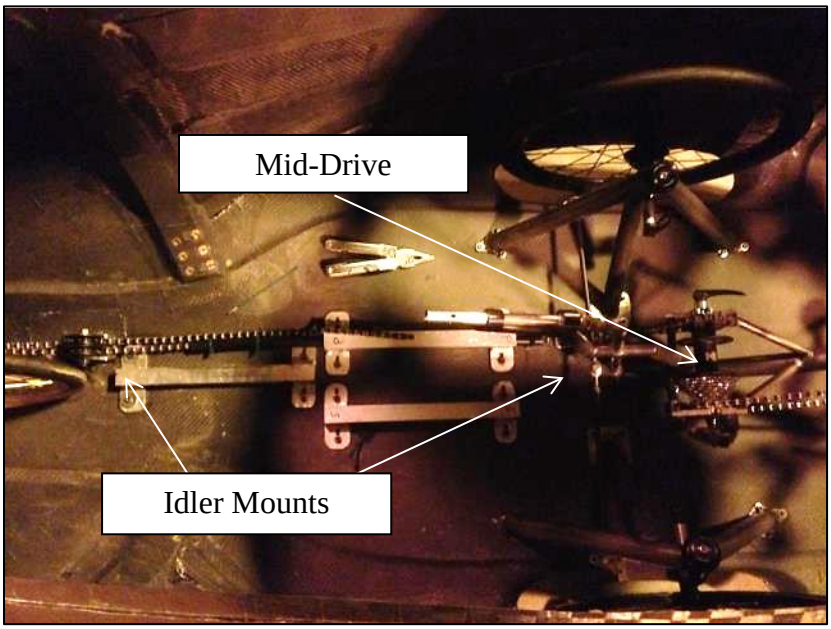

Figure 107. Installed drivetrain with seat removed for clarity.

Windshield Manufacturing

Due to the 3-D nature of the windshields on the vehicle, the team's traditional method of bending polycarbonate to fit and then adhering it with glue or tape was not feasible. Vacuum heat forming was pursued instead to create molded parts that would be easily installed and fastened to the fairing. While the current team had never performed heat shaping before, George Leone advised the team on the procedure.

The molds used for layups were used again for the heat shaping process. The plastic was heated to its specified glass temperature (250° for PETG and 350° for Polycarbonate) using a 3000 Watt calcium heat lamp (Figure 108). Temperature was consistently checked throughout the heating process with a hand-held infrared temperature sensor. Once the glass point had been reached, the plastic was transferred to the mold, where a vacuum seal was created with vacuum bag tape and a venturi device to apply pressure. The plastic was then held in the mold until room temperature had been again reached (approximately five minutes). The plastic was then trimmed and again heat shaped, if needed (Figure 109).

Figure 108. Heating setup for heat shaping the plastic

Figure 109. (Right) Team members sealing the vacuum bag during the front windshield heat shaping. The two top molds were bonded together to allow seamless heat-forming. (Left) The finished side windshield.

Problems encountered while heat forming were largely due to the way that the plastic was heated. A heat lamp is far from ideal for heating plastic evenly due to its spot heating nature. Instead, an oven would be ideal for this process; however no ovens were large enough to accommodate the large plastic sheets. Additionally, the method used to monitor the temperature was largely inaccurate and slow. If the plastic was over heated, it would bubble and become permanently damaged; if it was under heated, it would not fully shape to the contour and instead leave pleats in the plastic. Additionally, due to limited quantities and high expense of the heat shapeable plastic, only a few trial runs were available.

Figure 110. Bubbling defect on front windshield.

The front windshield provided the most challenge during shaping. Due to the high glass temperature of the Lexan (350°) sheet available, even heating was hard to achieve controllably with the heat lamp especially since that temperature exceeded that of the measuring device. Therefore, the team had to settle for a far inferior part with visible defects (Figure 110) such as pleats and minor bubbling.

Figure 111. Silicone caulking used to secure the windshield and fill the seams.

To attach the windshields to the vehicle, 5-minute epoxy was used to initially tack the windshields in place. Black silicone caulking was then used to fill in the seams between the plastic and the carbon fiber flange, providing weather-proofing and a sleek look (Figure 111).

Overall, the windshields were an improvement from the previous year's iterations, but still could have been improved. Firstly, mechanical fasteners such as rivets would be much more secure and less prone to temperature variations than the 5-minute epoxy. Additionally, the process of heat shaping could be improved by utilizing a more effective heating method and temperature monitoring method. Finally, more advanced methods such as true vacuum forming could be explored to improve part quality. The final vehicle with windshields can be seen in Figure 112.

Figure 112. Final vehicle with installed windshields.

Steering Knuckle Manufacturing

Aria suffered from highly inaccurate knuckle manufacturing, resulting in geometry that was up to 15 degrees off in a given parameter. Because the steering knuckles of the vehicle drive many of the critical steering and handling geometries, Aria handled poorly and did not inspire confidence in riders. Sweet Phoenix sought to improve upon the manufacturing techniques.

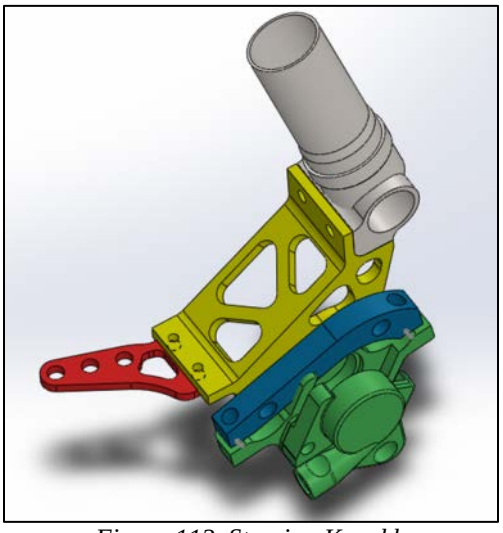

Figure 113. Steering Knuckles

Aria's knuckles were primarily weldments with primitive jigs used for alignment. Due to the proposed design for Sweet Phoenix's knuckles using fasteners instead of welds to accommodate the three dimensional angles, each component could be precisely machined and rely on fasteners to locate the critical mating points. Therefore, all components for the knuckles were machined on the Haas CNC Mini Mill. Using a CNC mill allowed the more complex shapes to be machined net shape to the specifications.

The three main components machined were the wheel axle bore, brake mount, and tie rod actuator (Figure 113). While all parts were comprised of relatively simple machining operations, the brake mounts required the most complex operations and most iterations (three) to achieve an acceptable final part. The initially proposed pocketing was foregone due to fixturing complexities and relatively little gains in weight savings. The axle bores were found to need a larger diameter than initially specified to fit a new wheel axle and thus had to be post-machined.

Figure 114. Welded bore and steerer.

Once the wheel axle bores were machined, precise miter profiles were done on the steerer tubes and the two were welded together using an angle jig (Figure 114). The welding was found to shrink the axle bore enough to require additional post-machining to accommodate the wheel axle. The installed final knuckle assemblies can be seen in Figure 115.

Figure 115. Assembled knuckles in vehicle.

Final Assembly

Once all vehicle sub-systems were manufactured, installation and assembly began. First, headset bearing races were press-fit into each headtube. The bottom bracket was installed into the bottom bracket shell, and the crankset installed on the bottom bracket. Steering column support bearings had been installed prior to welding. Steering column sections were inserted in their bearings and welded to the two universal joints. A derailleur was installed into the drive-side mid-drive dropout.

Next, each sub-frame component was bolted into place. Due to welding-induced heat distortion in some of the

components, several base plate mounting holes had to be bored out with a Dremel grinding tool in order to achieve alignment with the potted inserts in the fairing.

The knuckles were installed next, along with their steering and braking systems. Brake calipers were loosely installed on the knuckles, to be adjusted later. Next, the knuckles were installed into their respective supports and the bearings were adjusted. Rod ends were loosely installed in the ends of the steering tie rods, and bolted onto the bell crank and steering knuckles. Then, brake rotors were installed onto the front wheels, and the wheels were installed into the knuckles. At this point, the steering tie rods were adjusted to length to ensure parallel wheels when pointed straight. The brake calipers were adjusted and tightened.

To install the seat, the three seat rails were first bolted onto the fairing. At this point, the rear chain was routed from the mid-drive, through the front idler mount, left seat rail, and rear idler mount. The seat harness was threaded through slits in the seat at the shoulder and hip. The seat was then placed on the rails, and locked into its indexing holes on the front rails. The seat harness was bolted into the primary rollbar. Several issues arose during the seat installation process - the seat's alignment was not adequate to sit flat on all three rails, the locking pins did not fit in all the indexing holes, and the seat did not slide freely. Sufficient resolution of these issues required several days of tie rod adjustment, seat rail alignment, and Dremel grinding of the indexing holes.

Finally, the front chain was routed, a shift cable installed, and the derailleur adjusted. Brake cables were also installed and adjusted, including a Problem Solvers "Cable Doubler" to allow actuation of left and right brake calipers with a single lever. A twisting shifter and locking brake lever were installed on the steering wheel, which was attached to the end of the steering column.

Chapter 6: Design Verification

Table 42. Design verification plan.

Report Date 10/22/2014	Sponsor Cal Poly Human Powered Vehicle Team								REPORTING ENGINEER:			TriFiber Team
TEST PLAN									**TEST REPORT**			
Item No	Specification or Clause Reference	Test Description	Acceptance Criteria	Test Responsibility	Test Stage	SAMPLE Qty	SAMPLE Type	TIMING Start date	TIMING Finish date	TEST RESULTS Test Result	TEST RESULTS Qty Pass	TEST RESULTS Qty Fail	NOTES
1	Weight	Weigh final vehicle	55 lb	Matt	PV	1	C	2/23/2015	4/21/2015	65 lb	0	1	
2	Track Width	Measure distance	28 in	Matt	PV	1	C	2/23/2015	4/21/2015	27.5 in	1	0	
3	Wheelbase	Measure distance	43 in	Matt	PV	1	C	2/23/2015	4/21/2015	43.0 in	1	0	
4	Ground Clearance	Measure distance	4 in	Matt	PV	1	C	2/23/2015	4/21/2015	4 in	1	0	
5	Fwd Dist to Ground Visibility	Measure distance	20 ft	Matt	PV	1	C	2/23/2015	4/21/2015	18 ft	1	0	
6	Side Slope to Tip-over	Measure angle	25 deg	Peter	PV	1	C	2/23/2015	4/21/2015	34 deg	1	0	
7	Front Slope to Tip-over	Measure angle	15 deg	Peter	PV	1	C	2/23/2015	4/21/2015	42 deg	1	0	
8	Vertical Vehicle Stiffness	Apply calibrated weights to seat, measure deflection	2500 lb/in	Peter	PV	1	C	2/23/2015	4/21/2015	1350 lb/in	0	1	No complaints from riders; seemed to be adequate despite "unacceptable" result
9	Bottom Bracket Lateral Stiffness Under Pedal Load	Apply force to pedal, measure deflection	2500 lb/in	Peter	PV	1	C	2/23/2015	4/21/2015	1200 lb/in	0	1	Tolerance: ± 100 lb/in Prior to BB mount re-design: ~300 lb/in.
10	Drive Wheel Lateral Stiffness	Apply force to wheel rim, measure deflection	200 lb/in	Peter	PV	1	C	2/23/2015	4/21/2015	688 lb/in	1	0	
11	Rollbar Vert. Test SF	Calculate from FEA & verify on Instron	1.15	Trent	PV	1	C	2/23/2015	4/21/2015	0.76	0	1	Test failure of main rollbar only. FEA models - main rollbar model tuned, and equivalent full RPS model passed.
12	Rollbar Horiz. Test SF	Calculate from FEA & verify on Instron	1.15	Trent	PV	1	C	2/23/2015	4/21/2015	1.17	1	0	
13	Max Rider Height	Have tallest rider operate vehicle	74 in	Trent	PV	1	C	2/23/2015	4/21/2015	74 in	1	0	
14	Min Rider Height	Have shortest rider operate vehicle	65 in	Trent	PV	1	C	2/23/2015	4/21/2015	65 in	1	0	
15	Cargo Volume & Shape	Place package in cargo area	8 x 8 x 15 in box	Trent	PV	1	C	2/23/2015	4/21/2015	8 x 8 x 15 in box	1	0	
16	Max Cargo Weight	Test cargo container strength	10 lb	Trent	PV	1	C	2/23/2015	4/21/2015	20 lb	1	0	
17	Highest Gear	Calculate gear ratio	140 gear inches	Peter	PV	1	C	10/24/2014	10/31/2014	127 gear inches	0	1	Still resulted in 1st place Men's Sprint!
18	Lowest Gear	Calculate gear ratio	45 gear inches	Peter	PV	1	C	10/24/2014	10/31/2014	47 gear inches	0	1	
19	Stopping Distance from 15 mph	Measure distance	15 ft	Matt	PV	1	C	2/23/2015	4/21/2015	12 ft	1	0	
20	Speed at 200 W	Calculate from aerodynamic test data	25 mph	Matt	CV	1	A	10/18/2014	10/25/2014	Incomplete	0	0	Comparative analysis only.
21	Reflective Surface Area on Vertical Fairing Surfaces	Measure Surface Area	100 in^2	Peter	PV	1	C	2/23/2015	4/21/2015				
22	Forward Lighting System Brightness	Compare to manufacture specifications	200 lumens	Peter	PV	1	C	2/23/2015	4/21/2015	200 lumens	1	0	Objective altered from 1200 lumens to 200 lumens ("see" to "be seen")
23	Front Wheel Change Time	Time front wheel change	60 s	Matt	PV	1	C	2/23/2015	4/21/2015	30 s	1	0	
24	Rear Wheel Change Time	Time rear wheel change	120 s	Matt	PV	1	C	2/23/2015	4/21/2015	120 s	1	0	
25	Vehicle Production Costs	Maintain vehicle budget	$6,000	Matt	PV	1	C	2/23/2015	4/21/2015	$6,000	1	0	
26	Tire Life	Record run time	10 hrs	Trent	PV	1	C	2/23/2015	4/21/2015	> 10 hrs	1	0	
27	Serviceable Riding Hours	Log hours	100 hrs	Trent	PV	1	C	2/23/2015	4/21/2015	> 20 hrs (Incomplete)	0	0	
28	Production Man-Hours	Log hours	2500 hrs	Trent	PV	1	C	2/23/2015	4/21/2015	2220 hrs	1	0	
29	Assembly Man-Hours	Log hours	100 hrs	Trent	PV	1	C	2/23/2015	4/21/2015	220 hrs	1	0	

Design Verification Plan

Table 42 shows the filled out design verification plan. The team performed multiple tests to verify the design, and a sample of these tests is described in the following sections.

Rollover Protection System (RPS) Testing

Test Purpose

The rollover protection system is vital to the functionality of the vehicle in a crash situation and a well-designed and adequately tested system is paramount to success in the competition. As discussed in the RPS analysis section, the RPS system was re-designed for Sweet Phoenix to use the monocoque ribbing structure of the vehicle to carry the load instead of a single rollbar like in previous years' designs. However, to test this new system in its entirety, it would cost the team large amounts of manufacturing time and money. Therefore, the largest member, the rollbar closest to the rider's shoulders, was isolated and tested to confirm the FEA predictions. With the FEA confirmed, it would be reasonable to assume that the full RPS system would adequately meet the design criteria of 600 lbf vertical and 300 lbf horizontal with less than 2.0" and 1.5" of deflection, respectively.

Test Development

Traditionally, the team has performed the testing in manners similar to as seen in Figure 116. While this testing has traditionally scored well at competition, the team decided to explore alternative options to make the test more representative of a real crash experience, and thereby increase the safety of the vehicle. The ASME Rules give the following guidelines:

> *"The RPS system shall be evaluated based on two specific load cases – a top load representing an accident involving an inverted vehicle and a side load representing a vehicle fallen on its side. In all cases the applied load shall be reacted by constraints on the vehicle seat in an inverted or side position with drivers strapped in and clipped in to the pedals.* [12]*"*

A major flaw in the previous team's test was identified to be the reaction points used. The horizontal test was performed on the composites lab Instron machine with a constant rate of deflection and load readings being taken at a rate of 5 Hz. While this provided the most consistent loading and precise deflection measurements, this test was limited in the boundary

Figure 116. Horizontal (left) and vertical (right) test setups from previous years. The team deemed these not to be representative of reality.

conditions and reaction points that could be implemented due to size constraints. With reaction points being the shoulder point opposite the load, it was not reacted completely at the seat mounting points. Similarly, the vertical test fully encastred the bottom of the rollbar in concrete bolted to the Cal Poly Composites Lab strong-floor, while applying force with a hydraulic press. This setup gave poor force and deflection resolutions and was found to over-constrain the rollbar and cause excess stiffness. Therefore, other options were explored for both tests in hopes of creating a more precise, repeatable, and realistic test. The solutions the team came up with are described and shown in the figures below.

Horizontal

From the team's FEA analysis, the horizontal loading case was identified as the least critical loading case and was therefore tested first. The horizontal test was conducted using a custom test fixture with rigid mounts bolted to the strong floor in the composites lab, a pulley system to amplify the load, and a linear actuator to apply the load. The load was measured using a linear variable differential transformer (LVDT) and displacements were measured with dial indicators at a plate mounted to the end of the rollbar.

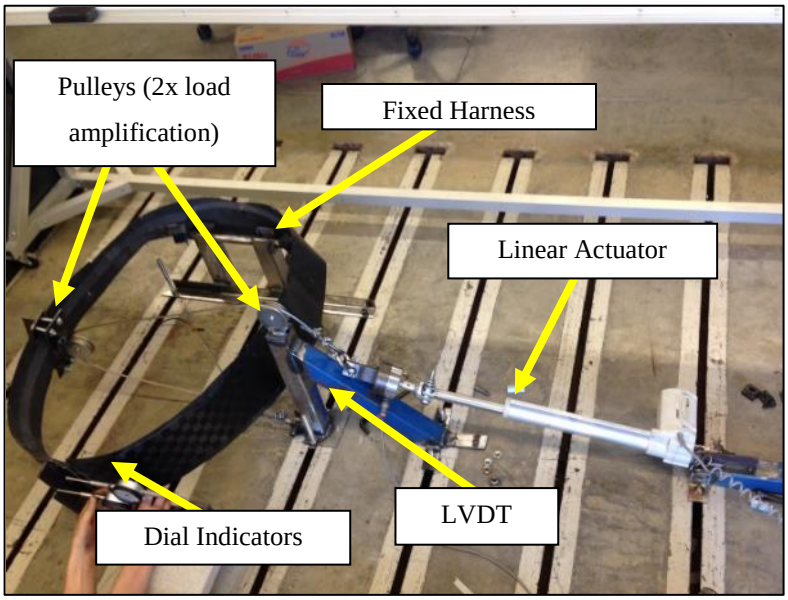

Figure 117. Horizontal RPS test setup.

The rollbar was constrained at the mounting location of the rider harness to simulate the rider reaction in the event of a crash, with the load being applied at the location of the shoulders of the tallest rider to simulate the maximum deflection. The first iteration of the test fixture was found to have excessive rotation at the mounting points, thereby not matching the FEA loading case. Additional gussets and strong floor mounts were added to create a fully fixed condition at the roll harness mounts. The final experimental test setup can be seen in Figure 117.

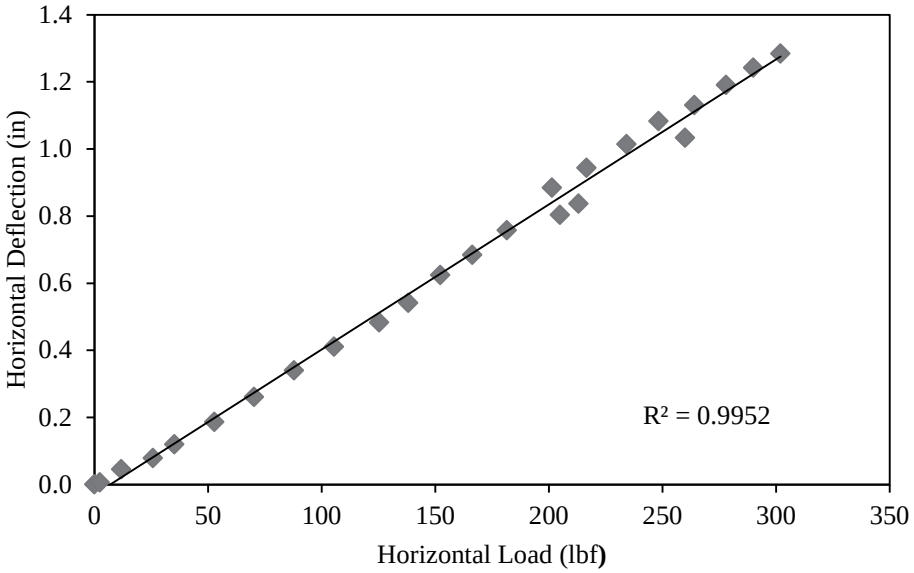

Figure 118. Results of the horizontal loading case applied to the roll bar.

The data collected from the test can be seen in Figure 118. Additionally, the results of the test and comparisons to the FEA results can be seen in Table 43. During the test, no indications of

failure were observed. Through this test, the team's FEA model was validated and the isolated rollbar met the design criteria. Therefore, it was concluded that the full roll structure would be fully adequate to take the required loads.

Table 43. Horizontal loading case results summary table.

Predicted Deflection (in)	Experimental Deflection (in)	Percent Error (%)	Displacement Safety Factor	Experimental stiffness (lbf/in)	Failure
0.971	1.284	32.2	1.17	233.7	NO

Vertical

From the team's finite element analysis, the vertical test was identified as the critical loading case. To perform the test, the rollbar was fixed in the same manner as for the horizontal test, using the pulley configuration shown below to apply the load at 12 degrees aft of vertical (rules mandated) at the topmost point of the rollbar. Dial indicators were set up such that the vertical and horizontal deflections relative to the vehicle ground plane would be measured (12 degrees from horizontal in this setup). A picture of the test setup can be seen in Figure 119 and the results of the test are tabulated in Table 44 along with comparisons to the FEA results.

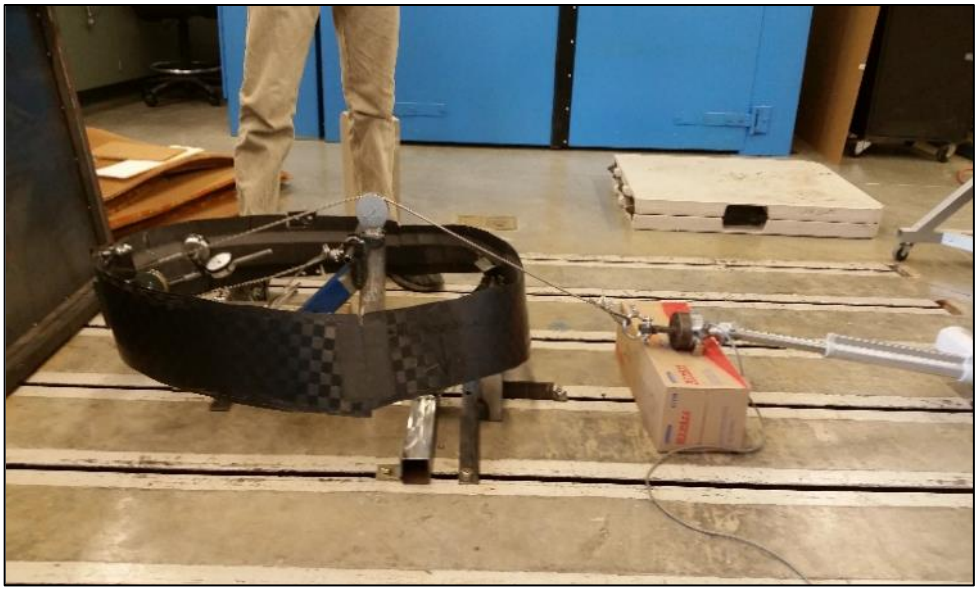

Figure 119. Vertical loading case rollbar test setup.

Failure occurred at around the 520 lbf load mark at the mounting locations. Data points became sparse at the higher loads due to safety concerns, and neither the exact deflection nor load were recorded at failure. Cyclic loading and stripped threads in the inserts were believed to be the root cause of failure. Inspection of the bolts after testing showed that they “tore out” through the inserts as seen in Figure 120 and that multiple inserts were cross threaded. However, from the potted insert testing performed, this failure is not typical of the inserts, as all testing showed face sheet failure before thread stripping. This is thought to have been caused by cyclic loading that occurred during the testing of the rollbar in the horizontal direction and four cycles to a 400 lbf vertical load to verify testing setup before proceeding to the 600 lbf load.

Figure 120. Close up of the boundary conditions (left) and failed potted inserts (right).

From this failure mode it can be concluded that the harness mounts had to be reinforced. For the final vehicle, it was decided to change to carbon steel inserts rather than the softer composite Torlon inserts used in this test to mitigate the cross threading and stripping issues. Because there were no indications of failure of the rollbar itself and the deflection curve showed a linear elastic response, it was concluded that the FEA model developed in the analysis section was validated. The experimental stiffness largely matched that seen with theoretical predictions, and when the curve in Figure 121 is extrapolated to 600 lb_f, the resulting deflection matches the theoretical deflection within 5%. Therefore, the roll structure FEA model can be verified to meet competition specifications based on exact same boundary conditions and load applications being used. Since it is not monetarily feasible to build another rollbar for testing, additional testing and analysis was required to confirm conformance to the competition rules.

Table 44. RPS Vertical load results summary table.

Predicted Deflection @ 600 lb_f (in)	Test Deflection (extrapolated 600 lb_f) (in)	Experimental Stiffness (lb_f/in)	Percent Error (%)	Failure (y/n)	Failure Load (lbf)	Failure Mode
2.778	2.640	227.3	-4.97	yes	520	Potted Inserts

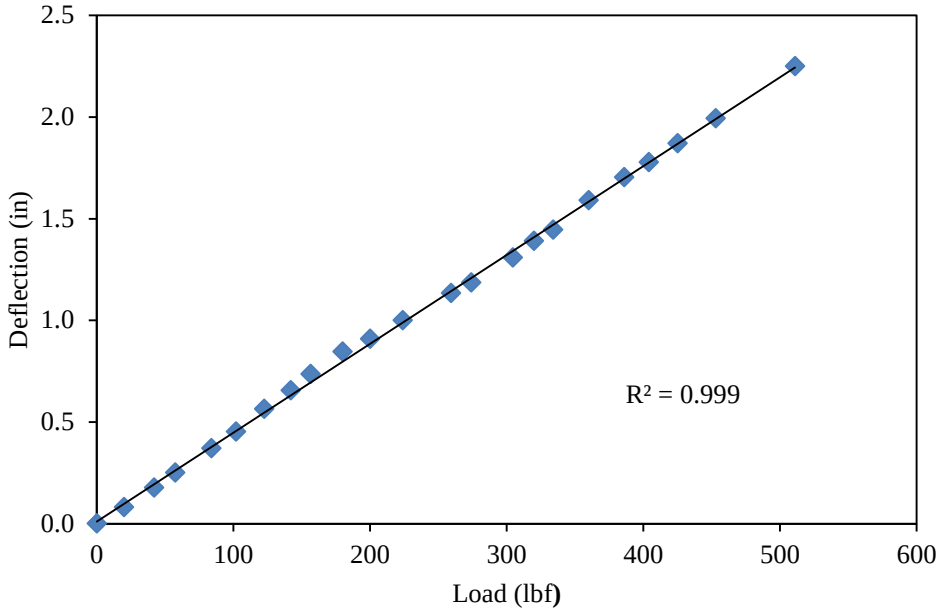

Figure 121. Vertical test deflection results.

Design Changes

After partial construction and testing of the final vehicle, three minor changes were made to the proposed designs.

Seat Bracket Mounting

The seat bracket initially conceived consisted of only a small bracket under the hips of the rider that was epoxied to the seat. The torsional loading of the seat was underestimated and the load path while pedaling was different than expected due to the weight shifting of the rider. The bracket frequently disbanded from the seat which in turn broke down the truss structure of the seat mounting. Lateral supports were proposed to fix this issue.

Two steel sheet metal plates were formed to the bottom of the sheet and struts were welded to them. This assembly was then welded to the sliding bracket at the pin sleeve locations and on top of the rails. The sheet metal plates were then epoxied to the carbon seat and 6 holes were drilled

through both for 6 bolts. Aluminum sleeves were bonded into the carbon seat to prevent bearing wear, and a foam pad was placed over the heads. The assembly was then bolted together and tested in the vehicle. While this layout added significant weight to the system, it provided a sturdy pedaling platform for the rider. No further design changes to the seat were needed.

Revised Drivetrain

The drivetrain caused the team many issues during the testing and refinement phase. The initial iteration of the drivetrain had enough friction to make turning the cranks near impossible with one's arm. The team identified four problems with the design:

1. Side by side chain routing caused excessive chain twist
2. Flexation / stripping potted inserts at the front idler mount
3. Single speed chain catching on iders
4. Catching of the chain, causing a popping noise during high pedaling loads

Problem one was fixed by creating new idler mounts that routed the chain top and bottom rather than side by side. This, however, caused problems with chain clearance with the seat. The chain had to be routed between the seat rails and bottom of the seat and through the seat rails. These positions caused very high chain angles and allowed for multiple places for the chain to rub or catch. However, it was deemed that with the mid-drive, there was no other way to route the chain without a complete redesign of the seat /tub.

Problem two manifested itself in stripped inserts and delamination at the front idler mount. To remedy this, an extra bolt was used with the front idler mount and longer bolts were used on the existing inserts. The delamination of the face sheet caused by the potted insert could not be fixed, however the team added two large washers and a thru-bolt at the delamination location to prevent it from spreading. While propagation of the delamination did occur, it did not compromise the other structures surrounding the affected area. The team deemed that the delamination was caused by an excess of members in the area or drilling of the potted inserts and propagated by the high loads.

Problem three stemmed from the fact that a single speed chain had to be used on the rear left drive hub. This increased the chain width from 3/32" to 1/8", causing the bought idlers to be

unusable. This was remedied by cutting off the channel walls of the idlers and using the idler mount walls as a guide for the chain.

The fourth problem was never remedied as its source could not be found. The team tried multiple diagnostic and solution techniques, but the concealed nature of much of the drivetrain made it hard to diagnose or solve. This problem would be the cause of multiple problems at competition and an overall disappointment for the team.

Dynamic Testing

Prior to competition, dynamic testing was completed in order to validate the required vehicle performance parameters outlined in the ASME rules. One of the parking structures on campus was used for testing due to the large flat open area available. Cones were set up to accurately represent obstacles encountered at competition as shown in Figure 122.

Figure 122. Slalom course testing (left). Braking distance testing (right).

Both the turning and slalom tests revealed the minimum turning radius of the vehicle was satisfactory to complete the tests. However, the rider noted that each turn required him to push the wheels to full-lock. Thus, the team decided it beneficial to decrease the turning radius by trimming additional carbon fiber from the front wheel wells as a means of providing more maneuverability in tight

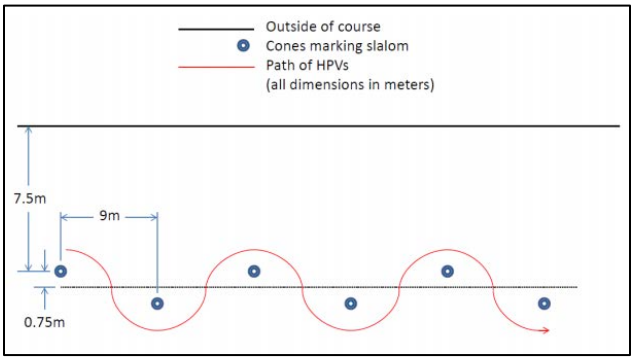

Figure 123. Slalom course layout [12].

corners.

The braking test was performed at the base of the parking structure ramp. An upright bike was ridden alongside the vehicle down the ramp during the tests in order to notify the rider when they had reached a speed of 15 mph. From this speed, they then stopped as fast as possible in the allotted 20 ft. distance. The results of the testing are outlined in Table 45 below.

Table 45. Dynamic testing summary.

Test	Details	Pass/Fail	Notes
Slalom Course	See Figure 124	Pass	Decrease turning radius
Turning Radius	Minimum 26 ft.	Pass	"
Braking	Stopping from 15 mph in 20 ft.	Pass	Stopped within 10 ft.

Throughout testing, one issue that became apparent was excessive lateral deflection of the bottom bracket mount while pedaling. Although this did not cause any derailments at the time, it was decided to minimize this deflection in hopes of mitigating any future chain management issues or carbon/steel interface problems. Therefore, after testing, three additional struts were welded to the bottom bracket mount (Figure 124) and the required potted inserts installed in the tub floor. Additional rider testing after the change revealed a significant decrease in the deflection and was deemed satisfactory for competition.

Figure 124. Additional struts welded to BB mount.

Throughout the testing and competition practice processes, the need for several ergonomic improvements became evident. The seat was equipped with removable butt, neck, and lumbar pads.

Competition Testing and Results

The most important testing of Sweet Phoenix was done at the 2015 ASME HPVC West competition, where 28 teams competed their vehicles. The weekend event consisted of the events as laid out in the HPVC West rules broken down in the background section.

Overall, Sweet Phoenix performed with few surprises. The drivetrain continued to be the biggest issue that plagued the team in all three dynamic events. The “popping” sounds continued to resonate when the vehicle was pedaled hard at low speed. Excessive drag was also seen during the speed event with relatively loud noise indicating a high amount of losses at speed. During the men’s speed event, a broken chain was also seen on a strong run by Judy. The broken chain happened at the quick link on the single speed chain, which initially suggested that it failed due to an overload of force not uncommon on standard bikes. While no more chains were broken during the speed event, the problem became more pronounced during the endurance event. Two chains were broken during the event along with multiple dropped chains. The team has thus equated the problem with the popping noise, or catching of the chain when it is under high chain load. The increased amount of quick accelerations caused the problem to become more apparent, and severely hindered the team’s performance during the endurance event.

The other limitation of the vehicle that was found at competition was the lack of excess turning radius less than the required 25 foot competition specification. While the vehicle met the requirement, it allowed no room for error or adjustment during the slalom and quick turn obstacles in the endurance event. While all pre-race tests were done on an uncrowded course, the addition of other vehicles showed that the perfect line wasn’t always possible. The wheel wells had to be extended during the endurance event to compensate and allow excess turning radius.

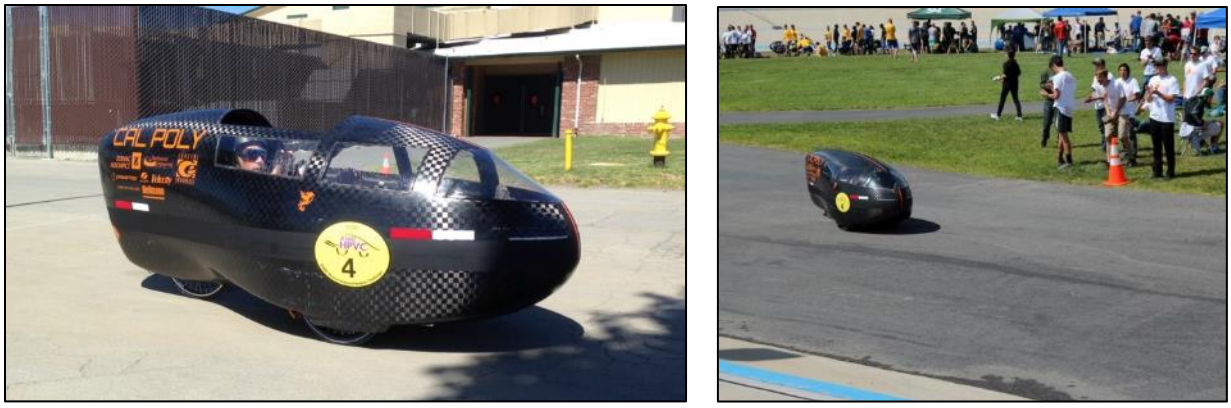

Figure 125. Sweet Phoenix at competition in the endurance race (left) and the sprint race (right).

During the endurance event, it was also found that some riders preferred to ride without the door, aiding in ventilation. This did not affect the riders' lap times significantly, but did allow for happier riders. It was thought that the relatively low speeds of the event allowed for leniency on aerodynamics. Additionally, one roll-over was caused by the largest rider not fully engaging the seat pins and railing a corner too hard. The seat shifted suddenly in a corner, causing the center of gravity to change and the vehicle to flip onto the door side. No injuries were caused and only cosmetic damages were done to the vehicle.

While the team had problems at competition, it was also overall happy with the results. Table 46 shows the results the team achieved, with notable performances in the men's speed and design events where the team achieved first place finishes.

Table 46. Competition result summary.

Main Event Awards	
Endurance Event	17th
Men's Speed	1st
Women's Speed	4th
Innovation	4th
Design	1st
Overall	7th
Special Awards	
Best Craftsmanship Award	

Chapter 7: Conclusions and Recommendations

The end goal of this senior project was to produce a vehicle that was capable of performing up to and beyond the standards set forth in the initial design phases. The true test of Sweet Phoenix's capabilities came at the 2015 ASME HPVC where the strengths and weaknesses of the vehicle were quickly realized. Overall the team was pleased with the individual performances in certain events, however the disappointment of a 7th place finish overall was tough to accept. As mentioned previously, the shortcomings of the drivetrain were a constant headache prior to and throughout competition where diagnosis of the issues were unsuccessful. However, these setbacks emphasized certain aspects of the engineering process that are essential to achieve the desired performance of a race vehicle.

The development of a reasonable schedule is critical to the overall success of a project. In years past, much of the work on the vehicle had been completed within the last couple of months prior to competition, inevitably creating oversights. This year, the team did a much better job of planning the sequence of construction from the start to accommodate testing in an effort to mitigate or diagnose problems such as the ones faced on Sweet Phoenix. However, the push in the build process took a hit over the last month before competition as many construction deadlines were missed, which cut into the testing window. Although some testing was performed, the amount of riding and time for diagnosis was not enough to correct the faults of the vehicle. As the team learned, insufficient testing can have undesirable results.

In a year that included a lot of unknowns, the team was generally pleased with the result of the vehicle design. As always though, there are some recommendations that would likely improve the design and performance of Sweet Phoenix. An obvious lesson learned from the year is the importance of a reliable and robust drivetrain as reiterated in the words of Cameron Christensen (old HPV member), "drivetrain, drivetrain, oh and drivetrain." The decision to utilize the mid-drive design had its pros and cons, but possibly the biggest downside was the added complexity, which introduced a myriad of design issues and interferences. As mentioned previously, extensive and thorough testing is essential to the success of the vehicle in competition and therefore even better planning and time management by the team would allow for troubleshooting of inevitable problems. In addition, further analysis and testing of the carbon to steel interface should be performed to better predict the structural characteristics of bolted joints

using potted-in inserts. Lastly, the success of non-faired or partially faired vehicles over the past few years has emphasized that success at HPVC is not linked to a fairing. The vehicles that tend to do well are relatively simple and reliable and some do not even have fairings, which is a testament to the utility-oriented direction competition has been moving in. Therefore a thorough analysis of the pros and cons of a fairing is necessary to justify the added time and effort put into the fairing construction.

Works Cited

[1] Zapletal, Erik. "Heavenly Angles." Racecar Engineering June 2001: 70-76. Print.

[2] Eland, Peter. "Steering." Peter Eland's Web Pages. N.p., 12 Mar. 2012. Web. 2 Oct. 2014.

[3] Gerlich, Matt, Alex Hawley, Philip Kinsley, Heather Kutz, Kevin Montoya, and Erik Nelson. Human Powered Vehicle Challenge. Rep. Flagstaff: Northern Arizona U, 2014. Print.

[4] Franklin, John. Cyclecraft. London: TSO, 2007. Print.

[5] Grether, Walter F. "Optical Factors In Aircraft Windshield Design As Related To Pilot Visual Performance." (1973). Web.

[6] "2013 ASME East Competition." Biking in a Big City. 8 May 2013. Web. 23 Oct. 2014.

[7] "Team Cygnus 2014 Bike." Cygnus Human Powered Team. 20 September 2014. Web. 23 Oct. 2014.

[8] "Trisled All Overzealous Record Breaking Trike." Trisled Factory Racing. 21 September 2014. Web. 23 Oct. 2014.

[9] The Chain Gang. “Human Powered Vehicle Frame Team Senior Project.” PDF. 15 March 2013

[10] "Installing a Potted-In Insert." *Marketing Masters*. Web. 20 Feb. 2015.

[11] "Tube Coping Calculator." Metalgeek.com, n.d. Web. 13 Feb. 2015.

[12] ASME. “ASME HPVC West Rules 2014.” Web. 15 November 2015

[13] Thomas, Henry. “Ergonomic Design.” Web. 17 October 2007.

Appendix A

Supplementary Analysis

Scoring Criteria

This guideline is an excerpt from the scoring sheet of the HPVC west score sheet. The competition puts less emphasis on the overall design and more emphasis on the detailed analysis and features of the vehicle. Performance based events account for 50% of the total score, where the innovation accounts for 20% and the design event accounts for the remaining 30%. Cal poly has traditionally performed well in the design, and sprint events, with weaker placements in the innovation and endurance events, leading to top 25% finishes overall.

Design Event	
General	5
Design	15
Analysis	25
Testing	25
Safety	20
Aesthetics	10
Design Event - Total	100
Report content largely non-original	100%
Late Report Submission (per day)	4%
Late for Static Judging or Safety Check	10%
Over Page Limit (per page)	3%
Report Does Not Conform to Outline	10%
Design - Rank	

Innovation Event	
Deign	10
Concept Evaluation	7
Learnings	7
Execution	6
Bonus	1
Innovation Event - Total	31
Report content largely non-original	100%
Late Report Submission (per day)	4%
Late for Presentation	10%
Over Page Limit (per page)	3%
Report not stand alone document	4%
Report Does Not Conform to Outline	10%
Innovation - Rank	

Women's Speed Event - Total	12.5
Fastest Speed (km/hr)	45.73
Women's Speed- Rank	

Men's Speed Event - Total	12.5
Fastest Speed (km/hr)	51.20
Men's Speed - Rank	

Endurance Event - Total	25
raw score	
Laps Completed	
Finish time (hr)	
Lap Length (km)	1.27
Avg Speed Minus Penalties (km/h)	
Avg Speed Minus Penalties (mph)	
Illegeal Start Assistance (m)	500
Damage or Loss of Parcel (m)	up to 500
Failure to Stop at Stop Sign, Complete Slalom, Hairpin Turn, or Quick Turn (m)	500
Safety Violation [Laps]	1 or more
Illegeal Lap [Laps]	1
Min/Max Driver Lap Violation [Laps]	1
Endurance - Rank	

Overall - Total	100

Previous Event Results

This table collects scoring information from the previous 3+ years of HPVC west competitions in order for trends to be identified. Major trends seen include the consistency of winning teams in placing in the top 10% in speed, innovation, and design event. The endurance event is less critical in determining the overall winner of the completion. This table will be used to evaluate potential concepts.

Bike Information			Women's Speed (mph, rank)		Men's Speed (mph, rank)		Endurance Event (mph, rank)		Innovation Event		Design Event	
Team	Year	Bike Notes	Rank	Speed (mph)	Rank	Speed (mph)	Rank	Speed (mph)	Rank	% Top Score	Rank	% Top Score
Cal Poly												
Atlas (2)	2008-09	Monocoque Tub Streamliner	3	31.58	2	34.89	2	18.59	N/A	N/A	1	100
Artemis (12)	2009-10	Rear Steer Streamliner	6	Drag Race	7		DNF	DNF	N/A	N/A	14	35.8
Lazarus (7)	2010-11	U-Joint Streamliner	3	27.8	3	36.2	8	15.12	N/A	N/A	4	86.5
Gemini (2)	2011-12	Monocoque Streamliner	2	Drag Race	2		3	16.4	3	87.1 (Solar Pannels)	1	100
Black Stallion (4)	2012-13	Leaning Delta Trike	7	29.67	5	40.1	6	12.5	8	79.1 (Rear View Camera)	2	95.1
Aria (6)	2013-14	CF Ridgid Tadpole Trike	8	22.36	7	27.24	17	7	4	86.5 (BCM Lugs)	3	96.6
Overall Winners												
U of Toronto	2010-11	Monocoque Tub Streamliner	1	35.85	2	40.67	4	10.6	N/A	N/A	3	90.8
Missouri S&T	2011-12	Suspension Streamliner	1	Drag Race	1	Drag Race	1	18.3	5	?	5	82.5
Rose Hulman	2012-13	Monocoque Tub Streamliner	1	38.56	1	48.21	12	11.3	1	100 (ABS)	3	90.1
Rose Hulman	2013-14	Leaning Delta Trike	6	23.46	3	31.38	4	13.7	1	100 (Regen Braking)	1	100
Catagory Winners												
Cal Poly (2)	2011-12(D)	Monocoque Streamliner										
Cal State Chico (4)	2011-12 (I)	Steel Streamliner	5	NDA	5	NDA	5	15.1	1	100	2	97.8
Missouri S&T (1)*	011-12 (MS)	Steel Suspension Streamliner										
Missouri S&T (1)*	011-12 (WS)	Steel Suspension Streamliner										
Missouri S&T (1)*	2011-12 (E)	Steel Suspension Streamliner										
Colorado State (2)	2012-13 (D)	Rigid Tadpole, Tent Fairing	4	30.8	6	38.83	3	13.2	4	81.7	1	100
Rose Hulman (1)*	2012-13 (I)	Monocoque Streamliner										
Rose Hulman (1)*	012-13 (WS)	Monocoque Streamliner										
Rose Hulman (1)*	012-13 (MS)	Monocoque Streamliner										
UC-Berkeley (6)	2012-2013 €	Monocoque Streamliner	6	30.4	9	36.7	2	14.1	16	45.3	11	66
Rose Hulman (1)*	2013-14 (D)	Leaning Delta Trike										
Rose Hulman (1)*	2013-14 (I)	Leaning Delta Trike										
UN-Reno (11)	013-14 (MS)	Aero Position Upright (Prone)	4	25.5	1	31.8	2	14.3	10	63.7	22	21.4
UC-Berkeley (16)	2013-14 E	Monocoque Streamliner	20	N/A	20	N/A	1	14.6	6	82.4	13	73.3
NAU (2)	013-14 (WS)	Rigid Tadpole Trike	1	28.8	4	27.8	3	14.3	2	86.7	2	97.6

Human Powered Vehicle 2015

Engineering Requirements (HOWS)

		Weight (Total 100)	Rider Min height (in)	Rider Max height (in)	Cargo Volume (in^3)	Cargo Weight Capacity (lbf)	Wheelbase (in)	Track Width (in)	Rollbar Vert. SF	Rollbar Horiz. SF	Vehicle Production Expenses ($)	Serviceable Years	Front Tire Change Time (s)	Rear Tire Change Time (s)	% Drivetrain Accessible From Door	Ground Clearance (in)	Top Speed @ 200 W (mph)	Top Gear (gear inches)	Low Gear (gear inches)	Percent Riders Uncomfortable(%)	Distance to Fwd Ground Visbility (ft)	Number of Reflective Surfaces	Total Lighting System Lumens	Vehicle Weight (lb)	Equiv. Aesthetic Judging Score	Vertical Seat Stiffness (lb/in)	BB Pedaling Stiffness (Lateral) (lb/in)	Drive Wheel Lateral Stiffness (lb/in)	Sideways Tip Angle (deg)	Forward Tip Angle (deg)	Tire life (hours)	Braking Distance from 15 mph (ft)	Production Man-Hours Required	Assembly Man-Hours Required	Aria (2014 Benchmark)
Customer Requirements	Fits Riders*	6	9	9																														2
	Adequate Cargo Capacity*	3			9	9																												2
	Compact Vehicle Size	2					9	9																3										3
	Weather Resistance	1																																4
	Crash Protection*	4							9	9																								3
	Low Cost	0									9																							1
	Vehicle Longevity	1										9																						4
	Ease of Maintenance	3											9	9	9																			3
	Easy/Fast Roadside Repair	2											9	9	3																			2
	Adequate Ground Clearance*	7														9																		5
	High Top Speed	5															9	9						3										3
	Efficient Drivetrain	6															3		9															4
	Wide Range of Gearing	5															3																	4
	Comfortable	3																		9														4
	Visibility (rider)*	8																			9													4
	External Visibility	1																				9	9											4
	Low Weight	5																						9										4
	Aesthetics	4																							9									5
	Optimal Stiffness	6																								9	9	9						3
	Static Stability	8						3																					3					1
	Dynamic Stability	7					3	3																					9	9				5
	Long Tire Life (scrubbing)	1																													9			2
	Short Braking Distance*	7																														9		2
	Ease of Manufacturing	4																															9	5
	Ease of Assembly/Fairing Integration	3																															9	4
	Targets		65	74	1000	10	35-45	25-35	1.15	1.15	8000	2	60	120	75	4	25	140	45	10	20	6	200	55	10	2500	2500	500	25	15	10	15	2500	100	
	Aria (2014 Benchmark)		TBD	TBD	TBD	TBD	46	32	1.25	1.25	5000	0.1	20	600	50	4	20	110	40	40	30	6	200	50	8.5	2500	1200	91	40	30	8	15	1800	200	

● = 9 Strong Correlation
○ = 3 Medium Correlation
△ = 1 Small Correlation
Blank No Correlation

Appendix B

Part & Assembly Drawings

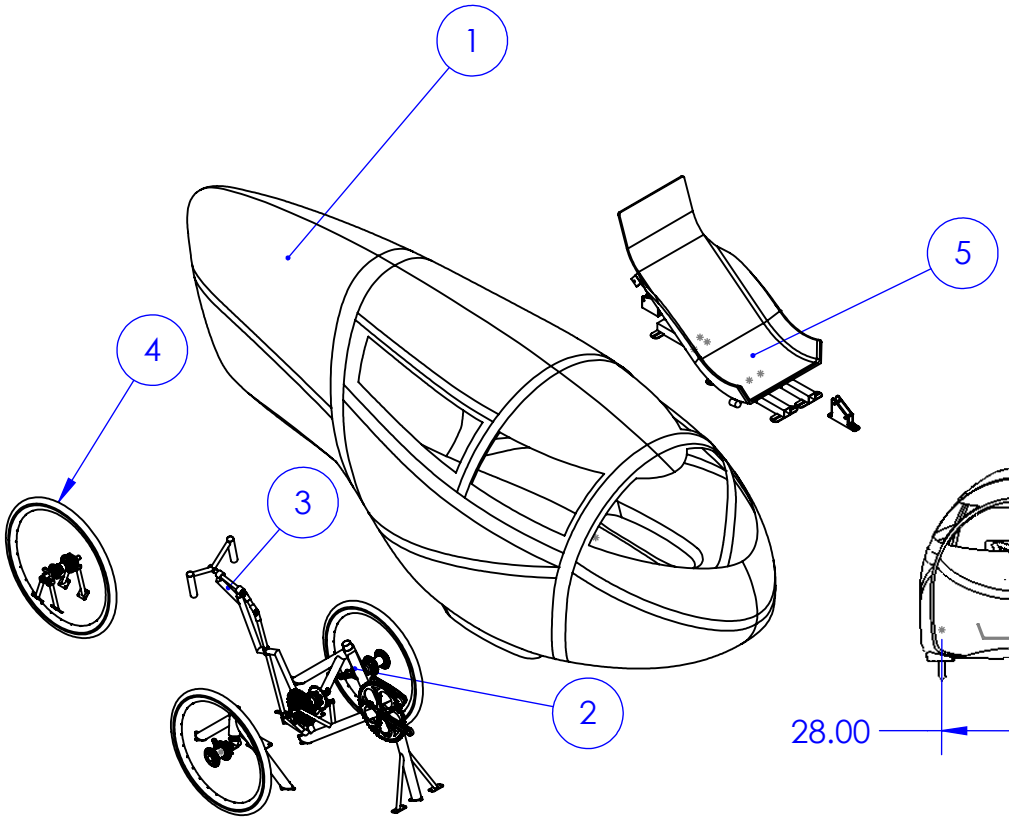

ISOMETRIC VIEW
SCALE 1:25

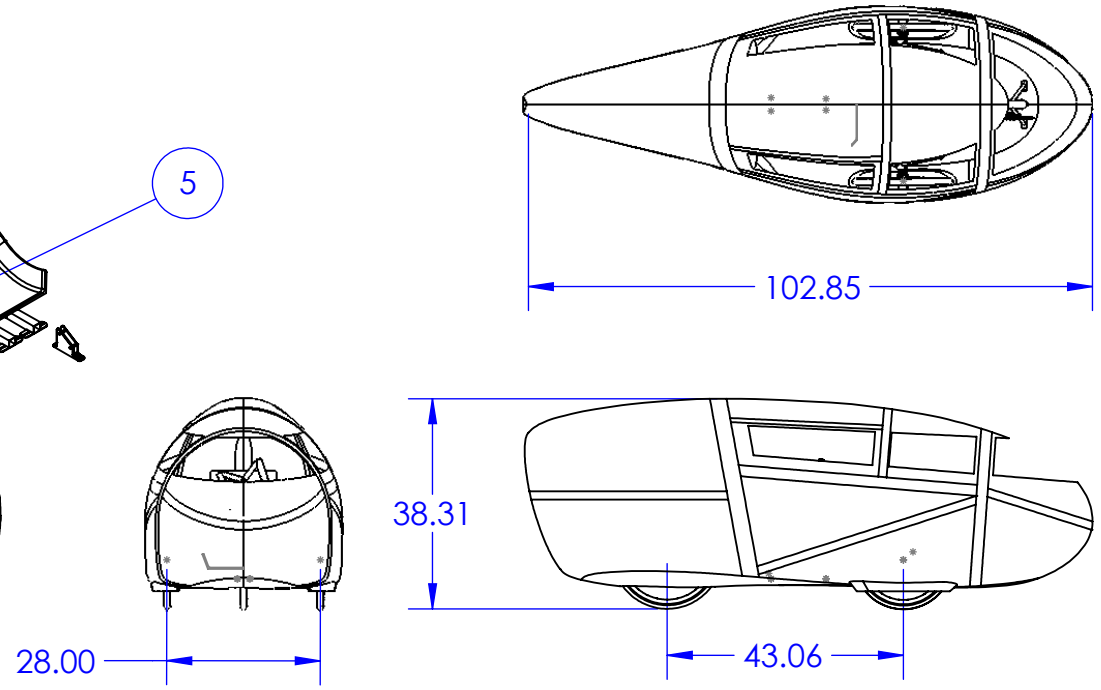

THREE VIEW
SCALE 1:35

BALLOON NO.	PART NUMBER	DESCRIPTION	QTY.
1	SP1500	FAIRING	1
2	SP1100	FRONT WHEEL SUPPORTS	1
3	SP1200	STEERING & BB	1
4	SP1400	REAR WHEEL ASSEMBLY	1
5	SP1300	MID VEHICLE ASSEMBLY	1

Cal Poly Mechanical Engineering HPV FRAME DESIGN	Title: FULL VEHICLE	Nxt Asb: NONE	Date: 09/26/2015	Drwn. By: MATT ALLEN
	Dwg. #: SP1000	Scale: AS NOTED	Material: VARIOUS	Chkd. By:

ITEM NO.	PART NUMBER	DESCRIPTION	QTY.
1	Brake Bracket		1
2	Bore		1
3	Tie Rod Plate		1
4	Steerer		1
5	Knuckle Mount		1

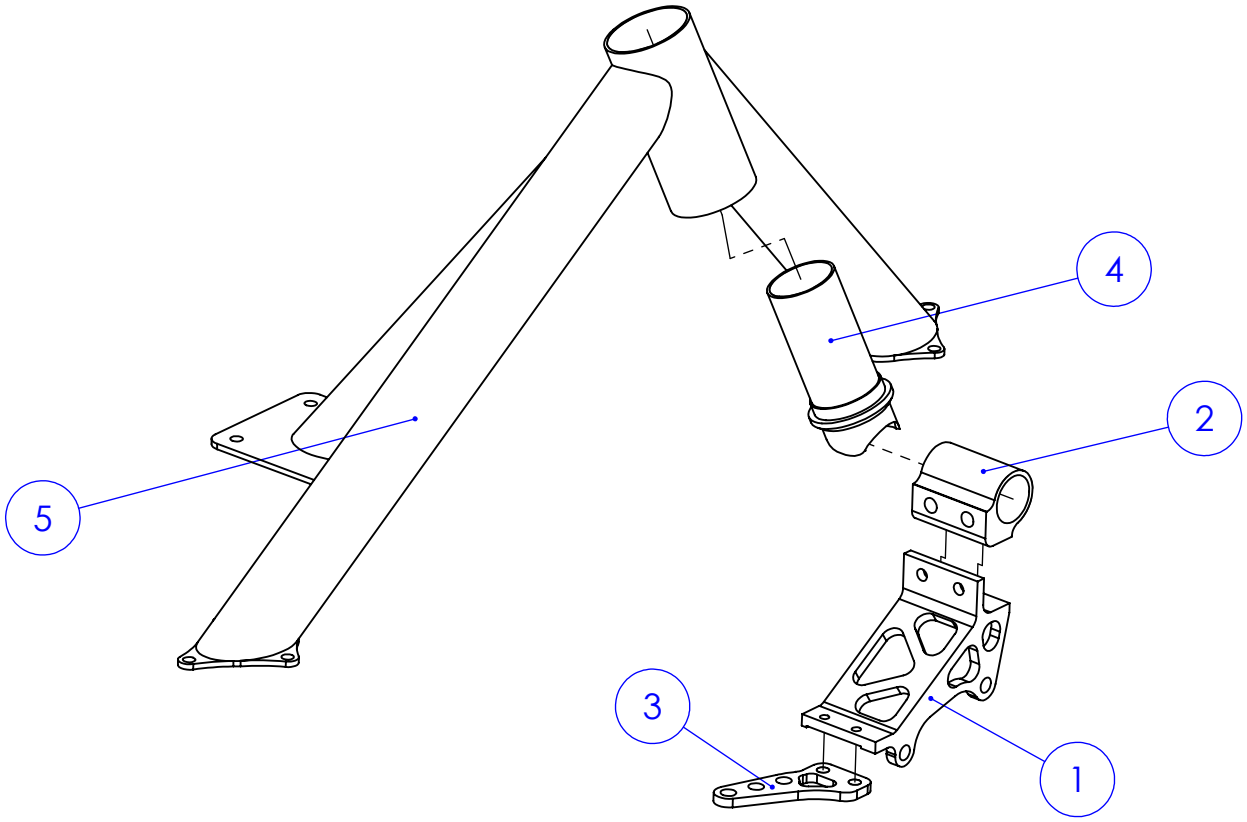

Cal Poly Mechanical Engineering HPV FRAME DESIGN	Title: FRONT WHEEL SUPPORTS	Nxt Asb: STEERING & BB	Date: 6/10/2015	Drwn. By: TRENT HELLMANN
	Dwg. #: SP1100	Scale: 1:3	Material: STEEL/ALUM.	Chkd. By:

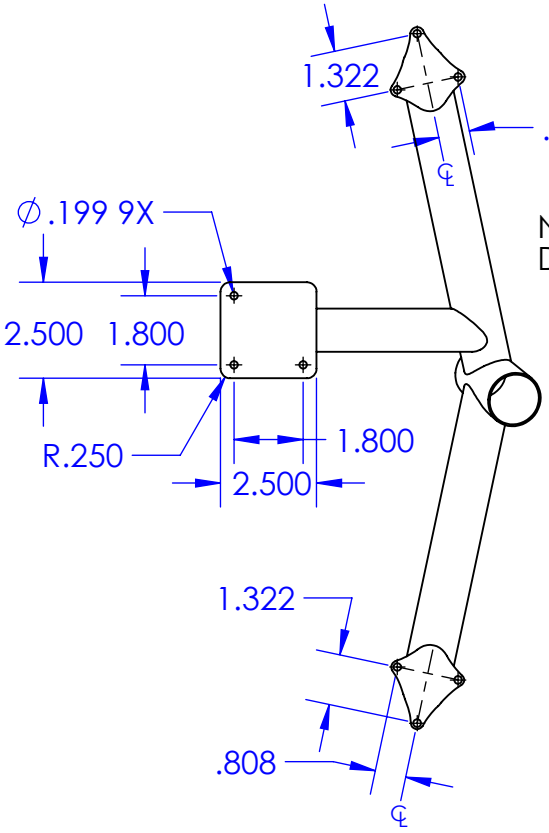

NOTE: "FEET" ARE HAND SHAPED, DIMENSIONS APPROXIMATE

NOTES
UNLESS OTHERWISE SPECIFIED:
1. ALL DIMENSIONS IN INCHES
2. TOLERANCES:
X.XX= ±.01
ANGLES= ±.1°
3. INSIDE TOOL RADIUS .01 MAX
4. BREAK SHARP EDGES .01 MAX

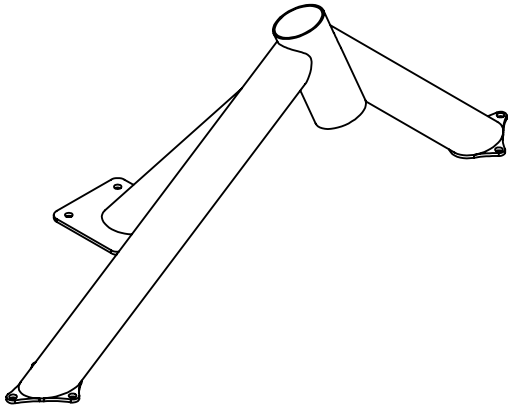

NOTE: ALL BASEPLATES USE 3/32" PLATE STOCK

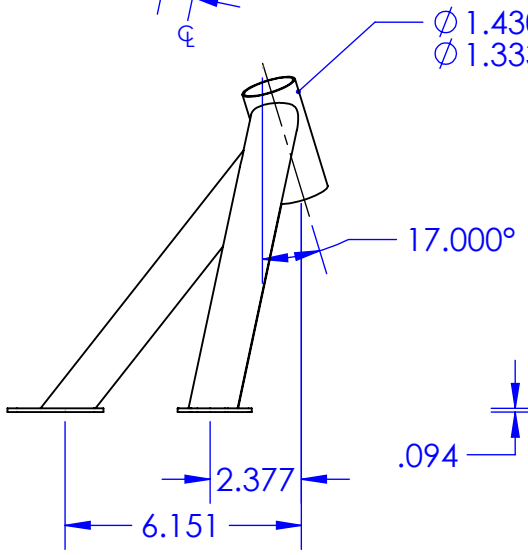

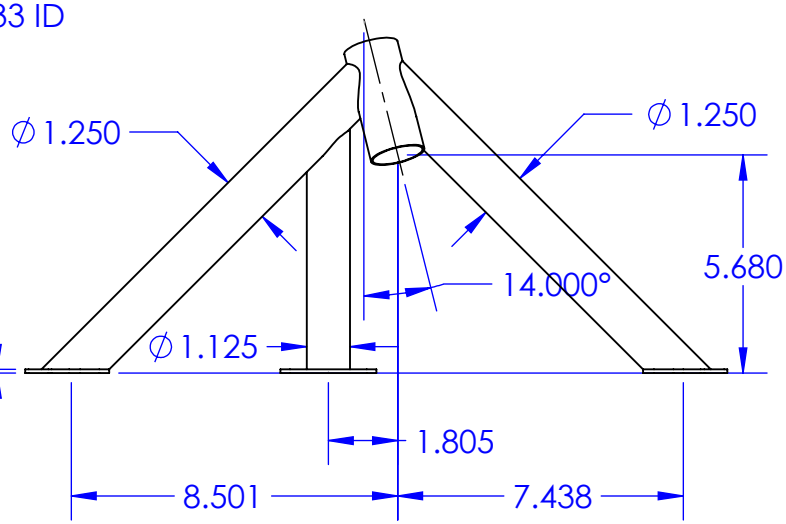

Cal Poly Mechanical Engineering HPV FRAME DESIGN	Title: KNUCKLE MOUNT	Nxt Asb: FRONT WHEEL SUPPORTS	Date: 6/10/2015	Drwn. By: TRENT HELLMANN
	Dwg. #: SP1101	Scale: 1:5	Material: 1020 STEEL	Chkd. By:

NOTES
UNLESS OTHERWISE SPECIFIED:
1. ALL DIMENSIONS IN INCHES
2. TOLERANCES:
X.XX= ± .01
ANGLES= ± .5°
3. INSIDE TOOL RADIUS .01 MAX
4. BREAK SHARP EDGES .01 MAX

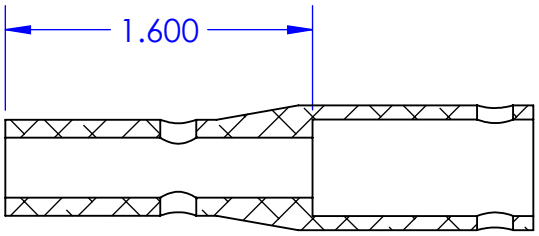

SECTION A-A

NOTE: SIZE "MEDIUM" : 2.750 LGTH
SIZE "LARGE" : 4.500 LGTH

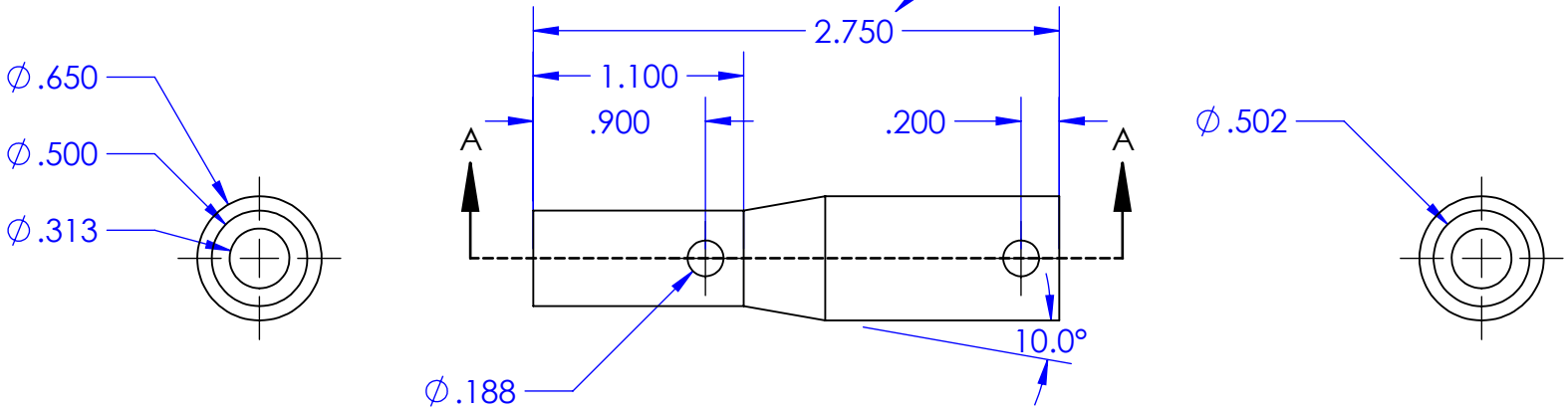

Cal Poly Mechanical Engineering HPV FRAME DESIGN	Title: STEERING COLUMN EXT.	Nxt Asb:	Date: 6/10/2015	Drwn. By: PETER AUMANN
	Dwg. #: SP1206	Scale: 1:1	Material: ALU 6061	Chkd. By:

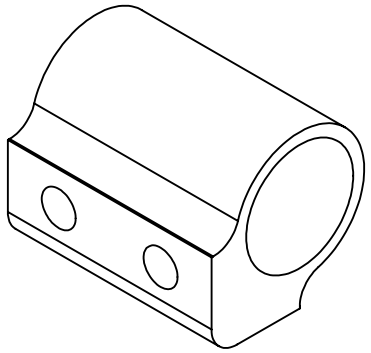

NOTES
UNLESS OTHERWISE SPECIFIED:
1. ALL DIMENSIONS IN INCHES
2. TOLERANCES:
   X.XX= ± .005
   ANGLES= ± 1°
3. INSIDE TOOL RADIUS .01 MAX
4. BREAK SHARP EDGES .01 MAX

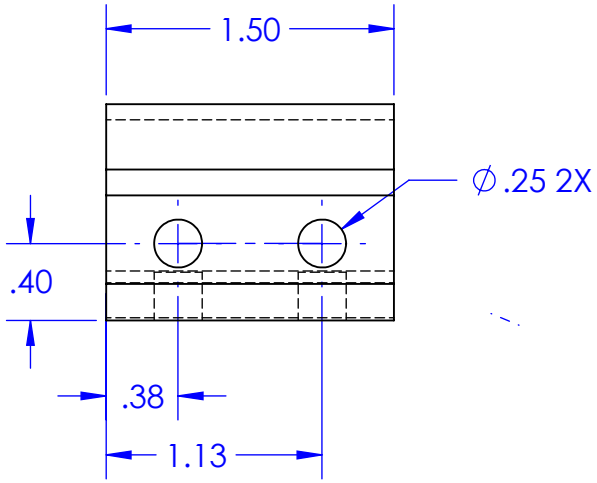

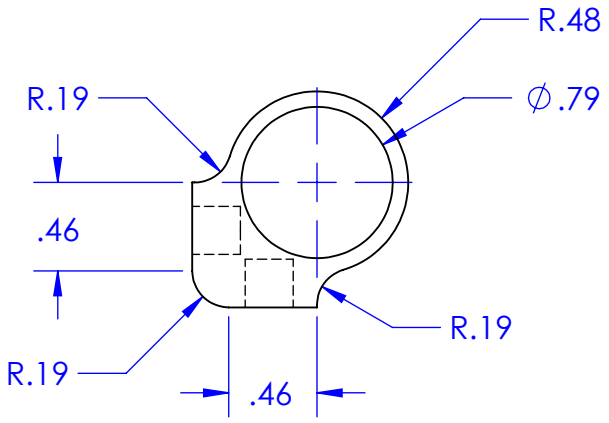

Cal Poly Mechanical Engineering HPV FRAME DESIGN	Title: Axel Bore	Nxt Asb: SP1100	Date: 08/02/2015	Drwn. By: Matt Allen
	Dwg. #: SP1102	Scale: 1:1	Material: 1018 Steel	Chkd. By:

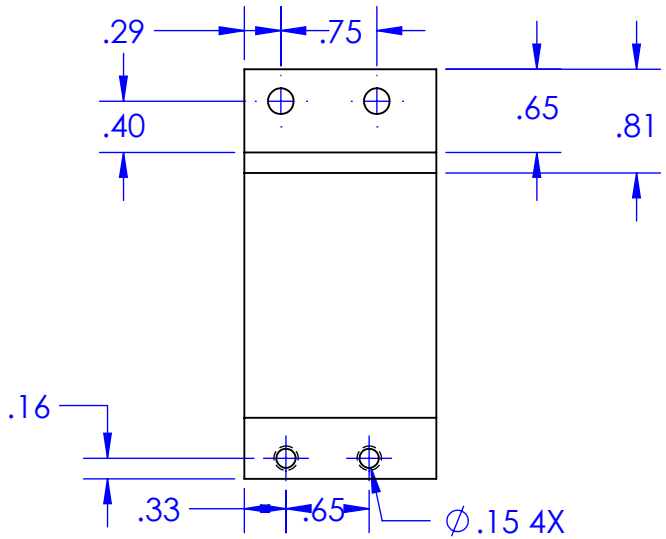

NOTES
UNLESS OTHERWISE SPECIFIED:
1. ALL DIMENSIONS IN INCHES
2. TOLERANCES:
X.XX= ±.005
ANGLES= ±.05°
3. INSIDE TOOL RADIUS .01 MAX
4. BREAK SHARP EDGES .01 MAX

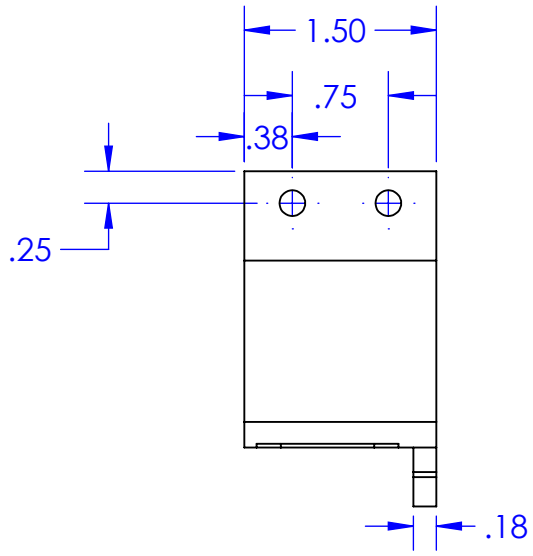

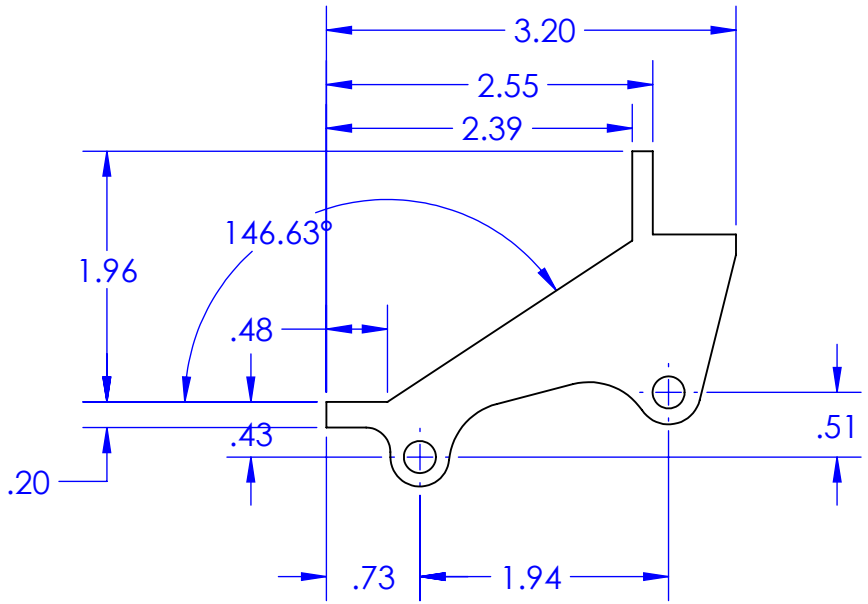

Cal Poly Mechanical Engineering HPV FRAME DESIGN	Title: Knuckle	Nxt Asb: 1100	Date: 08/02/2015	Drwn. By: Matt Allen
	Dwg. #: 1103	Scale: 1:1.5	Material: 6061-T6	Chkd. By:

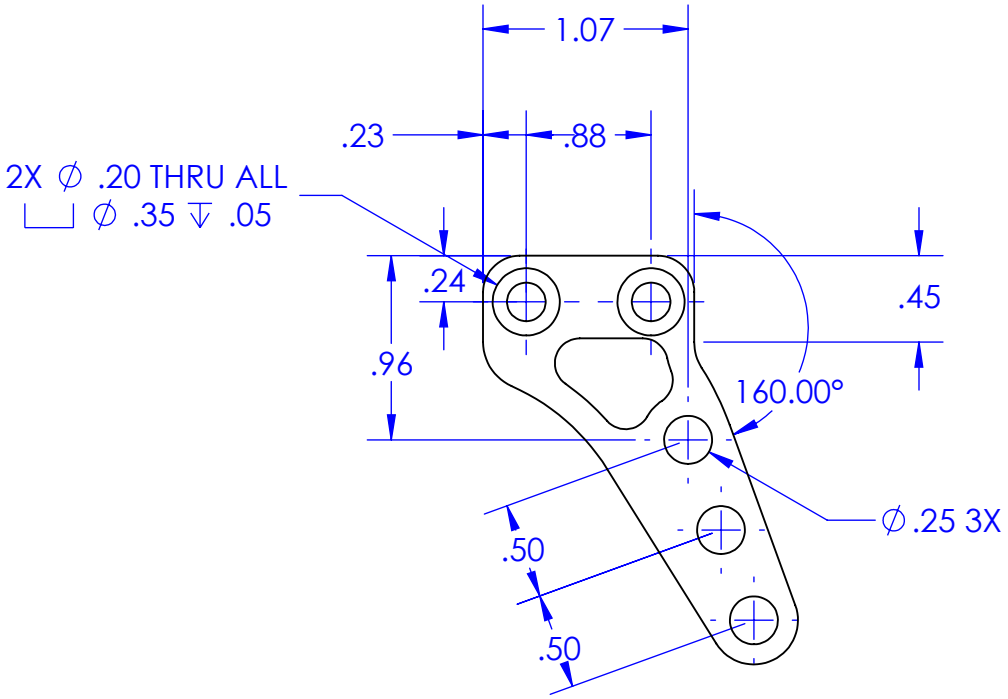

NOTES
UNLESS OTHERWISE SPECIFIED:

1. ALL DIMENSIONS IN INCHES
2. TOLERANCES:
   X.XX= ± .005
   ANGLES= ± .5°
3. INSIDE TOOL RADIUS .01 MAX
4. BREAK SHARP EDGES .01 MAX

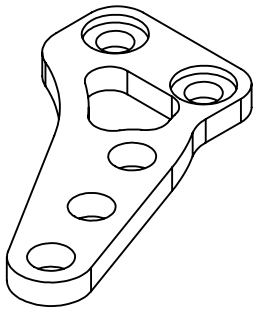

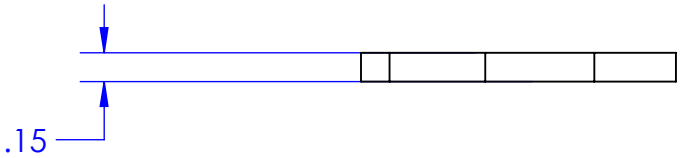

Cal Poly Mechanical Engineering HPV FRAME DESIGN	Title: Tie Rod Plate	Nxt Asb: SP1100	Date: 08/02/2015	Drwn. By: Matt Allen
	Dwg. #: SP1104	Scale: 1:1	Material: 6061-T6	Chkd. By:

ITEM NO.	PART NUMBER	DESCRIPTION	QTY.
1	SP1201	MID-DRIVE AND BB WELDMENT	1
2	SP1202	DRIVE SIDE DROPOUT	1
3	SP1203	NON-DRIVE SIDE DROPOUT	1
4	SP1204	BELL CRANK TAB	1
5	SP1205	STEERING COLUMN TUBING	1
6	SP1206	STEERING COLUMN EXTENSION STEM	1
7	SP1207A	MMC 5905K230 ROLLER BEARING	3
8	SP1207B	MMC 5905K250 ROLLER BEARING	1
11	SP1208	APEX MS-20270-A10	2
12	SP1209	TIE ROD	2
13	SP1210	MMC 6064K121 ROD END	4

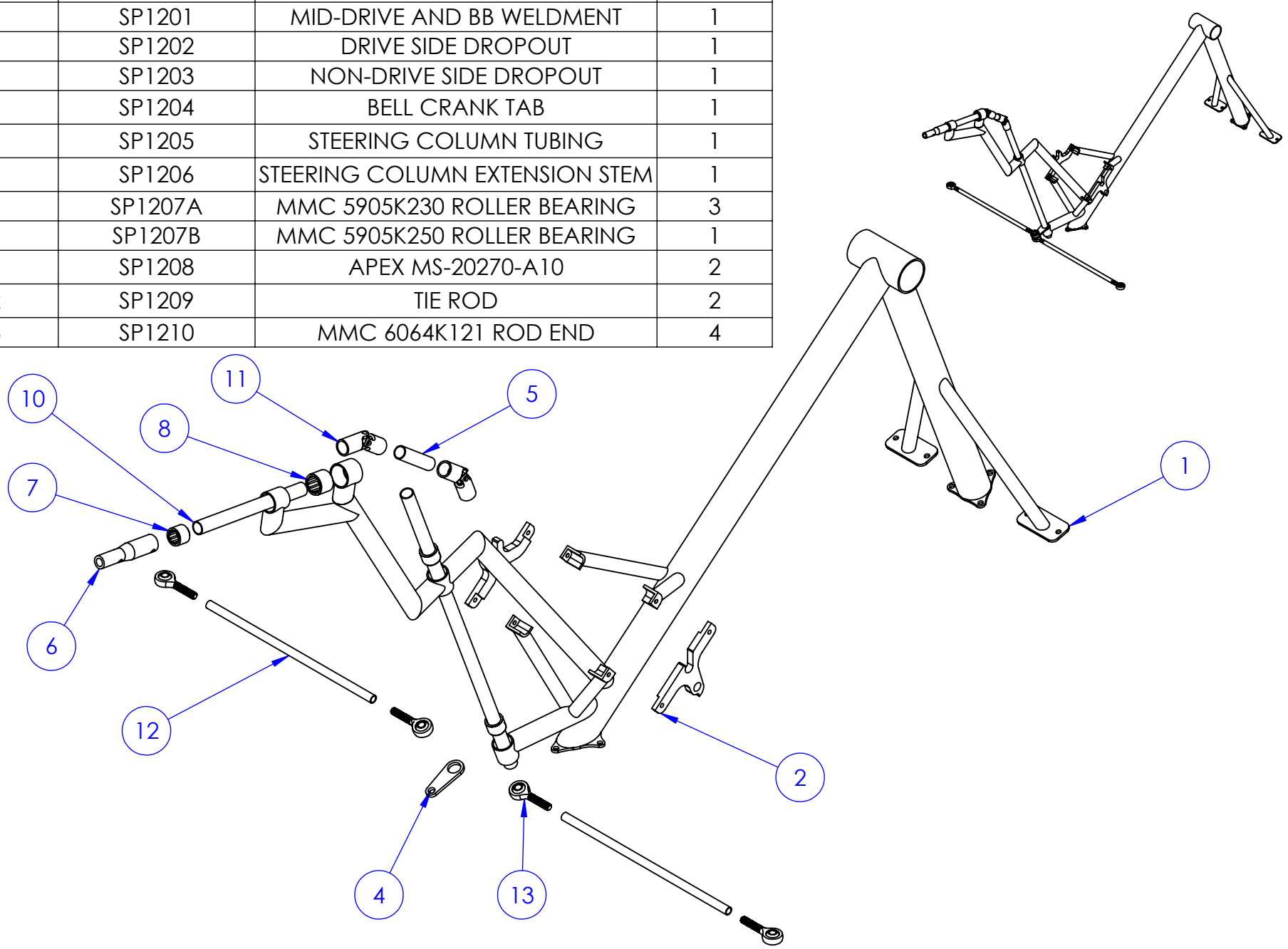

Cal Poly Mechanical Engineering HPV FRAME DESIGN	Title: STEERING & BB ASSY	Nxt Asb: SP1000	Date: 8/4/2015	Drwn. By: PETER AUMANN
	Dwg. #: SP1200	Scale: 1:5	Material: N/A	Chkd. By:

NOTES
UNLESS OTHERWISE SPECIFIED:

1. ALL DIMENSIONS IN INCHES
2. TOLERANCES:
   X.XXX= ±.005
   ANGLES= ±.1°
3. INSIDE TOOL RADIUS .01 MAX
4. BREAK SHARP EDGES .01 MAX

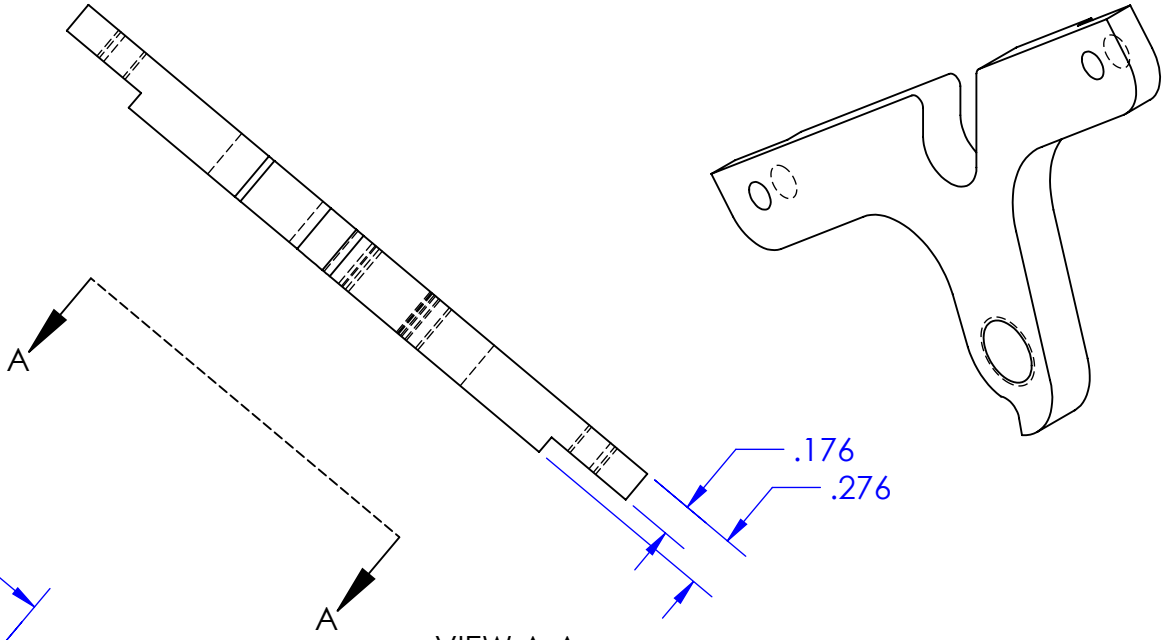

VIEW A-A
SCALE 1 : 1

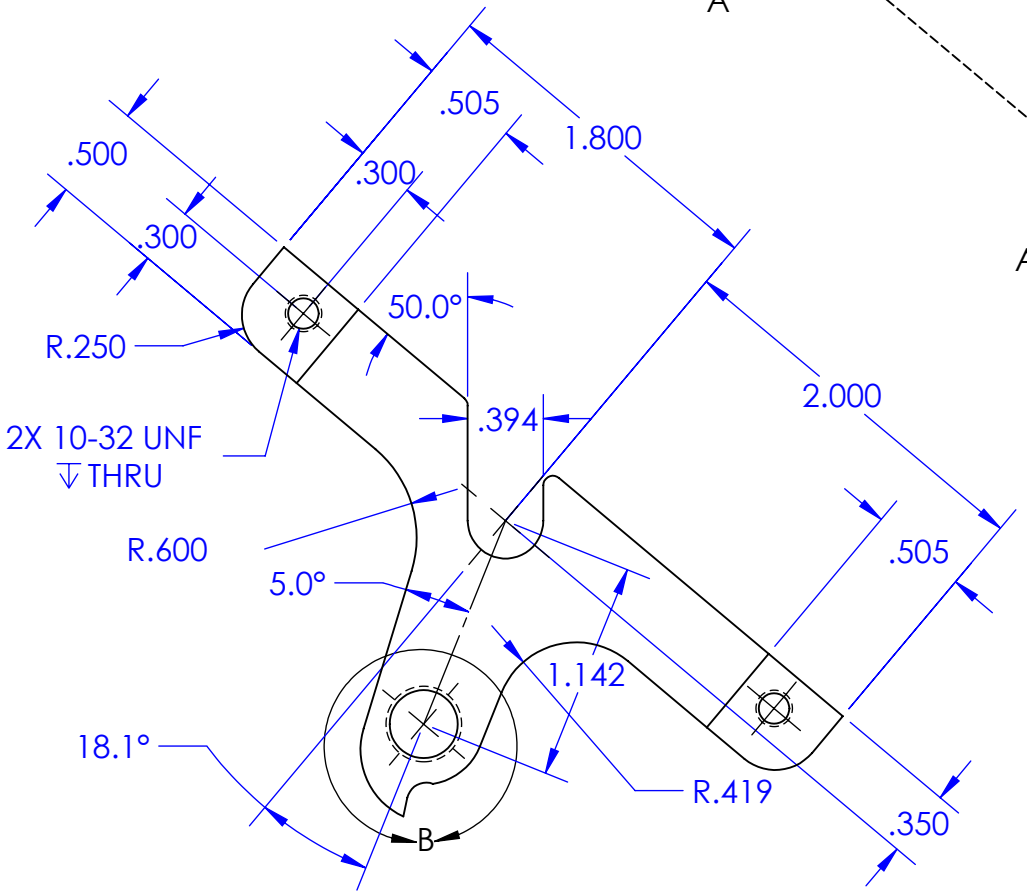

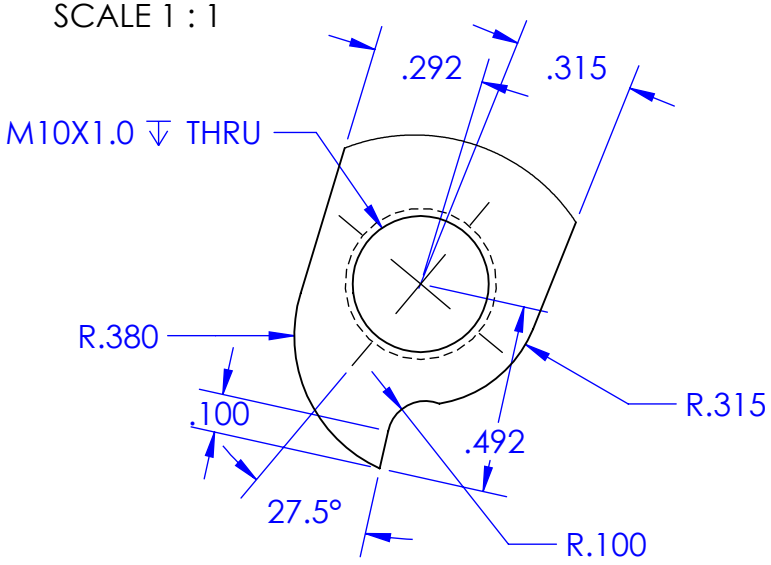

DETAIL B
SCALE 2 : 1

Cal Poly Mechanical Engineering HPV FRAME DESIGN	Title: DRIVE-SIDE DROPOUT	Nxt Asb: SP1200	Date: 8/2/2015	Drwn. By: PETER AUMANN
	Dwg. #: SP1201	Scale: 1:1	Material: AL 6061	Chkd. By:

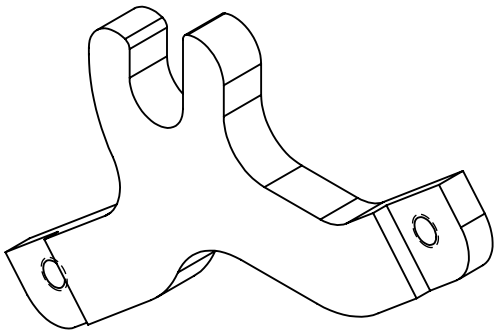

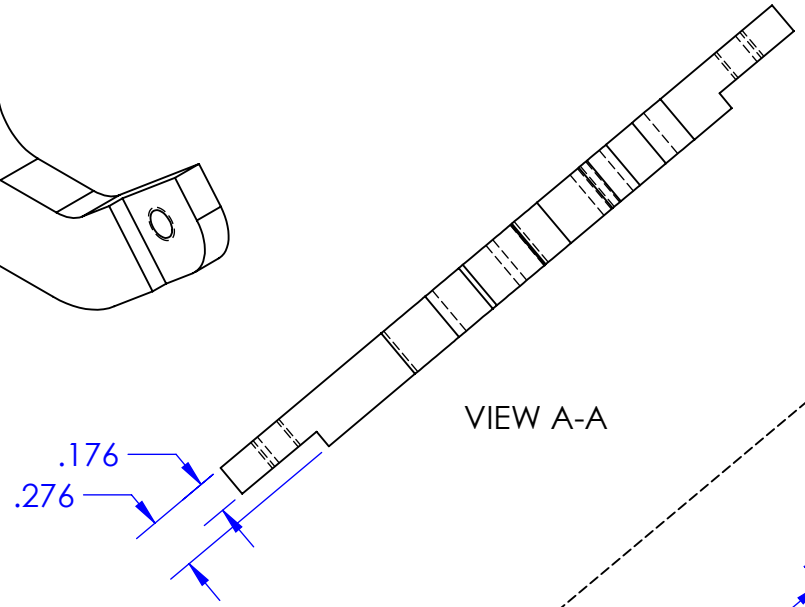

NOTES
UNLESS OTHERWISE SPECIFIED:
1. ALL DIMENSIONS IN INCHES
2. TOLERANCES:
   X.XxX= ± .005
   ANGLES= ± .1 °
3. INSIDE TOOL RADIUS .01 MAX
4. BREAK SHARP EDGES .01 MAX

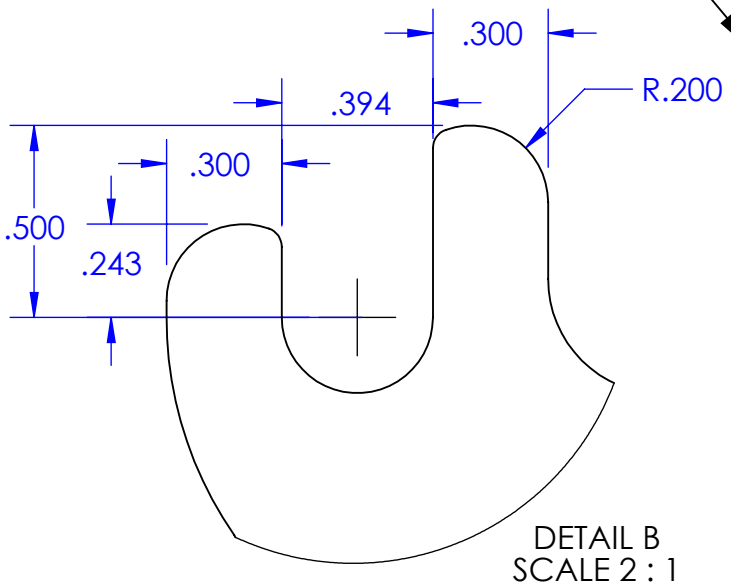

DETAIL B
SCALE 2 : 1

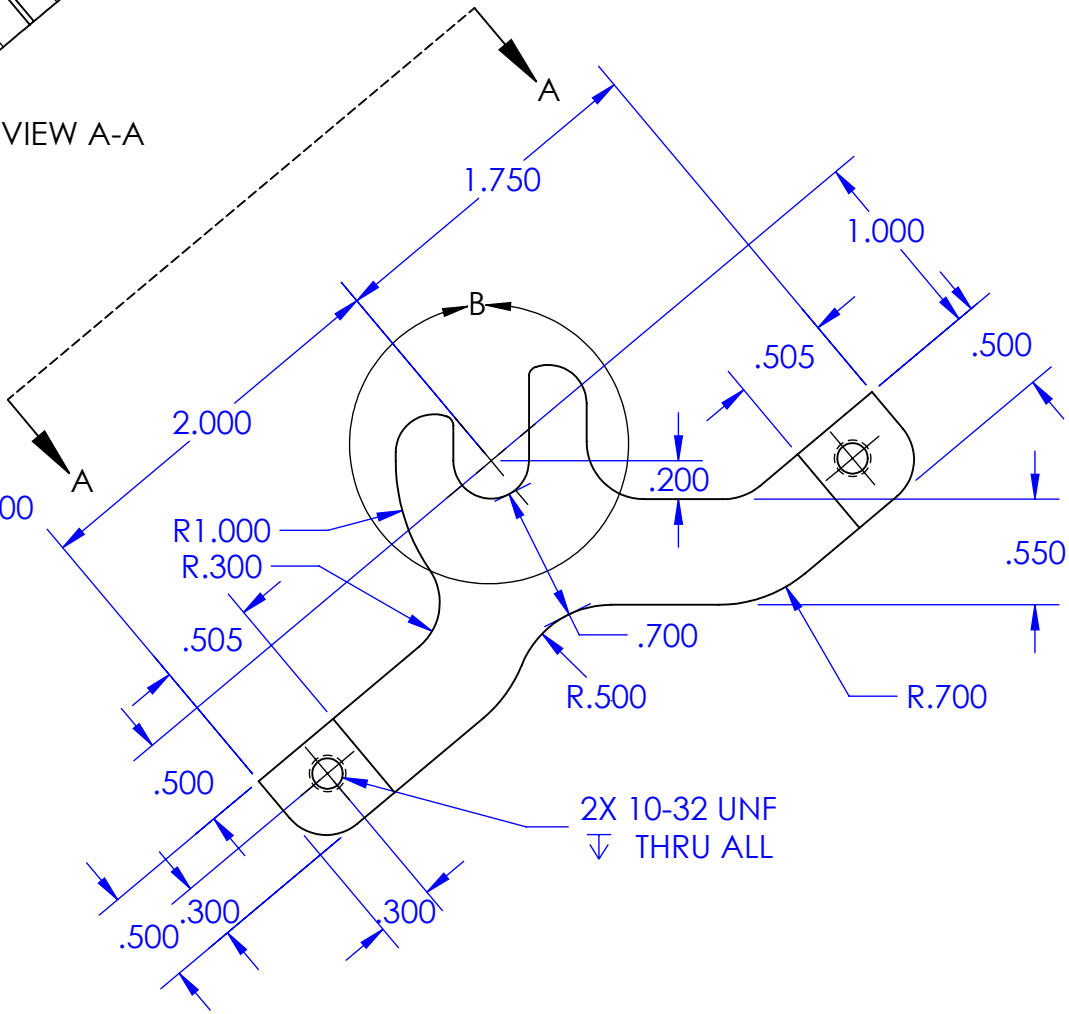

Cal Poly Mechanical Engineering HPV FRAME DESIGN	Title: NON-DRIVE SIDE DROPOUT	Nxt Asb: SP1200	Date: 8/2/2015	Drwn. By: PETER AUMANN
	Dwg. #: SP1203	Scale: 1:1	Material: AL 6061	Chkd. By:

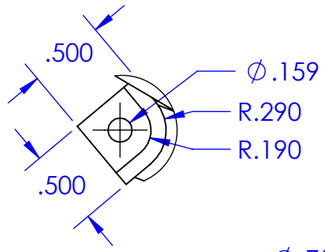

DETAIL C
SCALE 1 : 1

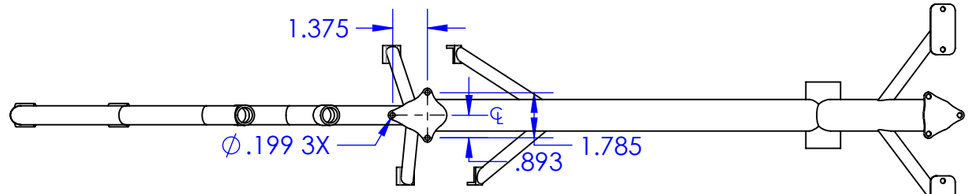

NOTE: "FEET" ARE HAND SHAPED,
DIMENSIONS APPROXIMATE

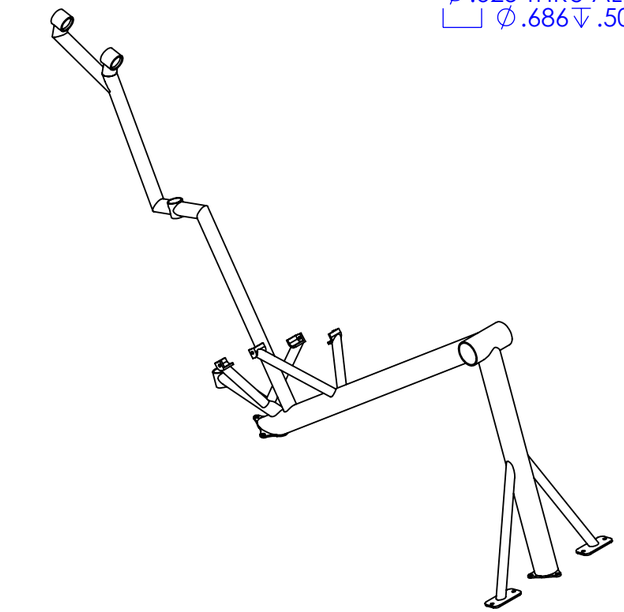

NOTE: THE LOCATION OF EACH STRUT IS
APPROXIMATE AS THEY ARE HAND MITERED

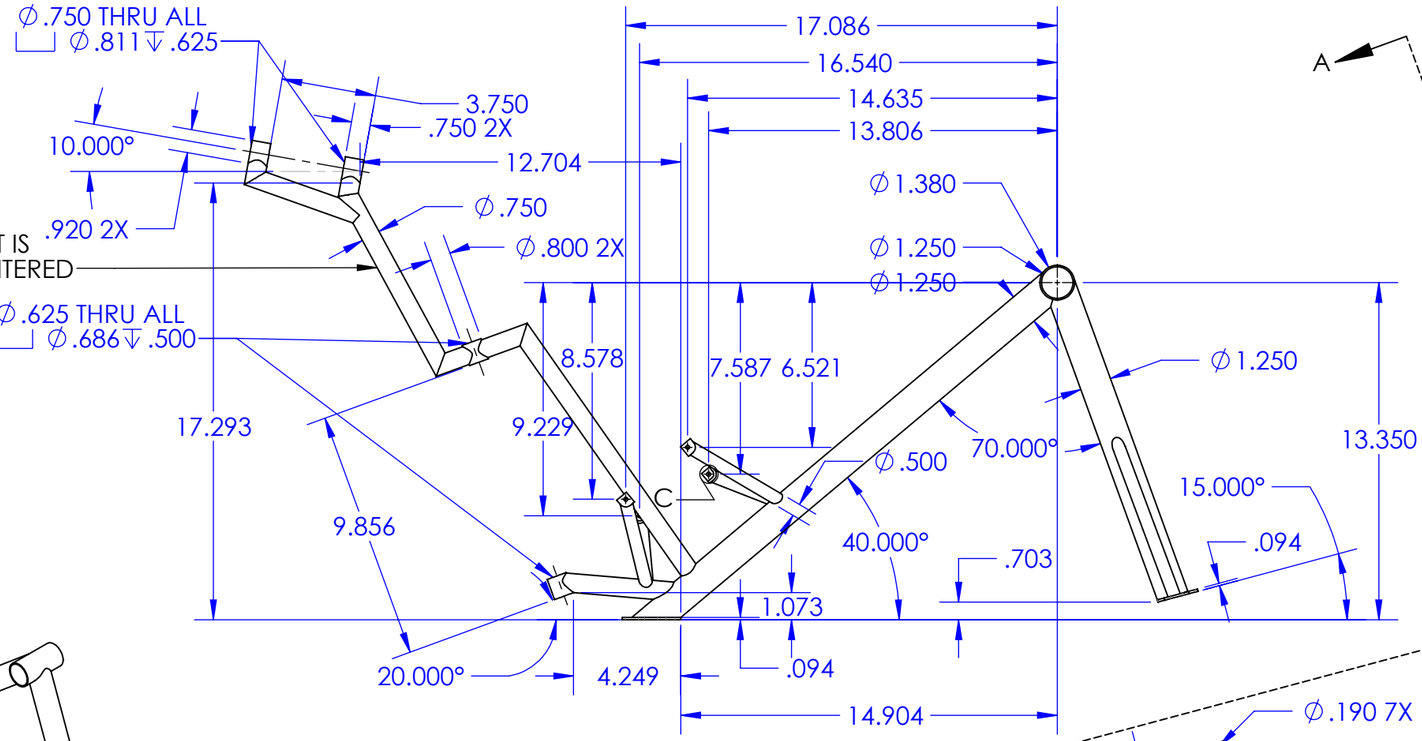

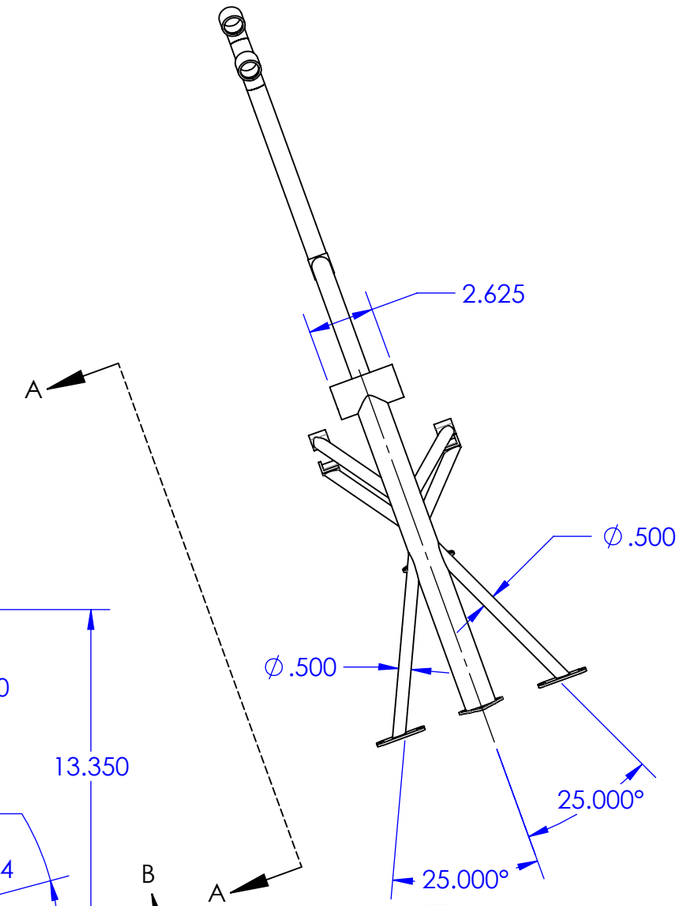

VIEW A-A
SCALE 1 : 6

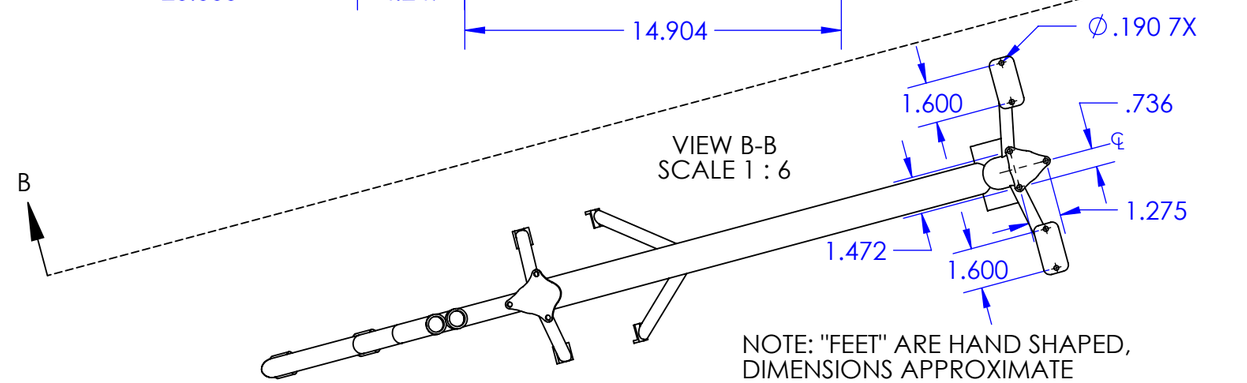

VIEW B-B
SCALE 1 : 6

NOTE: "FEET" ARE HAND SHAPED,
DIMENSIONS APPROXIMATE

NOTES
UNLESS OTHERWISE SPECIFIED:
1. ALL DIMENSIONS IN INCHES
2. TOLERANCES:
   X.XX=±.01
   ANGLES=±.1°
3. INSIDE TOOL RADIUS .01 MAX
4. BREAK SHARP EDGES .01 MAX

SolidWorks Educational Edition.
For Instructional Use Only.

Cal Poly Mechanical Engineering HPV FRAME DESIGN	Title: MID-DRIVE MOUNT	Nxt Asb: DROPOUT	Date: 6/10/2015	Drwn. By: TRENT HELLMANN
	Dwg. #: SP1201	Scale: 1:8	Material: 1020 STEEL	Chkd. By:

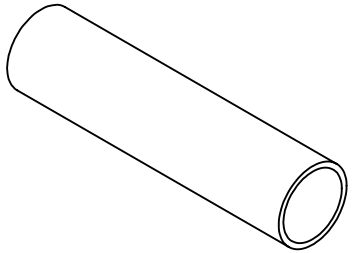

NOTES
UNLESS OTHERWISE SPECIFIED:
1. ALL DIMENSIONS IN INCHES
2. TOLERANCES:
   X.XXX= ± .002
   X.XX= ± .10
   ANGLES= ± 1°
3. INSIDE TOOL RADIUS .01 MAX
4. BREAK SHARP EDGES .01 MAX

MULTIPLE LENGTHS OF 0.500 TUBING USED
5. 2.00
6. 15.25

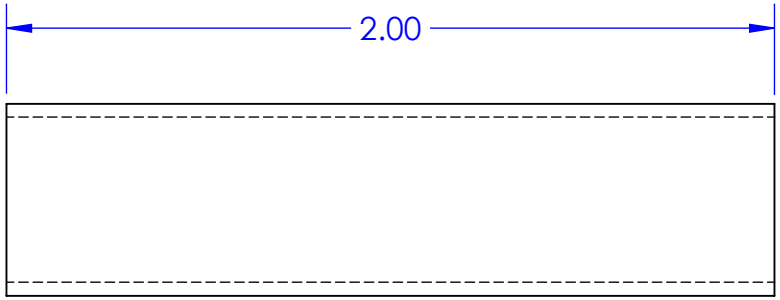

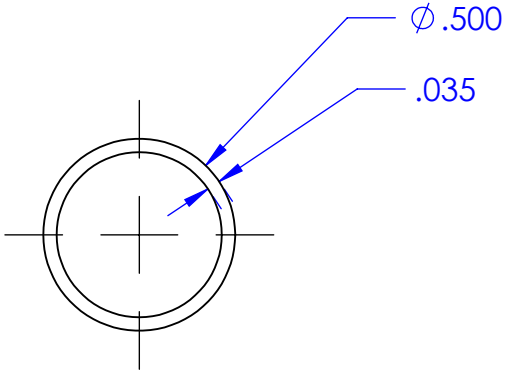

Cal Poly Mechanical Engineering HPV FRAME DESIGN	Title: STEERING COLUMN TUBING	Nxt Asb: SP1200	Date: 8/3/2015	Drwn. By: PETER AUMANN
	Dwg. #: SP1205	Scale: 2:1	Material: 4130 STEEL	Chkd. By:

Mirror part to create opposite side steerer

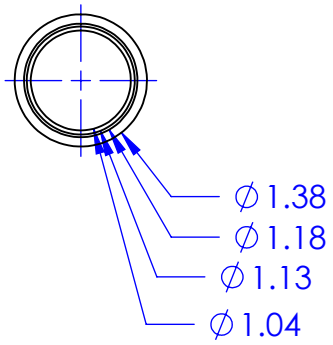

NOTES
UNLESS OTHERWISE SPECIFIED:
1. ALL DIMENSIONS IN INCHES
2. TOLERANCES:
X.XX= ±.01
ANGLES= ±.5°
3. INSIDE TOOL RADIUS .01 MAX
4. BREAK SHARP EDGES .01 MAX

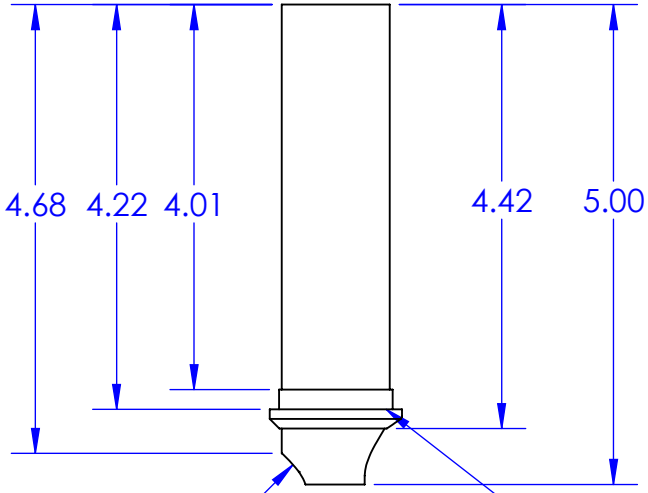

Miter profile at
56.5 degree angle

Press Stock Headtube Bearing cup to steerer

Cal Poly Mechanical Engineering HPV FRAME DESIGN	Title: Steerer tube	Nxt Asb: 1100	Date: 08/02/2015	Drwn. By: Matt Allen
	Dwg. #: 1101	Scale: 1:2	Material: 4041 Steel	Chkd. By:

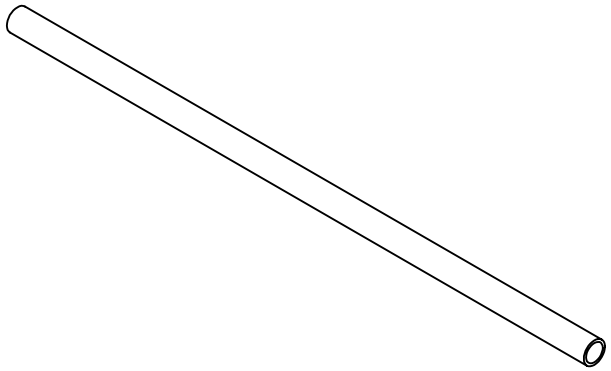

NOTES
UNLESS OTHERWISE SPECIFIED:
1. ALL DIMENSIONS IN INCHES
2. TOLERANCES:
   X.XXx= ± .010
   ANGLES= ± .1°
3. INSIDE TOOL RADIUS .01 MAX
4. BREAK SHARP EDGES .01 MAX

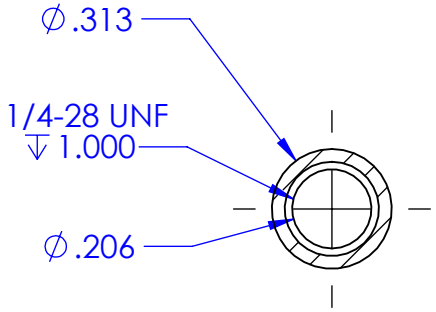

SECTION C-C
SCALE 2 : 1

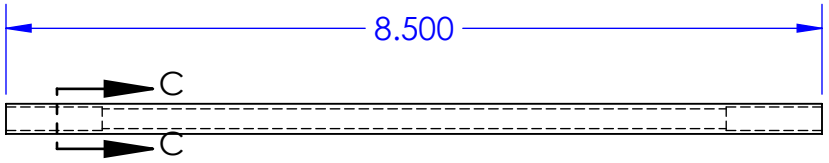

Cal Poly Mechanical Engineering HPV FRAME DESIGN	Title: TIE ROD	Nxt Asb: SP1200	Date: 8/4/2015	Drwn. By: PETER AUMANN
	Dwg. #: SP1209	Scale: 1:2	Material: 4130 STEEL	Chkd. By:

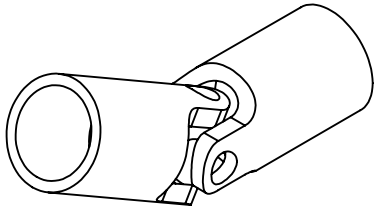

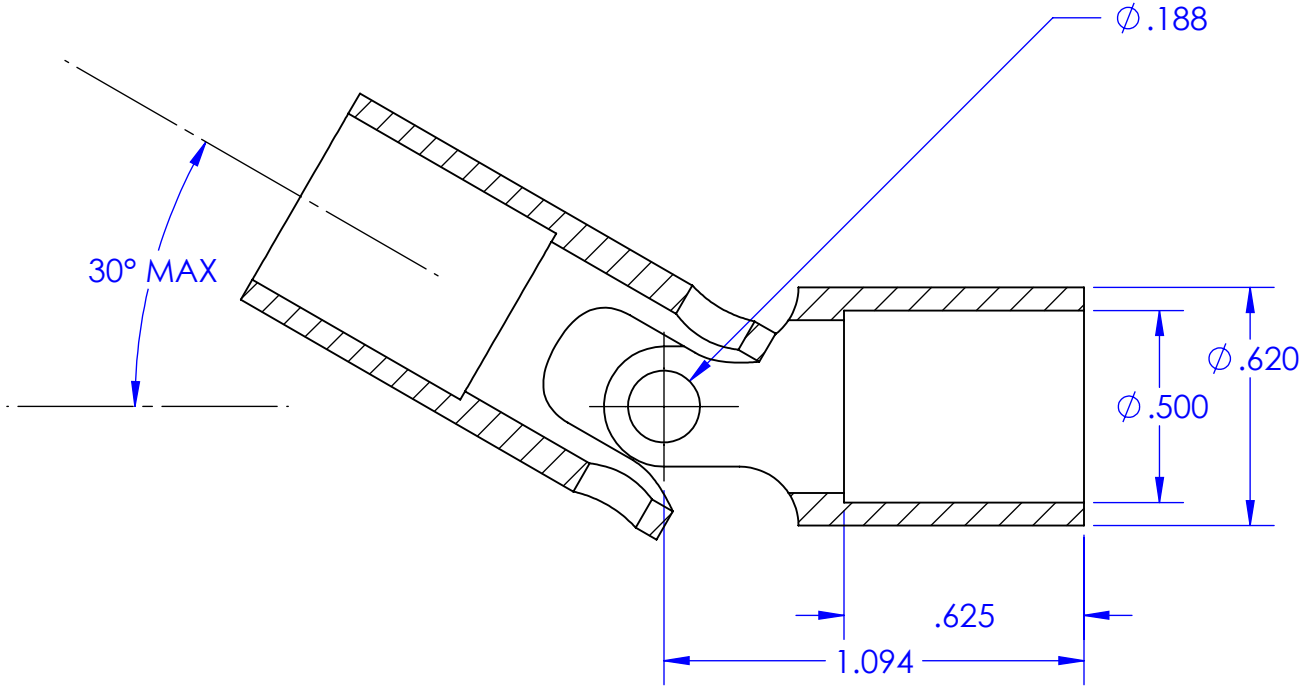

SECTION A-A
SCALE 2 : 1

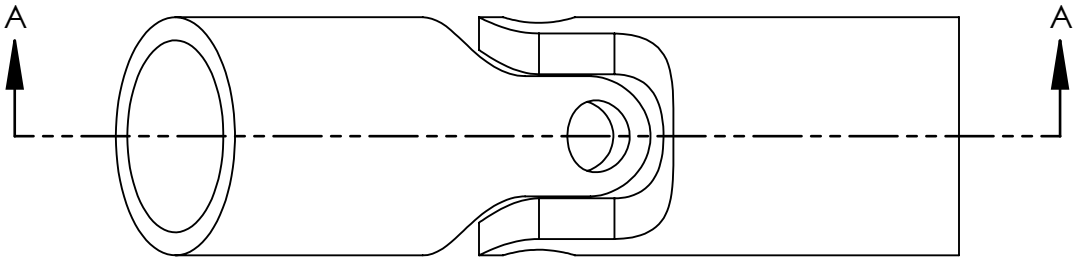

Cal Poly Mechanical Engineering HPV FRAME DESIGN	Title: APEX MS-20270-A10	Nxt Asb: SP1200	Date: 8/3/2015	Drwn. By: PETER AUMANN
	Dwg. #: SP1208	Scale: 2:1	Material: STEEL	Chkd. By:

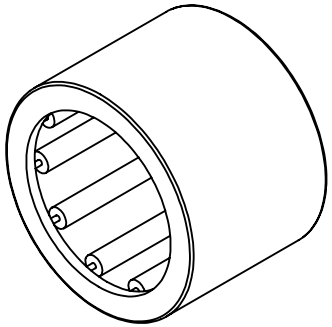

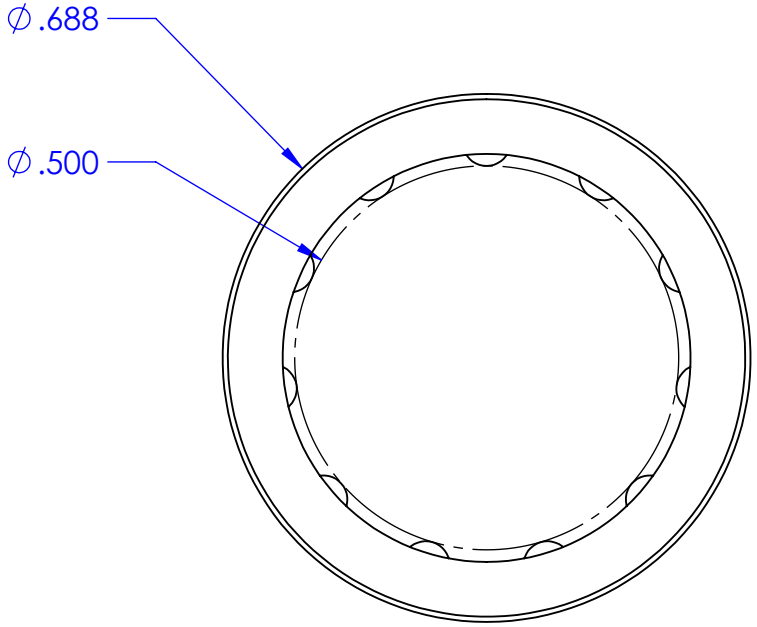

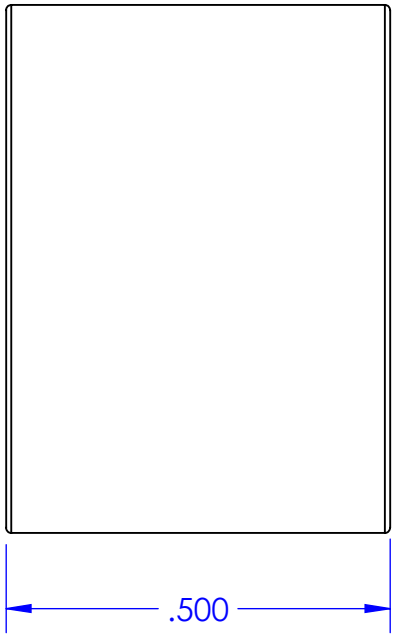

Cal Poly Mechanical Engineering HPV FRAME DESIGN	Title: MMC 5905K230	Nxt Asb: SP1200	Date: 8/3/2015	Drwn. By: PETER AUMANN
	Dwg. #: SP1207A	Scale: 4:1	Material: HARDENED STEEL	Chkd. By:

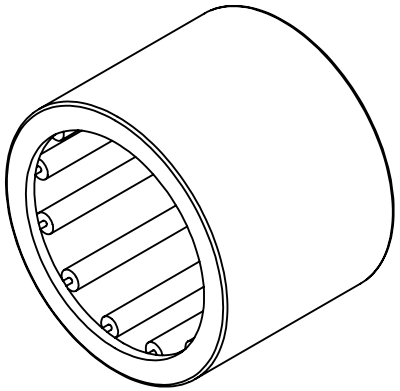

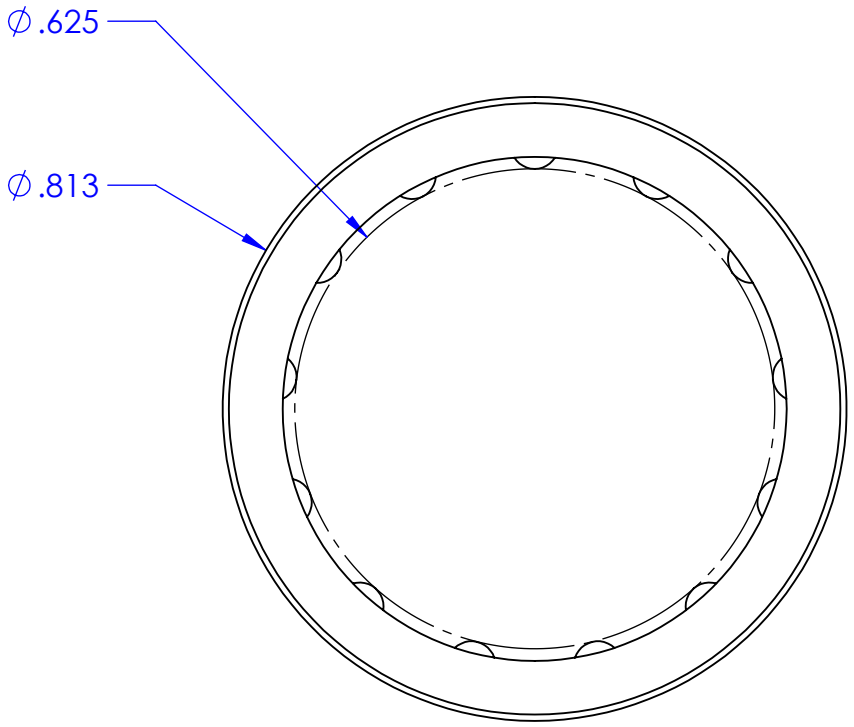

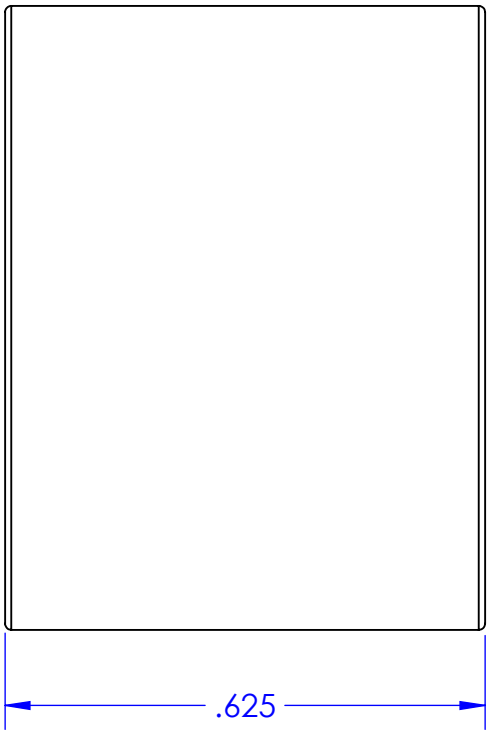

Cal Poly Mechanical Engineering HPV FRAME DESIGN	Title: MMC 5905K250	Nxt Asb: SP1200	Date: 8/3/2015	Drwn. By: PETER AUMANN
	Dwg. #: SP1207B	Scale: 4:1	Material: HARDENED STEEL	Chkd. By:

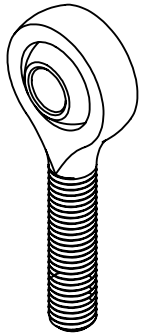

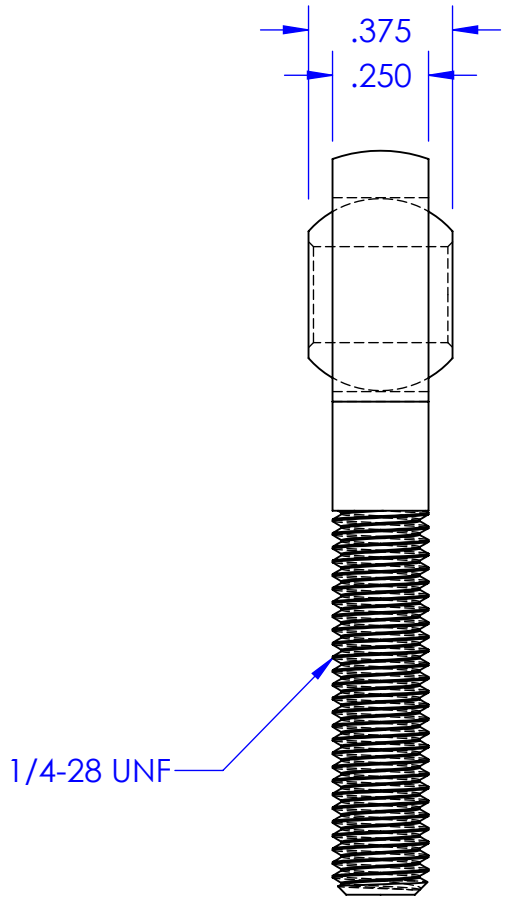

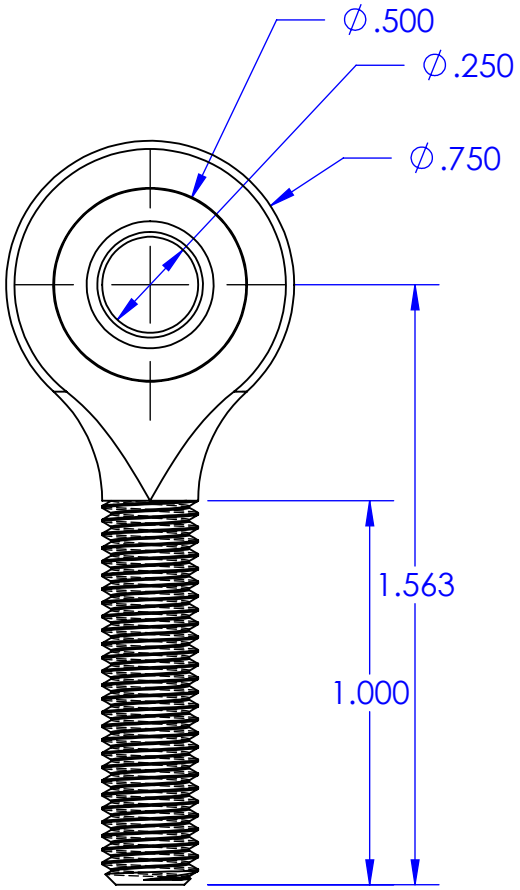

Cal Poly Mechanical Engineering HPV FRAME DESIGN	Title: MMC #60645K121	Nxt Asb: SP1200	Date: 8/3/2015	Drwn. By: PETER AUMANN
	Dwg. #: SP1210	Scale: 2:1	Material: STEEL	Chkd. By:

NOTES
Vendor Part, Critical Dimensions Only
McMaster 60656K121
1/4--28 1/4 inch Rod End

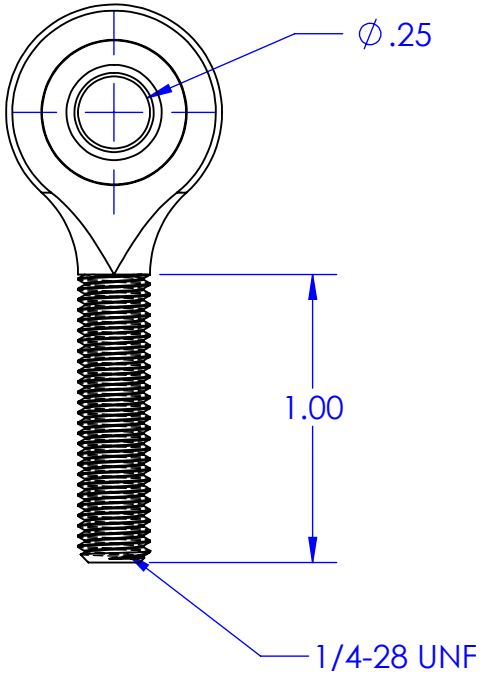

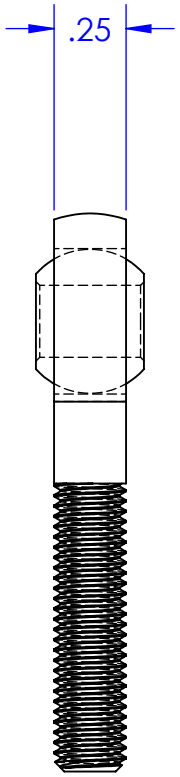

Cal Poly Mechanical Engineering HPV FRAME DESIGN	Title: 1/4 Rod End	Nxt Asb:SP1300	Date:07/23/2015	Drwn. By: Matt Allen
	Dwg. #: SP1309	Scale: 1:1	Material: Stainless	Chkd. By:

ITEM NO.	PART NUMBER	DESCRIPTION	QTY.
1	SP1301	SEAT SHELL	1
2	SP1302	SEAT RAILS	2
3	SP1303	FRONT BRACKETS	2
4	SP1304	REAR BRACKETS	1
5	SP1305	FRONT BRACKET SPANNER	1
6	SP1306	CP-K100TLO	2
7	SP1307	SEAT SUPPORTS	2
9	SP1308	UPPER TIE ROD	2
10	SP1309	LOWER TIE ROD	2
11	SP1310	MMC 6064K121 ROD END	8
12	SP1311	TOP SEAT BRACKET	2
14	SP1312	FRONT IDLER MOUNT	1
15	SP1313	REAR IDLER MOUNT	1

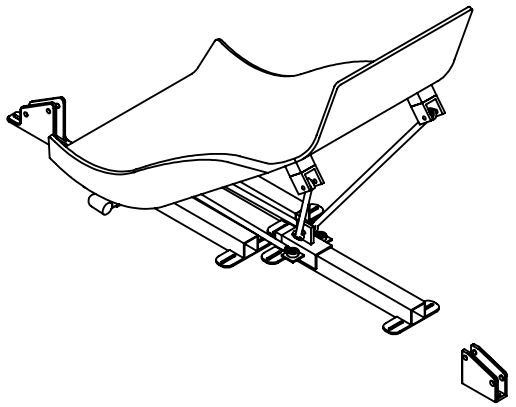

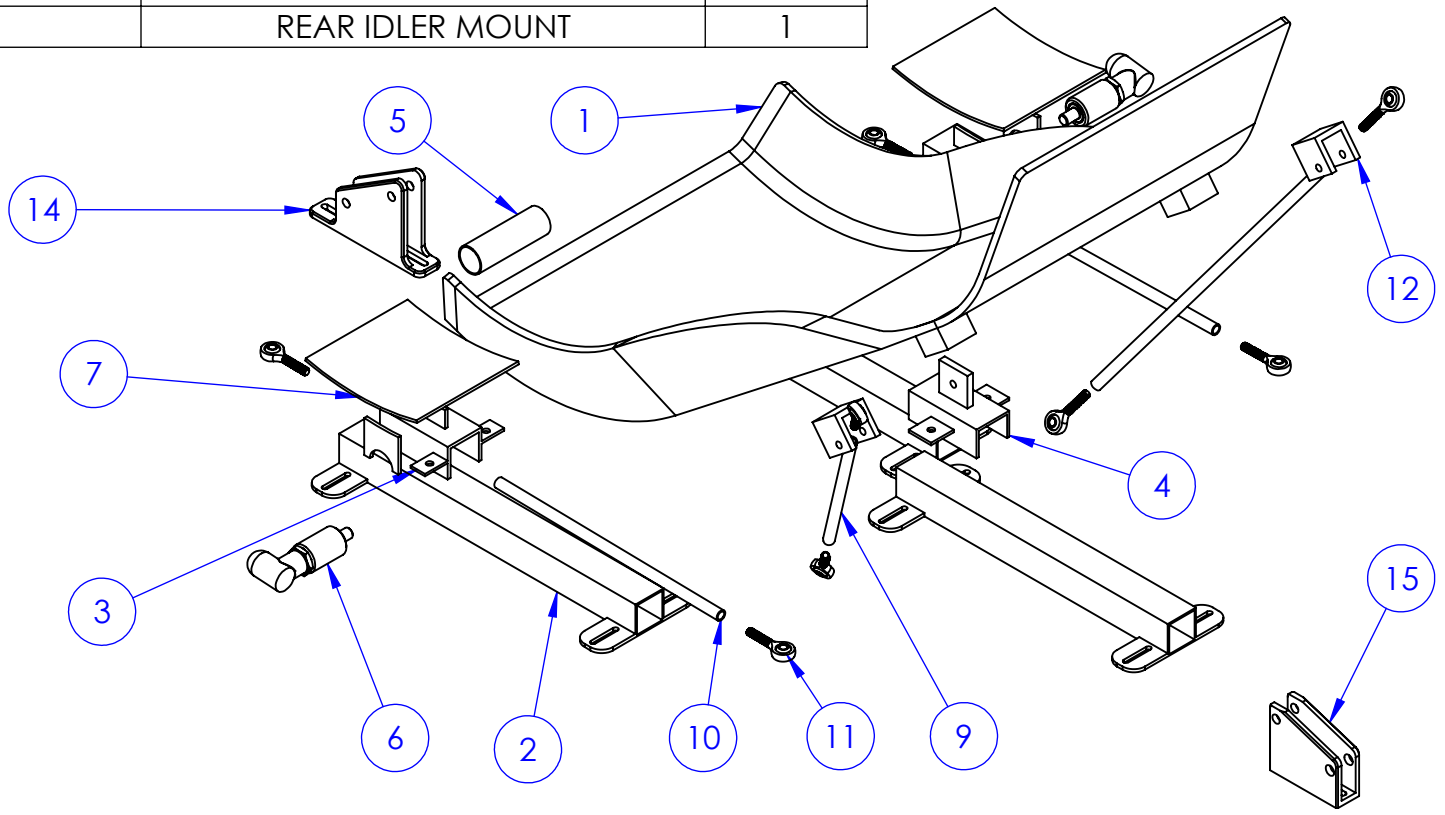

Cal Poly Mechanical Engineering HPV FRAME DESIGN	Title: SEAT & DRIVETRAIN SUBFRAME	Nxt Asb: SP1000	Date: 8/5/2015	Drwn. By: PETER AUMANN
	Dwg. #: SP1300	Scale: 1:6	Material: N/A	Chkd. By:

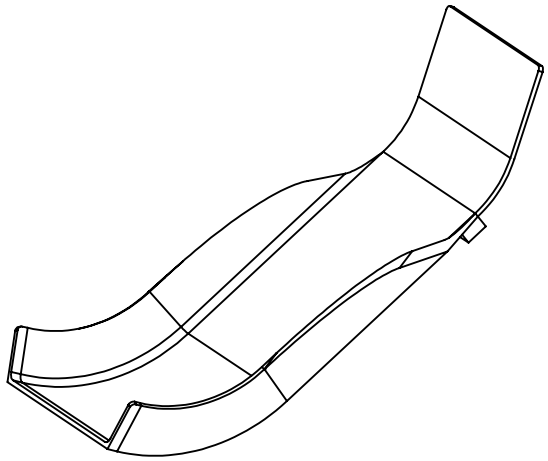

NOTES
UNLESS OTHERWISE SPECIFIED:
1. ALL DIMENSIONS IN INCHES
2. TOLERANCES:
   X.XX= ±.
   ANGLES= ± °
3. INSIDE TOOL RADIUS .01 MAX
4. BREAK SHARP EDGES .01 MAX

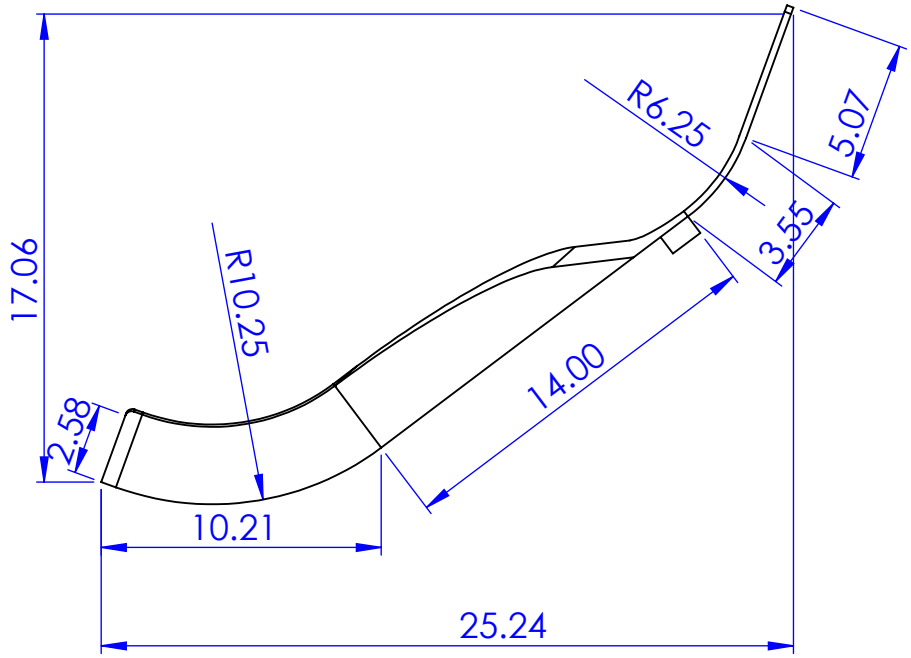

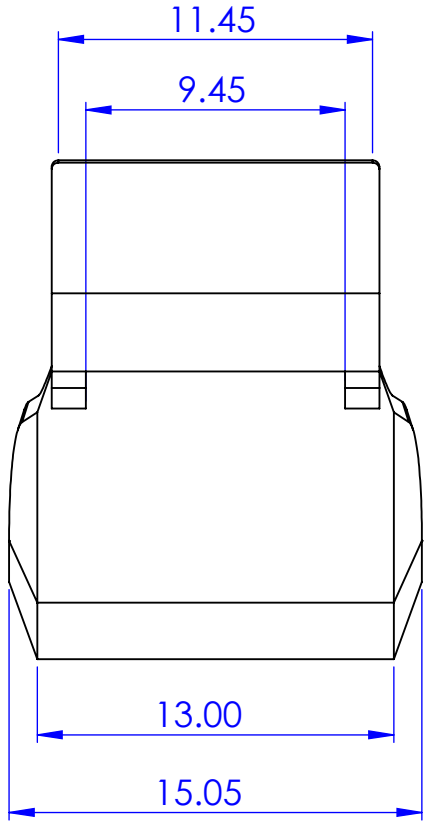

Thickness approximately .375 (see layup schedule)
Dimensions Approximate; use exact model for tool creation

Cal Poly Mechanical Engineering HPV FRAME DESIGN	Title: Seat	Nxt Asb: 1300	Date: 07/22/2015	Drwn. By: Matt Allen
	Dwg. #: 1301	Scale: 1:7	Material: Carbon	Chkd. By:

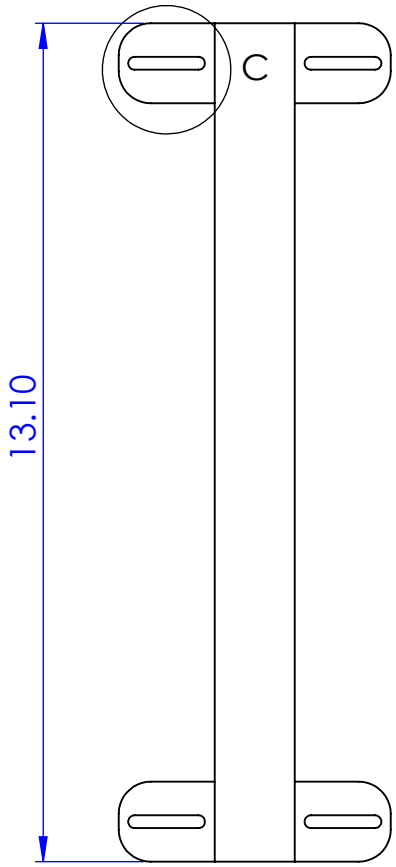

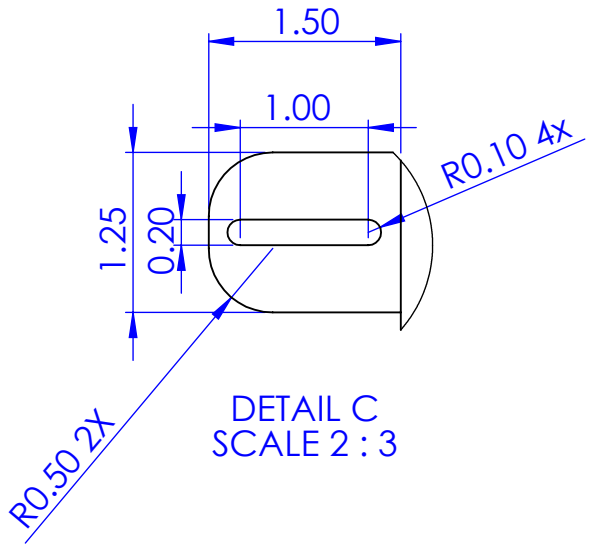

DETAIL C
SCALE 2 : 3

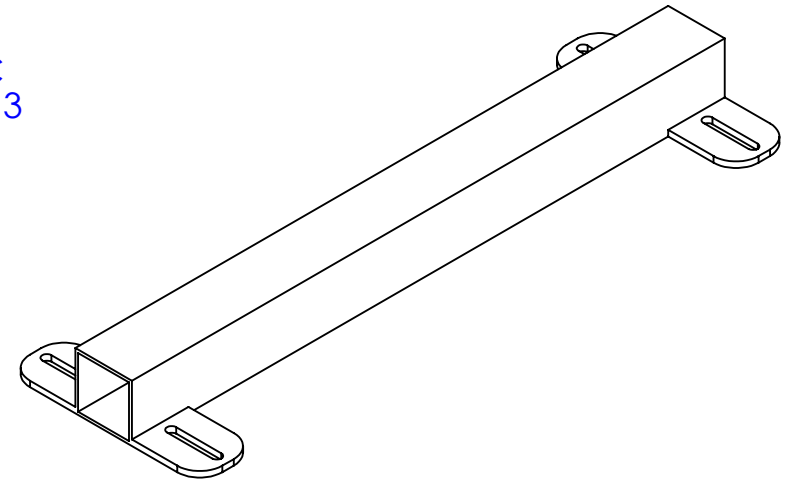

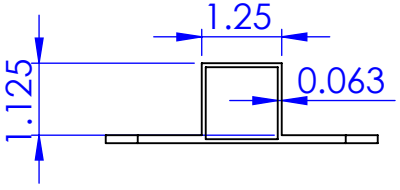

NOTES
UNLESS OTHERWISE SPECIFIED:

1. ALL DIMENSIONS IN INCHES
2. TOLERANCES:
   X.XX= ±.
   ANGLES= ± °
3. INSIDE TOOL RADIUS .01 MAX
4. BREAK SHARP EDGES .01 MAX

Cal Poly Mechanical Engineering HPV FRAME DESIGN	Title: Seat Rails	Nxt Asb: 1300	Date 7/22/2015:	Drwn. By: Matt Allen
	Dwg. #: 1302	Scale: 1:3	Material: 6061-T6 Al	Chkd. By:

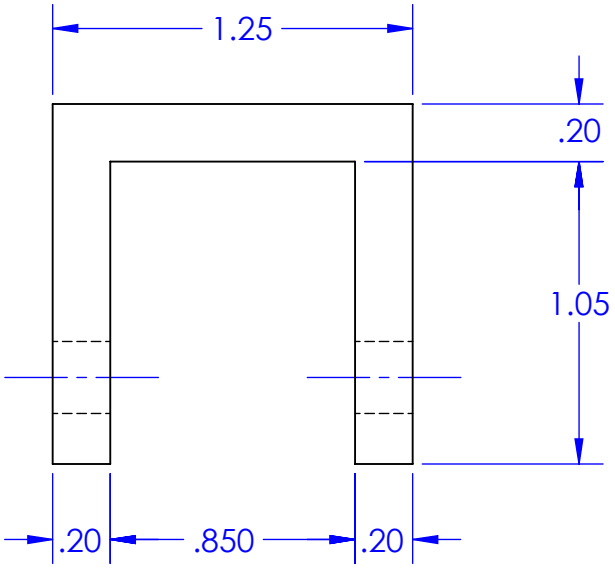

NOTES
UNLESS OTHERWISE SPECIFIED:
1. ALL DIMENSIONS IN INCHES
2. TOLERANCES:
X.XX= ± .01
ANGLES= ± 1 °
3. INSIDE TOOL RADIUS .01 MAX
4. BREAK SHARP EDGES .01 MAX

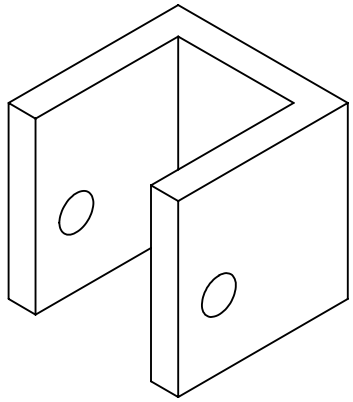

Scale 1:1

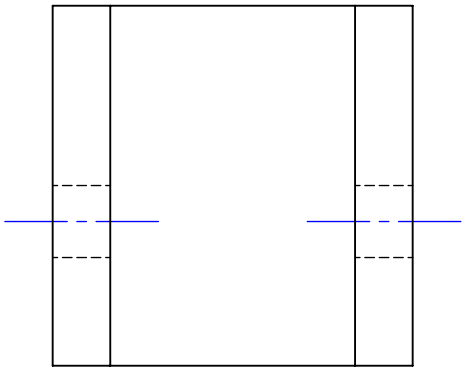

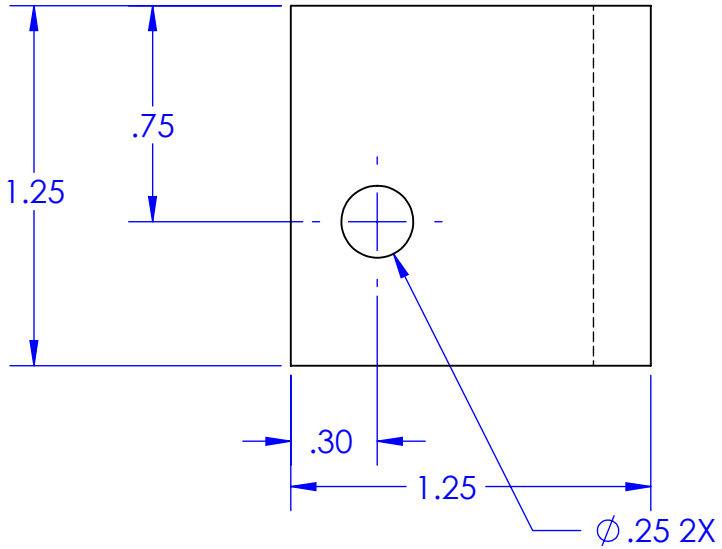

Cal Poly Mechanical Engineering HPV FRAME DESIGN	Title: Seat Top Bracket	Nxt Asb: SP1300	Date: 07/23/2015	Drwn. By: Matt Alle n
	Dwg. # SP1310:	Scale: 3:2	Material: 6061-T6	Chkd. By:

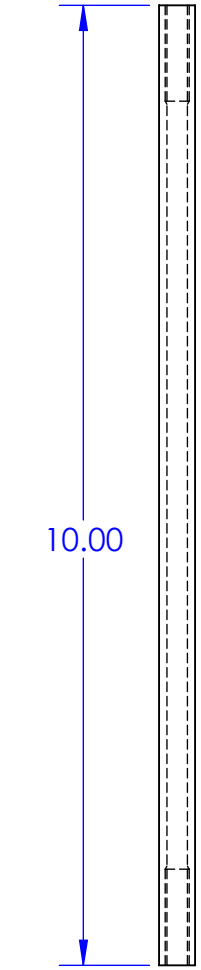

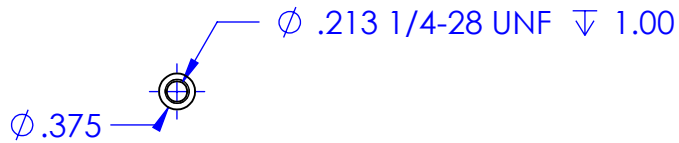

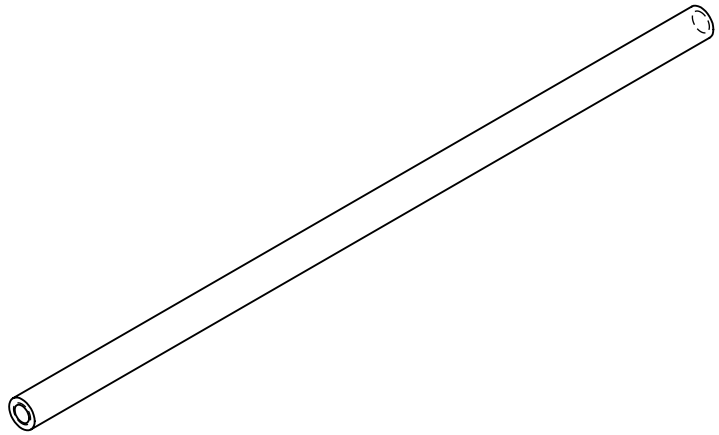

NOTES
UNLESS OTHERWISE SPECIFIED:

1. ALL DIMENSIONS IN INCHES
2. TOLERANCES:
   X.XX= ± .01.
   ANGLES= ± 1°
3. INSIDE TOOL RADIUS .01 MAX
4. BREAK SHARP EDGES .01 MAX

Cal Poly Mechanical Engineering HPV FRAME DESIGN	Title: Rear Seat Tie Rods	Nxt Asb: SP1300	Date: 07/23/2015	Drwn. By: Matt Allen
	Dwg. #: SP1307	Scale: 1:2	Material: 1018 Steel	Chkd. By:

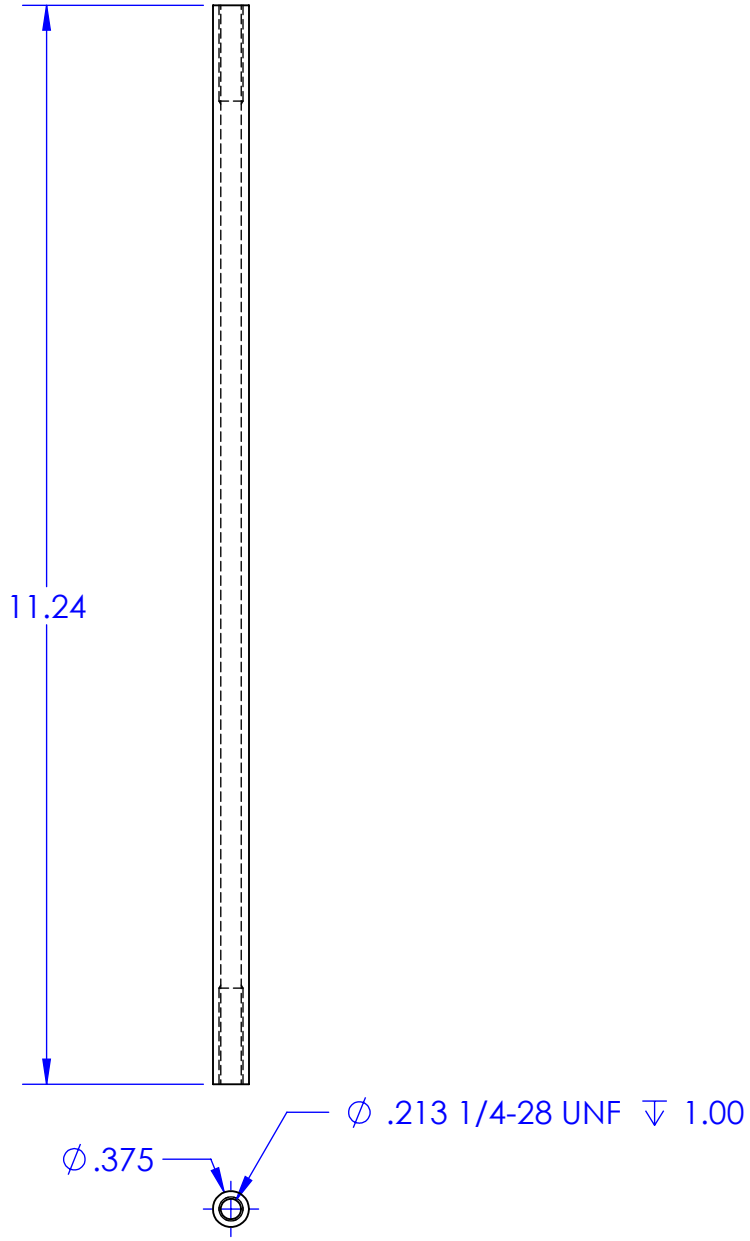

NOTES
UNLESS OTHERWISE SPECIFIED:

1. ALL DIMENSIONS IN INCHES
2. TOLERANCES:
   X.XX= ± .01
   ANGLES= ± 1°
3. INSIDE TOOL RADIUS .01 MAX
4. BREAK SHARP EDGES .01 MAX

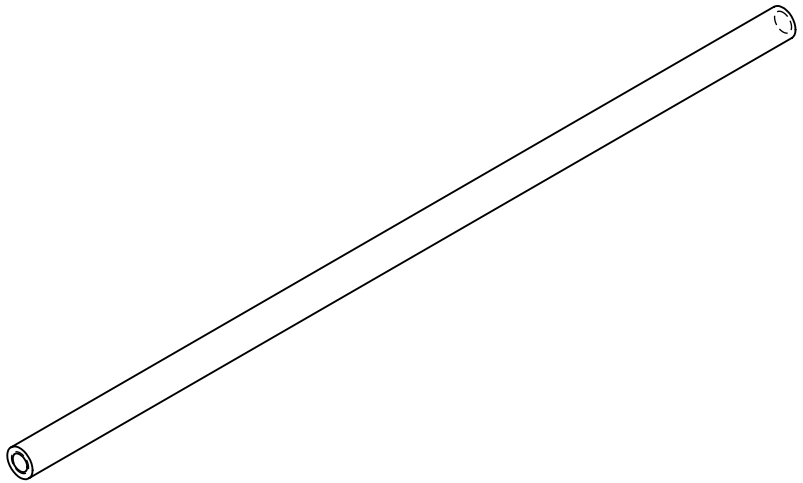

Cal Poly Mechanical Engineering HPV FRAME DESIGN	Title: Rear V Tie Rod	Nxt Asb:SP1300	Date: 07/23/2015	Drwn. By: Matt Allen
	Dwg. #: SP1308	Scale:1:2	Material: 1018 Steel	Chkd. By:

NOTES
UNLESS OTHERWISE SPECIFIED:

1. ALL DIMENSIONS IN INCHES
2. TOLERANCES:
   X.XX= ±0.01
   ANGLES= ±1 °
3. INSIDE TOOL RADIUS .01 MAX
4. BREAK SHARP EDGES .01 MAX

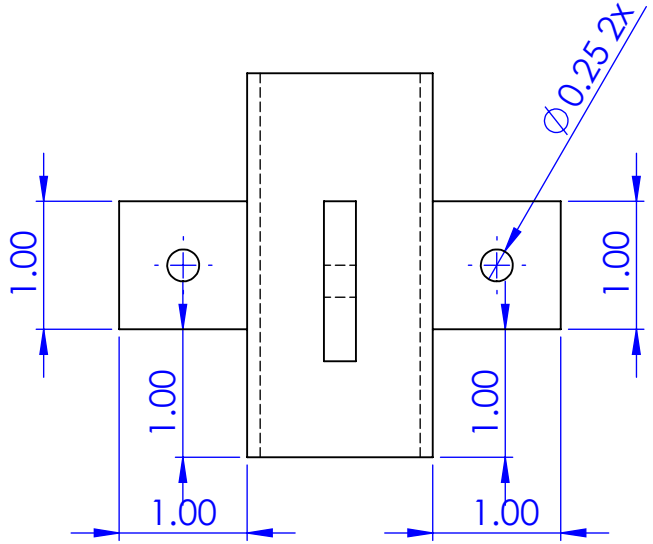

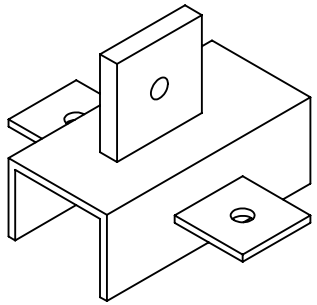

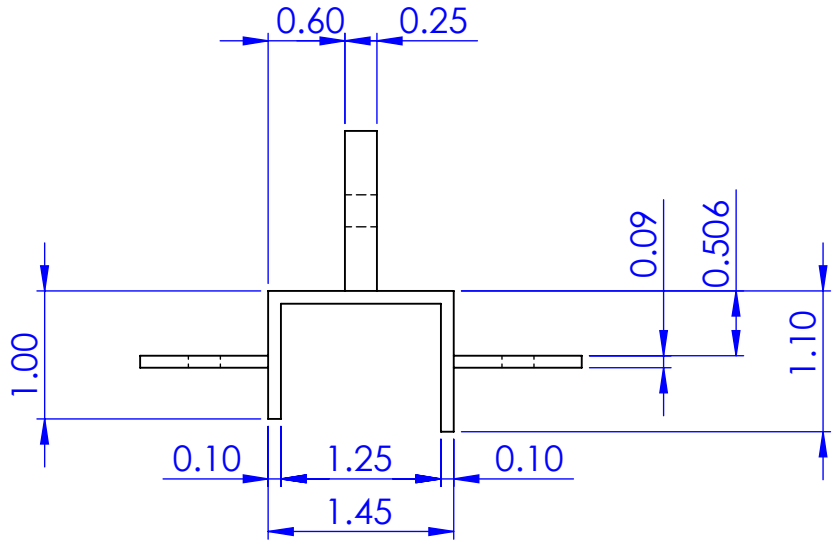

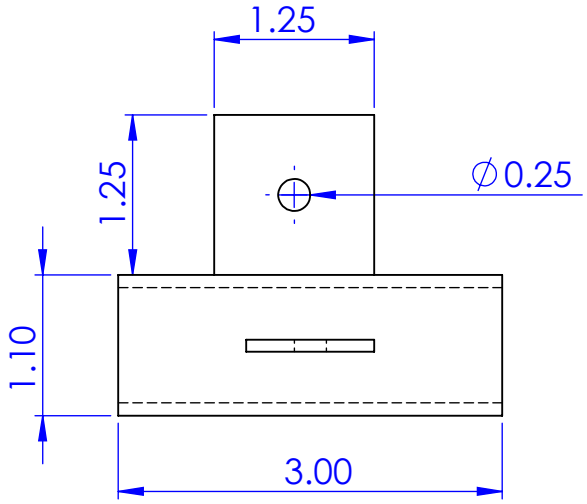

Cal Poly Mechanical Engineering HPV FRAME DESIGN	Title: Rear Seat Bracket	Nxt Asb: SP1300	Date: 07/22/2015	Drwn. By: Matt Allen
	Dwg. #: SP1304	Scale: 1:1.5	Material: 1018 Steel	Chkd. By:

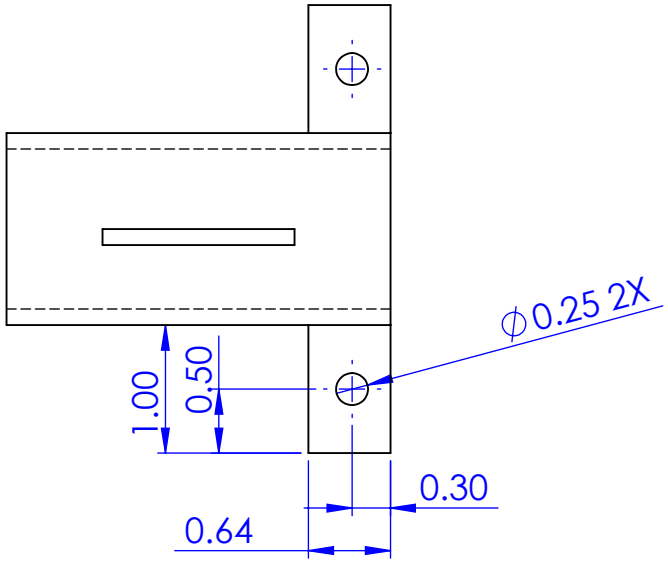

NOTES
UNLESS OTHERWISE SPECIFIED:
1. ALL DIMENSIONS IN INCHES
2. TOLERANCES:
X.XX= ±.
ANGLES= ± °
3. INSIDE TOOL RADIUS .01 MAX
4. BREAK SHARP EDGES .01 MAX

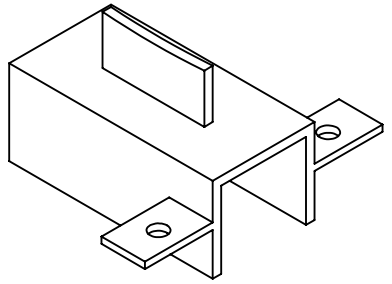

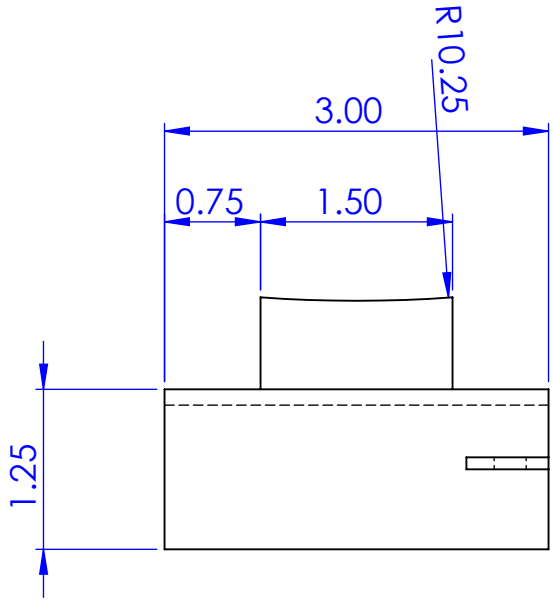

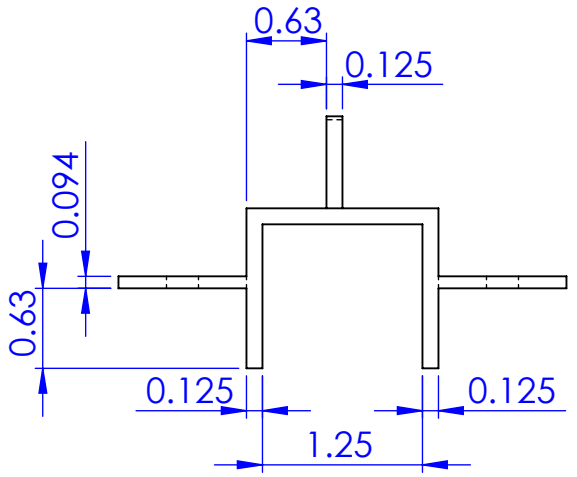

Cal Poly Mechanical Engineering HPV FRAME DESIGN	Title: F Seat Bracket	Nxt Asb: SP1300	Date: 07/22/2015	Drwn. By: Matt Allen
	Dwg. #: SP1303	Scale: 1:1.5	Material: 1018 Steel	Chkd. By:

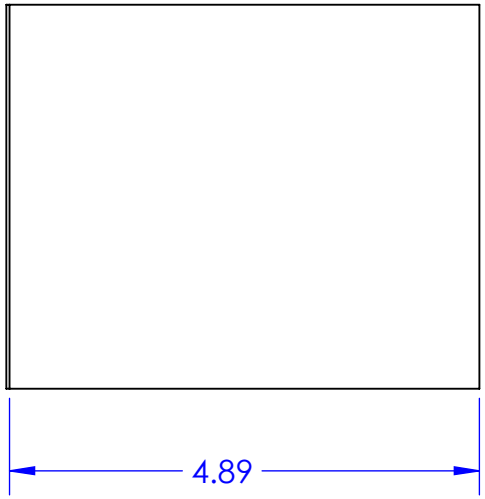

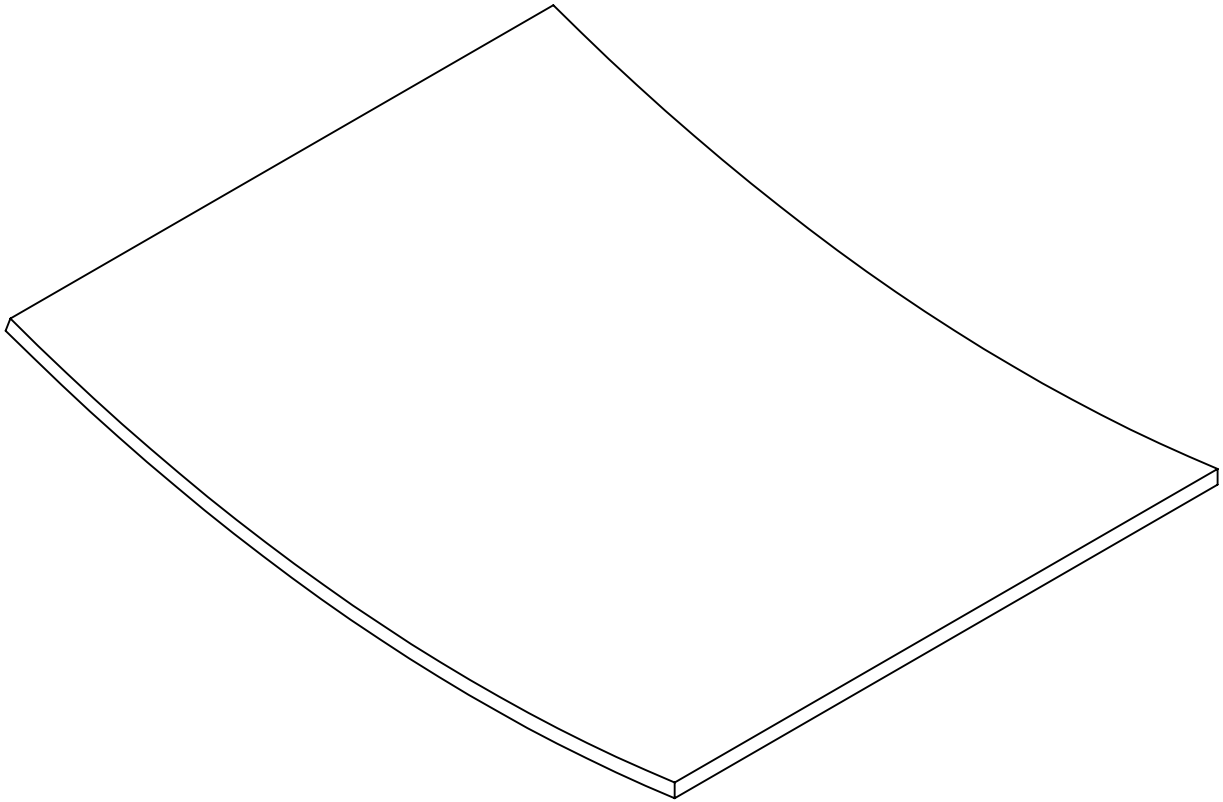

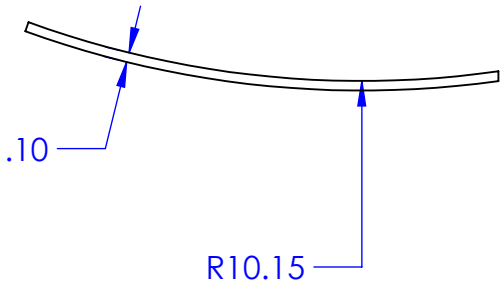

NOTES
UNLESS OTHERWISE SPECIFIED:
1. ALL DIMENSIONS IN INCHES
2. TOLERANCES:
X.XX= ±.01
ANGLES= ±1°
3. INSIDE TOOL RADIUS .01 MAX
4. BREAK SHARP EDGES .01 MAX

Cal Poly Mechanical Engineering HPV FRAME DESIGN	Title: Seat Support	Nxt Asb: SP1300	Date: 07/23/2015	Drwn. By: Matt Allen
	Dwg. #: SP1306	Scale: 1:2	Material: 1018 Steel	Chkd. By:

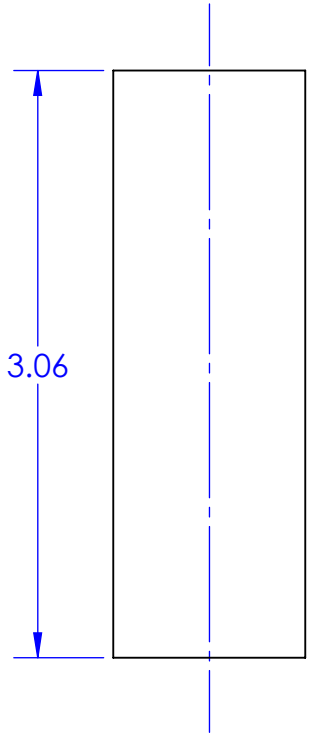

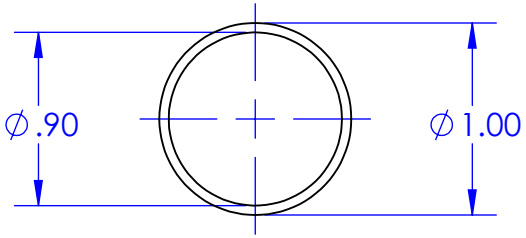

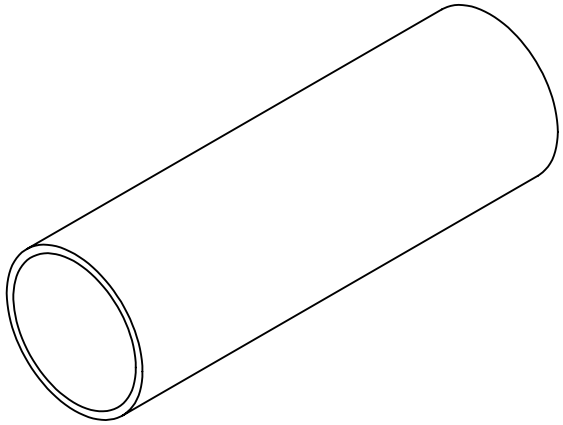

NOTES
UNLESS OTHERWISE SPECIFIED:

1. ALL DIMENSIONS IN INCHES
2. TOLERANCES:
   X.XX= ± .01
   ANGLES= ± 1°
3. INSIDE TOOL RADIUS .01 MAX
4. BREAK SHARP EDGES .01 MAX

Cal Poly Mechanical Engineering HPV FRAME DESIGN	Title: Seat Tube Spanner	Nxt Asb: SP1300	Date: 07/22/2015	Drwn. By: Matt Allen
	Dwg. #: SP1305	Scale: 1:1	Material: 1018 Steel	Chkd. By:

NOTES
UNLESS OTHERWISE SPECIFIED:
1. ALL DIMENSIONS IN INCHES
2. TOLERANCES:
X.XX= ±.01
ANGLES= ±1°
3. INSIDE TOOL RADIUS .01 MAX
4. BREAK SHARP EDGES .01 MAX

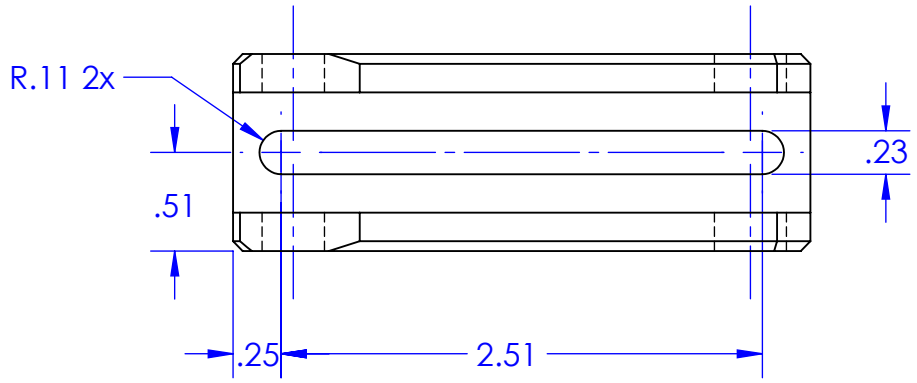

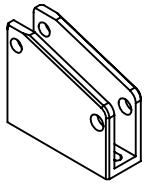

Scale 1:4

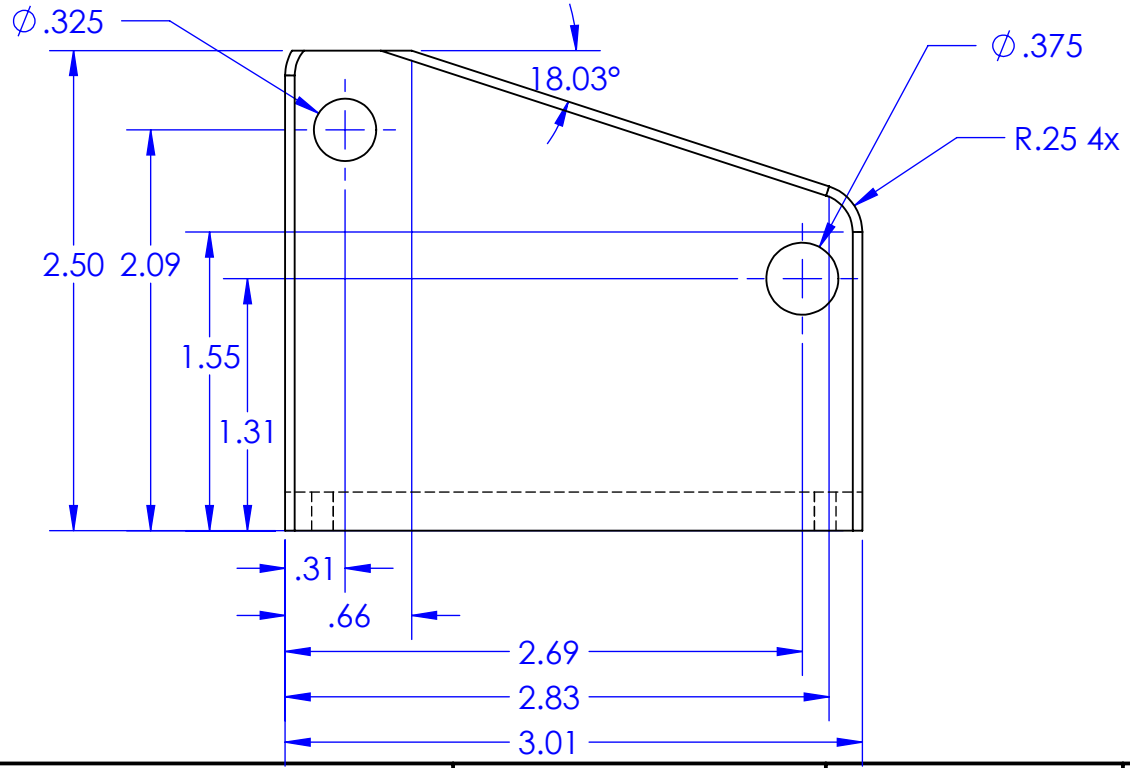

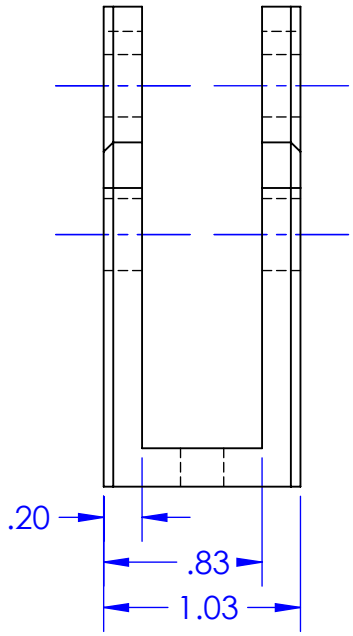

Cal Poly Mechanical Engineering HPV FRAME DESIGN	Title: Rear Idler Mount	Nxt Asb:SP1300	Date:07/23/2015	Drwn. By:Matt Allen
	Dwg. #:SP1313	Scale:1:1	Material: 6061-T6 Al	Chkd. By:

NOTES
UNLESS OTHERWISE SPECIFIED:
1. ALL DIMENSIONS IN INCHES
2. TOLERANCES:
X.XX= ±.01
ANGLES= ±1°
3. INSIDE TOOL RADIUS .01 MAX
4. BREAK SHARP EDGES .01 MAX

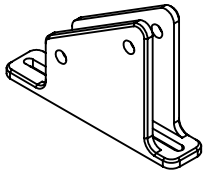

Scale 1:4

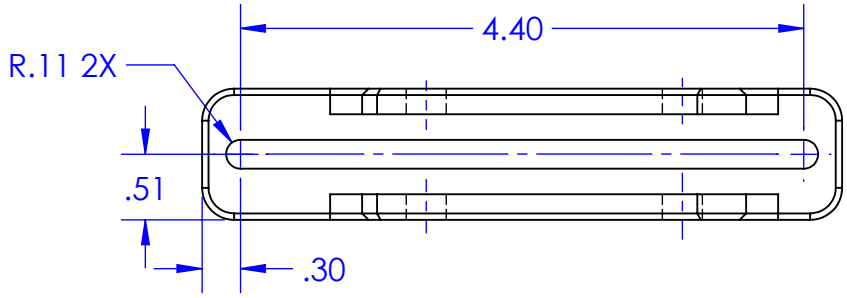

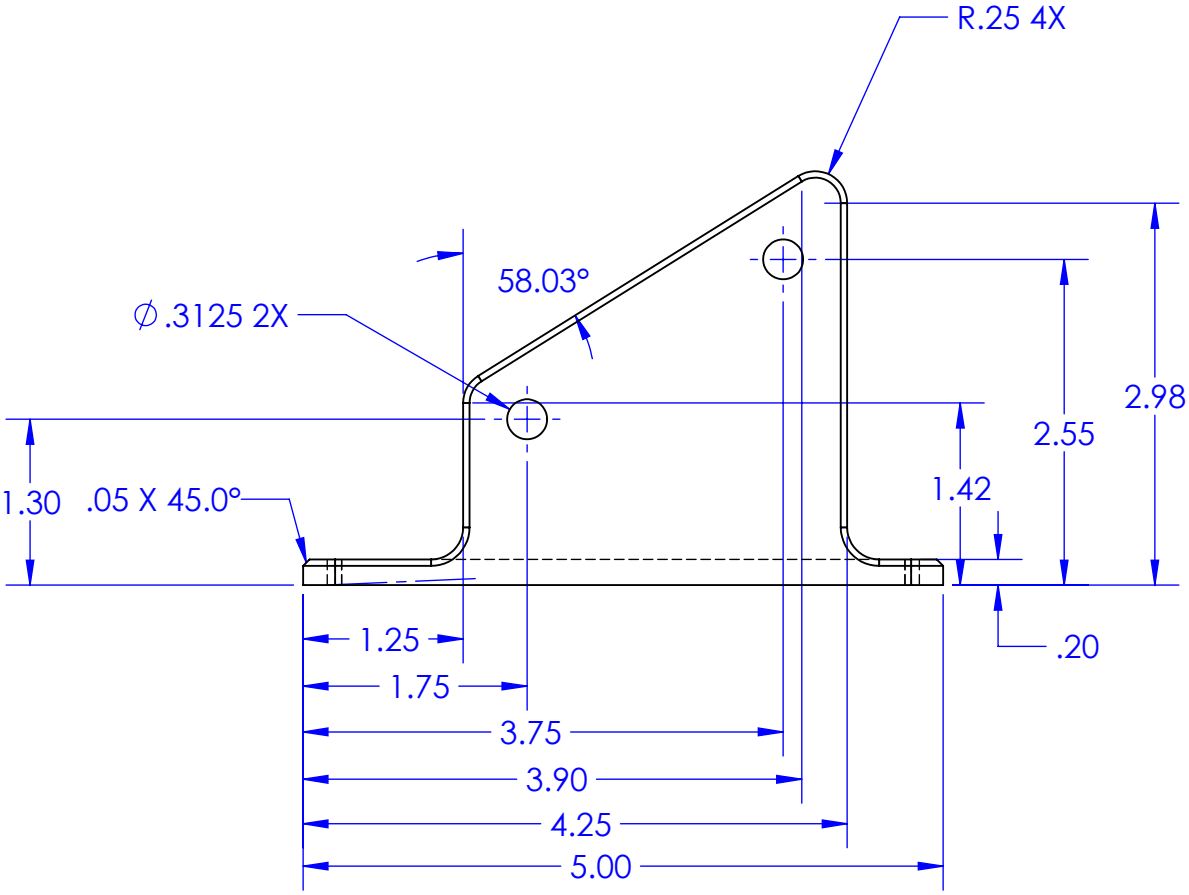

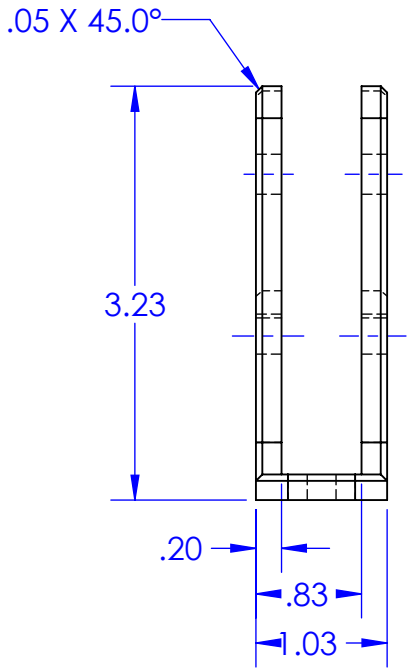

Cal Poly Mechanical Engineering HPV FRAME DESIGN	Title: Front Idler Mount	Nxt Asb: SP1300	Date: 07/23/2015	Drwn. By: Matt Allen
	Dwg. #: SP1311	Scale: 1:2	Material: 6061-T6 Al	Chkd. By:

NOTES
Key Dimensions only
Fixturewerks T-Handle Spring Loaded Pin
Part Number: CP-K100TLO

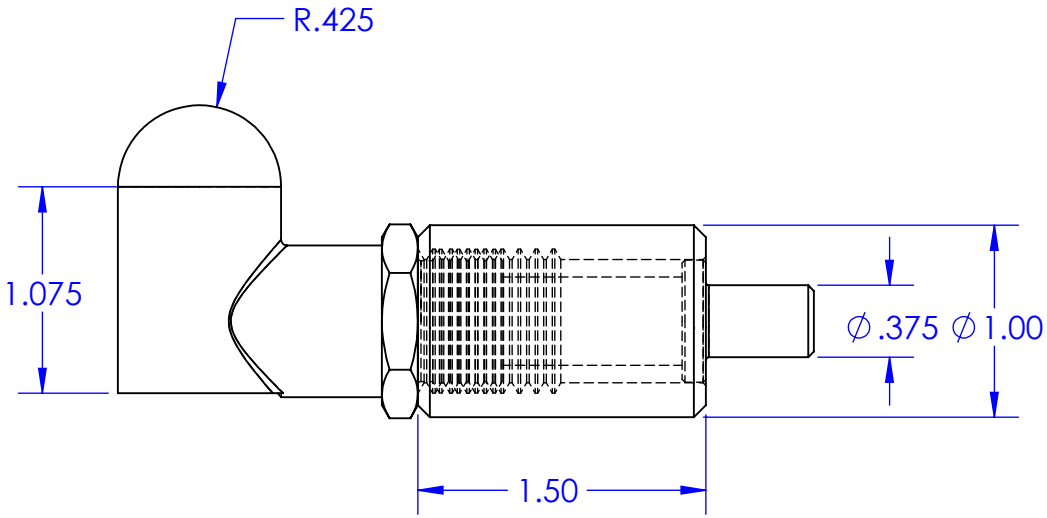

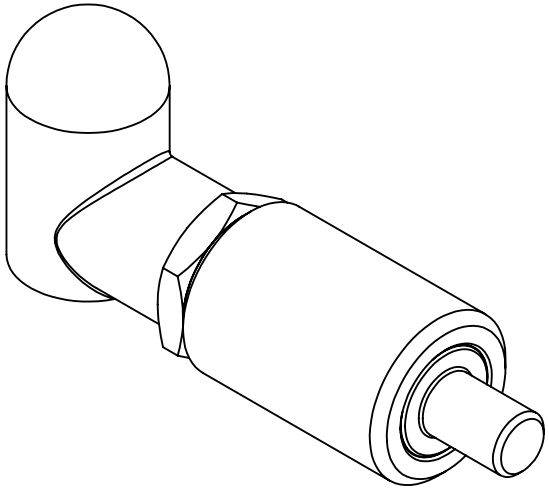

Cal Poly Mechanical Engineering HPV FRAME DESIGN	Title: T-Handle Pin	Nxt Asb: SP1300	Date: 07/22/2015	Drwn. By: Matt Allen
	Dwg. #: SP1306	Scale: 1:1	Material: Steel	Chkd. By:

ITEM NO.	PART NUMBER	DESCRIPTION	right/QTY.
1	steel dropout mount_6_10_15	NOVA CYCLES #NOV_DROP_MSET_TRK (MODIFIED)	1
2	aluminum BMX dropout_6_10_15		1
3	chainring bolt - male_6_10_15		2
4	chainring bolt - female_6_10_15		2

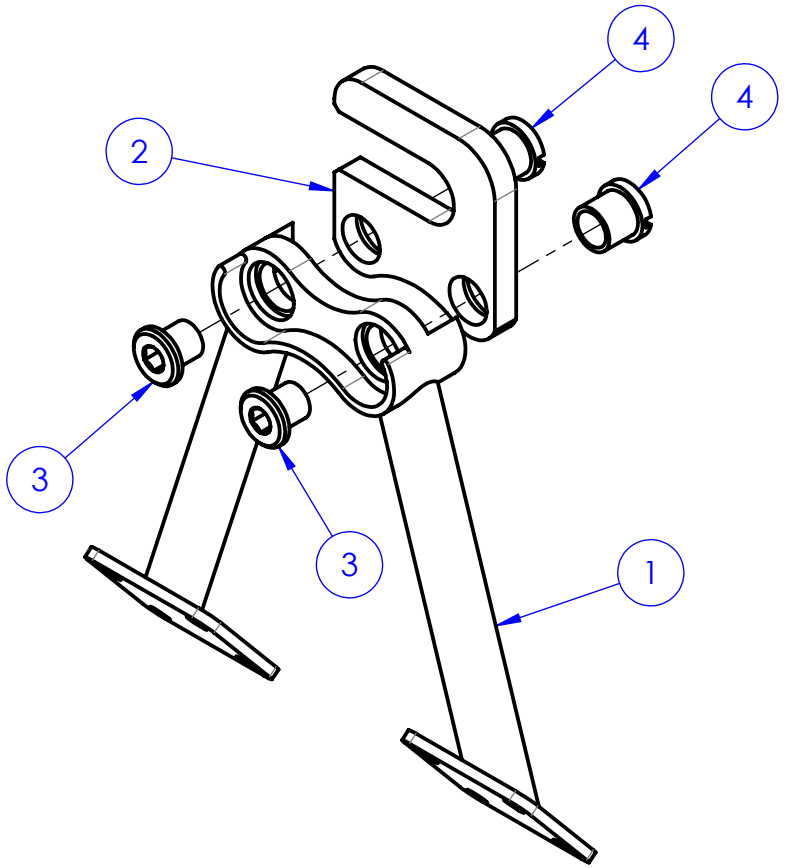

NOTES
UNLESS OTHERWISE SPECIFIED:
1. ALL DIMENSIONS IN INCHES
2. TOLERANCES:
X.XX= ±.
ANGLES= ± °
3. INSIDE TOOL RADIUS .01 MAX
4. BREAK SHARP EDGES .01 MAX

Cal Poly Mechanical Engineering HPV FRAME DESIGN	Title: REAR DROPOUT ASSY	Nxt Asb: FULL VEHICLE	Date: 6/10/2015	Drwn. By: PETER AUMANN
	Dwg. #: SP1400	Scale:1:1	Material:	Chkd. By:

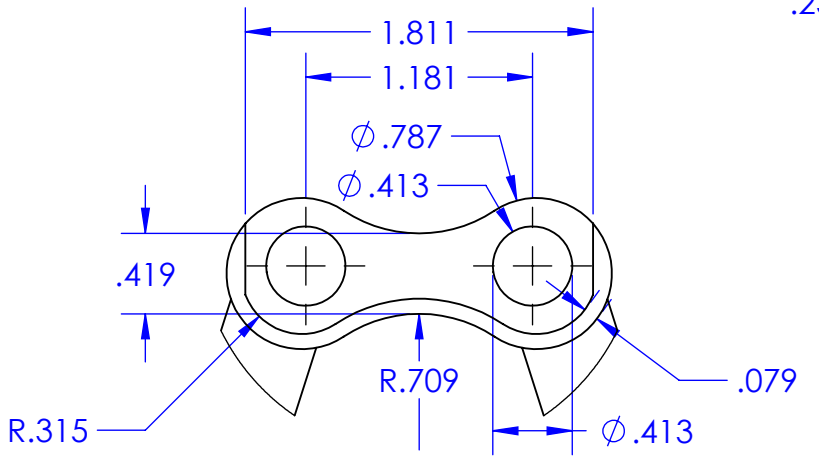

DETAIL J

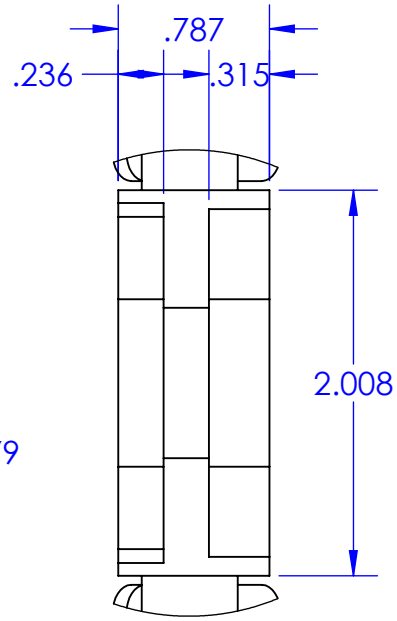

SECTION K-K

NOTES
UNLESS OTHERWISE SPECIFIED:
1. ALL DIMENSIONS IN INCHES
2. TOLERANCES:
X.XX= ± .01
ANGLES= ± .1°
3. INSIDE TOOL RADIUS .01 MAX
4. BREAK SHARP EDGES .01 MAX

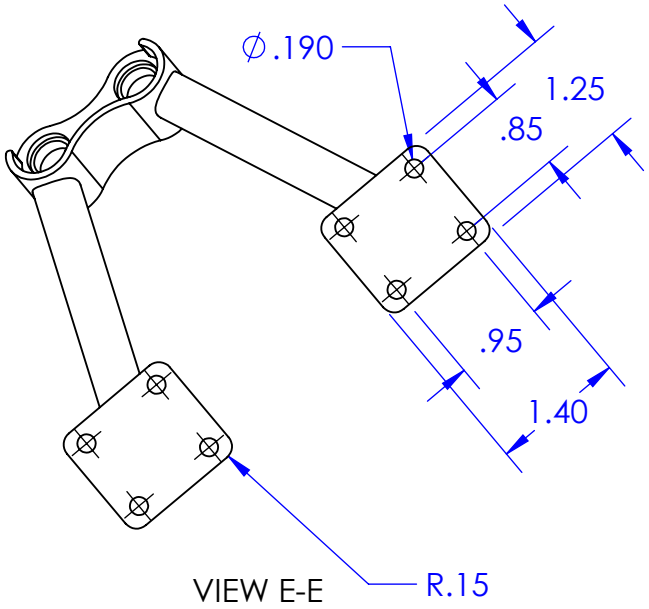

VIEW E-E

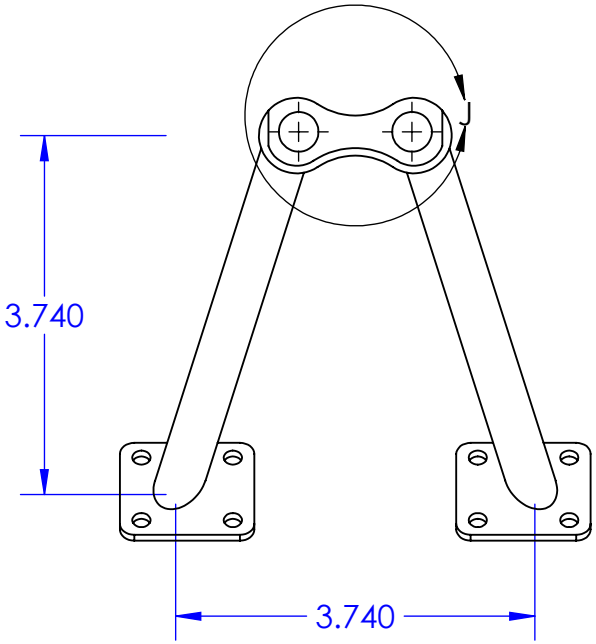

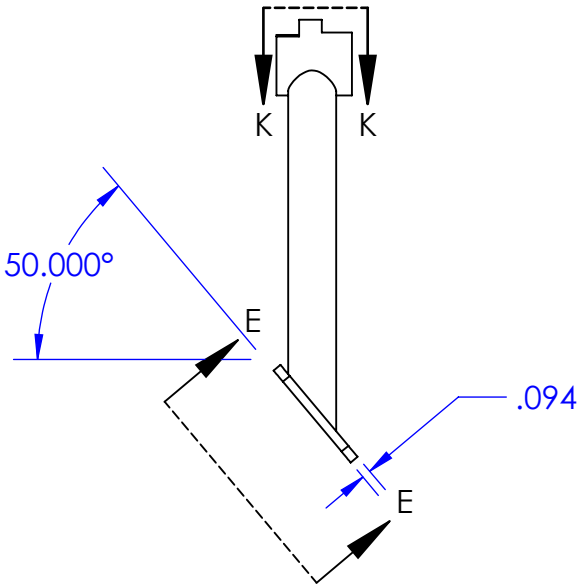

NOTE: "FEET" ARE HAND SHAPED, DIMENSIONS APPROXIMATE

Cal Poly Mechanical Engineering HPV FRAME DESIGN	Title: STEEL DROPOUT MOUNT	Nxt Asb: REAR DROPOUT	Date: 6/10/2015	Drwn. By: PETER AUMANN
	Dwg. #: SP1401	Scale: 1:2	Material: STEEL	Chkd. By:

NOTES
UNLESS OTHERWISE SPECIFIED:
1. ALL DIMENSIONS IN INCHES
2. TOLERANCES:
X.XX= ± .01
ANGLES= ± 0.1°
3. INSIDE TOOL RADIUS .01 MAX
4. BREAK SHARP EDGES .01 MAX

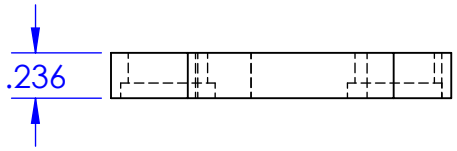

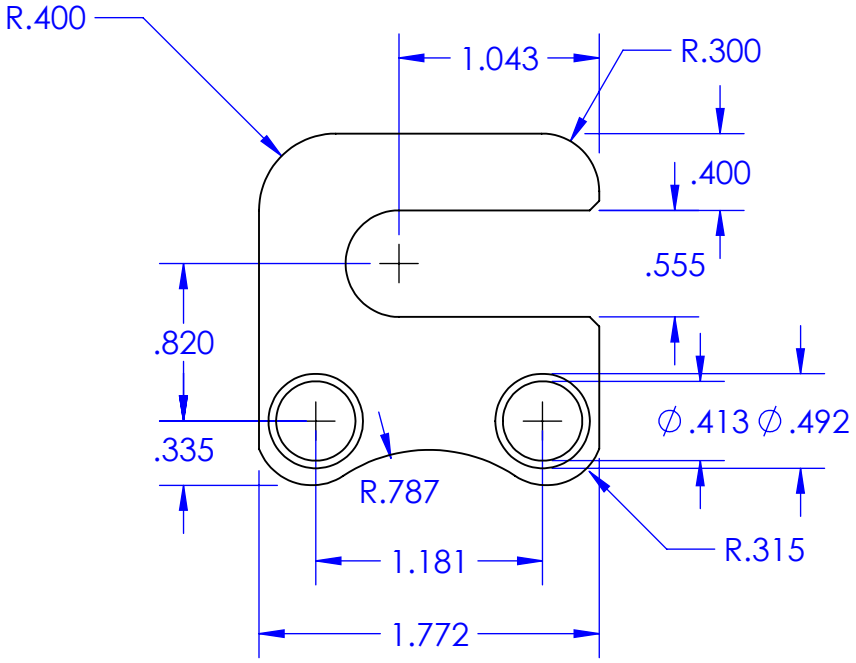

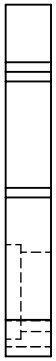

Cal Poly Mechanical Engineering HPV FRAME DESIGN	Title: ALU REAR DROPOUT	Nxt Asb: REAR DROPOUT	Date: 6/10/2015	Drwn. By: PETER AUMANN
	Dwg. #: SP1402	Scale: 1:1	Material: ALUMINUM 6061	Chkd. By:

NOTES
UNLESS OTHERWISE SPECIFIED:
1. ALL DIMENSIONS IN INCHES
2. TOLERANCES:
X.XX= ±0.01
ANGLES= ±0.1°
3. INSIDE TOOL RADIUS .01 MAX
4. BREAK SHARP EDGES .01 MAX

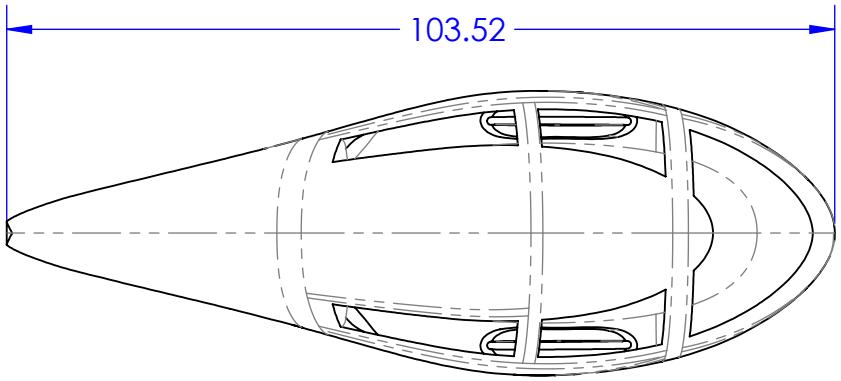

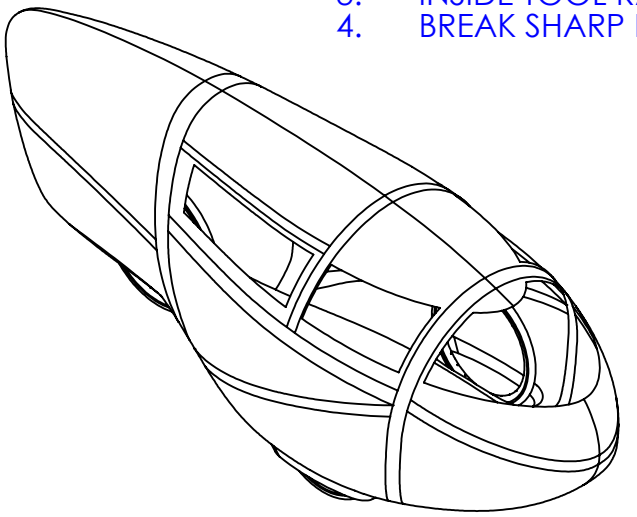

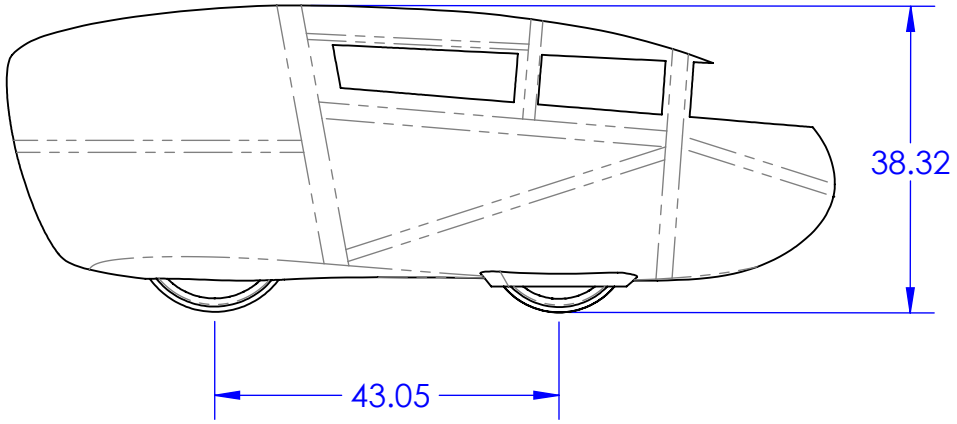

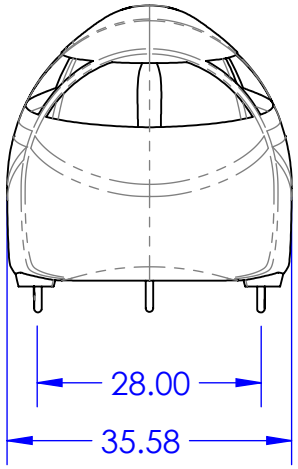

Cal Poly Mechanical Engineering HPV FRAME DESIGN	Title: FAIRING	Nxt Asb: FULL VEHICLE	Date: 6/10/2015	Drwn. By: TRENT HELLMANN
	Dwg. #: SP1500	Scale: 1:24	Material: CARBON FIBER	Chkd. By:

ITEM NO.	PART NUMBER	DESCRIPTION	QTY.
1	TSLOTbar	80/20 #1515 EXTRUSION	2
2	TSLOTbar	80/20 #1515 EXTRUSION	5
3	TSLOTbar	80/20 #1515 EXTRUSION	1
4	TSLOTbar	80/20 #1515 EXTRUSION	2
5	TSLOTbar	80/20 #1515 EXTRUSION	1
6	TSLOTbar	80/20 #1515 EXTRUSION	2
7	TSLOTbar	80/20 #1515 EXTRUSION	2
8	90degBracket	80/20 # 4332 BRACKET	4
9	90degBracket	80/20 # 4295 BRACKET	16
10	rear dropout aligner_v2		1
11	BBshell	68 MM, BSA THREAD	1
12	BBbracket		1
15	TSLOTpivotarm		8
16	steereraligner		2
17	8020-4312	80/20 # 4312 PLATE	2

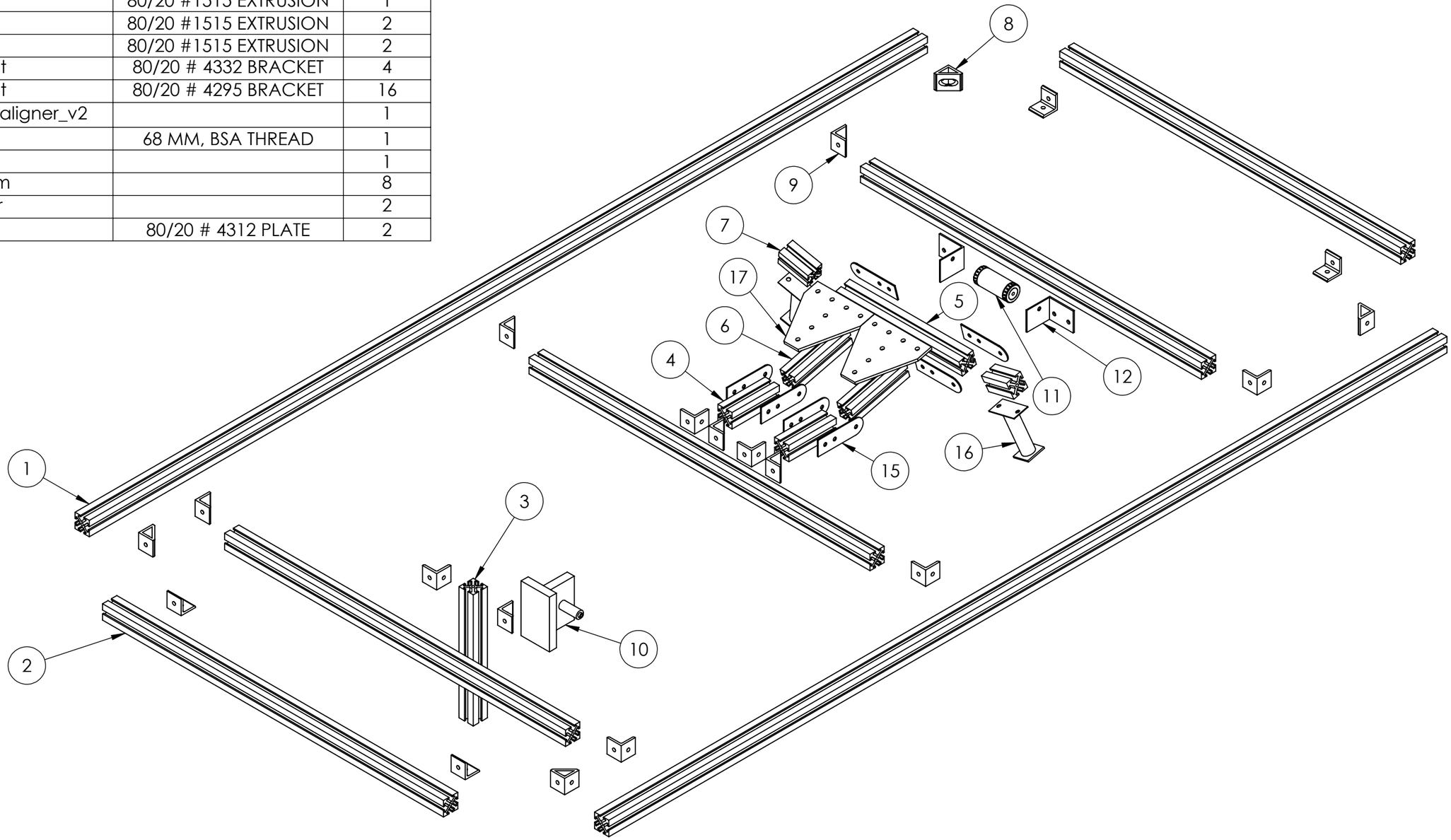

Cal Poly Mechanical Engineering HPV FRAME DESIGN	Title: ALIGNMENT JIG	Nxt Asb:	Date: 6/12/2015	Drwn. By: PETER AUMANN
	Dwg. #: SP2000	Scale: 1:8	Material:	Chkd. By:

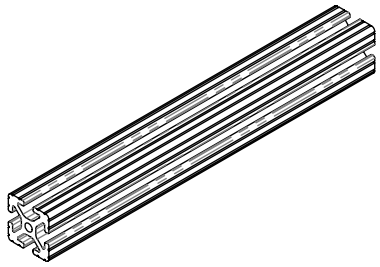

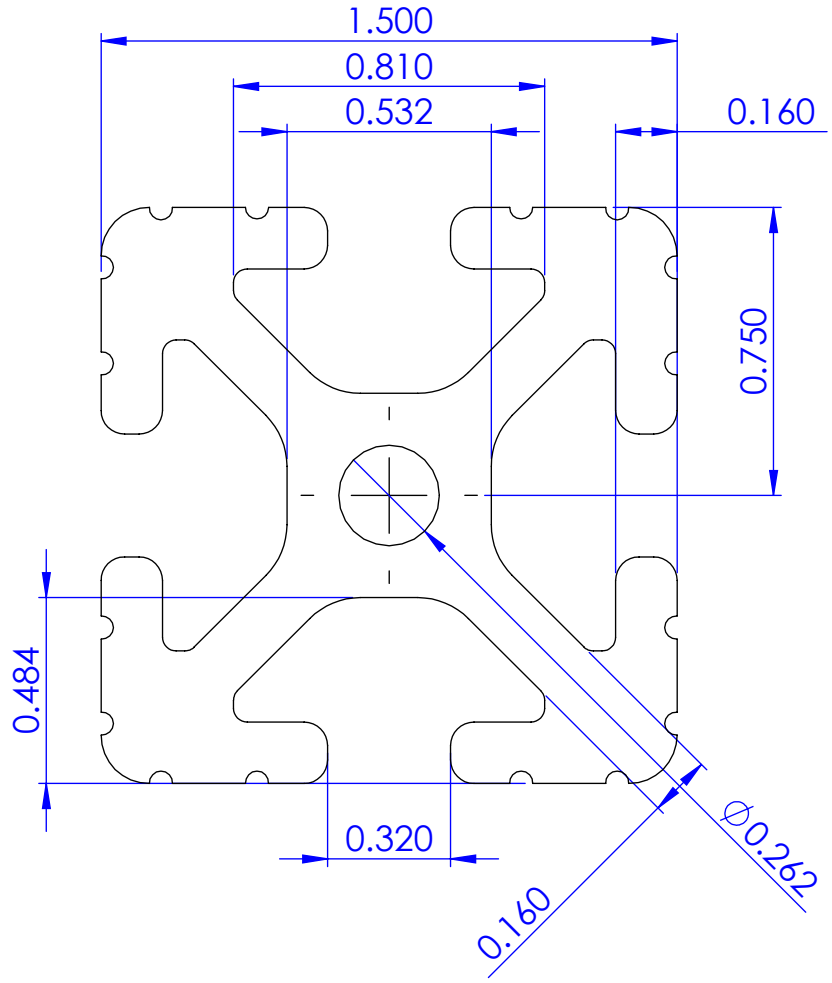

Cal Poly Mechanical Engineering HPV FRAME DESIGN	Title: 80/20 1515 EXTRUSION	Nxt Asb: ALIGNMENT JIG	Date: 6/12/2015	Drwn. By: 80/20, INC.
	Dwg. #:	Scale: 2:1	Material: ALUMINUM	Chkd. By: PETER AUMANN

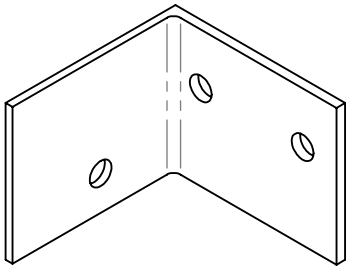

NOTES
UNLESS OTHERWISE SPECIFIED:
1. ALL DIMENSIONS IN INCHES
2. TOLERANCES:
   X.XX= ± .005
   ANGLES= ± .1°
3. INSIDE TOOL RADIUS .01 MAX
4. BREAK SHARP EDGES .01 MAX

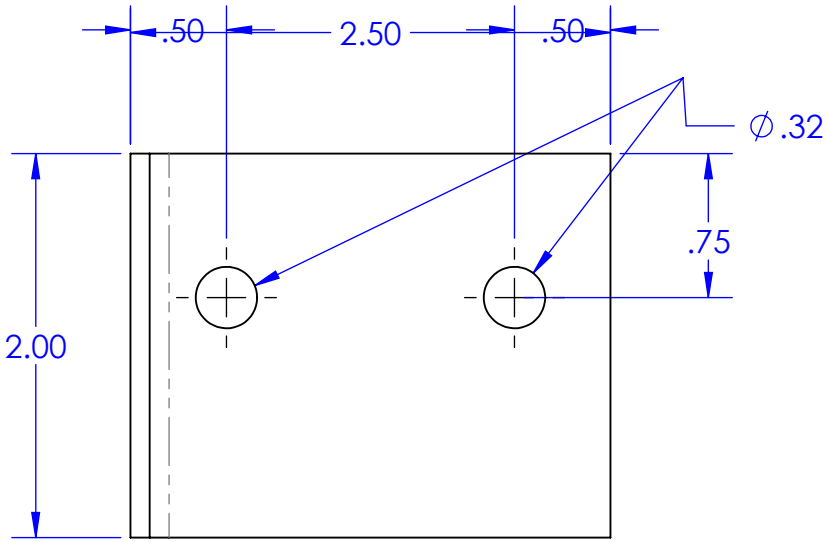

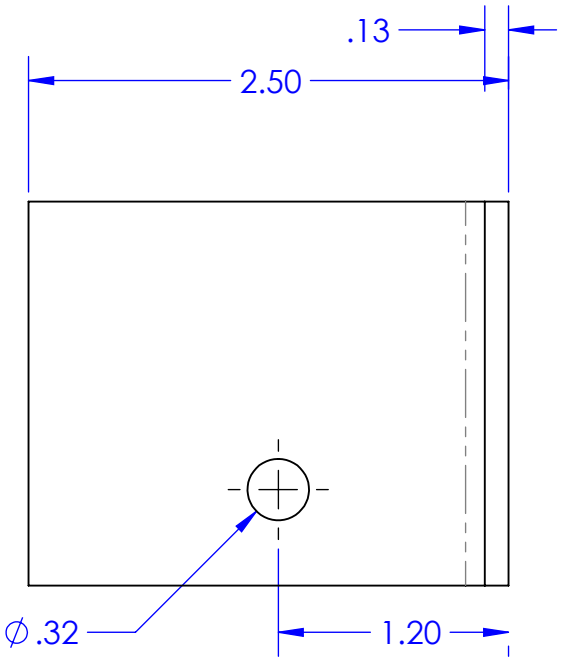

Cal Poly Mechanical Engineering HPV FRAME DESIGN	Title: BB ALIGNMENT BRACKET	Nxt Asb:ALIGNMENT JIG	Date: 6/10/2015	Drwn. By: PETER AUMANN
	Dwg. #: SP2003	Scale: 1:1	Material: ALUMINUM	Chkd. By:

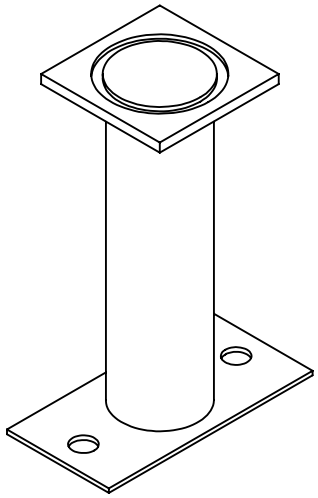

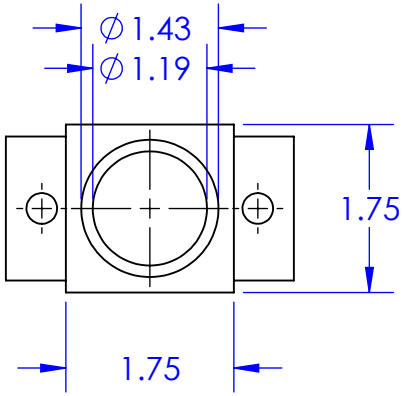

NOTES
UNLESS OTHERWISE SPECIFIED:
1. ALL DIMENSIONS IN INCHES
2. TOLERANCES:
X.XX= ± .05
ANGLES= ± .1°
3. INSIDE TOOL RADIUS .01 MAX
4. BREAK SHARP EDGES .01 MAX

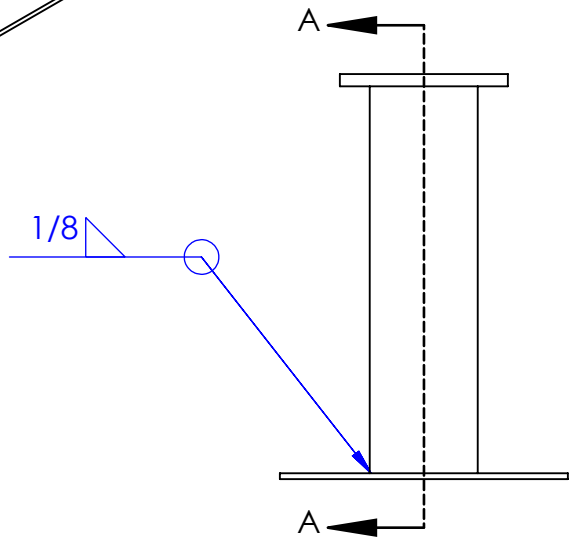

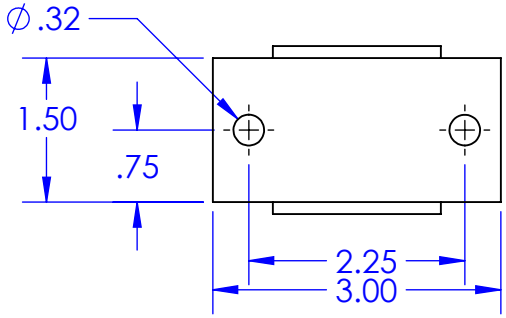

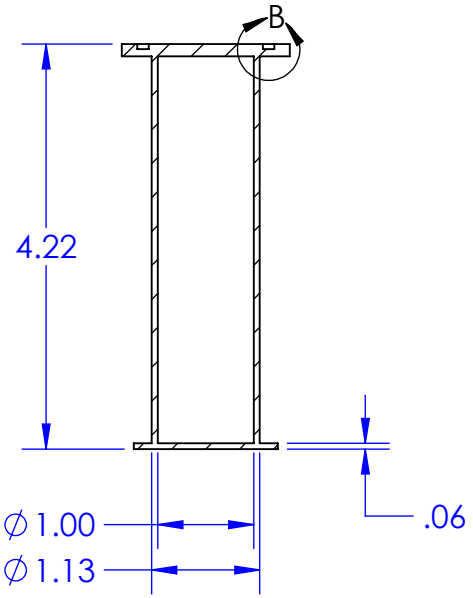

SECTION A-A

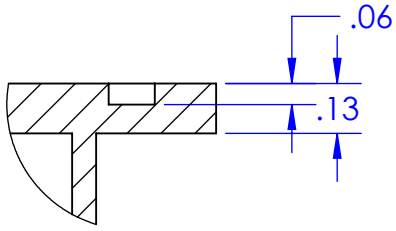

DETAIL B
SCALE 2 : 1

Cal Poly Mechanical Engineering HPV FRAME DESIGN	Title: HEADTUBE LOCATOR	Nxt Asb: ALIGNMENT JIG	Date: 6/10/2015	Drwn. By: PETER AUMANN
	Dwg. #: SP2005	Scale: 1:1	Material: STEEL	Chkd. By:

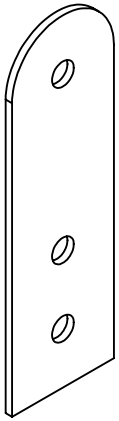

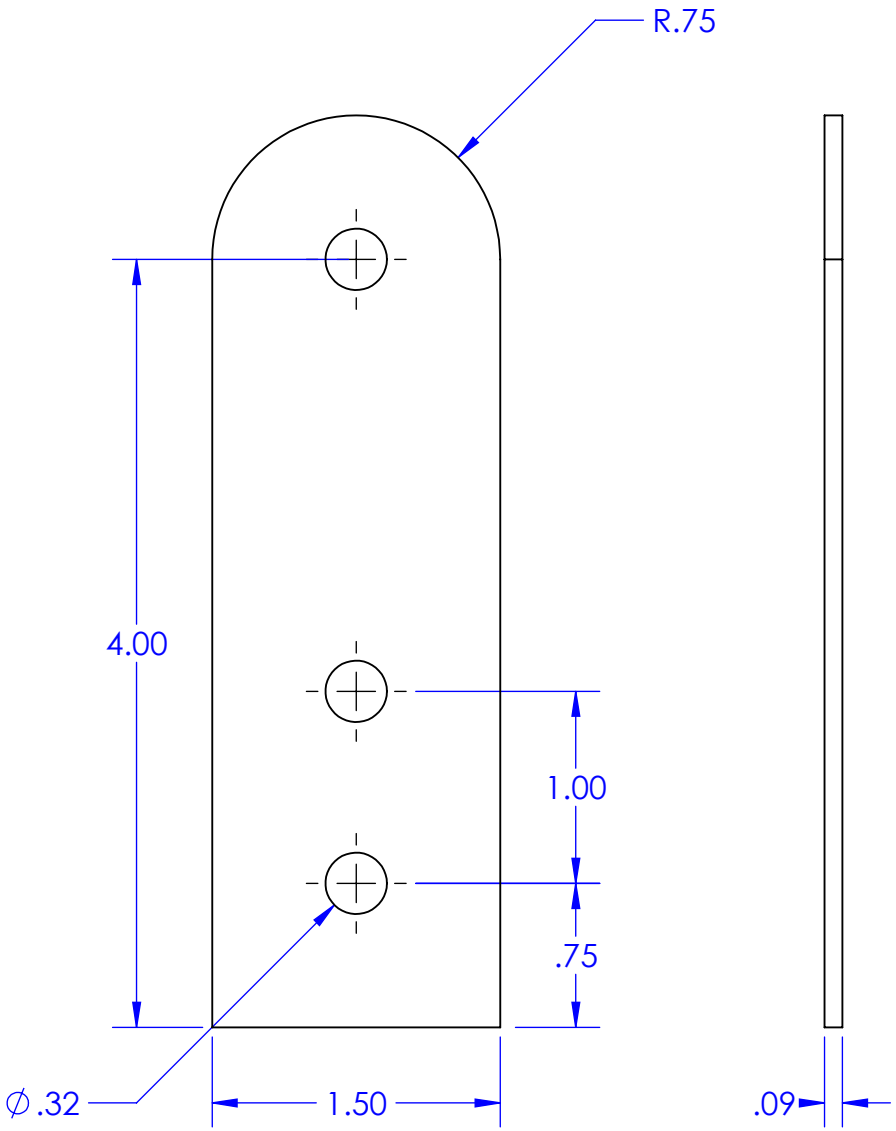

NOTES
UNLESS OTHERWISE SPECIFIED:
1. ALL DIMENSIONS IN INCHES
2. TOLERANCES:
X.XX= ± .05
ANGLES= ± .1°
3. INSIDE TOOL RADIUS .01 MAX
4. BREAK SHARP EDGES .01 MAX

Cal Poly Mechanical Engineering HPV FRAME DESIGN	Title: 80/20 ANGLE BRACKET	Nxt Asb: ALIGNMENT JIG	Date: 6/10/2015	Drwn. By: PETER AUMANN
	Dwg. #: SP2006	Scale: 1:1	Material: STEEL	Chkd. By:

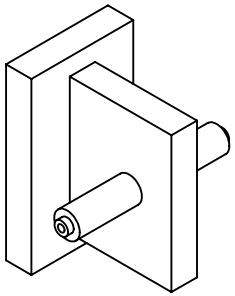

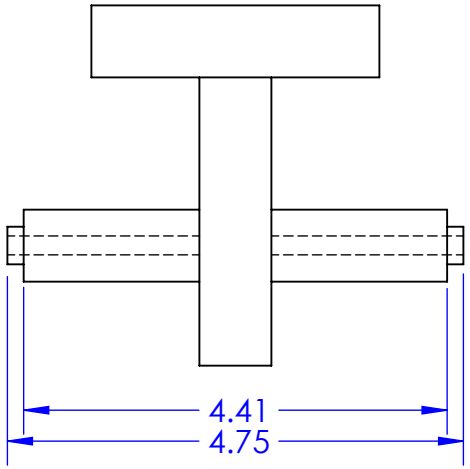

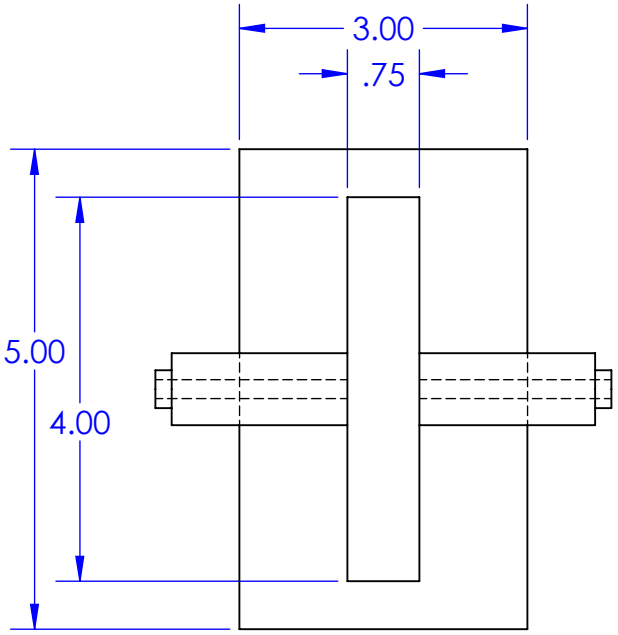

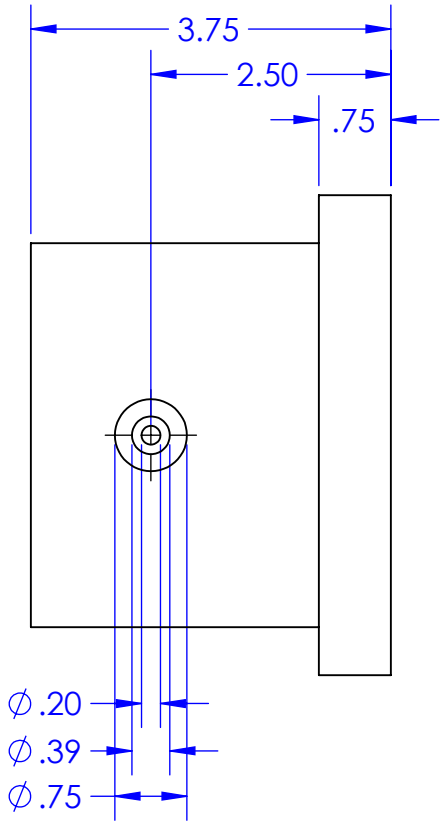

NOTES
UNLESS OTHERWISE SPECIFIED:

1. ALL DIMENSIONS IN INCHES
2. TOLERANCES:
   X.XX= ±.01
   ANGLES= ±.5°
3. INSIDE TOOL RADIUS .01 MAX
4. BREAK SHARP EDGES .01 MAX

Cal Poly Mechanical Engineering HPV FRAME DESIGN	Title: REAR DROPOUT LOCATOR	Nxt Asb: ALIGNMENT JIG	Date: 6/12/2015	Drwn. By: PETER AUMANN
	Dwg. #: SP2004	Scale: 1:2	Material: WOOD, ALU	Chkd. By:

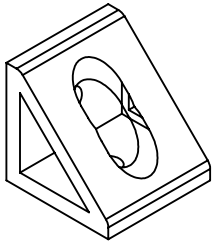

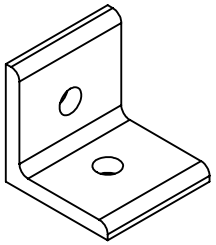

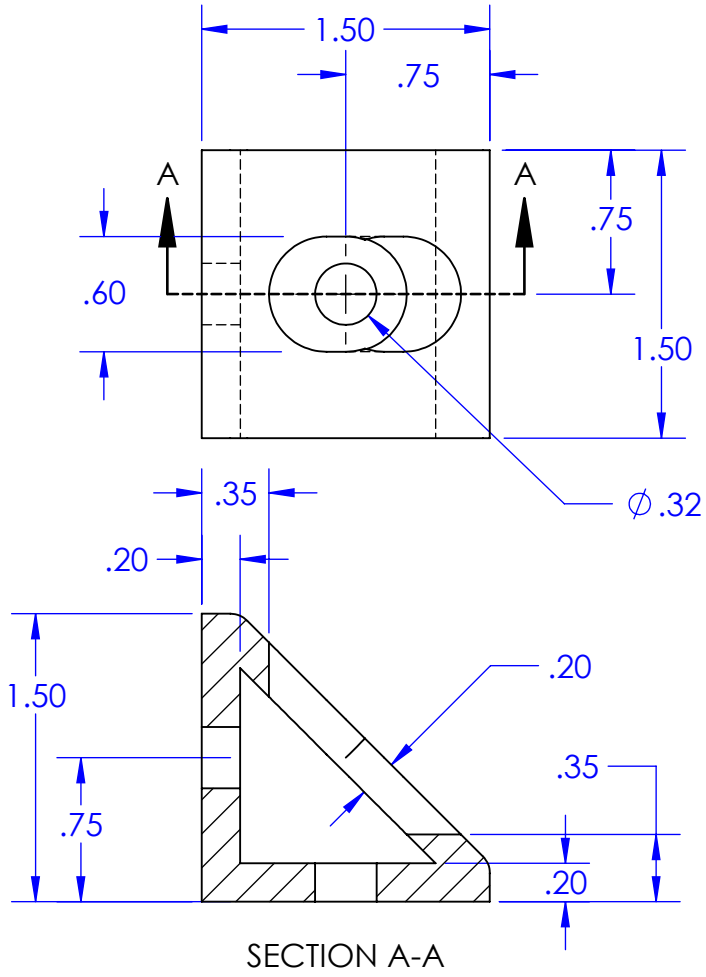

SECTION A-A

NOTE: 80/20 PART NO. 4332

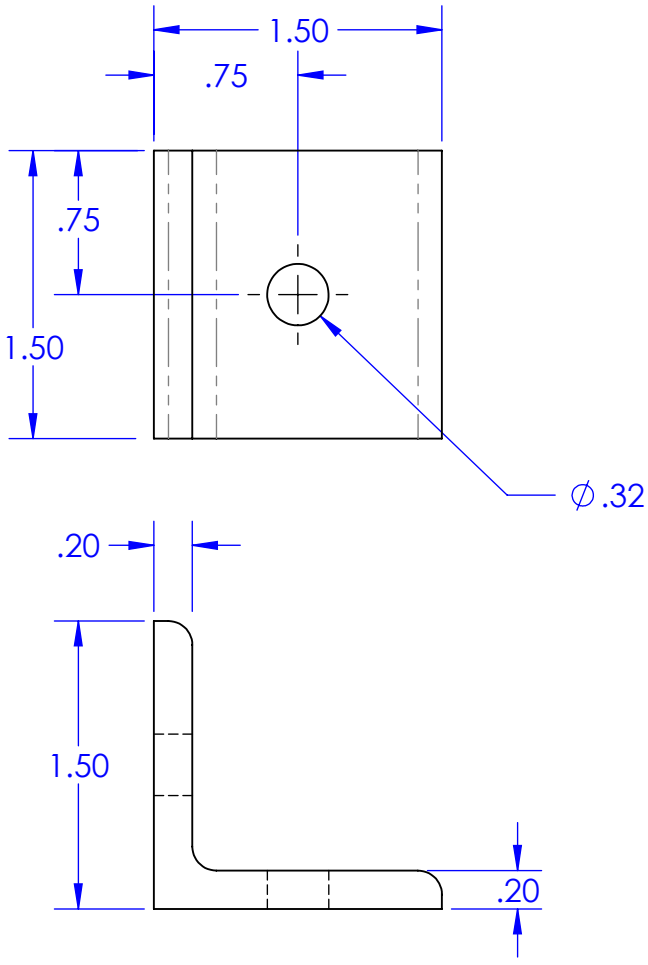

NOTE: 80/20 PART NO. 4295

Cal Poly Mechanical Engineering HPV FRAME DESIGN	Title: 80/20 ANGLE BRACKETS	Nxt Asb: ALIGNMENT JIG	Date: 6/10/2015	Drwn. By: PETER AUMANN
	Dwg. #:	Scale: 1:1	Material: ALUMINUM	Chkd. By:

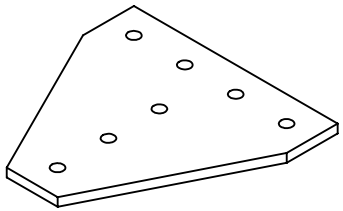

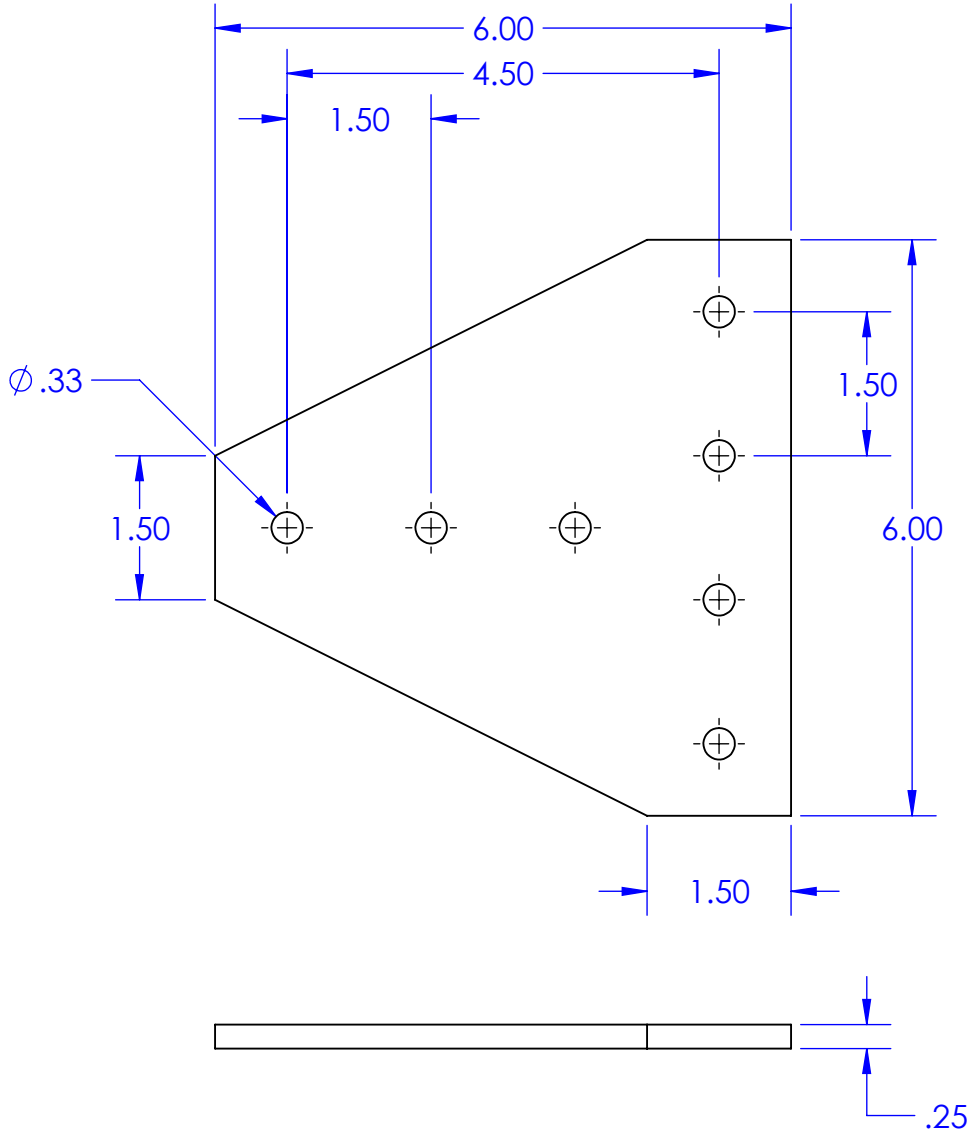

Cal Poly Mechanical Engineering HPV FRAME DESIGN	Title: 80/20 TEE BRKT # 4312	Nxt Asb: ALIGNMENT JIG	Date: 6/12/2015	Drwn. By: 80/20, INC.
	Dwg. #: SP2007	Scale: 1:2	Material: ALUMINUM	Chkd. By: PETER AUMANN

Appendix C

Scanned Hand Calculations

10/13/14

Loading Cases

Speedbump/Pothole Impact

*note: validated w/ strain gauge testing

Overall Bike weight = 220 lbf
70/30 weight dist'n
↑ front

Initial

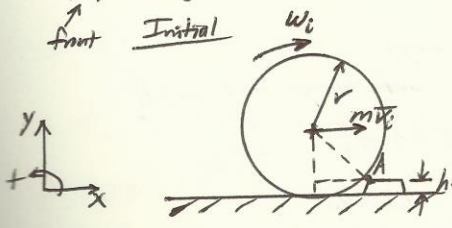

Wheel Properties

$r = 9"$ (to outside of tire)

$M = \frac{77\,lbf}{32.174\,ft/s^2} = 2.39\,slugs$

$\bar{I} = \frac{mr^2}{2} = \frac{\left(2.39\frac{lbf\cdot s^2}{ft}\right)(9in.)^2\left(\frac{ft^2}{144in.^2}\right)}{2} = 0.673\,lbf\cdot ft\cdot s^2$

Impulse

*note: Gravity is negligible compared to impulse

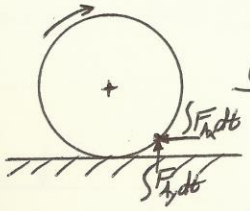

Conserv. of Linear Momentum

$x: m\bar{V}_{i_x} + \int_{t_i}^{t_f} F_{A_x}dt = m\bar{V}_{f_x} \leftarrow \bar{V}_f\cos\theta$

$y: m\bar{V}_{i_y}^{\,0} + \int_{t_i}^{t_f} F_{A_y}dt = m\bar{V}_{f_y} \leftarrow \bar{V}_f\sin\theta$

Final

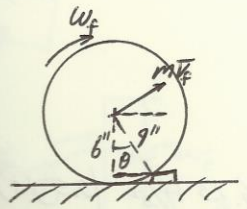

$\theta = \cos^{-1}\left(\frac{6}{9}\right) = 48.2°$

Rolling w/o slip $\Rightarrow \bar{V}_i = \omega_i r$

Fixed axis rotation (A) $\Rightarrow \bar{V}_f = \omega_f r$

$\Rightarrow -m\omega_i r + \int_{t_i}^{t_f} F_{A_x}dt = m\omega_f r\cos\theta$ (a)

$\int_{t_i}^{t_f} F_{A_y}dt = m\omega_f r\sin\theta$ (b)

Conservation of angular momentum

$\bar{I}\omega_i + \sum\int_{t_i}^{t_f} M_G\,dt = \bar{I}_G\omega_f$

$\Rightarrow \int_{t_i}^{t_f}\sum M_G\,dt = r\sin\theta\int F_{A_y}dt - r\cos\theta\int F_{A_x}dt$

$\Rightarrow \bar{I}\omega_i + r\sin\theta\int F_{A_y}dt - r\cos\theta\int F_{A_x}dt = \bar{I}\omega_f$ (c)

→ Combine a, b, c:

$\Rightarrow \bar{I}\omega_i + m\omega_f r^2\sin^2\theta + m\omega_f r^2\cos^2\theta + m\omega_i r^2\cos\theta = \bar{I}\omega_f$

$-m\omega_f r^2(1)$

$\Rightarrow \omega_f(\bar{I} + mr^2\cos\theta) = \omega_f(\bar{I} + mr^2)$

$\Rightarrow \omega_f = \frac{\omega_i(\bar{I} + mr^2\cos\theta)}{\bar{I} + mr^2}$

$\Rightarrow$ Assuming impulse forces do not vary w/ time

$$F_{Ax} = \frac{-m\omega_i r + m\omega_f r\cos\theta}{\Delta t} \qquad F_{Ay} = \frac{-m\omega_f r\sin\theta}{\Delta t}$$

$\Delta t \rightarrow$ length of impact

~~Δt~~ From 410 testing, $\Delta t \approx 0.0667s$ @ 10mph

- assume linear relation between impact ~~and~~ time and speed?

$\Rightarrow \Delta t$ @ 20mph = 0.033 s 29.33 ft/s $\downarrow$ 39.11 rad/s $\omega = \frac{v}{r}$

$\Rightarrow F_{Ax} =$ ~~[illegible]~~ 1048 lbf
$F_{Ay} =$ ~~[illegible]~~ 1203 lbf $\rightarrow$ highly influenced by Δt

~~$\frac{0.0667s}{10\ mph} = \frac{}{18mph}$~~ 0.037

| Braking Loading Case |

see pg. 10

Assumptions:

1. max load occurs just before skidding
2. constant deceleration from ~~15~~ mph → 0 in ~~10~~ 15 ft (comp. specified)

Kinematics

$$a = \frac{V_f^2 - V_i^2}{2\Delta x}$$

$$\Rightarrow a_x = \frac{(0\ ft/s)^2 - (22\ ft/s)^2}{2(15\ ft)} = 16.13\ ft/s^2 \ (0.5 g's)$$

$$\alpha = \frac{a}{r_0} = \frac{16.13\ ft/s^2}{0.75\ ft} = 21.5\ rad/s^2$$

$$m_w = \frac{1.5\ lbf}{32.174\ ft/s^2} = 0.0466\ slugs$$

W/ horizontally oriented brake caliper:

$$F_B = \frac{m_w r_0^2 \alpha + F_f r_0}{r_i} = \frac{(0.0466\ slugs)(0.75ft)^2(21.5\ rad/s^2) + (110\ lbf)(.75ft)}{0.525\ ft}$$

$$m_{Tot} = \frac{220\ lbf}{32.174\ ft/s^2} = 6.84\ slugs$$

$\Rightarrow F_B = 158\ lbf$

where:

$$F_f = m_{Tot} a_x = (6.84\ slugs)(16.13\ ft/s^2) = 110\ lbf$$

Axle Loads:

Sweet Phoenix:
$x_1 = 2.1\ ft.$
$x_2 = 1.48\ ft.$
$x_3 = 1.24\ ft.$

$$F_R = W - F_w = 220 - F_w = 52.9\ lbf$$

$$F_w = \frac{F_R x_1 + F_f x_3}{x_2} = \frac{(220 - F_w)\,2.1ft + (110\ lbf)(1.24ft.)}{1.48\ ft.}$$

$$\Rightarrow F_w = 312.2 - 1.42F_w + 92.2$$

$$\Rightarrow F_w = 167.1\ lbf$$

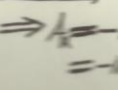

$$\Rightarrow A_x = -ma_x + F_B + F_f = -111 + 158 + 110 = 157\ lbf$$

$$A_y = F_w = 167.1\ lbf$$

Rider Ingress/Egress

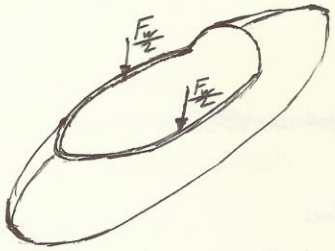

F_w (heaviest rider) = 175 lbf

- apply to supporting ribs halfway between knee roller and RRS
- avoid excessive deflection

Rider standing on tub:

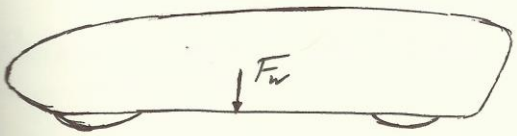

* assume 2 point loads @ rider's feet ($F_w/2$)

Pedal Loading

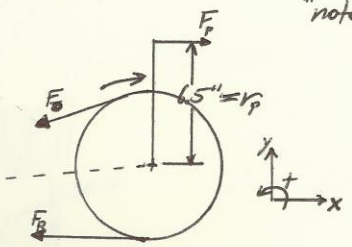

* notes: - assuming all load on one pedal
- 165 mm cranks
- chain orientation will likely change

Pedal Force

$P = F_p v$

Steady State

N [revs/min]

P - power [Watts or $\frac{ft \cdot lbf}{s}$]

Try 80 rpm @ 250 W:

$\Rightarrow F_p = \frac{P}{v}$

$= \frac{(250\ W)\left(\frac{0.738\ ft\cdot lbf/s}{1\ W}\right)}{[illegible]}$

$= [illegible]$

$\Rightarrow F_p = \frac{(250\ W)\left(\frac{0.738\ ft\cdot lbf/s}{1\ W}\right)}{[illegible]}$

$r_{CR} = 8\frac{1}{8}"\ (54\text{-tooth?}) = 0.677\ ft.$

$r_{cog} = 1\frac{7}{8}"\ (smallest) = 0.156\ ft.$

* note: rolling w/o slip $r_{cog} = 4"\ (largest)$

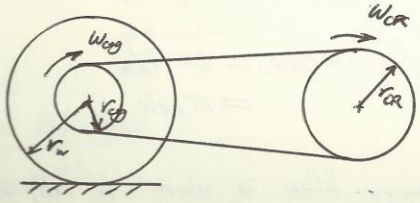

$\omega_{CR} = N_{CR}\frac{revs}{min}\left[\frac{2\pi\ rad}{rev}\right]\left[\frac{1\ min}{60\ s}\right] = 0.105\,N_{CR} \Rightarrow V_{pedal} = r_p\,\omega_{CR}$

pedal velocity

Speed of rear wheel:

$\frac{N_{cog}}{N_{CR}} = \frac{r_{CR}}{r_{cog}} \Rightarrow N_{cog} = N_{CR}\left(\frac{r_{CR}}{r_{cog}}\right)$

$\Rightarrow \omega_{cog} = 0.105\,N_{cog} = N_{CR}\left(\frac{r_{CR}}{r_{cog}}\right)(.105)$

$= \omega_{wheel}$

$\Rightarrow V_{wheel} = r_w \cdot \omega_{cog}$

$\Rightarrow V_{wheel} = r_w\,(.105)\left(\frac{r_{CR}}{r_{cog}}\right)N_{CR}$ ← rider input

Rollover

Start-up load:

Try 15 rpm @ 500 w

$$\Rightarrow F_p = \frac{(500\,w)\left(\frac{0.738\,lbf\text{-}ft/s}{1\,w}\right)}{(0.54\,ft)(.105)(15\,rpm)} = 430\,lbf$$

- Check fatigue loading on BB support during analysis

Torque loading on BB

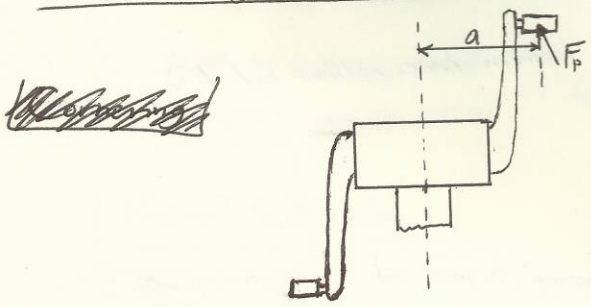

Cornering

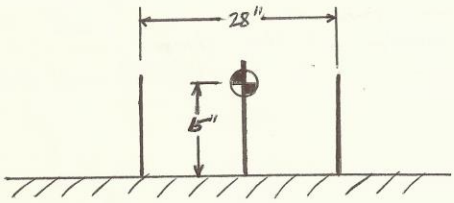

Max g's as determined from stability analysis $\approx 0.6\,g = 19.3\,ft/s^2$

Min radius of curvature = 26 ft.

$$a_n = \frac{V^2}{\rho} \Rightarrow V = \sqrt{a_n \rho} = \sqrt{(19.3\,ft/s^2)(26\,ft.)} = 22.9\,ft/s = 15\,mph$$

FBD

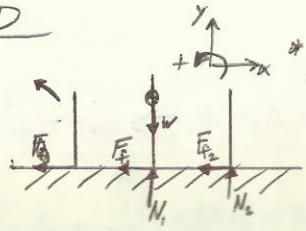

* Assuming bike is about to roll, w/ weight on outside wheel & rear wheel

KD

Equations of Motion

Overall Bike Weight = 220 lbf

$\Rightarrow m = \frac{220\,lbf}{32.174\,ft/s^2} = 6.84\,slugs$

$\Sigma F_x = ma_x$

$\Rightarrow -F_{f_1} - F_{f_2} = -ma_x$

$\Rightarrow F_{f_1} + F_{f_2} = 6.84\,slugs\,(19.3\,ft/s^2)$

$\Rightarrow F_{f_1} + F_{f_2} = 132\,lbf$

$\Sigma F_y = 0$

$\Rightarrow N_1 + N_2 = W$

$\Rightarrow N_1 = 66\,lbf$

$N_2 = 154\,lbf$

Assuming 70/30 weight ratio

$\Rightarrow N_2 = 2.33 N_1$

$F_f = \mu_s N$

$\Rightarrow \mu_s (N_1 + N_2) = 132\,lbf$

$\Rightarrow \mu_s = 0.6$ ← reasonable as $\mu_{s\,max}$ for rubber tire on asphalt is 0.9

$\Rightarrow F_{f_1} = 39.6\,lbf$

$F_{f_2} = 92.4\,lbf$

Rollbar Loading

Per 2015 ASME rules (pg. 10)

Side Load/Top Load

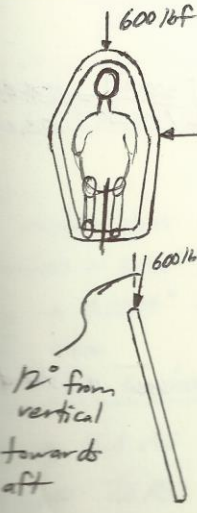

Note: Loads should not be applied concurrently in analysis or testing

"Roll bar is acceptable if 1) there is no indication of permanent deformation, fracture, or delamination on either the roll bar or the vehicle frame, 2) the max. elastic deformation is less than 2" for top load and 1.5" for side load."

Req'd Max. Deflections

Top load → $\delta_{max} < 2"$

Side load → $\delta_{max} < 1.5"$

[Wind Tunnel] Data Analysis 10/29/14

Velocity Calculations:

Pitot-static Tube:

$(P_T - P) = \rho_{H_2O} g h$ ← note: h is read from pressure transducer display, in units of [in. H_2O]

$\rho_{H_2O} = 1.93$ slug/ft.^{3}

$g = 32.174$ ft/s^2

h (enclosed wheels) $= 5.129$ in H_2O

$\Rightarrow P_T - P = (1.93 \text{ slug/ft.}^3)(32.174 \text{ ft/s}^2)(5.129 \text{ in } H_2O)\left(\frac{1 \text{ ft}}{12 \text{ in}}\right) = 26.54$ lbf/ft.^{2}

Ambient Conditions:

$p_{amb} = 14.57$ psia

$T_{amb} = 70.628°F = 530.3°R$

$\rho_{air} = \frac{p_{amb}}{RT_{amb}}$

$\rightarrow R = 53.33$ ft-lbf/lbm-°R

$\Rightarrow \rho_{air} = \frac{(14.57 \text{ lbf/in.}^2)\left(\frac{144 \text{ in.}^2}{1 \text{ ft.}^2}\right)}{(53.33 \text{ ft-lbf/lbm-°R})(530.3°R)}\left(\frac{1 \text{ slug}}{32.174 \text{ lbm}}\right) = 0.0023$ slug/ft.^{3}

$V = \sqrt{\frac{2(P_T - P)}{\rho_{air}}} = \sqrt{\frac{2(26.54 \text{ lbf/ft.}^2)}{0.0023 \text{ slug/ft.}^3}} = 151.9$ ft/s $\left[\frac{1 \text{ mi}}{5280 \text{ ft}}\right]\left[\frac{3600 \text{ s}}{1 \text{ hr}}\right] = 103.6$ mph

W/ Wheels Out → $V = 103.4$ mph

Drag Data/Calculations:

- we had to tare off drag from the sting as we did not use a shroud

$\Rightarrow D_{sting} = 0.866$ lbf

Total Drag

Wheels enclosed: $D_e = 2.089$ lbf

Wheels out: $D_o = 2.130$ lbf

Net Drag (Model)

$D_{m_e} = 1.223$ lbf

$D_{m_o} = 1.264$ lbf

Dimensional Analysis

$D_{actual} = \frac{\rho_{air}}{\rho_{m\,air}}\left(\frac{V}{V_m}\right)^2\left(\frac{l}{l_m}\right)^2 D_m$ ← model drag

(ρ_{air} / $\rho_{m\,air}$: assumed equal)

1/6 scale models, scaling velocity by 6 $\Rightarrow V_{actual} = \frac{103.4 \text{ mph}}{6} = 17.2$ mph

$\Rightarrow D_{actual} = [illegible](\frac{1}{16})^2(\frac{6}{1})^2 D_m$

$\Rightarrow D_{actual} = D_m$

$\Rightarrow$ **Wheels Enclosed**

@ 17.3 mph → D = 1.223 lbf

Wheels Out

@ 17.2 mph → D = 1.264 lbf

Conclusion:

Wheels enclosed variation is a 3.3% reduction in drag force. Even w/ increased frontal area (less drag due to lessened turbulence @ wheels. This coupled w/ manufacturing considerations led us to choose the wheels enclosed model

Power Output Required @ Speed:

$P = F \cdot V$

$\Rightarrow P = (1.223\ lbf)(17.3\ mph)(\frac{1\ hr}{3600\ s})(\frac{5280\ ft}{1\ mi})(\frac{1.356\ W}{1\ lbf\ ft/s}) = 42\ Watts$

$C_d A = \frac{2D}{\rho_{air} V^2}$

$= \frac{2(1.223\ lbf)}{(0.0023\ slug/ft^3)(25.3\ ft/s)^2} = 1.659$

Core Sizing / Layup Selection

Notes

- using carbon cloth (3k likely)
- 3k thickness = 0.009" (Seller composited)
- Tetreme → 0.0024" thickness
- Divinycell core

→ Goal is to obtain initial sizing for core & layup schedule for use in Abaqus from which further refinement is possible
→ aiming for target vertical stiffness of 2500 lbf/in

Seller 3k Carbon Cloth Matl. Properties

$E_1 = E_{22} = 12.6$ Msi

$G = 7.6$ Msi

$\nu_{12} = \nu_{21} = 0.021$

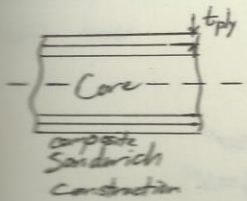

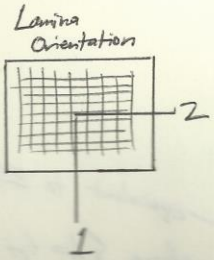

Data obtained from 2012 Senior Project team → performed Instron testing w/ 0-90 & ±45 specimens

Divinycell we have:

L = 9" → 11g

$\frac{lbf}{ft^2}\left[\frac{144\ in^2}{1\ ft^2}\right]$

0.055 g/in³ = 52 kg/m³

3K-Area density

4½" 2ft-6grams

3 parts → $\frac{3g}{[illegible]} = [illegible]$

$[illegible]\left[\frac{[illegible]}{1g}\right] = 0.001345\ lbf/in^2$

Appendix D

Vendor supplied component specifications and data sheets

FREKOTE®

700-NC™

October 2009

PRODUCT DESCRIPTION

700-NC™ provides the following product characteristics:

Technology	Mold Release
Appearance	Clear, colorless[LMS]
Chemical Type	Solvent Based Polymer
Odor	Solvent
Cure	Room temperature cure
Cured Thermal Stability	≤400 °C
Application	Release Coatings
Application Temperature	13 to 135 °C
Specific Benefit	• No chlorinated solvents • High gloss finish • High slip • No contaminating transfer • No mold build-up

700-NC™ offers excellent release properties for the most demanding applications and is a great all-purpose release agent. 700-NC™ releases epoxies, polyester resins, thermoplastics, rubber compounds and most other molded polymers.

TYPICAL PROPERTIES OF UNCURED MATERIAL

Specific Gravity @ 25 °C 0.755 to 0.764[LMS]

Flash Point - See MSDS

GENERAL INFORMATION

This product is not recommended for use in pure oxygen and/or oxygen rich systems and should not be selected as a sealant for chlorine or other strong oxidizing materials

For safe handling information on this product, consult the Material Safety Data Sheet (MSDS).

Mold Preparation

Cleaning:

Mold surfaces must be thoroughly cleaned and dried. All traces of prior release must be removed. This may be accomplished by using Frekote® PMC or other suitable cleaner. Frekote® 915WB™ or light abrasives can be used for heavy build-up.

Sealing New/Repaired Molds:

Occasionally, green or freshly repaired molds are rushed into service prior to complete cure causing an increased amount of free styrene on the mold surface. Fresh or "production line" repairs, new fiberglass and epoxy molds should be cured per manufacturer's instructions, usually a minimum of 2 -3 weeks at 22°C before starting full-scale production. Fully cured previously unused molds should be sealed before use. This can be accomplished by applying one to two coats of an appropriate Frekote® mold sealer, following the directions for use instructions. Allow full cure of the appropriate Frekote® mold sealer before you apply the first coat of 700-NC™ as outlined in the directions of use.

Directions for use:

1. 700-NC™ can be applied to mold surfaces at room temperature up to 135°C by spraying, brushing or wiping with a clean lint-free, cloth. When spraying ensure a dry air source is used or use an airless spray system. Always use in a well ventilated area.
2. Wipe or spray on a smooth, thin, continuous, wet film. Avoid wiping or spraying over the same area that was just coated until the solvent has evaporated. If spraying, hold nozzle 20 to 30cm from mold surface. It is suggested that small areas be coated, working progressively from one side of the mold to the other.
3. Initially, apply 2 to 3 base coats allowing 5 to 10 minutes between coats for solvent evaporation .
4. Allow the final coat to cure for 15 to 20 minutes at 22°C.
5. Maximum releases will be obtained as the mold surface becomes conditioned to 700-NC™. Performance can be enhanced by re-coating once, after the first few initial pulls.
6. When any release difficulty is experienced, the area in question can be "touched-up" by re-coating the entire mold surface or just those areas where release difficulty is occurring.
7. **NOTE**: 700-NC™ is moisture sensitive, keep container tightly closed when not in use. The product should always be used in a well ventilated area.
8. **Precaution:** Users of closed mold systems(rotomolding) must be certain that solvent evaporation is complete and that all solvent vapors have been ventilated from the mold cavity prior to closing the mold. An oil-free compressed air source can be used to assist in evaporation of solvents and ventilation of the mold cavity.

Mold Touch up

Touch up coats should only be applied to areas where poor release is noticed and should be applied using the same method as base coats. This will reduce the possibility of release agent or polymer build-up. The frequency of touch ups will depend on the polymer type, mold configuration, and abrasion parameters.

Loctite Material Specification[LMS]

LMS dated May 10, 2006. Test reports for each batch are available for the indicated properties. LMS test reports include selected QC test parameters considered appropriate to specifications for customer use. Additionally, comprehensive controls are in place to assure product quality and consistency. Special customer specification requirements may be coordinated through Henkel Quality.

Storage
The product is classified as flammable and must be stored in an appropriate manner in compliance with relevant regulations. Do not store near oxidizing agents or combustible materials. Store product in the unopened container in a dry location. Storage information may also be indicated on the product container labelling.
Optimal Storage: 8 °C to 21 °C. Storage below 8 °C or greater than 28 °C can adversely affect product properties. Material removed from containers may be contaminated during use. Do not return product to the original container. Henkel cannot assume responsibility for product which has been contaminated or stored under conditions other than those previously indicated. If additional information is required, please contact your local Technical Service Center or Customer Service Representive.

Conversions
(°C x 1.8) + 32 = °F
kV/mm x 25.4 = V/mil
mm / 25.4 = inches
µm / 25.4 = mil
N x 0.225 = lb
N/mm x 5.71 = lb/in
N/mm² x 145 = psi
MPa x 145 = psi
N·m x 8.851 = lb·in
N·m x 0.738 = lb·ft
N·mm x 0.142 = oz·in
mPa·s = cP

Note
The data contained herein are furnished for information only and are believed to be reliable. We cannot assume responsibility for the results obtained by others over whose methods we have no control. It is the user's responsibility to determine suitability for the user's purpose of any production methods mentioned herein and to adopt such precautions as may be advisable for the protection of property and of persons against any hazards that may be involved in the handling and use thereof. In light of the foregoing, **Henkel Corporation specifically disclaims all warranties expressed or implied, including warranties of merchantability or fitness for a particular purpose, arising from sale or use of Henkel Corporation's products. Henkel Corporation specifically disclaims any liability for consequential or incidental damages of any kind, including lost profits.** The discussion herein of various processes or compositions is not to be interpreted as representation that they are free from domination of patents owned by others or as a license under any Henkel Corporation patents that may cover such processes or compositions. We recommend that each prospective user test his proposed application before repetitive use, using this data as a guide. This product may be covered by one or more United States or foreign patents or patent applications.

Trademark usage
Except as otherwise noted, all trademarks in this document are trademarks of Henkel Corporation in the U.S. and elsewhere. ® denotes a trademark registered in the U.S. Patent and Trademark Office.

Reference 0.0

PRODUCT DATA

Chemlease® 15 Sealer

Mold Sealer

Description

Chemlease® 15 Sealer is a high performance sealer developed to condition and seal mold surfaces, reduce mold porosity and act as a base for new or reconditioned molds.

Benefits

- Reduces porosity problems.
- Provides an excellent base coat for all types of release agents.
- Compatible with fiberglass, aluminum, steel, and most solid or dense surfaces
- Shortens break-in time.
- High temperature stability - 850°F/450°C

Chemlease® solvent carriers contain no Class I or II registered ozone depleting substances.

Application Instructions

Wiping

1. Mold surface must be thoroughly cleaned to remove all traces of wax, release agents, and other sealers. We recommend Chemlease® Mold Cleaner.
2. Surface should be dry and free of contaminants.
3. Saturate clean cotton cloth (not dripping) and wipe on a smooth continuous film of no more than a few square feet at a time.
4. Wait until the Chemlease® 15 Sealer film starts to evaporate (approximately 3-20 seconds) and while film is still wet, wipe the surface with a second clean dry cotton cloth using a circular motion from the outside working inward until the film is left dry and clear. A cold mold surface may require a longer waiting period before wiping off excess material.
5. Repeat above procedures until entire mold surface has been covered. Usually only one coat is necessary.
6. Allow to cure for one hour before applying mold release. *Note: Cold temperatures increase time necessary for cure. Cure time can be accelerated by elevating mold temperature to 200°F for 30 minutes.*

Spraying

1. Mold surface must be thoroughly cleaned to remove all traces of wax, release agents, and sealers.
2. To apply by spraying use a hand held manual spray bottle or a dry air system. It is important that all containers and spray lines be thoroughly clean and dry.
3. Keep spray nozzle 10 to 15 inches from mold surface and apply a smooth, thin continuous film. Do not allow to run or drip (by over applying).
4. While film is still wet, wipe the surface with a clean dry cotton cloth using a circular motion from the outside working inward until film is left dry and clean.
5. Repeat above procedures until the entire mold surface is covered overlapping slightly to ensure complete coverage. Usually only one coat is necessary.
6. Allow to cure for one hour before applying mold release. *Note: Cold temperatures increase time necessary for cure. Cure time can be accelerated by elevating mold temperature to 200°F for 30 minutes.*

Important

The recommended number of coats and cure times are a general guideline found to be more than sufficient in a broad spectrum of molding conditions. When molding products with extreme geometries or experiencing low-humidity conditions in the shop, the customer may find the need to extend the cure time between coats and increase the number of coats applied to the mold. The efficiency of a release film is best determined through a combination of tape tests and experimentation.

Troubleshooting Tips

1. Keep container closed at all times when not in use.
2. Mold must be thoroughly cleaned and dried before application.
   Note: A good test to tell if the mold is clean is to use a small piece of masking tape (approximately 1" in width) on the mold surface. Sufficient resistance should be felt when removing the tape.
3. Material should be clear with no noticeable precipitate. If cloudy or milky, material is contaminated.
4. Areas of application should be well ventilated.

Packaging

Chemlease® 15 Sealer is available in 1 and 4 gallon containers.

Safety Data

Material Safety Data Sheets are available for all Chemlease® products and should be consulted prior to use of the product.

Chem-Trend L.P.
1445 W. McPherson Park Drive, P.O. Box 860, Howell, MI 48844.0860
Telephone: 517.546.4520 Facsimile: 517.548.5370 US/Canada: 800.727.7730

Precision Board Plus™
PBLT-10

COASTAL ENTERPRISES

Manufacturers of Precision Board

P.O. Box 4875
Orange, CA 92863-4875
(714) 771.4969
(800) 845.0745
Fax: (714) 771.6422
Email: hdu@precisionboard.com
www.precisionboard.com

Product Data Sheet

DESCRIPTION & APPLICATION:

PBLT-10 is a rigid, High Density Urethane, (HDU), Tooling/Modeling board designed for Prototype Machining, Water Jet Cutting, Pattern Making, Thermoforming, Prepreg Composite Layup Tooling, Vacuum Form Tooling, Tool Path Proofing, Lost Wax Casting Masters, Master Model Making, Artistic Carving Blocks, Indoor and Outdoor Signage. PBLT Plus is made in the USA.

Precision Board Plus PBLT is formulated with eco-friendly, "Green" urethane components. The new Plus material has a Certified "Carbon Foot Print" of 3 to 1 and a Certified "Rapidly Renewable Green Resource Content" of 23.9%. This means each 3"x 4'x8' sheet of PBLT-20 saves 38.5 pounds of plastic material which assists meeting LEED requirements for obtaining USGBC and ICC 700 building credits.

Precision Board Plus **does not contain**: **CFCs or VOCs.** See MSDS for details.

Precision Board Plus PBLT comes in standard sizes of 20"x60", 24"x60", 30"x80", 45"x60" 4'x8', 4'x10', 5'x8' and 5'x10'. Thickness ranges from 1/2" to 24". Custom bonded blocks available in any size. PBLT Densities are 4, 6, 8, 10, 12, 15, 18, 20, 30, 34, 40, 48, 60, 70, & 75 pcf. Other densities available.

Precision Board Plus is **non-abrasive**, can be machined with HSS bits or cut with any standard cutting tool. PBLT's tight cell structure allows adjusting spindle speed & table feed to produce either chips or dust as desired. Check Coastal's on-line Onsrud Router Search guide for most efficient cutter bit for desired speeds & feeds. PBLT Plus does not outgas or affect prepreg resin cure.
See FAQ for important oven/autoclave ramping procedures and other pertinent information. **

PBLT can be bonded to itself or most other substrates using Coastal Enterprises' one part urethane adhesives: PB Bond-240 and PB Fast Set or EP-76, a two part, epoxy adhesive.

PHYSICAL PROPERTIES:

Density	ASTM D-1623	10 lbs/Cubic Foot
Compressive Strength	ASTM D-1621	158 psi
Compressive Modulus	ASTM D-1621	5,120 psi
Tensile Strength	ASTM D-1623	134 psi
Tensile Modulus	ASTM D-1623	1,867 psi
Shear Strength	ASTM C-273	79 psi
Shear Modulus	ASTM C-273	1,094 psi
Flexural Strength Method 1A	ASTM D-790	190 psi
Flexural Modulus Method 1 A	ASTM D-790	8,031 psi
Hardness Shore D	ASTM D-2240	9
Elongation		8.0%
Dimensional Stability	ASTM D-2126	1.2% Max.
Water Absorption	ASTM D-2842	0.9% by Vol. after 96 hrs.
Closed Cell Content	ASTM D-2856	97%
"K" Value Insulation Factor	ASTM C-177	0.338
Impact Resistance	0˚F 4.6 oz. 1" Dia. 9'6" drop	No cracking observed
Freeze Thaw	ASTM D-2126, 25 Cycles	No disbonding or distortion occurred
Mold and Mildew Resistance	ASTM D-3273	Does not support growth
Dielectric Constant	ASTM D-1678	1.3
Maximum Service Temperature	Dry	200˚ F
Coefficient of Thermal Expansion (CTE)		23 X 10^{-6} ˚F
Glass Transition	DMA/TMA	237˚F
Specific Heat @ 77˚F	ASTM E-1269	0.235
Precision Board does not contain: Chlorinated Fluorocarbons (CFC's) or Volatile Organic Compounds (VOC's)		
Flammability Tests:	FAR 25.853 Vertical Burn	Pass
	MIL P 26514 Burn Test	Pass
	ASTM D-1692-74 Burn Test	Pass
	ASTM D635-06 Burn Test	Pass

Follow heat temperature ramping of 1˚F up per minute & 2˚F down per minute. See FAQ for additional data.

Any Questions please contact Coastal Enterprises Company

(800) 845-0745

www.PrecisionBoard.com

Form 171 8/19/13

GE
Plastics
Specialty Film & Sheet

Lexan* 9030 Sheet
Product Datasheet

Description

Lexan* 9030 sheet is the standard grade of Lexan sheet without UV protected nor Mar resistant surface treatment. Lexan 9030 sheet combines high impact and temperature resistance with optical clarity and can be utilized for secondary glazing behind existing glazing for economical protection against breakage or intrusion. Lexan 9030 sheet can be cut, sawn, drill, milling and bent easily using standard workshop equipment without the risk of cracking and breakage and is therefore an excellent candidate for fabricating a wide range of indoor applications such as machine guards etc. Lexan 9030 sheet can be easily thermoformed into complex parts while retaining its excellent properties necessary for demanding applications such as vandal proof street furniture. Lexan 9030 sheet may be decorated using a wide variety of modern techniques such as painting and screen printing.

Typical Property Values ◆

Property	Test Method	Unit	Value
Physical			
Density	ISO 1183	g/cm³	1.2
Water absorption, 24 hours	ISO 62	mg.	10
Water absorption, saturation /23°C	ISO 62	%	0.35
Mould shrinkage	ASTM-D955	%	0.6-0.8
Poison's ratio	ASTM-D638	-	0.38
Mechanical			
Tensile stress at yield 50 mm/min	ISO 527	MPa	60
Tensile stress at break 50 mm/min	ISO 527	MPa	70
Tensile strain at yield 50 mm/min	ISO 527	%	6
Tensile strain at break 50 mm/min	ISO 527	%	120
Tensile modulus 1 mm/min	ISO 527	MPa	2350
Flexural stress at yield 2 mm/min	ISO 178	MPa	90
Flexural modulus 2 mm/min	ISO 178	MPa	2300
Hardness H358/30 95	ISO 2039/1	MPa	95
Impact			
Charpy impact, notched	ISO 179/2C	kJ/m²	35
Izod impact, unnotched 23°C	ISO 180/1U	kJ/m²	NB
Izod impact, unnotched -30°C	ISO 180/1U	kJ/m²	NB
Izod impact, notched 23°C	ISO 180/1A	kJ/m²	65
Izod impact, notched -30°C	ISO 180/1A	kJ/m²	10

◆ These property values have been derived from Lexan* resin data for the material used to produce this sheet product. These property values may differ for color grades. These typical values are not intended for specification purposes. If minimum certifiable properties are required please contact your local GE- Plastics, Specialty Film & Sheet representative. All values are measured at least after 48 hours storage at 23°C/50% relative humidity. All properties are measured on injection molded samples. All samples are prepared according ISO 294.

* Lexan is a trademark of General Electric Company.

GE
Plastics
Specialty Film & Sheet

Lexan* 9030 Sheet
Product Datasheet

Typical Property Values (continued)◆

Property		Test Method	Unit	Value
Thermal				
Vicat B/120		ISO 306	°C	145
HDT/Ae, 1.8 MPa edgew. 120*1*04/s=100		ISO 75	°C	127
Thermal conductivity		DIN52612	W/m.°C	0.2
Coef.of Lin.Therm.Exp.extr. 23-80°C		DIN53752	1/°C	7.00E-05
Ball pressure test 125 ±2°C		IEC335-1	-	Passes
Thermal Index. Electrical Properties		UL746B	°C	100
Thermal Index. Mech. prop.with impact		UL746B	°C	100
Thermal Index. Mech.prop.w/o impact		UL746B	°C	100
Electrical				
Volume Resistivity		IEC93	Ohm.cm	1015
Relative Permittivity	50Hz	IEC250	-	3
Dissipation Factor	1Mhz	IEC250	-	2.9
Dissipation Factor	5Hz	IEC250	-	0.0009
Dissipation Factor	1 Mhz	IEC250	-	0.01
Arc Resistance Tungsten		ASTM-D495	sec.	119
Optical				
Light transmission [1] 3 mm		ASTM-D1003	%	89

◆ These property values have been derived from Lexan* resin data for the material used to produce this sheet product. These property values may differ for color grades. These typical values are not intended for specification purposes. If minimum certifiable properties are required please contact your local GE –Plastics, Specialty Film & Sheet representative. All values are measured at least after 48 hours storage at 23°C/50% relative humidity. All properties are measured on injection molded samples. All samples are prepared according ISO 294.

1) Light transmission value may vary by + or - 5%.

* Lexan is a trademark of General Electric Company.

GE
Plastics
Specialty Film & Sheet

Lexan* 9030 Sheet
Product Datasheet

Sound reduction

Installing Lexan 9030 sheet as secondary glazing behind glass meets the acoustic requirements of today's glazing.

Acoustic insulation DIN 52210 - 75 Rw (Db)

Lexan 9030 thickness	Air space in mm	Glass	Rw in Db
4 mm	85	6 mm	39
5 mm	85	6 mm	40
6 mm	85	6 mm	42
8 mm	85	6 mm	44

Thermal Insulation

When using Lexan 9030 sheet in combination as secondary glazing behind glass considerable energy savings can be achieved.

K-Values

Lexan 9030 thickness	Air space in mm	Glass	K-Value in W/m2 K
4 mm	20-60	4 mm	2.77
5 mm	20-60	4 mm	2.73
6 mm	20-60	4 mm	2.72

Steel ball impact test

Norm prEN356

Lexan 9030 sheet meets the highest impact performance required by the European Norm prEN356 for security glazing. A steel ball of 4.11 kg. with a diameter of 100 mm is freely dropped from different heights onto the glazing specimen. The steel ball must impact the specimen 3 times. Lexan 9030 sheet reached the highest standard required by the test at a thickness of 5 mm and above.

Category of resistance	Drop Height mm	Total number of strikes	Code designation for category of resistance	Impact energy per stroke
P1A	1500	3 in a triangle	EN 356 P1A	62 Joule
P2A	3000	3 in a triangle	EN 356 P2A	123 Joule
P3A	6000	3 in a triangle	EN 356 P3A	247 Joule
P4A	9000	3 in a triangle	EN 356 P4A	370 Joule
P5A	9000	3 x 3 in a triangle	EN 356 P5A	370 Joule

Classification table for the resistance of security glazing products according to European Norm prEN356

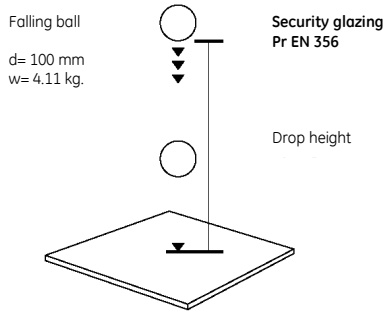

Glazing guidelines

Thermal expansion allowance

When installing Lexan 9030 sheet in a frame care should be taken to allow free expansion of the sheet. In general: Thermal expansion of the sheet is approximately 3 mm per linear meter.

Internal overglazing

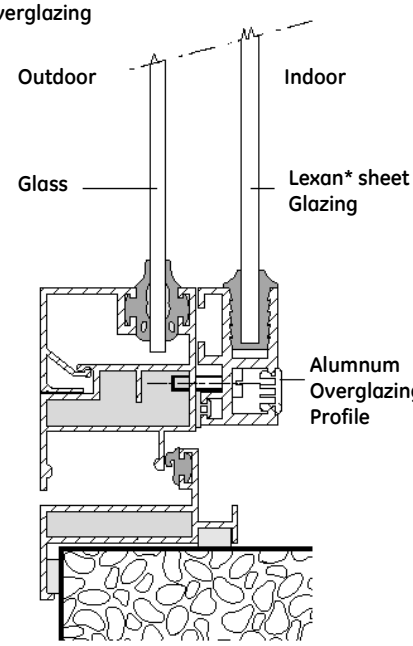

Sheet edge engagement

The required sheet edge engagement of Lexan 9030 sheet the glazing profiles is around 20 mm

Gaskets/Sealants

When using glazing compounds it is essential that the compound accepts thermal expansion movements and that compatible with Lexan 9030 sheet.
Silicone sealants and Neoprene, EPT or EPDM Rubber gaskets (65 shore) are generally recommended.

Thickness recommendation

Lexan 9030 sheet thickness recommendation installed as secondary glazing behind glass.

Shortest sheet side	Lexan 9030 sheet thickness
<400 mm	3 mm
<650 mm	4 mm
<900 mm	5 mm
<1200 mm	6 mm
<1400 mm	8 mm

GE
Plastics
Specialty Film & Sheet

Lexan* 9030 Sheet
Product Datasheet

Cleaning

Small area's: wash sheet with a solution of mild soap and lukewarm water using a soft cloth or sponge.
Large area's: clean surface with a high pressure water and/ or steam cleaner.
Note: do not use abrasive cleaners or detergents or sharp instruments which may scratch the sheet.

Forming, fabricating, finishing

Cutting, drilling and milling

Circular saws, band saws, jig saws and common hacksaws, all with fine toothed panel blades, can be used for trouble free cutting of Lexan* 9030 sheet. Standard high speed steel twist drill or carbide tipped drills can be used for drilling holes in Lexan 9030 sheet. Lexan 9030 sheet can be machined using conventional milling machines fitted with standard high speed knife cutting tools. During above mentioned operations the Lexan 9030 sheet must be always securely clamped to avoid rough cut edge by undesirable vibration and the masking should be left on the sheet to prevent surface damage by scratching.

Cold curving

Cold curving of Lexan 9030 sheet is acceptable for shapes having a radius of 100 times the sheet thickness or greater.

Sheet thickness	Minimum allowable radius
2 mm	200 mm
3 mm	300 mm
4 mm	400 mm
5 mm	500 mm
6 mm	600 mm
8 mm	800 mm

Cold line bending

Cold line bending of Lexan 9030 sheet as metal is possible when taking into account the following guidelines.

- Use hydraulic bent equipment
- Protective masking should be left during bending process
- Angle max. 45 degree at sheet thickness ³ 8 mm
- Angle max. 90 degree at sheet thickness <8 mm
- Use sharp bending knife
- Bending operation should be performed quickly
- Over bending is required to achieve the desired angle after stress relaxation
- Smooth and notch free edge of Lexan 9030 sheet to avoid side cracking

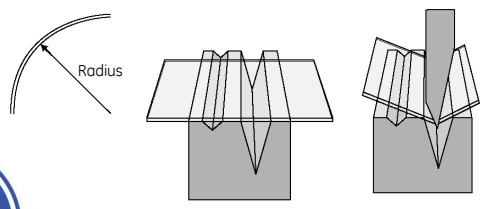

Thermoforming techniques for Lexan 9030 sheet

Vacuum forming

Lexan 9030 sheet is may be suitable to vacuum forming. It allows deep draw ratios, equal wall thickness distribution and it can be formed into complex shapes using standard thermoforming equipment which is equipped with its own sandwich type of heating devices. Lexan 9030 sheet has a forming temperature range of 185 - 205°C.

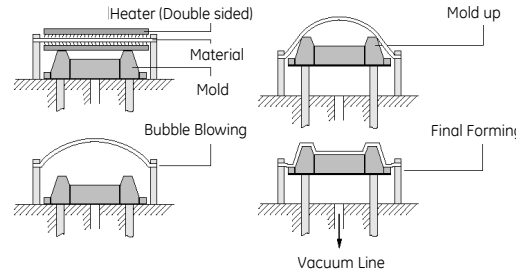

Drape forming

The process involves placing the sheet, without the masking and mould in a hot circulating oven. The temperature is raised to the point where th Lexan 9030 sheet sags (between 140 - 155°C) and conforms to the shape of the mold.

Typical drape forming set-up

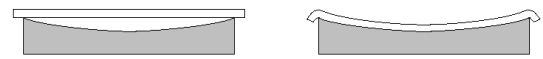

Pressure forming

Pressure forming is basically the same as vacuum forming. However, during the final forming stage compressed air is applied to the positive side of the mould to force the sheet to conform more closely to the mould. The result is a component with sharp features and detailed geometry.

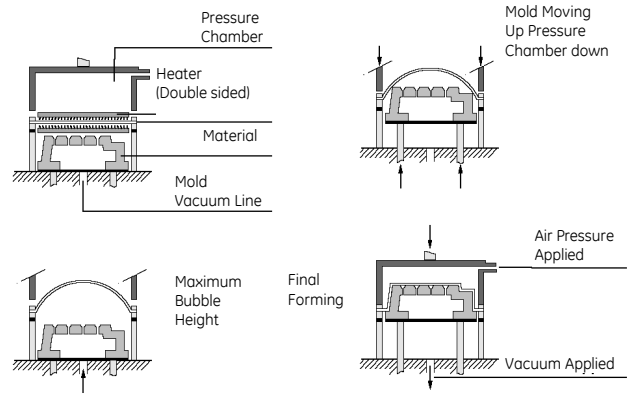

GE
Plastics
Specialty Film & Sheet

Lexan* 9030 Sheet
Product Datasheet

Twin sheet forming
Twin sheet forming is a vacuum forming technology whereby two sheets are formed at the same time, producing an application with hollow sealed section. The connection joint between the two parts is obtained by melting of the two materials and the exposed pressure of the mould.
No additional glue or other adhesive is therefor necessary.

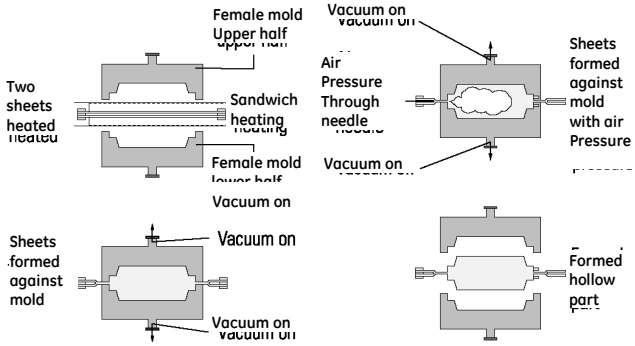

Pre-drying
It is extremely important to ensure that Lexan 9030 sheets are free of moisture prior to thermoforming. A hot circulation oven set at 120°C is recommended.

Sheet thickness	Drying time
2 mm	3 hours
3 mm	4 hours
4 mm	10 hours
5 mm	16 hours
6 mm	24 hours

Decorating

Painting
Lexan 9030 sheet can be painted without surface treatment other than cleaning. Provided certain basic recommendations are followed, most techniques used to apply paint to other material, can be used for Lexan 9030 sheet. Paint systems for Lexan 9030 sheet are readily available as standard items from various manufacturers.
Use only recommended paint

Painting systems

Supplier	Paints	Thinner	Comments
AKZO	Autocryl	-	2K Acrylic
Coatings	01-69004	06-302007	Primer/2K/PUR
	Class 45		Top
coat/2K/PUR			
Diegel	PA 21	24896	1K Flex. acrylic
Schaepman	C1 F57	VOA 462	Acrylic
	C1 W28	Water	Acrylic/water
based			
	C4 P212	VOA421/H4P4	2K Acrylic
Herberts	R 47633	-	2K Primer
	41605	11098	Basecoat BMW
mete			
	R4790	-	2K Clear coat
	R4780	-	2K One layer
system			
Becker	TH 130	NT19 2K	Top coat
	DJ-331-5176	ET-134 1K	Primer (flexible)
	TC 132	-	2K Clear coat
HSH	Interplan 1000		1K Water-
based			
Morton	L446	U987	1K Acrylic Syst.

NB For information regarding application techniques and property values please contact the relevant paint supplier.

Screen process printing
Screen printing is a well established process that offer a wide variety of options for a decorative finish. Approved Lexan 9030 sheet screen paints, when applied to flat, uniformed sheet are handled in the same manner as screen paints fit other plastic material.

Silk Screen Inks

Supplier	Inks
Sericol	Seritec TH Polyplast PY
	Plastipure PP
Wiederhold	HG/PK/PK-Jet
Visprox	TCI 8700/STR 5700/TCP 9900
Diegel	HV/Z
Gibbon Inks & Coating Ltd.	Matercryl
	Polyvin/Marlerstyrene
Coates	Vynaglaze/Vynafresh/Touchkey
Pröll	Jet 200/Thermo-Jet/Noriprint PS
Marabu	Marastar SR/Maraplast D

Anti static treatment/cleaning
Lexan 9030 sheet tends to build up a static charge. It is often necessary to clean and discharge surface prior to painting and screen printing. Special anti static formulations are available which reduce the static charge. Cleaning prior to thermoforming Lexan 9030 sheet it is recommended that dust is blown off with unionizing air.

Anti-static Products

Company/Supplier	Product/Brand Name
American Cyanamid Co.	Cyastat SN50
AKZO Chemicals	No. 03643
Morton	S154

GE
Plastics
Specialty Film & Sheet

Lexan* 9030 Sheet
Product Datasheet

Fire performance

Lexan 9030 sheet has good fire behavior characteristics. Lexan sheet does not contribute significantly to the spread of fire or to the generation of toxic gases.
For details please contact your local sales office.

Light transmission

Transparent Lexan 9030 sheet have excellent light transmission, dependent of thickness between 84 - 87%.

Product Availability •)

Product code:	Lexan 9030
Standard gauge:	0.75 – 1 – 1.5 mm
Standard width:	625 x 1250, 2050x 3050 mm
Standard length:	1250 x 1250, 2050 x 6050 mm
Standard colors:	transparent code 112 and opal white code 82103
Texture:	blue print
Masking:	
top side	Coex opal white PE
bottom side	Coex transparent PE

•) Other gauges and other dimensions upon request and are subject to minimum order quantities. Dimensions only for 0.75 mm

Chemical resistance

Taking into account the complexity of chemical compatibility, all chemicals which come into contact with Lexan 9030 sheet should be tested. Consult our technical service center for more technical info.

A Quality Product from Hawkeye Industries, Inc.

Duratec® Polyester **EZ Sanding Primer**

An exceptionally easy-to-sand primer, that can be polished to a smooth, porosity-free surface.

Uses: for surfacing patterns for composite molds, and where an easy sanding, high build primer is required.. Apply over tooling board, MDF, brick, concrete, plaster and clay.

Features:

Builds rapidly and provides a surface that sands quickly.

- Use less sandpaper
- Reduce sanding labor

Easy to spray from HVLP guns. Low porosity, fine smooth surface.

- Start sanding with a fine grit, reduce dust and film loss.
- Build up to 30 mils.

Adhesion to most epoxies.

- Heat distortion temperature of 83° C, 180° F
- Not recommended for use on CNC patterns over a low (less than 120° F) HDT tooling putty.

Use Instructions:

Assure that the work area is at least 60°F, and that the Duratec and the part that will be sprayed are at least 60° F. Compressed air must be free of water.

1. Mix the Duratec EZ Sanding Primer with a paint shaker or drill-mounted mixer. Use a stir stick to scrape the bottom of the container before mixing.

714-061 White

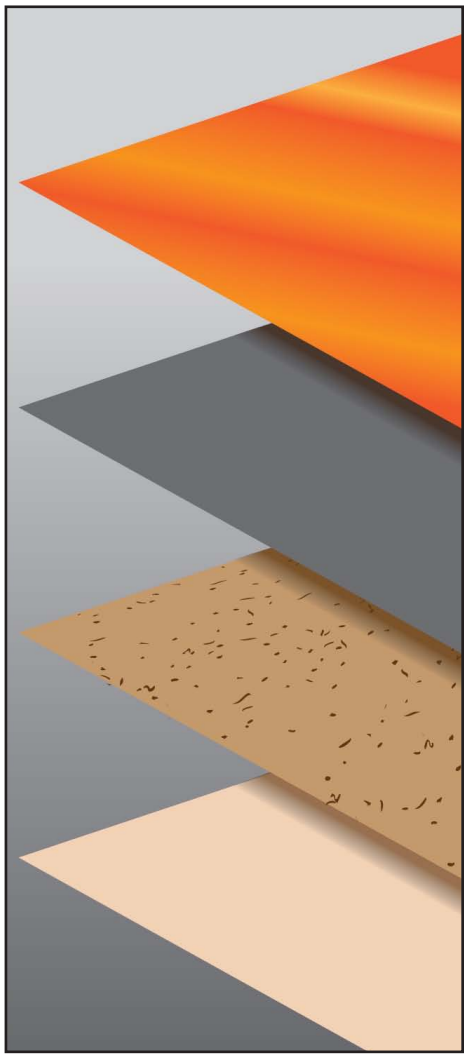

Hawkeye Industries
P. O. Box 415, Bloomington, CA 92316
(USA) 800-977-0060 • (Outside USA) 909-546-1160 • Fax 909-546-1161
Email: hawkeyesales@hawkeyeind.com • www.duratec1.com

Product Properties: All time calculations are based on temperatures of 77°F, 25°C

As measured on a Brookfield Viscometer Model RVF, Spindle #2 at 20 rpm	2900 cps +/- 150 cps
Thixotropic	6.5
Gel Time: Sample based on a 100 g mass catalyzed at 2 percent with mekP	22 min +/- 2 min
Weight per Gallon	11.8 lb., 5.36 kg
Coverage per Gallon:	
10 mil thickness (wet-dry)	110-115 ft^2
250 micron thickness (wet-dry)	10.2-10.7 m^2

Duratec Polyester EZ Sanding Primer is among the many fine Duratec products marketed worldwide by Hawkeye Industries Inc.

Revised 07-15-15

Hawkeye Industries
P. O. Box 415, Bloomington, CA 92316
(USA) 800-977-0060 • (Outside USA) 909-546-1160 • Fax 909-546-1161
Email: hawkeyesales@hawkeyeind.com • www.duratec1.com

A Quality Product from Hawkeye Industries Inc.

Duratec® Polyester **Sealer**

A low viscosity, rapid curing, penetrating sealer that anchors lacquers, urethanes, polyesters, vinyl esters and most epoxies to a variety of substrates

Usage

For surfacing composite plugs and patterns and for sealing woods and veneers, plaster, concrete, and GRP surfaces.

Features

Save time and add quality with Duratec Polyester Sealer.

Here's why you should choose Duratec Polyester Sealer–

Easy to apply – Spray, brush or roll.

Rapid curing–surfaces are ready for topcoats in 1 to 2 hours.

Deep penetration–allows primers and topcoats to bond to a variety of substrates.

Duratec Polyester Sealer

823A Clear

Hawkeye Industries Inc.
P O Box 415 Bloomington, CA 92316
Tel 909-546-1160; Toll Free 800-977-0060; Fax: 909-546-1161
Email hawkeyesales@hawkeyeind.com Web www. duratec1.com

Product No. 823 Clear

Duratec Polyester Sealer

Product Properties

All time calculations are based on temperatures of 77°F, 25°C

Viscosity

As measured on a Brookfield Viscometer Model RVF, Spindle #2 at 20 rpm 80 cps

Thixotropic Index 0

Gel Time

Sample based on a 100 g mass catalyzed at 2 percent with mekP 10-14 min

Weight per Gallon 8.59 lb., 3.89 kg

Rev 07-15-15

Hawkeye Industries Inc.
P O Box 415 Bloomington, CA 92316
Tel 909-546-1160; Toll Free 800-977-0060; Fax: 909-546-1161
Email hawkeyesales@hawkeyeind.com Web www. duratec1.com

105 Epoxy Resin® / 206 Slow Hardener®

Technical Data Sheet

105 System
105/206

General Description

105/206 Epoxy is used for general coating and bonding applications when extended working and cure time are needed or to provide adequate working time at higher temperatures.

105/206 forms a high-strength, moisture-resistant solid with excellent bonding and barrier coating properties. It will wet out and bond to wood fiber, fiberglass, reinforcing fabrics, foam and other composite materials, and a variety of metals.

105/206 Epoxy can be thickened with WEST SYSTEM fillers to bridge gaps and fill voids and can be sanded and shaped when cured. With roller applications, it has excellent thin-film characteristics, allowing it to flow out and self-level without "fish-eyeing." Multiple coats of 105/206 Epoxy create a superior moisture barrier and a tough, stable base for paints and varnishes. It is formulated without volatile solvents resulting in a very low VOC content. It has a relatively high flash point, no strong solvent odor and does not shrink after curing. It is not intended for clear coating natural finished wood.

Handling Characteristics

Mix ratio by volume (300 Mini Pump ratio)	5 parts resin : 1 part hardener
by weight	5.36 : 1
Acceptable ratio range by weight	4.84 : 1 to 6.19 :1
Mix viscosity (at 72°F) ASTM D-2393	725 cps
Pot life (100g at 72°F)	20 to 25 minutes
Working time, thin film*	90 to 110 minutes
Cure to a solid, thin film*	10 to 15 hours
Cure to working strength	1 to 4 days
Minimum recommended temperature	60°F (16°C)

**Epoxy cures faster at higher temperatures and in thicker applications.*

Physical Properties of Cured Epoxy

Specific gravity	1.18
Hardness (Shore D) ASTM D-2240	83
Compression yield ASTM D-695	11,500 psi
Tensile strength ASTM D638	7,300 psi
Tensile elongation ASTM D-638	4.5%
Tensile modulus ASTM D-638	4.60E+05psi
Flexural strength ASTM D-790	11,800 psi
Flexural modulus ASTM D-790	4.50E+05
Heat deflection temperature ASTM D-648	123°F
Onset of Tg by DSC	126°F
Ultimate Tg	139°F

Storage/Shelf Life

Store at room temperature. Keep containers closed to prevent contamination. With proper storage, resin and hardeners should remain usable for many years. After a long storage, verify the metering accuracy of the pumps. Mix a small test batch to assure proper curing.

Over time, 105 Resin will thicken slightly and will therefore require extra care when mixing. Repeated freeze/thaw cycles during storage may cause crystallization of 105 Resin. Warm resin to 125°F and stir to dissolve crystals. Hardener may darken with age, but physical properties are not affected by color. Be aware of a possible color shift if very old and new hardener are used on the same project.

Gougeon Brothers, Inc.
P.O. Box 908
Bay City, MI 48707

866-937-8797

westsystem.com

October, 2014

105 Epoxy Resin® / 209 Extra Slow Hardener®

Technical Data Sheet

105 System
105/209

General Description

105/209 Epoxy is used for general coating and bonding applications in extremely warm and/or humid conditions or when extended working time is desired at room temperature. Provides approximately twice the working time of 206 Slow Hardener.

105/209 forms a high-strength, moisture-resistant solid with excellent bonding and barrier coating properties. It will wet out and bond to wood fiber, fiberglass, reinforcing fabrics, foam and other composite materials, and a variety of metals.

105/209 Epoxy can be thickened with WEST SYSTEM fillers to bridge gaps and fill voids and can be sanded and shaped when cured. With roller applications, it has excellent thin-film characteristics, allowing it to flow out and self-level without "fish-eyeing." Multiple coats of 105/209 Epoxy creates a superior moisture barrier and a tough, stable base for paints and varnishes. It is formulated without volatile solvents resulting in a very low VOC content. It has a relatively high flash point, no strong solvent odor and does not shrink after curing. It is not intended for clear coating natural finished wood.

Handling Characteristics

Mix ratio by volume (300 Mini Pump ratio)	3 parts resin : 1 part hardener
by weight	3.68 : 1
Acceptable ratio range by weight	3.30 : 1 to 4.03 : 1
Mix viscosity (at 72°F) ASTM D-2393	650 cps
Pot life (100g at 72°F)	40-50 minutes
Working time, thin film*	3 to 4 hours
Cure to a solid, thin film*	20 to 24 hours
Cure to maximum strength	4 to 9 days
Minimum recommended temperature	70°F (21°C)

**Epoxy cures faster at higher temperatures and in thicker applications.*

Physical Properties of Cured Epoxy

Specific gravity	1.16
Hardness (Shore D) ASTM D-2240	82
Compression yield ASTM D-695	12,000 psi
Tensile strength ASTM D-638	7,300 psi
Tensile elongation ASTM D-638	3.6%
Tensile modulus ASTM D-638	3.98E+05 psi
Flexural strength ASTM D-790	12,500 psi
Flexural modulus ASTM D-790	3.97E+05
Heat deflection temperature ASTM D-648	117°F
Onset of Tg by DSC	122°F
Ultimate Tg	130°F
Annular shear fatique @ 100,000 cycles	9,900 lb

Storage/Shelf Life

Store at room temperature. Keep containers closed to prevent contamination. With proper storage, resin and hardeners should remain usable for many years. After a long storage, verify the metering accuracy of the pumps. Mix a small test batch to assure proper curing.

Over time, 105 Resin will thicken slightly and will therefore require extra care when mixing. Repeated freeze/thaw cycles during storage may cause crystallization of 105 Resin. Warm resin to 125°F and stir to dissolve crystals.

Hardener may darken with age, but physical properties are not affected by color. Be aware of a possible color shift if very old and new hardener are used on the same project.

Gougeon Brothers, Inc.
P.O. Box 908
Bay City, MI 48707

866-937-8797

westsystem.com

April, 2015

PLASCORE®

PN2 Aerospace Grade Aramid Fiber Honeycomb

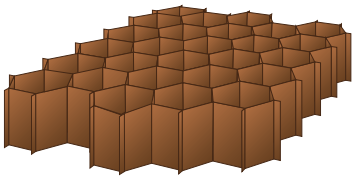

Description:

PN2 aerospace grade aramid fiber honeycomb exhibits outstanding flammability properties. It is manufactured from DuPont Nomex® paper (or equivalent) and coated with a heat resistant phenolic resin.

Applications:

PN2 honeycomb uses include aircraft galleys, flooring, partitions, aircraft leading and trailing edges, missile wings, radomes, antennas, military shelters, fuel tanks, helicopter rotor blades and navy bulkhead joiner panels.

Features:

- Fire resistant (self extinguishing)
- High strength to weight ratio
- Corrosion resistant
- Excellent dielectric properties
- Thermally insulating
- High toughness
- Excellent creep and fatigue performance
- Good thermal stability
- Densities as low as 1.5 lb/ft^3 (24 kg/m^3)
- Over expanded cell configuration suitable for forming simple curves
- Compatible with most adhesives used in sandwich composites

Availability:

PN2 honeycomb is available in sheets, blocks or cut to size pieces in both regular hexagonal and over expanded (OV) cell configurations.

Cell Sizes:	1/8" - 1/4"	
Densities:	1.8 pcf - 9.0 pcf	
Sheet "Ribbon" (L):	48" typical	
Sheet "Transverse" (W):	96" typical	
Tolerances:	Length:	+ 3", - 0" (36" for OV)
	Width:	+ 6", - 0"
	Thickness:	± .006" (under 2" thick)
	Density:	± 10%
	Cell Size:	± 10%

NOTE: Special dimensions, sizes, tolerances and specifications can be provided upon request.

PN2 aerospace grade aramid fiber honeycomb is specified as follows:

Material - Cell Size - Density - Cell Configuration

Note: 1/8" OV core can be over expanded only to a maximum of 20% over nominal cell size.

®Nomex is a registered trademark of E.I. DuPont de Nemours, Wilmington, Delaware.

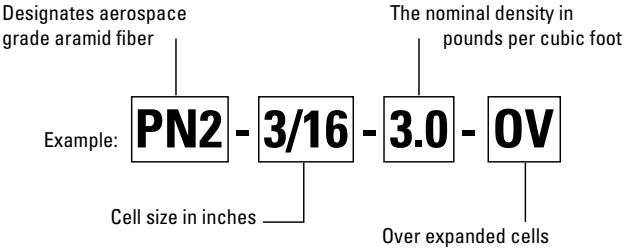

PN2 Mechanical Properties

PLASCORE® Honeycomb Designation	DENSITY		COMPRESSIVE (BARE) STRENGTH (psi/MPa)				PLATE SHEAR "L" DIRECTION STRENGTH (psi/MPa)				PLATE SHEAR "L" DIRECTION MODULUS (ksi/GPa)		PLATE SHEAR "W" DIRECTION STRENGTH (psi/MPa)				PLATE SHEAR "W" DIRECTION MODULUS (ksi/GPa)	
			TYP		MIN		TYP		MIN		TYP		TYP		MIN		TYP	
	lb/ft³	kg/m³	psi	MPa	psi	MPa	psi	MPa	psi	MPa	ksi	GPa	psi	MPa	psi	MPa	ksi	GPa
PN2-1/8-1.8	1.8	29	85	0.59	74	0.51	75	0.52	60	0.41	3.8	0.026	45	0.31	32	0.22	1.7	0.012
PN2-1/8-3.0	3.0	48	290	2.00	200	1.38	205	1.41	140	0.97	6.7	0.046	105	0.72	74	0.51	3.5	0.024
PN2-1/8-4.0	4.0	64	515	3.55	350	2.41	275	1.90	215	1.48	8.6	0.059	150	1.04	108	0.74	4.7	0.032
PN2-1/8-5.0	5.0	80	700	4.83	540	3.72	325	2.24	265	1.83	10.8	0.074	215	1.48	130	0.90	6.2	0.042
PN2-1/8-6.0	6.0	96	930	6.41	700	4.83	360	2.48	320	2.21	12.9	0.089	245	1.69	150	1.03	7.5	0.052
PN2-1/8-8.0	8.0	128	1700	11.72	1170	8.07	420	2.90	400	2.76	16.7	0.115	295	2.03	200	1.38	10.6	0.073
PN2-1/8-9.0	9.0	144	2145	14.79	1450	10.00	445	3.07	425	2.93	18.7	0.129	315	2.17	240	1.65	11.2	0.077
PN2-3/16-1.8	1.8	29	90	0.62	74	0.51	70	0.48	50	0.34	3.3	0.023	45	0.31	30	0.21	1.8	0.013
PN2-3/16-2.0	2.0	32	125	0.86	93	0.64	95	0.66	70	0.48	4.5	0.031	55	0.38	40	0.28	2.5	0.017
PN2-3/16-3.0	3.0	48	300	2.07	200	1.38	185	1.28	140	0.97	6.1	0.042	110	0.76	67	0.46	4.1	0.028
PN2-3/16-4.0	4.0	64	515	3.55	350	2.41	235	1.62	215	1.48	8.2	0.056	165	1.14	112	0.77	5.5	0.038
PN2-1/4-1.5	1.5	24	70	0.48	54	0.37	55	0.38	45	0.31	2.8	0.019	35	0.24	23	0.16	1.7	0.012
PN2-1/4-2.0	2.0	32	130	0.90	93	0.64	90	0.62	70	0.48	3.8	0.026	55	0.38	36	0.25	2.4	0.017
PN2-1/8-3.0-OV	3.0	48	270	1.86	200	1.38	165	1.14	100	0.69	5.0	0.035	115	0.79	80	0.55	4.0	0.027
PN2-3/16-1.8-OV	1.8	29	95	0.66	75	0.52	60	0.41	35	0.24	2.2	0.015	60	0.41	36	0.25	3.3	0.023
PN2-3/16-2.0-OV	2.0	32	115	0.79	90	0.62	70	0.48	50	0.34	2.4	0.016	70	0.48	40	0.28	3.9	0.027
PN2-3/16-3.0-OV	3.0	48	280	1.93	250	1.72	115	0.79	75	0.52	3.3	0.023	135	0.93	75	0.52	6.6	0.045
PN2-3/16-4.0-OV	4.0	64	495	3.41	350	2.41	160	1.10	100	0.69	4.1	0.028	195	1.34	120	0.83	9.4	0.065
PN2-3/8-3.0-OV	3.0	48	250	1.72	200	1.38	105	0.72	60	0.41	2.8	0.020	135	0.93	80	0.55	6.5	0.045

NOTE: The above data is based on variable sample sizes and is subject to change with continued manufacturing and testing of PN2 honeycomb core blocks per MIL-C-81986 at room temperature.

Plascore, Inc., employs a quality management system that is AS/EN/JISQ 9100, ISO 9001:2008 and ISO 14001:2004 certified.

PLASCORE®

Corporate Headquarters

Plascore Incorporated
615 N. Fairview St.
Zeeland, MI 49464-0170

Phone (616) 772-1220
Toll Free (800) 630-9257
Fax (616) 772-1289
Email sales@plascore.com
Web www.plascore.com

Europe

Plascore GmbH&CoKG
Feldborn 6
D-55444 Waldlaubersheim
Germany

Phone +49(0) 6707-9143 0
Fax +49(0) 6707-9143 40
Email sales.europe@plascore.com
Web www.plascore.de

NAS1832 thru NAS1836, Inserts

For Composite or Honeycomb Panel Fastening

These **NAS1832 thru NAS1836**, Potted in Inserts are the standard for fastening in composite or honeycomb panels. The panel is first prepared by drilling or routing a hole or holes in the panel as necessary, depending on whether or not the insert is a through hole insert or a closed end insert. After preparing the hole and securing the insert in place with the NAS1837 adhesive tab (comes with inserts), then the adhesive or epoxy as recommended by the panel or aircraft manufacturer is forced in through one of the potting holes until it is forced out of the other hole or slot which acts as a vent hole. After the proper curing time and procedures are followed, remove the tab, clean up as required and then fasten items to the newly installed insert as appropriate.

Please use Part Number Diagram, Tables and pictures, to select inserts

When selecting length on all except NAS1833 and NAS1834, allow .040”min between insert and back skin

Basic#
NAS1832,Threaded, Closed end, Med Flange
NAS1833,Threaded, Open end, Med Flange
NAS1834,Thru Hole, Open end, Med Flange
NAS1835,Threaded, Closed end, Large Flange
NAS1836,Threaded, Closed end, Small Flange

Special Feature
- (dash) = Locking Thread Element
N = Non Locking Thread Element
K = *for NAS1834 only, Countersunk end, use a -(dash) for flat end.*

NAS1832 - 3 - 4 M

Material
- (dash) = Carbon steel
A = Aluminum 2024t3 or T351
C = Corrosion Resistant Steel 303

Size
of Threads
or Hole

Plating / Lube
Blank = Cad II plating, (Steel)
M = Black moly lubed Threads
P = Cad II plated (Cres)
S = Silver plated (Cres)
Note: Cres inserts should be plated or have black moly in threads to prevent galling.
These options not avail with NAS1834. Steel will be Cad II, Cres will be passivated.

Length specification number / increments
NAS1832, one or more digits / .125 incr.
NAS1833, three digits / .001 increments
NAS1834, three digits / .001 increments
NAS1835, fixed length, see item's table
NAS1836, one or more digits / .031 incr.

Continued.....

NAS1832 thru NAS1836, Inserts

For Composite or Honeycomb Panel Fastening....Continued

NAS1832 series, Potted in Insert, Medium Flange, Threaded with Closed End				
NAS1832	Threads	Flange	Installation Hole size	Length Minimum
-06	6-32	.560	.561-.566	.370
-08	8-32			
-3	10-32			
-4	1/4-28	.685	.686-.691	.500
-5	5/16-24			
-6	3/8-24	.841	.842-.847	

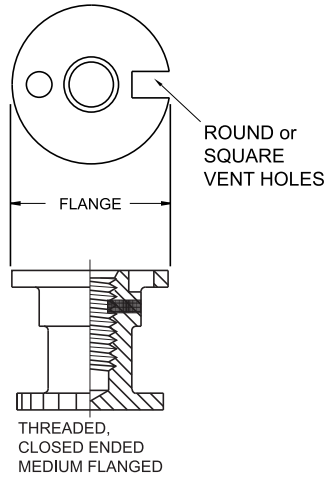

Note:
Do not specify less than minimum lengths shown on Tables !

NAS1833 series, Potted in Insert, Medium Flange, Threaded with Open End				
NAS1833	Threads	Flange	Installation Hole size	Length Minimum
-06	6-32	.560	.561-.566	.250
-08	8-32			
-3	10-32			
-4	1/4-28	.685	.686-.691	.312
-5	5/16-24			
-6	3/8-24	.841	.842-.847	.375

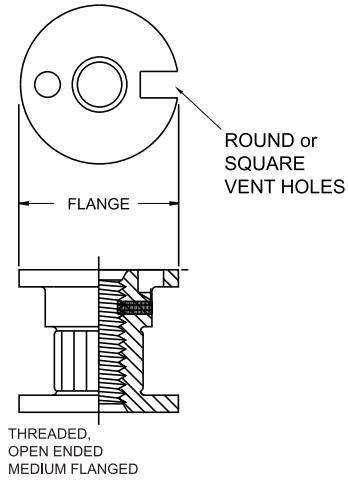

Installation Tabs are supplied with each Insert
If you need extras see the part numbers below for each series and size of insert

NAS1832, 1833, and 1834 all use the tab with part # **NAS1837T3** for thread sizes 06,08 & 3.
NAS1832, 1833, and 1834 all use the tab with part # **NAS1837T6** for thread sizes 4 and 5.
NAS1835, all use **NAS1837T7** they only come in thread sizes 3 and 4.
NAS1836 sizes 06, 08 & 3, use **NAS1837T2**, for size 4 use **NAS1837T4**

Continued.....

NAS1832 thru NAS1836, Inserts

For Composite or Honeycomb Panel Fastening....Continued

NAS1834 series, Potted in Insert, Medium Flange, UN-Threaded with Open End, Plain or Countersunk Bottom

NAS1834	Thru-Hole Size	Flange	Installation Hole size	Length Minimum
-06	.139-.145	.560	.561-.566	.250
-08	.168-.174			
-3	.195-.201			
-4	.256-.263	.685	.686-.691	.312
-5	.315-.322			
-6	-376-.383	.841	.842-.847	.375

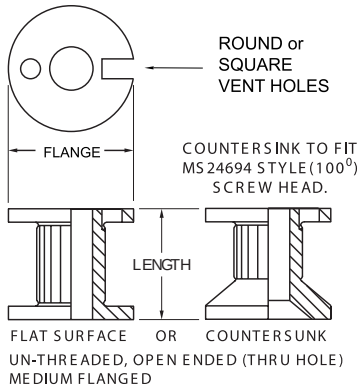

NAS1835 series, Potted in Insert, Large Flange, Floating Nut Element, Closed End.

NAS1835	Threads	Flange	Installation Hole size	Length
-08	8-32	.685	.686-.691	.37
-3	10-32			.43
-4	1/4-28	.748	.749-.755	.56
-5	5/16-24	.810	.811-.817	.75
-6	3/8-24	.873	.874-.880	.81

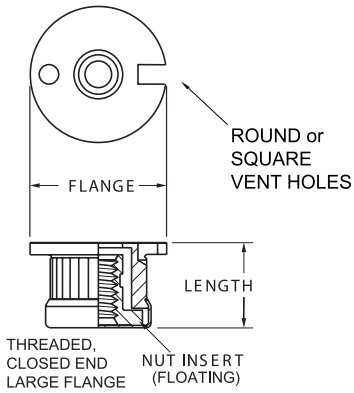

NAS1836 series, Potted in Insert, Small Flange, Threaded with Closed End

NAS1836	Threads	Flange	Installation Hole size	Length Minimum
-06	6-32	.451	.452-.457	.217
-08	8-32			
-3	10-32			
-4	1/4-28	.498	.499-.504	.279

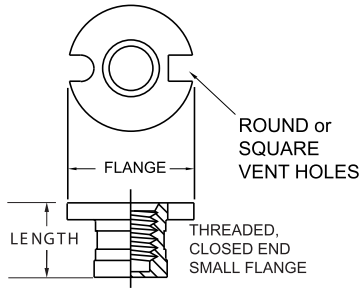

 Documents in this book for REFERENCE ONLY, not intended for design. Not guaranteed for accuracy.

DIAB Divinycell® H 45 Sandwich Core Material

Categories: Other Engineering Material; Composite Core Material; Polymer

Material Notes: Divinycell H has been widely used over many years in virtually every application area where sandwich composites are employed including the marine (leisure, military and commercial), land transportation, wind energy, civil engineering/infrastructure and general industrial markets. In its application range, Divinycell H has the highest strength to density ratio. It exhibits at both ambient and elevated temperatures impressive compressive strength and shear properties. In addition the ductile qualities of Divinycell H make it ideal for applications subject to fatigue, slamming or impact loads.

Other key features of Divinycell H include consistent high quality, excellent adhesion/peel strength, excellent chemical resistance, low water absorption and good thermal/acoustic insulation. Divinycell H is compatible with virtually all commonly used resin systems (polyester, vinyl ester and epoxy) including those with high styrene contents. Its good temperature performance with high residual strength and good dimensional stability makes Divinycell H ideal for hand laminating, vacuum bagging, RTM (resin transfer molding) or vacuum infusion.

Continuous operating temperature is -200 to 70°C. The foam can be used in sandwich structures, for outdoor exposure, with external skin temperatures up to 85°C. Normally Divinycell H can be processed up to 90°C with minor dimensional changes. Maximum processing temperature is dependent on time, pressure and process conditions.

Information Provided by DIAB

Vendors: No vendors are listed for this material. Please click here if you are a supplier and would like information on how to add your listing to this material.

Physical Properties	Metric	English	Comments
Density	0.0480 g/cc	0.00173 lb/in³	ISO 845

Mechanical Properties	Metric	English	Comments
Tensile Strength, Ultimate	1.40 MPa	203 psi	Perpendicular to the plane; ASTM D1623
Elongation at Break	12 %	12 %	In Shear; ASTM C273
Tensile Modulus	0.0550 GPa	7.98 ksi	Perpendicular to the plane; ASTM D1623
Compressive Strength	0.600 MPa	87.0 psi	Perpendicular to the plane; ASTM D1621
Compressive Modulus	0.0500 GPa	7.25 ksi	Perpendicular to the plane; ASTM D1621
Shear Modulus	0.0150 GPa	2.18 ksi	ASTM C273
Shear Strength	0.560 MPa	81.2 psi	ASTM C273

Thermal Properties	Metric	English	Comments
CTE, linear	22.2 µm/m-°C	12.3 µin/in-°F	
Maximum Service Temperature, Air	70.0 °C	158 °F	Continuous
Minimum Service Temperature, Air	-200 °C	-328 °F	Continuous

DIAB Divinycell® H 45 Sandwich Core Material

Categories: Other Engineering Material; Composite Core Material; Polymer

Material Notes: Divinycell H has been widely used over many years in virtually every application area where sandwich composites are employed including the marine (leisure, military and commercial), land transportation, wind energy, civil engineering/infrastructure and general industrial markets. In its application range, Divinycell H has the highest strength to density ratio. It exhibits at both ambient and elevated temperatures impressive compressive strength and shear properties. In addition the ductile qualities of Divinycell H make it ideal for applications subject to fatigue, slamming or impact loads.

Other key features of Divinycell H include consistent high quality, excellent adhesion/peel strength, excellent chemical resistance, low water absorption and good thermal/acoustic insulation. Divinycell H is compatible with virtually all commonly used resin systems (polyester, vinyl ester and epoxy) including those with high styrene contents. Its good temperature performance with high residual strength and good dimensional stability makes Divinycell H ideal for hand laminating, vacuum bagging, RTM (resin transfer molding) or vacuum infusion.

Continuous operating temperature is -200 to 70°C. The foam can be used in sandwich structures, for outdoor exposure, with external skin temperatures up to 85°C. Normally Divinycell H can be processed up to 90°C with minor dimensional changes. Maximum processing temperature is dependent on time, pressure and process conditions.

Information Provided by DIAB

Vendors: No vendors are listed for this material. Please click here if you are a supplier and would like information on how to add your listing to this material.

Physical Properties	Metric	English	Comments
Density	0.0480 g/cc	0.00173 lb/in³	ISO 845

Mechanical Properties	Metric	English	Comments
Tensile Strength, Ultimate	1.40 MPa	203 psi	Perpendicular to the plane; ASTM D1623
Elongation at Break	12 %	12 %	In Shear; ASTM C273
Tensile Modulus	0.0550 GPa	7.98 ksi	Perpendicular to the plane; ASTM D1623
Compressive Strength	0.600 MPa	87.0 psi	Perpendicular to the plane; ASTM D1621
Compressive Modulus	0.0500 GPa	7.25 ksi	Perpendicular to the plane; ASTM D1621
Shear Modulus	0.0150 GPa	2.18 ksi	ASTM C273
Shear Strength	0.560 MPa	81.2 psi	ASTM C273

Thermal Properties	Metric	English	Comments
CTE, linear	22.2 µm/m-°C	12.3 µin/in-°F	
Maximum Service Temperature, Air	70.0 °C	158 °F	Continuous
Minimum Service Temperature, Air	-200 °C	-328 °F	Continuous

Table 47. 3K 2x2 twill carbon fiber material properties (provided by Dr. Mello).

Stiffness	
E_{11} (psi)	1.00E+07
E_{22} (psi)	1.00E+07
G_{12} (psi)	9.30E+05
G_{13} (psi)	9.30E+05
G_{23} (psi)	4.65E+05
ν_{12}	0.05
Strength	
F_{1t} (psi)	1.00E+05
F_{2t} (psi)	1.00E+05
F_6 (psi)	1.00E+04
Failure Strains	
ε_{1t}	0.010
ε_{2t}	0.010
γ_{12}	0.022

Appendix E

Detailed Supporting Analysis

```
function[xd] = accsim(t,x)

global g Mrider Mbike rho Crr CdA eff P opt Pmax1 Pmax2 gain;

% Define power ramp-up with time relationship
if opt <= 1; % power profile for 1500 ft sprint
    P = gain*min(0.12*t^2+200,(Pmax1+100)-2*t)*.73756*eff; % converted to lb-ft/s
elseif opt <= 2; % power profile for corner acceleration
    P = gain*Pmax2*.73756; % converted to lb-ft/s
end

% P = 500;

xd = [0;0];

% Find starting force
Fin0 = (Mbike+Mrider)*g*0.7/3; % mu sub s = 0.7; divide by 3 for rwd

% Define force from power profile
Fin = min(Fin0,P/(eff*x(2))); % avoids spinout of rear tire

xd(1) = x(2);
xd(2) = (-0.5*rho*x(2)^2*CdA+Fin)/(Mrider+Mbike)-g*Crr;
```

```
%% HPV Acceleration Simulator

clc; clear; close all;

%% Define Variables

% Hold these constant
global g;
g = 32.174; % ft/s^2
global rho;
rho = 2.33E-3; %slg/ft^3 @ 70F

% Change these
global Mrider;
Mrider = 150/g; % slg (xxx lb/g = slg)
global Mbike;
Mbike = 50/g;
% global Pmax;
% Pmax = 600*.73756; % lbf-ft/s, (xxx W -> BG)
global Crr;
Crr = .005; % coeff. of rolling resistance
global CdA;
CdA = 1.69; % ft^2, Aria from CFD
global eff;
eff = 0.75; % drivetrain efficiency
global opt;
global Pmax1;
Pmax1 = 400; % W, max rider output in sprint
global Pmax2;
Pmax2 = 225; % W, rider output from corners
global gain;
gain = 1; % create training improvement parameter

%% Run accsim for 1500 ft sprint, create plot

opt = 1; % select sprint power profile
tspan = 90;
v0 = 0;

[t,x] = ode45(@accsim, [0 tspan], [0 v0]);
x(:,2) = x(:,2).*15./22;

% plot(t,x(:,1))
%
% figure
plot(x(:,1),x(:,2),'k','LineWidth',3) % Plot speed vs distance, baseline
axis([0 2600 0 35])
xlabel('Distance (ft)')
ylabel('Speed (mph)')
title('Half Mile Sprint Race')
hold on
```

```
Mbike = 40/g; % 20% lighter bike
[t,x] = ode45(@accsim, [0 tspan], [0 v0]);
x(:,2) = x(:,2).*15./22;
plot(x(:,1),x(:,2),'g','LineWidth',3)
Mbike = 50/g; % reset bike weight

% CdA = 1.69*.8; % 20% less air drag
% [t,x] = ode45(@accsim, [0 tspan], [0 v0]);
% x(:,2) = x(:,2).*15./22;
% plot(x(:,1),x(:,2),'b','LineWidth',3)
% CdA = 1.69; % reset drag coefficient

gain = 1.2; % 20% stronger rider
[t,x] = ode45(@accsim, [0 tspan], [0 v0]);
x(:,2) = x(:,2).*15./22;
plot(x(:,1),x(:,2),'c','LineWidth',3)
gain = 1; % reset gain

% 2015 Projections
gain = 1.25; % 25% stronger rider
CdA = .23*7.9; % wind tunnel estimation
Mbike = 60/g; % 60 lb bike
[t,x] = ode45(@accsim, [0 tspan], [0 v0]);
x(:,2) = x(:,2).*15./22;
plot(x(:,1),x(:,2),'r--','LineWidth',3)
legend('Aria','20% lighter vehicle','20% stronger rider','2015 bike',4)
% legend('Aria','20% lighter vehicle','20% less air drag','20% stronger rider','2015↙
bike',2)
hold off

gain = 1; % Reset values to Aria
CdA = 1.69;
Mbike = 50/g;

%% %% Run accsim for 100 ft acceleration, create plot

opt = 2; % select endurance power profile
tspan = 6;
v0 = 20; % initial speed, fps

[t,x] = ode45(@accsim, [0 tspan], [0 v0]);
x(:,2) = x(:,2).*15./22;

figure
plot(x(:,1),x(:,2),'k','LineWidth',3) % Plot speed vs distance, baseline
axis([0 100 min(x(:,2)) x(65,2)])
xlabel('Distance (ft)')
ylabel('Speed (mph)')
title('100 ft Acceleration from Corner')
hold on
```

```
Mbike = 40/g; % 20% lighter bike
[t,x] = ode45(@accsim, [0 tspan], [0 v0]);
x(:,2) = x(:,2).*15./22;
plot(x(:,1),x(:,2),'g','LineWidth',3)
Mbike = 50/g; % reset bike weight

% CdA = 1.69*.8; % 20% less air drag
% [t,x] = ode45(@accsim, [0 tspan], [0 v0]);
% x(:,2) = x(:,2).*15./22;
% plot(x(:,1),x(:,2),'b','LineWidth',3)
% CdA = 1.69; % reset drag coefficient

gain = 1.2; % 20% stronger rider
[t,x] = ode45(@accsim, [0 tspan], [0 v0]);
x(:,2) = x(:,2).*15./22;
plot(x(:,1),x(:,2),'c','LineWidth',3)
gain = 1; % reset rider strength

% 2015 Bike Projections
gain = 1.2; % 25% stronger rider
CdA = .23*7.9; % wind tunnel estimation
Mbike = 60/g; % 60 lb bike
[t,x] = ode45(@accsim, [0 tspan], [0 v0]);
x(:,2) = x(:,2).*15./22;
plot(x(:,1),x(:,2),'r--','LineWidth',3)

legend('Aria','20% lighter vehicle','20% stronger rider','2015 projection',4)
% legend('Aria','20% lighter vehicle','20% less air drag','20% stronger rider','2015↙
bike',2)
hold off

%% Other Notes

% Find power ramp to achieve max speed in min energy output
%
%   Work = 0
%   for loop over length of vector
%       Work = Work + Fnet(i)*(x(i+1)-x(i))
%   end
%
% Then play with the power ramp until 'Work' is minimized, and still
% achieve 95% of max speed at x = 1500 ft, with Pmax <= 600 Watts
```

Table 48. Rider body measurements and position measurements derived from SolidWorks 2-D model.

	Rider	Trent	Peter	Matt	Judy	Zach	Shannon	Mike	Alex
BODY MEASUREMENTS (in)	Femur	16.5	18.0	16.5	18.0	16.5	15.5	17.0	18.0
	Tibia	17.8	17.0	17.0	16.0	15.5	16.0	15.5	21.0
	Torso	26.0	22.5	22.5	23.0	22.0	22.0	22.5	26.5
	Lower Head	7.0	6.0	6.5	6.5	5.5	6.0	6.0	6.0
	Upper Head	5.5	5.0	5.0	5.5	5.0	5.5	6.0	6.0
	Shoulder Width	18.0	16.0	17.5	19.0	15.5	16.5	17.5	18.5
	Hip Width	13.5	12.0	14.0	13.0	12.5	14.0	13.5	14.5
POSITION MEASUREMENTS (in)	Back Angle	42.0	46.0	45.0	46.0	47.0	46.0	46.0	44.0
	Hip Angle	124.3	123.7	123.4	121.8	122.6	122.6	122.1	123.9
	Hip Joint Height	8.5	10.5	10.0	9.5	11.0	10.5	10.0	8.5
	Seat Surface Height	4.0	6.5	5.5	5.0	6.5	6.0	5.5	4.0
	Seat Thickness	0.0	2.5	1.5	1.0	2.5	2.0	1.5	0.0
	Eye Height	32.9	32.7	32.4	32.5	32.6	32.3	32.2	32.9
	Top of Head Height	38.4	37.7	37.4	38.0	37.6	37.8	38.2	38.9
	Shoulder Height	25.9	26.7	25.9	26.0	27.1	26.3	26.2	26.9
	Knee Height	25.8	28.2	27.4	27.4	27.7	26.8	27.2	26.9
	CG Height	14.7	15.9	15.4	15.0	16.3	15.8	15.4	14.9
	Hip Joint - BB	34.8	35.8	34.2	34.7	32.8	32.3	33.2	39.5
	Rider CG - BB	35.8	36.8	35.2	35.7	33.8	33.3	34.2	40.5
	Shoulders - BB	54.1	51.4	50.1	50.7	47.8	47.6	48.9	58.6
	Visibility Distance	363.0	359.0	369.0	363.0	340.0	356.0	376.0	393.0

[in]	Rider	Trent	Peter	Matt	Judy	Zach	Shannon	Mike	Alex	**GOALS**
BODY MEASUREMENT	Femur	16.5	18.0	16.5	18.0	16.5	15.5	17.0	18.0	
	Tibia	17.8	17.0	17.0	16.0	15.5	16.0	15.5	18.0	
	Torso	26.0	22.5	22.5	23.0	22.0	22.0	22.5	26.5	
	Lower Head	7.0	6.0	6.5	6.5	5.5	6.0	6.0	6.0	
	Upper Head	5.5	5.0	5.0	5.5	5.0	5.5	6.0	6.0	
	Shoulder Width	18.0	16.0	17.5	19.0	15.5	16.5	17.5	18.5	
	Hip Width	13.5	12.0	14.0	13.0	12.5	14.0	13.5	14.5	
	Weight	165	140	165	160	125	125	145	170	
ARIA	Back Angle	39	39	39	39	39	39	39	39	
	Hip Angle	131	131	131	131	131	131	131	131.1	
	Knee Angle	58	62	53	56	41	35	45	67	
	Seat Surface Height	9	9	9	9	9	9	9	9	
	Hip Joint Height	13.5	13.5	13.5	13.5	13.5	13.5	13.5	13.5	
	Eye Height	36.9	33.7	34.2	34.5	32.9	33.4	33.7	36.2	
	Top of Head Height	42.4	38.7	39.2	40.0	37.9	38.9	39.7	42.2	
	Shoulder Height	29.9	27.7	27.7	28.0	27.4	27.4	27.7	30.2	
	Knee Height	30.2	30.8	29.8	30.2	29.0	28.7	29.3	31.3	
	CG Height	19.7	18.9	18.9	19.0	18.8	18.8	18.9	19.9	
	Hip Joint - BB	30.5	30.5	30.5	30.5	30.5	30.5	30.5	30.5	
	Rider CG - BB	31.5	31.5	31.5	31.5	31.5	31.5	31.5	31.5	
	Shoulders - BB	50.7	48.0	48.0	48.4	47.6	47.6	48.0	51.1	
	Visibility Distance	262	409	369	350	499	437	409	287	
	Combined CG Height	19.1	18.3	18.5	18.5	18.1	18.1	18.3	19.3	
	Combined CG - BB	31.4	31.4	31.4	31.4	31.4	31.4	31.4	31.4	
	Combined CG - Front	13.4	13.4	13.4	13.4	13.4	13.4	13.4	13.4	
	Combined % R	0.29	0.29	0.29	0.29	0.29	0.29	0.29	0.29	
	Combined % F	0.71	0.71	0.71	0.71	0.71	0.71	0.71	0.71	
	Roll acceleration (g's)	0.60	0.62	0.62	0.62	0.63	0.63	0.62	0.59	
	Hairpin test speed (mph)	15.3	15.7	15.6	15.6	15.8	15.8	15.6	15.2	
	Hairpin SF @ 12 mph	1.02	1.04	1.04	1.04	1.05	1.05	1.04	1.02	
	Braking tip (g's)	0.43	0.43	0.43	0.43	0.43	0.43	0.43	0.43	
	Braking test distance (m)	5.75	5.75	5.75	5.75	5.76	5.76	5.75	5.75	
	Braking test SF	1.04	1.04	1.04	1.04	1.04	1.04	1.04	1.04	
2015 BIKE	Back Angle	42	46	45	46	47	46	46	44	
	Hip Angle	123	123	123	121	121	122	121	122	122
	Hip Joint Height	8.5	10.5	10	9.5	10.5	10.5	10	8.5	
	Seat Surface Height	4.0	6.5	5.5	5.0	6.0	6.0	5.5	4.0	
	Seat Thickness	0.0	2.5	1.5	1.0	2.0	2.0	1.5	0.0	0-3
	Eye Height	32.9	32.7	32.4	32.5	32.1	32.3	32.2	32.9	
	Top of Head Height	38.4	37.7	37.4	38.0	37.1	37.8	38.2	38.6	39
	Shoulder Height	25.9	26.7	25.9	26	26.6	26.3	26.2	26.9	
	Knee Height	25.1	27.1	26.2	26.2	26.2	25.9	26.0	25.9	28
	CG Height	14.7	15.9	15.4	15.0	15.8	15.8	15.4	14.9	
	Hip Joint - BB	32.6	33.7	32.2	32.6	30.8	30.3	31.2	34.3	
	Rider CG - BB	33.6	34.7	33.2	33.6	31.8	31.3	32.2	35.3	
	Shoulders - BB	51.9	49.4	48.1	48.5	45.8	45.6	46.8	53.3	
	Visibility Distance	337	337	344	338	349	332	349	347	350
	Combined CG Height	14.1	14.8	14.6	14.2	14.6	14.6	14.5	14.2	15
	Combined CG - BB	33.1	33.9	32.8	33.1	31.8	31.4	32.1	34.4	
	Combined CG - Front	15.6	16.4	15.3	15.6	14.3	13.9	14.6	16.9	
	Combined % R	0.36	0.38	0.36	0.36	0.33	0.32	0.34	0.39	0.36
	Combined % F	0.64	0.62	0.64	0.64	0.67	0.68	0.66	0.61	0.67
	Roll acceleration (g's)	0.63	0.59	0.62	0.63	0.64	0.65	0.64	0.60	0.57
	Hairpin test speed (mph)	15.8	15.2	15.6	15.7	15.8	15.9	15.9	15.3	
	Hairpin SF @ 15 mph	1.05	1.01	1.04	1.04	1.06	1.06	1.06	1.02	
	Braking tip (g's)	0.47	0.48	0.47	0.47	0.45	0.44	0.45	0.49	0.41
	Braking test distance (m)	5.21	5.09	5.27	5.21	5.47	5.55	5.41	5.00	
	Braking test SF	1.15	1.18	1.14	1.15	1.10	1.08	1.11	1.20	

Trike (units: in, lb)	Track Width	Wheel-base (L)	Weight	CG height	CG to front	CG to rear	% F	% R	BB to front	BB to CG
Aria	32	46.8	49	13.6	13.2	33.6	0.72	0.28	18	31.2
2014-2015	28	43	55	12	14.19	28.81	0.67	0.33	17.5	31.69

Frame Stiffness Testing Data

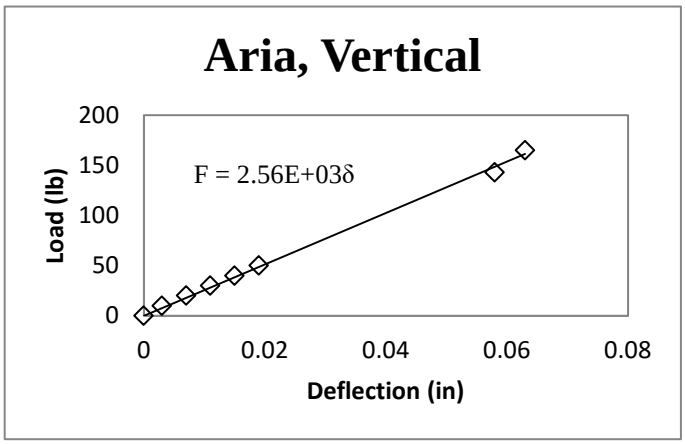

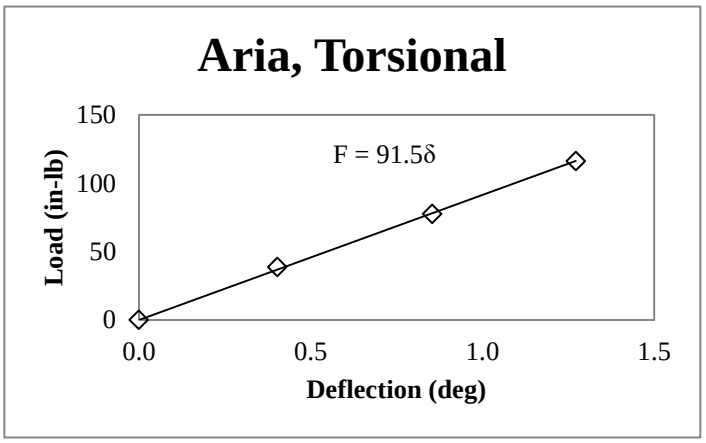

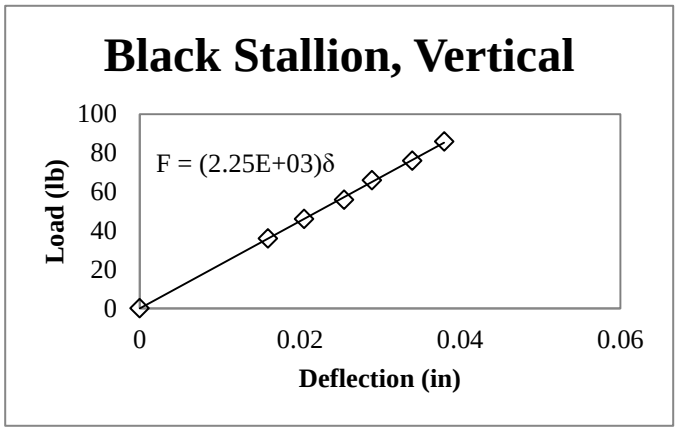

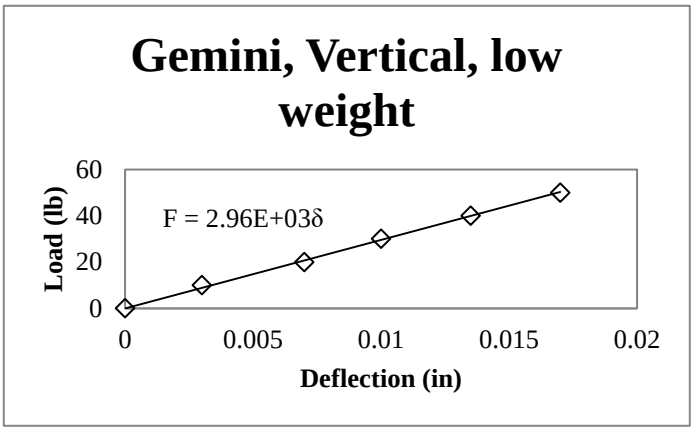

Wheel Stiffness Testing Data

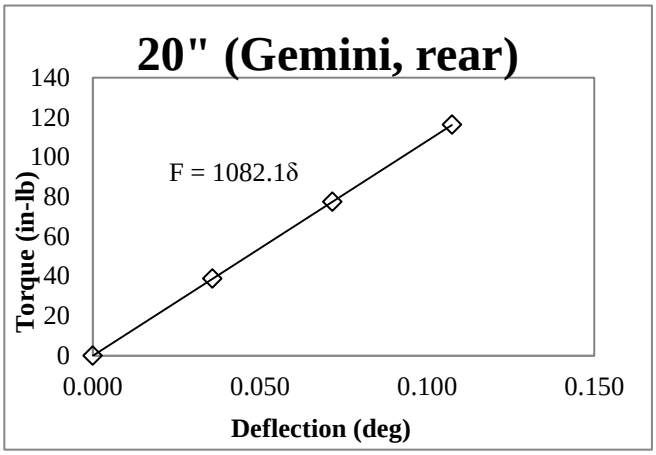

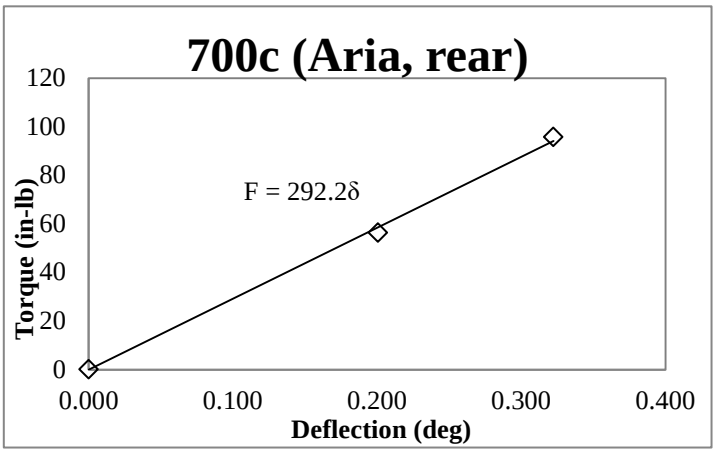

Table 49. Wind tunnel testing raw data (wheels enclosed model).

	ΔP		V_0=2.139				
Trial	Static Taps	Pitot-Tube	Drag (readout, V)	Δ Drag (V)	Drag (kg)	Total Drag (lbf)	Model Drag (lbf)
1	5.094	5.137	1.936	-0.203	0.949	2.093	1.227
2	5.087	5.125	1.933	-0.206	0.963	2.124	1.258
3	5.083	5.132	1.933	-0.206	0.963	2.124	1.258
4	5.083	5.126	1.937	-0.202	0.945	2.082	1.216
5	5.085	5.129	1.933	-0.206	0.963	2.124	1.258
6	5.089	5.128	1.936	-0.203	0.949	2.093	1.227
7	5.083	5.132	1.941	-0.198	0.926	2.041	1.175
8	5.087	5.126	1.937	-0.202	0.945	2.082	1.216
9	5.09	5.123	1.942	-0.197	0.921	2.031	1.165
10	5.088	5.128	1.936	-0.203	0.949	2.093	1.227

Table 50. Wind tunnel testing raw data (wheels out model).

	ΔP		V_0=2.137				
Trial 1	Static Taps	Pitot-Tube	Drag (readout, V)	Δ Drag (V)	Drag (kg)	Total Drag (lbf)	Model Drag (lbf)
1	5.087	5.142	1.930	-0.208	0.973	2.144	1.278
2	5.087	5.116	1.929	-0.209	0.977	2.155	1.289
3	5.085	5.135	1.930	-0.208	0.973	2.144	1.278
4	5.086	5.132	1.934	-0.204	0.954	2.103	1.237
5	5.087	5.142	1.932	-0.206	0.963	2.124	1.258
6	5.084	5.105	1.932	-0.206	0.963	2.124	1.258
7	5.088	5.116	1.934	-0.204	0.954	2.103	1.237
8	5.094	5.12	1.929	-0.209	0.977	2.155	1.289
9	5.081	5.107	1.931	-0.207	0.968	2.134	1.268
10	5.086	5.106	1.933	-0.205	0.959	2.113	1.247

Appendix F

Gantt Chart

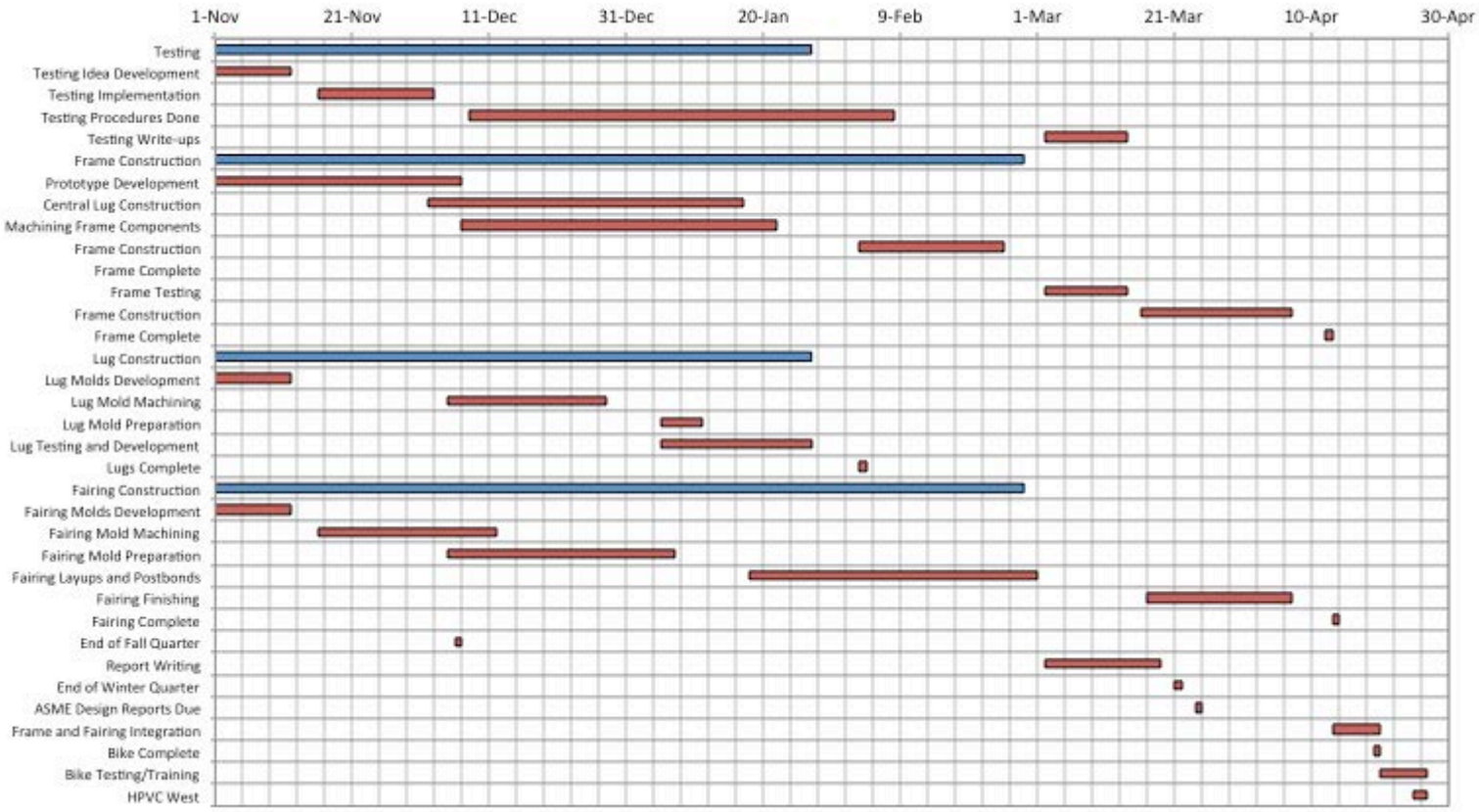
1-Nov
21-Nov
11-Dec
31-Dec
20-Jan
9-Feb
1-Mar
21-Mar
10-Apr
30-Apr
Testing
Testing Idea Development
Testing Implementation
Testing Procedures Done
Testing Write-ups
Frame Construction
Prototype Development
Central Lug Construction
Machining Frame Components
Frame Construction
Frame Complete
Frame Testing
Frame Construction
Frame Complete
Lug Construction
Lug Molds Development
Lug Mold Machining
Lug Mold Preparation
Lug Testing and Development
Lugs Complete
Fairing Construction
Fairing Molds Development
Fairing Mold Machining
Fairing Mold Preparation
Fairing Layups and Postbonds
Fairing Finishing
Fairing Complete
End of Fall Quarter
Report Writing
End of Winter Quarter
ASME Design Reports Due
Frame and Fairing Integration
Bike Complete
Bike Testing/Training
HPVC West